HOW PLANTS MANAGE EPISODES OF DROUGHT STRESS: FROM SIGNALING TO EMBOLISM RESISTANCE OF PLANT ORGANS

A Dissertation

Presented to the Faculty of the Graduate School

of Cornell University

In Partial Fulfillment of the Requirements for the Degree of

Doctor of Philosophy

by

Annika Erika Huber

August 2019

HOW PLANTS MANAGE EPISODES OF DROUGHT STRESS: FROM SIGNALING TO EMBOLISM RESISTANCE OF PLANT ORGANS

Annika Erika Huber, Ph.D.

Cornell University 2019

Water shortage is the most limiting factor for plant growth and development. Nevertheless, the current state of science is far from understanding drought stress behavior in plants and the mechanisms leading to drought stress resistance. This thesis investigates long-distance signaling types (hydraulic, electrical, chemical) preceding the onset of stomatal closure, studies the role of hydraulic integrity of plant organs (root, stem, petiole) during and after drought stress periods on stomatal conductance, and investigates xylem network characteristics that determine hydraulic efficiency (hydraulic flow per unit xylem area) and embolism resistance.

In the first study, I exposed sunflowers (*Helianthus annuus*) to two different drought stress treatments and measured simultaneously and continuously stomatal conductance, acoustic emissions events (AE), and surface-level electrical signals. Changes in organ-level water potential and leaf-level abscisic acid (ABA) concentration were also measured on a subset of plants throughout the experiment. I found that hydraulic signals precede the onset of stomatal closure while surface potentials shifted concurrently with the onset of stomatal closure. Leaf-level ABA concentration did not change until after stomata were closed.

In the second study, six different plant species (*Helianthus annuus*, *Populus x*

canadensis, Acer saccharum, Acer saccharinum, Picea glauca, Tsuga canadensis) were exposed to increasing drought stress intensities with subsequent rewatering events. At each drought intensity, I measured water potential, relative water content, and embolism thresholds of roots, stems, and petioles using cryo-microscopy and single vessel injection technique. These results were compared to established hydraulic vulnerability curves (PLC curves). Results showed that leaf petiole xylem vessels were the most susceptible to embolism formation, while root and stem xylem vessels were highly drought resistant. Stomatal closure was not correlated to xylem cavitation events since cavitation only occurred during higher drought stress intensities. After rewatering, embolism events in the petiole xylem vessels recovered for all species, while poplar plants shed their leaves. In *Acer saccharum* we found that stem xylem vessel embolism increased after rewatering. Additionally, I found a disparity between PLC curves and plant organ water potentials experienced during drought periods.

Lastly, xylem networks of three ring- (*Quercus montana, Fraxinus pennsylvanica, Carya ovata*) and three diffuse-porous tree species (*Fagus sylvatica, Liriodendron tulipifera, P. x canadensis*) were reconstructed to understand the topology of vascular networks. Fluid simulation models of each network were performed to predict the resistance of hydraulic conductivity as a function of vessel dropout within the network. I found that the combination of different network presentations advanced the understanding of xylem networks. Additionally, xylem dropout analysis revealed that all six examined xylem networks experience a 50% loss in hydraulic conductivity with a xylem vessel dropout fraction between 0.01-0.04%, despite the degree of xylem vessel connectivity differing among the tree species.

BIOGRAPHICAL SKETCH

Annika Erika Huber was born in Bayreuth, Germany. Growing up on the countryside she always loved being outside and discovering nature. At the age of 10 she announced she would become a plant doctor. Following her passion, she started a bachelor's degree in Biology at the University of Bayreuth after she graduated from the German high school. In her bachelor's degree she deepened her understanding in ecology and biodiversity and in ecosystems and its components. Annika finished her studies with a bachelor thesis focusing on *Quercus robur* and *Quercus petraea*: Influence of flooding on stem growth. After she received her bachelor's degree in 2008, she decided to deepen her understanding on woody plant species and therefore she started a master's degree in Forest and Wood Science at the Technical University of Munich. During her master's she majored in timber-raw material and wood based products, mountain forests, and forest ecosystems-soil and stand. In the summer of 2012, she completed her study with her Master thesis focusing on carbon assimilation and transpiration of beech and spruce trees under inter- and intraspecific competition. In fall 2012 she came to Cornell University and started a Ph.D. program with Dr. Taryn Bauerle in the field of Horticulture, School of Integrative Plant Science. Her work focused on drought signaling and hydraulic integrity of plant organs during drought stress.

To my family and husband.

Thank you for your endless support.

ACKNOWLEDGMENTS

This thesis encompasses the hard work of many people. I would like to offer my special thanks to my advisor Taryn Bauerle for her valuable and constructive suggestions during the planning and the development of this research. I also would like to express my appreciation to my committee members Peter Melcher, Miguel Piñeros, and Tim Setter who assisted me in lab work and enriched my thesis with many stimulating discussions. Additionally, I would like to thank undergraduate research assistants Tommi Schieder, Hannah Fuller, Andrew Harner, Erika Bucior, as well as our lab technician Max Heitner for many hours of image analysis and their support in the greenhouse. I also appreciated my fellow lab mates Juana Muñoz Ucros and Marie Zwetsloot. For my work, I spent countless hours in the Cornell Center for Material Research, and I would like to thank John Grazul and Malcolm Thomas for all of their efforts in this area. Without their assistance and time, I would not have been able to accomplish all of the image acquisition. Lastly, I deeply thank my family and friends for their unconditional support and cheering. My husband, Erik Huber, who helped me not only with data analysis but even more valuable to me, he helped me not to forget that there is a world outside Cornell campus.

TABLE OF CONTENTS

CHAPTER 1

INTRODUCTION

1.1 Importance of drought stress research in plants:

Water shortage is one of the most limiting factors for plant growth (Cattivelli *et al.*, 2008). Persistent drought periods can have detrimental effects on plant development and productivity (Barnabás *et al.*, 2008) leading to major losses in field crop yields (Boyer *et al.*, 2013) and causing worldwide tree diebacks (Ciais *et al.*, 2005; Allen *et al.*, 2010). In agricultural settings, a reduction in crop yields due to water shortages has become an increasing threat that affects food prices and food security (Vicente-Serrano *et al.*, 2014; Glotter and Elliott, 2016; Tian *et al.*, 2016). On an ecosystem scale, drought periods have been correlated with major tree diebacks across many biomes, including mangroves (Duke *et al.*, 2017), temperate forests (Hogg *et al.*, 2008), tropical forests (Phillips *et al.*, 2009), and chaparral (Venturas *et al.*, 2016). Since one severe drought event can result in the death of millions of trees (Asner *et al.*, 2015), it is not surprising that tree diebacks alter plant biodiversity as well as cause changes in ecosystem services such as provisioning services (food, lumber, water), cultural services (recreation), and habitat control (flood and erosion presentation) with negative impact on mankind (Breshears *et al.*, 2011).

Future climate is predicted to exhibit more frequent and prolonged drought periods which will be accompanied by heat waves, exacerbating the drought stress on plants (Meehl *et al.*, 2007; Seager *et al.*, 2007; Prudhomme *et al.*, 2014). Therefore, predicting plants' reactions to drought in changing climate conditions has become one

of the most urgent research areas in plant ecophysiology. Yet, predicting plants' responses to changing environmental conditions remains difficult because the precise physiological mechanisms underlying plant behavior during drought stress periods are poorly understood. In general, the hydraulic integrity of the water column has been identified as playing a major role in plant productivity and survival during drought (Anderegg *et al.*, 2012; Nardini *et al.*, 2013; Venturas *et al.*, 2016). The integrity of the hydraulic system is crucial for providing plants with enough water for all aspects of plant life, ranging from growth to photosynthesis and reproduction. However, under prolonged drought periods, the integrity of the water column is prone to disruption (Tyree and Dixon, 1986). Depending on the severity of the disruption within the hydraulic system, the water being supplied to the plant tissues can be reduced or even stopped. By closing their stomates at the beginning of drought stress periods, plants try to maintain the integrity of the water column (Sparks and Black, 1999). However, the manner in which stomatal closure is integrated on a whole plant level to the hydraulic system is not known, nor are the fundamental characteristics of hydraulic networks which would lead to a more robust hydraulic system (Venturas *et al.*, 2017). Understanding plant behavior during drought will allow scientists to make predictions of where, when, and how vegetation will be affected by future climatic variations and will support management decisions in agricultural as well as silvicultural settings.

1.2 The current state of drought stress research of plants:

Water is transported in plants under tension from the roots to the leaves via the water conducting tissue (xylem) following a negative water potential gradient in the soil-

plant-air continuum (SPAC) (Dixon, 1914). The driving force for the water flow is the difference in water potential between the relatively hydrated soil and the subsaturated atmosphere. The tension, acting on the water column during the water transport, puts the air nuclei in the xylem sap into a metastable condition, meaning the air nuclei are prone to spontaneously cavitate (formation of small air bubbles) (Tyree and Dixon, 1986). Under increasing tensions, these initial cavitation events can transform into embolisms as the surrounding air within the xylem tissue diffuses into the cavitated space. The air embolism can fill an entire sector of xylem vasculature (Tyree and Sperry 1989).

Embolism thresholds of stems are used as a proxy for drought resistance in plants (Cochard *et al.*, 1996; Nardini and Salleo, 2000; Vogt, 2001; Cordero and Nilsen, 2002; Davis *et al.*, 2002; Lo Gullo *et al.*, 2003; Pita *et al.*, 2003; Tyree *et al.*, 2003; Maherali *et al.*, 2004; McDowell *et al.*, 2008). During periods of water shortages, the overall magnitude of the water potential gradient becomes greater in the soil-plant-air continuum, raising the tension on the water column, which increases local embolism events (Fig. 1.1a,b). The threshold for embolism formation is plant and plant organ specific, making it difficult to predict these events (Melcher *et al.*, 2001; Maherali *et al.*, 2004, 2006). If the tension in the water column continues to increase, local embolism events can expand in the xylem network by being aspirated via pits into neighboring xylem conduits (air-seeding). Thus, embolism events decrease the hydraulic conductivity of the xylem network and this diminishes the water supply to distal plant organs (Tyree and Sperry, 1989) (Fig. 1.1c). Pits are porous membranes (cellulosic meshes) that form laterally between two neighboring xylem vessels and

serve as ports for water and gas exchange (Fig. 1.1d). The thickness, as well as the porosity of the membrane, highly affects the vulnerability to embolism (Schmid and Machado, 1968; Sano *et al.*, 2005; Jansen *et al.*, 2009). The weaker the cellulosic mesh of the pit pores, the more prone the xylem vessel network is to air-seeding.

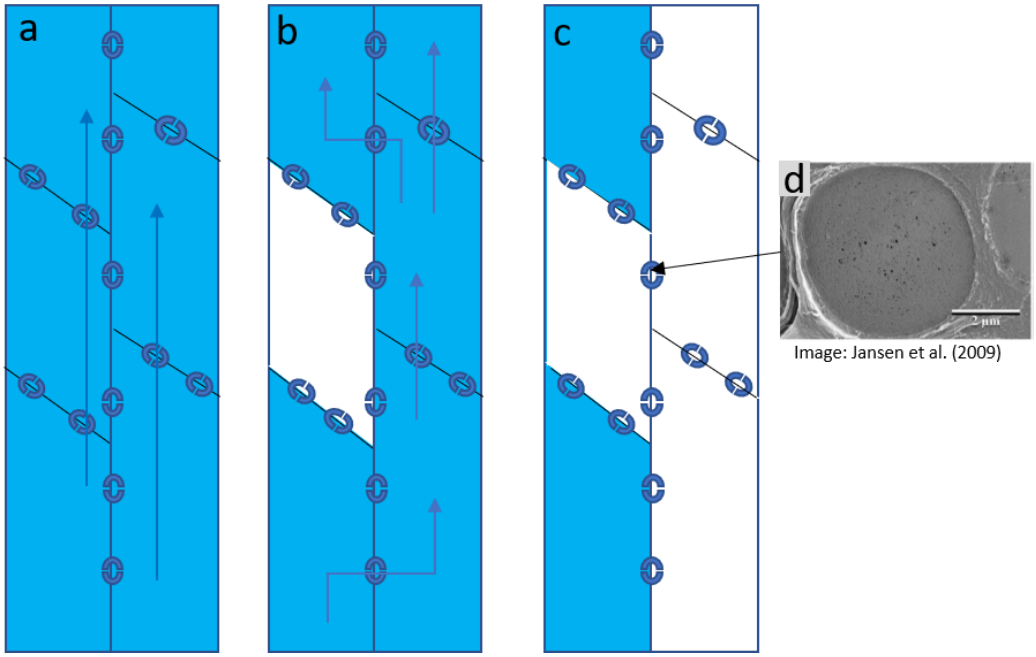

Figure 1.1: Xylem vessels under well-hydrated (a), moderate drought (b), and severe drought (c) conditions. Vessels are connected via pits(d) (SEM image from *Jansen et al.* 2007). Blue arrows indicate water flow. All vessels are water conducting under well hydrated conditions and water can move freely through pits. Under moderate drought stress conditions embolism threshold is reached and vessel start cavitating. However, water can be diverted through pits. Under severe drought conditions, embolism spread through pits in adjacent vessels and interrupt the water flow.

Zimmermann (1983) characterized embolism patterns at the organ-scale and formulated the segmentation hypothesis, which states that distal plant organs, such as roots and petioles, are most prone to cavitation events and therefore less drought stress resistant. Thus, roots and leaves are referred to as safety valves (Bucci *et al.*, 2013).

Less carbon per gram tissue is needed to produce roots and petioles than is needed to produce stems (Zimmermann, 1983). Therefore, plants can sacrifice distal organs first. Today, there is general agreement that the stem is the plant organ most resistant to cavitation (Nardini *et al.*, 2003; Choat *et al.*, 2005; Jacobsen *et al.*, 2007; Bucci *et al.*, 2008; Hao *et al.*, 2008), even though it has not always been supported (Cochard *et al.*, 1992, 1997). However, there is no consensus if the roots or the petioles are more prone to embolism events. The reason for this uncertainty is that very little research has compared plant organs across an individual plant (Choat *et al.*, 2005; Rodriguez-Dominguez *et al.*, 2018). Nevertheless, the high embolism vulnerability of distal plant organs has been shown to preserves the hydraulic integrity of stems

Early embolism events in leaves are thought to be connected to stomatal closure, even though there is still a debate if cavitation events initiate stomatal closure, or if stomatal closure occurs prior to leaf embolism events (Nardini and Salleo, 2000). Either way, there is a broad consensus that the water status of the leaves is strongly correlated with the onset of stomata closure (Saliendra *et al.*, 1995; Cochard *et al.*, 1996; Salleo *et al.*, 2000; Brodribb *et al.*, 2003; Jacobsen *et al.*, 2008), which advocates hydraulic signals as one signal type initiating stomatal closure. Nevertheless, the definitive signal type and origin preceding the onset of stomatal closure is still unknown.

Plants transfer information through three different signal types: hydraulic, chemical, and electrical (Huber and Bauerle, 2016). Because signal integration is highly complex and not well understood, all three signal types have been proposed as the primary contributor to stomatal closure (Zhang and Davies, 1989; Fromm and

Eschrich, 1993; Christmann *et al.*, 2007). The main difference between these different signal types is the transportation speed (Huber and Bauerle, 2016). Hydraulic signals are thought to be the quickest transported signal type. Pressure waves that are released during embolism formation can travel up to the speed of sound (Malone, 1993). However, other hydraulic signals, like turgor pressure changes of parenchyma cells, can occur before embolism formation and are observed to be transmitted slower, with an average speed of 20 cm s^{-1} (Boari and Malone, 1993). Electrical signal propagation speeds are comparable to hydraulic signals. Electrical signals control stomatal control in response to a plethora of different biotic and abiotic stressors (Huber and Bauerle, 2016) but they have never been monitored *in situ* to play a role in stomatal closure during drought stress periods. Chemical signals have the lowest signal speed, with 0.17 cm s^{-1} (Evans and Morris, 2017). However, they are the most discussed signal type. Besides the numerous different chemical signals (Huber and Bauerle, 2016), hormonal signals have been thoroughly discussed as playing a role in stomatal closure (e.g. Assmann, 2010). Yet, in the absence of a single experiment recording all three signal types simultaneously, the primary signal type initiating stomatal closure (chemical, hydraulic, or electric) remains uncertain.

1.3 Defining drought stress tolerance of plants:

Defining a reliable method to predict stomatal closure and drought stress resistance of plants is an active research area. A common method to predict these two plant characteristics is to quantify the percentage of hydraulic conductivity loss across a range of negative water potentials (PLC curves), which are often performed on plant

stems (Lo Gullo *et al.*, 2003; Tyree *et al.*, 2003; McDowell *et al.*, 2008) (Fig. 1.2).

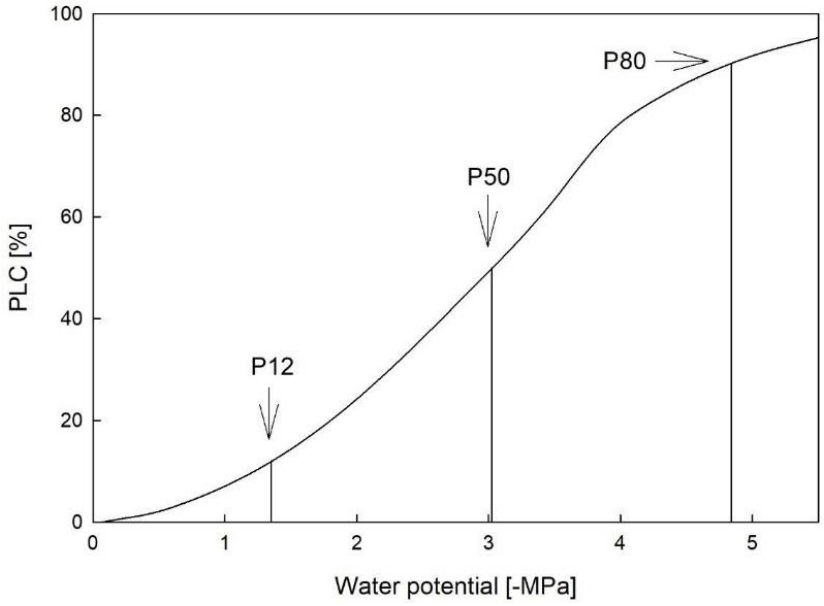

Figure 1.2: Hydraulic vulnerability curves (PLC curves) show the relationship between percentage loss of hydraulic conductivity and decreasing water potentials. PLC curves are often used to predict plant performance during drought stress periods. The water potential that induces a 12% loss of hydraulic conductivity (P_{12}) is used to predict the onset of stomatal closure. The water potential that initiates 50% loss of hydraulic conductivity (P_{50}) is used to compare plant resistance to embolism events among plant species. The water potential causing a 90% loss of hydraulic conductivity (P_{90}) is said to be the point of no return in angiosperm trees (no embolism repair and consequently plant death), in conifers this point is P_{50}.

Different percentages of hydraulic conductivity losses have been used as proxies to predict tree performance at the beginning and during drought stress periods, and even for possible drought stress recovery. For example, the water potential at which 12% of hydraulic conductivity loss occurs (P_{12}), also referred to as air entry value (Pe) because conductivity loss starts increasing rapidly beyond this value, has been identified to be the potential threshold above which stomatal closure occurred in many tree species (Meinzer *et al.*, 2009 Torres-Ruiz *et al.*, 2013), and the water potential at

which 50% loss of hydraulic conductivity is reached (P_{50}) is used to compare drought stress resistance among plants (e.g. Melcher *et al.*, 2001; Maherali *et al.*, 2004; Maherali *et al*., 2006). Lastly, the water potential inducing around 90% conductivity loss in angiosperms (Barigah *et al.*, 2013; Urli *et al.*, 2013; Anderegg *et al.*, 2016) and 50% loss in conifers (Brodribb and Cochard, 2009; Brodribb *et al.*, 2010) is referred to as the point of no return, meaning that most trees will likely die if they experience this level of hydraulic conductivity loss. While average P_{50} values of tree species lie between -2.5 to -5 MPa, some trees can have far lower P_{50} values, such as -14.1 MPa as measured in *Juniperus pinchotii* (Willson *et al.*, 2008). However, there are several shortcomings in the use of PLC curves to predict plant behavior during drought. For example, while the hydraulic conductivity loss in PLC curves is attributed to embolism events (Tyree and Sperry, 1988; Cochard *et al.*, 1992; Lobo *et al.*, 2018), there are other mechanisms such as extra-xylary cavitation events and tissue collapse that can reduce hydraulic conductivity without the occurrence of embolism events (Brodribb and Holbrook, 2005; Zhang *et al.*, 2016). Additionally, methods required to generate PLC curves are invasive and therefore prone to disturb the hydraulic integrity of the specimens. Finally, the value of using stem-level P_{50} values as a criterion to assess whole plant response to drought is not strongly grounded in biological relevance, for example: P_{50} values do not account for differences in plant organ vulnerabilities and it is questionable if plants in situ reach the range of water potentials which are induced during PLC measurements. Thus, studies that rely only on assessing plant drought response from stem P_{50} values are not ideal in predicting whole plant responses to drought stress.

Understanding drought responses on a whole plant level, rather than on an organ level, is crucial for predicting drought tolerance and drought impact on plant growth and productivity. The first step in accomplishing this long term goal is set forth in this dissertation, which aims to increase the understanding of the connection between stomatal control and plant hydraulics during and after drought stress periods. The objectives are 1) to investigate the signaling cascade of hydraulic, chemical, and electrical signals prior to and after stomatal closure and link these signal types to PLC curves and organ water potentials to identify the signal types most likely involved in stomatal closure, 2) to examine the hydraulic integrity of plant organs during different drought stress intensities and a subsequent rewatering event to understand organ impact on stomatal conductance during and after drought stress periods, and 3) to perform network analysis on ring- and diffuse-porous tree species to identify network properties that increase network resistance to cavitations.

1.4 References

Allen CD, Macalady AK, Chenchouni H, *et al.* 2010. A global overview of drought and heat-induced tree mortality reveals emerging climate change risks for forests. Forest Ecology and Management **259**, 660–684.

Anderegg WRL, Berry JA, Smith DD, Sperry JS, Anderegg LDL, Field CB. 2012. The roles of hydraulic and carbon stress in a widespread climate-induced forest die-off. Proceedings of the National Academy of Sciences of the United States of America **109**, 233–237.

Anderegg WRL, Klein T, Bartlett M, Sack L, Pellegrini AFA, Choat B, Jansen S.

2016. Meta-analysis reveals that hydraulic traits explain cross-species patterns of drought-induced tree mortality across the globe. Proceedings of the National Academy of Sciences **113**, 5024–5029.

Asner GP, Brodrick PG, Anderson CB, Vaughn N, Knapp DE, Martin RE. 2015. Progressive forest canopy water loss during the 2012–2015 California drought. Proceedings of the National Academy of Sciences **113**, E249–E255.

Assmann SM. 2010. Absciscic acid signal transduction in stomatal response. In: Davies PJ, ed. Plant hormones. Heidelberg London New York: Springer, 399–420.

Barigah TS, Charrier O, Douris M, Bonhomme M, Herbette S, Améglio T, Fichot R, Brignolas F, Cochard H. 2013. Water stress-induced xylem hydraulic failure is a causal factor of tree mortality in beech and poplar. Annals of Botany **112**, 1431–1437.

Barnabás B, Jäger K, Fehér A. 2008. The effect of drought and heat stress on reproductive processes in cereals. Plant, Cell and Environment **31**, 11–38.

Boari F, Malone M. 1993. Wound-induced hydraulic signals: survey of occurrence in a range of species. Journal of Experimental Botany **44**, 741–746.

Boyer JS, Byrne P, Cassman KG, *et al.* 2013. The U.S. drought of 2012 in perspective: a call to action. Global Food Security **2**, 139–143.

Breshears DD, López-Hoffman L, Graumlich LJ. 2011. When ecosystem services crash: preparing for big, fast, patchy climate change. AMBIO **40**, 256–263.

Brodribb TJ, Bowman DJMS, Nichols S, Delzon S, Burlett R. 2010. Xylem function and growth rate interact to determine recovery rates after exposure to

extreme water deficit. New Phytologist **188**, 533–542.

Brodribb TJ, Cochard H. 2009. Hydraulic failure defines the recovery and point of death in water-stressed conifers. Plant Physiology **149**, 575–584.

Brodribb TJ, Holbrook NM. 2005. Water stress deforms tracheids peripheral to the leaf vein of a tropical conifer. Plant Physilogy **137**, 1139–1146.

Brodribb TJ, Holbrook NM, Edwards EJ, Gutiérrez M V. 2003. Relations between stomatal closure, leaf turgor and xylem vulnerability in eight tropical dry forest trees. Plant, Cell and Environment **26**, 443–450.

Bucci SJ, Scholz FG, Goldstein G, Meinzer FC, Franco C, Zhang Y, Hao G. 2008. Water relations and hydraulic architecture in Cerrado trees : adjustments to seasonal changes in water availability and evaporative demand. Brazilian Journal of Plant Physiology **20**, 233–245.

Bucci SJ, Scholz FG, Peschiutta ML, Arias NS, Meinzer FC, Goldstein G. 2013. The stem xylem of Patagonian shrubs operates far from the point of catastrophic dysfunction and is additionally protected from drought-induced embolism by leaves and roots. Plant, Cell and Environment **36**, 2163–2174.

Cattivelli L, Rizza F, Badeck FW, Mazzucotelli E, Mastrangelo AM, Francia E, Marè C, Tondelli A, Stanca AM. 2008. Drought tolerance improvement in crop plants: an integrated view from breeding to genomics. Field Crops Research **105**, 1–14.

Choat B, Lahr EC, Melcher PJ, Zwieniecki MA, Holbrook NM. 2005. The spatial pattern of air seeding thresholds in mature sugar maple trees. Plant, Cell and Environment **28**, 1082–1089.

Christmann A, Weiler EW, Steudle E, Grill E. 2007. A hydraulic signal in root-to-shoot signalling of water shortage. The Plant Journal **52**, 167–174.

Ciais P, Reichstein M, Viovy N, *et al.* 2005. Europe-wide reduction in primary productivity caused by the heat and drought in 2003. Nature **437**, 529–533.

Cochard H, Breda N, Grainer A, Aussenac G. 1992. Vulnerability to air embolism of three European species (*Quercus petraea* (Matt) Liebl , *Q pubescens* Wild, *Q robur* L). Annals of Forest Science, 225–233.

Cochard H, Bréda N, Granier A. 1996. Whole tree hydraulic conductance and water loss regulation in Quercus during drought: evidence for stomatal control of embolism ? Annals of Forest Science **53**, 197–207.

Cochard H, Peiffer M, Gall K LE, Granier A. 1997. Developmental control of xylem hydraulic resistances and vulnerability to embolism in *Fraxinus excelsior* L.: impacts on water relations. Journal of Experimental Botany **48**, 655–663.

Cordero RA, Nilsen ET. 2002. Effects of summer drought and winter freezing on stem hydraulic conductivity of Rhododendron species from contrasting climates. Tree Physiology **22**, 919–928.

Davis SD, Ewers FW, Sperry JS, Portwood KA, Crocker MC, Adams GC. 2002. Shoot dieback during prolonged drought in *Ceanothus* (Rhamnaceae) chaparral of California: a possible case of hydraulic failure. American Journal of Botany **89**, 820–828.

Dixon HH. 1914. *Transpiration and the ascent of sap in plants*. London: Macmillan and Company.

Duke NC, Kovacs JM, Griffiths AD, Preece L, Hill DJE, Van Oosterzee P, Mackenzie J, Morning HS, Burrows D. 2017. Large-scale dieback of mangroves in Australia's Gulf of Carpentaria: a severe ecosystem response, coincidental with an unusually extreme weather event. Marine and Freshwater Research **68**, 1816–1829.

Evans MJ, Morris RJ. 2017. Chemical agents transported by xylem mass flow propagate variation potentials. Plant Journal **91**, 1029–1037.

Fromm J, Eschrich W. 1993. Electric signals released from roots of willow (*Salix viminalis* L.) change transpiration and photosynthesis. Journal of Plant Physiology **141**, 673–680.

Glotter M, Elliott J. 2016. Simulating US agriculture in a modern Dust Bowl drought. Nature Plants **3**, 1–6.

Lo Gullo MA, Salleo S, Rosso R, Trifilò P. 2003. Drought resistance of 2-year-old saplings of Mediterranean forest trees in the field: relations between water relations, hydraulics and productivity. Plant and Soil **250**, 259–272.

Hao GY, Hoffmann WA, Scholz FG, Bucci SJ, Meinzer FC, Franco AC, Cao KF, Goldstein G. 2008. Stem and leaf hydraulics of congeneric tree species from adjacent tropical savanna and forest ecosystems. Oecologia **155**, 405–415.

Hogg EH (Ted), Brandt JP, Michaelian M. 2008. Impacts of a regional drought on the productivity, dieback, and biomass of western Canadian aspen forests. Canadian Journal of Forest Research **38**, 1373–1384.

Huber AE, Bauerle TL. 2016. Long-distance plant signaling pathways in response to multiple stressors: the gap in knowledge. Journal of Experimental Botany **67**,

2063–2079.

Jacobsen AL, Agenbag L, Esler KJ, Pratt RB, Ewers FW, Davis SD. 2007. Xylem density, biomechanics and anatomical traits correlate with water stress in 17 evergreen shrub species of the Mediterranean-type climate region of South Africa. Journal of Ecology **95**, 171–183.

Jacobsen AL, Pratt RB, Davis SD, Ewers FW. 2008. Comparative community physiology: nonconvergence in water relations among three semi-arid shrub communities. New Phytologist **180**, 100–113.

Jansen S, Choat B, Pletsers A. 2009. Morphological variation of intervessel pit membranes and implications to xylem function in angiosperms. American Journal of Botany **96**, 409–419.

Lobo A, Torres-Ruiz JM, Burlett R, *et al.* 2018. Assessing inter- and intraspecific variability of xylem vulnerability to embolism in oaks. Forest Ecology and Management **424**, 53–61.

Maherali H, Moura CF, Caldeira MC, Willson CJ, Jackson RB. 2006. Functional coordination between leaf gas exchange and vulnerability to xylem cavitation in temperate forest trees. Plant, Cell and Environment **29**, 571–583.

Maherali H, Pockman WT, Jackson RB. 2004. Adaptive variation in the vulnerability of woody plants to xylem cavitation. Ecology **85**, 2184–2199.

Malone M. 1993. Hydraulic signals. Philosophical Transactions of the Royal Society B: Biological Sciences **341**, 33–39.

McDowell N, Pockman WT, Allen CD, *et al.* 2008. Mechanisms of plant survival and mortality during drought: why do some plants survive while others

succumb to drought? New Phytologist **178**, 719–739.

Meehl GA, Arblaster JM, Tebaldi C. 2007. Contributions of natural and anthropogenic forcing to changes in temperature extremes over the United States. Geophysical Research Letters **34**, L19709.

Meinzer FC, Johnson DM, Lachenbruch B, McCulloh K a., Woodruff DR. 2009. Xylem hydraulic safety margins in woody plants: coordination of stomatal control of xylem tension with hydraulic capacitance. Functional Ecology **23**, 922–930.

Melcher PJ, Goldstein G, Meinzer FC, Yount DE, Jones TJ, Holbrook NM, Huang CX. 2001. Water relations of coastal and estuarine *Rhizophora mangle*: xylem pressure potential and dynamics of embolism formation and repair. Oecologia **126**, 182–192.

Nardini A, Battistuzzo M, Savi T. 2013. Shoot desiccation and hydraulic failure in temperate woody angiosperms during an extreme summer drought. New Phytologist **200**, 322–329.

Nardini A, Salleo S. 2000. Limitation of stomatal conductance by hydraulic traits: sensing or preventing xylem cavitation? Trees **15**, 14–24.

Nardini A, Salleo S, Raimondo F. 2003. Changes in leaf hydraulic conductance correlate with leaf vein embolism in *Cercis siliquastrum* L. Trees **17**, 529–534.

Phillips OL, Aragão LEOC, Lewis SL, *et al.* 2009. Drought sensitivity of the Amazon rainforest. Science **323**, 1344–1347.

Pita P, Gascó A, Pardos JA. 2003. Xylem cavitation, leaf growth and leaf water potential in *Eucalyptus globulus* clones under well-watered and drought

conditions. Functional Plant Biology **30**, 891–899.

Prudhomme C, Giuntoli I, Robinson EL*, et al.* 2014. Hydrological droughts in the 21st century, hotspots and uncertainties from a global multimodel ensemble experiment. Proceedings of the National Academy of Sciences **111**, 3262–3267.

Rodriguez-Dominguez CM, Carins Murphy MR, Lucani C, Brodribb TJ. 2018. Mapping xylem failure in disparate organs of whole plants reveals extreme resistance in olive roots. New Phytologist **218**, 1025–1035.

Saliendra N, Sperry J, Comstock J. 1995. Influence of leaf water status on stomatal response to humidity, hydraulic conductance, and soil drought in *Betula occidentalis*. Planta **196**, 357–366.

Salleo S, Nardini A, Pitt F, Gullo MA. 2000. Xylem cavitation and hydraulic control of stomatal conductance in Laurel (*Laurus nobilis* L.). Plant, Cell and Environment **23**, 71–79.

Sano Y, Okamura Y, Utsumi Y. 2005. Visualizing water-conduction pathways of living trees: selection of dyes and tissue preparation methods. Tree Physiology **25**, 269–75.

Schmid R, Machado R. 1968. Pit membranes in hardwoods - fine structure and development. Protoplasma **66**, 185–204.

Seager R, Ting M, Held I, *et al.* 2007. Model projections of an imminent transition to a more arid climate in southwestern North America. Science **316**, 1181–1184.

Sparks JP, Black RA. 1999. Regulation of water loss in populations of *Populus trichocarpa*: the role of stomatal control in preventing xylem cavitation. Tree

Physiology **19**, 453–459.

Tian H, Ren W, Tao B, *et al.* 2016. Climate extremes and ozone pollution: a growing threat to China's food security. Ecosystem Health and Sustainability **2**, e01203.

Tyree MT, Dixon MA. 1986. Water stress induced cavitation and embolism in some woody plants. Physiologia Plantarum **66**, 397–405.

Tyree MT, Engelbrecht MJ, Vargas G, Kursar TA. 2003. Desiccation tolerance of five tropical seedlings in Panama. Relationship to a field assessment of drought performance. Plant Physiology **132**, 1439–1447.

Tyree MT, Sperry JS. 1988. Do woody plants operate near the point of catastrophic xylem dysfunction caused by dynamic water stress? Answers from a model. Plant Physiology **88**, 574–580.

Tyree MT, Sperry JS. 1989. Vulnerability of xylem to cavitation and embolism. Annual Review of Plant Physiology and Plant Molecular Biology **40**, 19–38.

Torres-Ruiz JM, Diaz-Espejo A, Morales-Sillero A, Martín-Palomo MJ, Mayr S, Beikircher B, Fernández JE. 2013. Shoot hydraulic characteristics, plant water status and stomatal response in olive trees under different soil water conditions. Plant and Soil **373**, 77–87.

Urli M, Porté AJ, Cochard H, Guengant Y, Burlett R, Delzon S. 2013. Xylem embolism threshold for catastrophic hydraulic failure in angiosperm trees. Tree Physiology **33**, 672–683.

Venturas MD, MacKinnon ED, Dario HL, Jacobsen AL, Pratt RB, Davis SD. 2016. Chaparral shrub hydraulic traits, size, and life history types relate to species mortality during California's historic drought of 2014. PLoS ONE **11**,

1–22.

Venturas MD, Sperry JS, Hacke UG. 2017. Plant xylem hydraulics: what we understand, current research, and future challenges. Journal of Integrative Plant Biology **59**, 356–389.

Vicente-Serrano SM, Lopez-Moreno JI, Beguería S, *et al.* 2014. Evidence of increasing drought severity caused by temperature rise in southern Europe. Environmental Research Letters **9**.

Vogt UK. 2001. Hydraulic vulnerability, vessel refilling, and seasonal courses of stem water potential of *Sorbus aucuparia* L. and *Sambucus nigra* L. Journal of Experimental Botany **52**, 1527–1536.

Willson CJ, Manos PS, Jackson RB. 2008. Hydraulic traits are influenced by phylogenetic history in the drought-resistant, invasive genus *Juniperus* (Cupressaceae). American Journal of Botany **95**, 299–314.

Zhang J, Davies WJ. 1989. Abscisic acid produced in dehydrating roots may enable the plant to measure the water status of the soil. Plant, Cell and Environment **12**, 73–81.

Zhang Y-J, Rockwell FE, Graham AC, Alexander T, Holbrook NM. 2016. Reversible leaf xylem collapse: a potential "circuit breaker" against cavitation. Plant Physiology **172**, 2261–2274.

Zimmermann MH. 1983. *Xylem structure and the ascent of sap*. New York: Springer Verlag.

CHAPTER 2

LONG-DISTANCE PLANT SIGNALING PATHWAYS IN RESPONSE TO MULTIPLE STRESSORS: THE GAP IN KNOWLEDGE[1]

2.1 Introduction

The immobility of plants distinguishes their lifestyle from animals, requiring plant recognition of external stimuli within their environment necessary for survival. Plants regularly encounter a wide range of abiotic and biotic stresses, whose individual elicited plant responses are abundant within the scientific literature (Mohr and Cahill, 2003; Wang *et al.*, 2003; Choi *et al.*, 2014; Torres-Ruiz *et al.*, 2014). Less represented, although perhaps more realistic in natural settings, are simultaneous stresses that represent either multiple, within or across, abiotic and biotic stress types. Such stress combinations can result in either specific or integrated signaling cascades that warrant further empirical attention in an attempt to gain a more realistic representation of plant response(s) to their environment.

Typical environmental stressors are commonly classified as abiotic or biotic. Abiotic stresses are caused by physical conditions such as salt, water, light, heat, and cold stress. Abiotic stress alone can reduce major crop plants' yield by more than 50% (Bray *et al.*, 2000). A plant's ability to react to these stressors and survive in light of

---

[1] This chapter has previously been published and can be found with the following citation: **Huber AE, Bauerle TL**. 2016. Long-distance plant signaling pathways in response to multiple stressors: the gap in knowledge. Journal of Experimental Botany **67**, 2063–2079.

changing environmental conditions depends on effective defense mechanism(s) and signaling pathways leading to an increased tolerance to their surroundings (Zebelo and Maffei, 2015). Biotic stressors can be either herbivorous or pathogenic in nature (Maffei and Bossi, 2006), with both herbivore and plant-pathogen interactions often highly specific and dependent on both the plant species as well as the stressor type (Bonaventure *et al.*, 2011; Bricchi *et al.*, 2012).

Defense mechanisms can be extremely costly for the plant. Therefore, plants have developed a defense response system which can be quickly activated in response to stressors and can affect the entire plant body. This so called systemic acquired resistance (SAR) is accomplished by either the transport of defense metabolites or through the production of new defense components (Heil and Ton, 2008; Mittler and Blumwald, 2015). SAR is acquired by a modification of gene transcription patterns leading to an overall increase in plant fitness to a broader spectrum of biota as well as environmental conditions (Ryals *et al.*, 1996; Gilroy *et al.*, 2014).

To date, there is a multitude of information available on stress/defense responses of plants when exposed to an individual stressor. However, in the field, plants are rarely exposed to single stressors, but instead, often face a combination of stressors which may result in unique plant responses (Hewezi *et al.*, 2008). The importance of deciphering the complexity of stress responses to combined stressors is exemplified in the context of current climate change predictions. Warmer temperatures and changes in precipitation events produce not only assorted stress intensities but an array of stress combinations (Jia and Davies, 2007), including enhanced herbivore pressure due to faster growth rates (Bale *et al.*, 2002), and increased plant water stress levels

resulting from an increased evaporative demand (Barber *et al.*, 2000) caused by increased temperature to name a few. It is not surprising that the impact of both abiotic and biotic stresses on a plant's life can be severe, and often result in either decreased plant productivity or weakened plant defense mechanisms (Ewers and Fisher, 1989; Wang *et al.*, 2001).

Regardless of whether a stressor is solitary or in combination with other stressors, plants have developed several long-distance signaling pathways enabling the plant to react quickly and ideally cope with imposing stress(s). To date, we recognize three distinct long-distance signaling types: 1) hydraulic, 2) chemical, and 3) electrical, that not only differ in their chemical nature but also in their propagation speeds (Fig. 2.1).

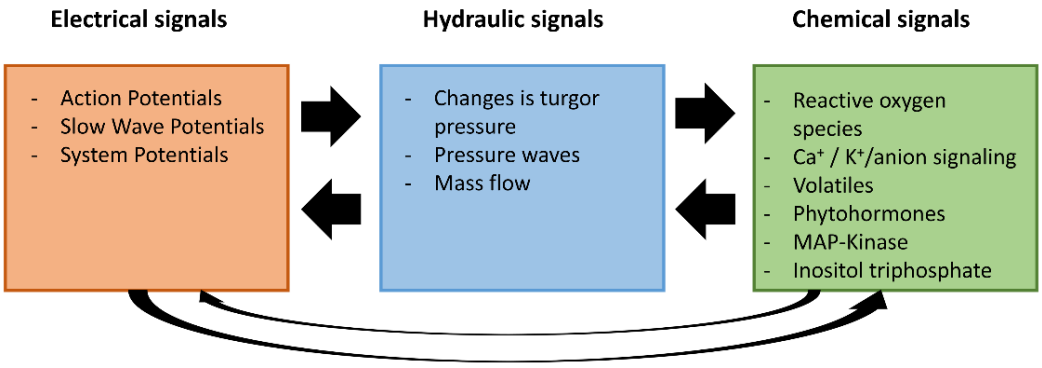

Figure 2.1: Overview of electrical, hydraulic, and chemical long-distance signals in plants. Boxes represent different subcategories of signaling types. All three signaling pathways are most probably interwoven (black arrows).

To respond adequately to stressors, plants may employ different signaling pathways and use "master regulators" like transcription factors or turgor/ osmosensors to interconnect these pathways (Christmann et al., 2013; Wang et al., 2003). However, the complementation and fine tuning of these signals, both their specificity and

generality, especially in response to combined stressors, require critical further examination.

In the following paragraphs, we focus on hydraulic, chemical, and electrical signaling pathways, their interaction and integration. We discuss overlapping signaling cascades, physiological factors influencing plant stress responses, and highlight the importance of stress intensity and accumulating stressors on signaling within plants and elaborate on the question of how plants orchestrate long distance signals as a means to react to biotic and abiotic stressors accordingly.

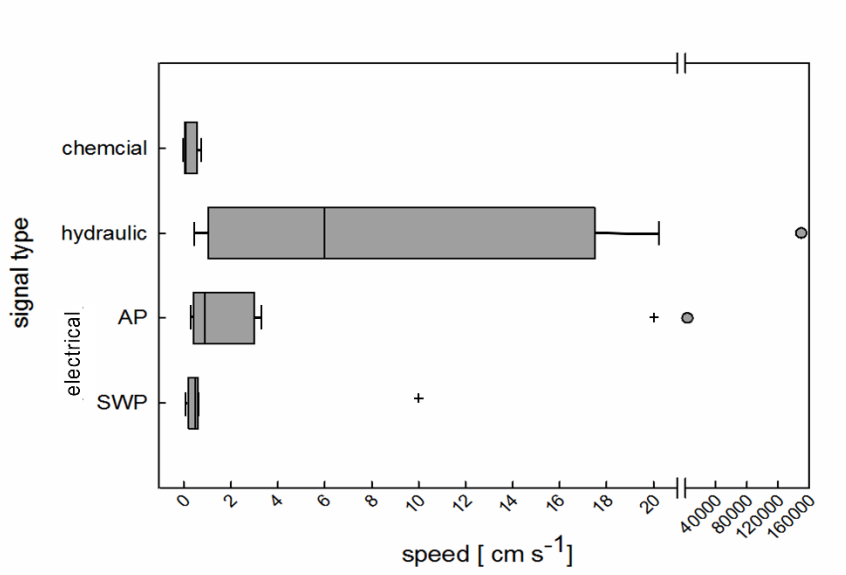

Figure 2.2: Signal speed ranges plus standard errors of chemical, hydraulic, and electrical signals [action potentials (APs), slow wave potentials (SWPs)] in plants (in cm s^{-1}). Plus symbols represent outliers of the box plot. Data points > 4000 cm s^{-1} were not included in the boxplot statistics but are represented on the graph by circles. Note the break in the x-axis in order to accommodate the range of data points.

2.2 Signal Types

2.2.1 Hydraulic signals

Water is the connecting medium between plant organs and is responsible for nutrient exchange and maintenance of metabolic processes, making water an excellent medium for fast information exchange. Water in plants is transported under tension along the soil-plant-air continuum (Zimmermann, 1983) due to an increasing water potential difference, largely determined by the soil water availability and the vapor pressure deficit (Comstock, 2002). In most climates, the driest (most negative) component in the soil-plant-air continuum is the atmosphere and the least negative the soil, causing the water to be pulled through the plant to the leaves (Steudle, 2001). In light of hydraulic signal transmission, this same pathway is utilized and integrated with adjacent living cells.

Hydraulic signals orchestrate the physiological behavior of plants on a daily basis, through the regulation of cell expansion rates (Westgate and Boyer, 1984; Tang and Boyer, 2002, 2003) which are mainly controlled by the cell's turgor pressure (Taiz, 1984) and fluctuate with a decrease in soil water status, an increase in evaporation demand (Bouchabké *et al.*, 2006), or through herbivore feeding (Alarcon and Malone, 1994). These pressure changes originate in the xylem vessel conduits and because of low axial resistance can be propagated rapidly into surrounding cells (Bramley *et al.*, 2007) and potentially, throughout the whole plant. However, pressure changes cannot be perceived by dead cells, e.g. xylem conduits, and therefore must be decoded by adjacent parenchyma cells. Moreover, parenchyma cells can perceive and undergo pressure changes (turgor changes) themselves via elastic and resistant cell walls

(Tyree and Yang, 1990). Due to the high elasticity modulus, higher volumes of water must be moved in and/or out the parenchyma cells in order to detect a pressure change in the system (Malone, 1993). Additionally, it is likely that parenchyma cells are also able to translate hydraulic signals into a physiological signal with the help of mechano-sensitive channels in the plasma membrane (see review: Árnadóttir and Chalfie, 2010; Christmann *et al.*, 2013)

Depending on the imposed stressor, pressure changes can be either positive, through an expansion of the xylem fluid, or negative, due to a tension increase in the xylem sap column as a result of a decrease in the water potential gradient within the plant. It is important to mention, that in most cases, the change in cell turgor is just a secondary by-product of initial changes in the tension within the xylem conduit and occurs after the xylem sap tension is altered (Lopez *et al.*, 2014) resulting in water movement into or out of cells seeking water potential equilibrium (Tyree and Yang, 1990). Xylem tension can also be positively altered (decreased xylem tension or even pressure pulses) by either expanding the water in the vascular tissue, by heating or burning the leaves (Stahlberg and Cosgrove, 1997*a*) or relocation of water through mechanical bending by wind or artificial means (Lopez *et al.*, 2014). Drought can also influence cell turgor pressure positively through the displacement of water in the surrounding tissues or even by preceding pressure pulses within the xylem (pressure travels faster than fluid) provoked by cavitation events or conduit collapse (Bramley *et al.*, 2007; Vandeleur *et al.*, 2014). However, this mechanism is not well explored and more hypothesis than data currently exist. A strong correlation has been recorded between cavitation events and the initiation of stomatal closure during drought periods

(Cochard et al., 1996; Salleo et al., 2001), but it is unclear if the increasing pressure pulses or the displaced water initiate stomatal closure during progressive increases in xylem tension. Hydraulic pulses might also help to explain why a decrease in stomatal conductance during drought can occur in some plants irrespective of leaf turgor (Gollan *et al.*, 1986) or Ψ_{leaf} (Gowing *et al.*, 1990; Davies and Zhang, 1991; Yao *et al.*, 2001).

Negative alteration of the xylem tension (increased tension) can be caused by abiotic stressors like salt and drought stress (Neumann *et al.*, 1988; Bréda *et al.*, 2006), that initiate similar signaling pathways (Zhu, 2001). During osmotic or drought stress, the initiation of the hydraulic signal is in the root, the organ first exposed to the water shortage, transmitted through the stem to the leaves where parenchyma cells perceive the signal (Endo *et al.*, 2008; Christmann *et al.*, 2013) and trigger the production of the phytohormone ABA to initiate stomatal closure (Bauer *et al.*, 2013). The importance of ABA as the short-distance signal initiating stomatal closure and not the hydraulic signal was shown by (Christmann et al., 2007). The authors suppressed the hydraulic signal in Arabidopsis (*Arabidopsis thaliana*) plants by maintaining the leaf turgor pressure during root exposure to drought stress. However, as soon as ABA was exogenously added to the leaves, the stomata closed. Contrary, in grapevine hydraulic signals initiate stomatal closure, while ABA maintains stomatal closure (Tombesi *et al.*, 2015). Consequently, these different results indicate the complexity of signal transduction pathways and emphasize the need of further research to decipher the mechanism plants use to decode hydraulic signals (Christmann *et al.*, 2013)

2.2.2 Chemical signals

Chemical signals are the most frequently discussed signals in plants, underlining their importance in plant stress response(s) (see Table 2.1).

Table 2.1: Molecules involved in chemical signaling pathways related to abiotic and biotic stress conditions and their respective references.

Chemical signal type	**References (reviews)**
Secondary messengers:	
Calcium fluxes	Pandey *et al.*, 2000; Sathyanarayanan and Poovaiah, 2004; Medvedev, 2005
Potassium fluxes	Zebelo and Maffei, 2015
Anion fluxes	Garcia-Brugger *et al.*, 2006
Inositol triphosphate	Xiong and Zhu, 2003; Tuteja and Sopory, 2008
Reactive oxygen compounds	Fujita *et al.*, 2006; Laloi *et al.*, 2007; Maffei *et al.*, 2007*a*
Signaling cascade	
MAP-Kinase	Nakagami *et al.*, 2005; Fujita *et al.*, 2006
Chemical response	
Volatile compounds	Holopainen, 2004; Baldwin, 2006; Maffei *et al.*, 2007*a*; Dicke and Baldwin, 2010; Zebelo and Maffei, 2015
Plant hormones	Reymond and Farmer, 1998; Kunkel and Brooks, 2002; Fujita *et al.*, 2006

However, despite their indispensability in plant stress/defense response initiation, it is still questionable if chemicals are exclusively a short-distance stress signal. Evidence against their long-distance transport ability is given in several experiments showing that plant hormones crucial for plant stress/defense responses are incapable of traveling over longer distances and have propagation speeds that are slow in

comparison to hydraulic and/or electrical signals (see Table 2.2).

Table 2.2: Propagation speed, mode of action of hydraulic, chemical and electrical signals (SP = system potential; SWP = slow wave potential; AP = action potential).

Signal type	Speed	Mode of action	Plant	Author:
Hydraulic	< 2 cm min^{-1}	Changes in cell turgor (cell pressure probe) upon water stress treatment	*Arabidopsis thaliana*	(Christmann *et al.*, 2007)
	10 cm s^{-1}	Changes in leaf thickness (pressure transducer) upon wounding	*Triticum durum Desf.* cv. *Iva*	(Malone, 1992)
	20 cm s^{-1}	Changes in leaf thickness (pressure transducer) upon wounding	*Prunus avium* *Tilia cordata* *Lycopersicum esculentum* *Lycopersicum esculentum* *Zea mays* (10 additional species)	(Boari and Malone, 1993)
	150000 cm s^{-1}	Theoretical pressure wave propagation	Any plant	(Malone, 1993)
	Almost simultaneously with mechanical bending	Pressure sensors in apoplast correlated with bending	*Arpinus betulus* L., *Ilex aquifolium* L., *Pinus sylvestris* L., *Cupressus sempervirens* L., *Taxus baccata* L.	(Lopez *et al.*, 2014)
Transportation	0.01 cm s^{-1}	Phloem transportation	*Triticum aestivum* L.	(Fisher, 1990)

speeds of sap		rate		
	25 cm s^{-1}	Xylem flow rate	*Triticunz aestivum* cv. Gabo	(Passioura, 1972)
Chemical	~ 0.04 cm s^{-1}	Calcium wave upon salt stress	*Arabidopsis thaliana*	(Choi et al., 2014)
	0.7 cm s^{-1}	Solute transport	*Zea mays*	(Boari and Malone, 1993)
	3-5 min (signal speed 0.05 cm s^{-1})	Increase in JA after wounding	*Arabidopsis thaliana*	(Glauser *et al.*, 2008)*
	0.14 cm s^{-1}	Reactive oxygen species in apoplast upon wounding, heat, cold, high-intensity light, and salinity stresses	*Arabidopsis thaliana*	(Miller *et al.*, 2009)
Electrical	0.08-0.2 cm s^{-1}	SP initiated by wounding	*Vicia faba* *Hordeum vulgare*	(Zimmermann et al. 2009)
	0.08-0.5 cm s^{-1}	SWP preceded by hydraulic signals (positive pressure steps)	*Cucumis sativus* L. cv. Burpee Pickler	(Stahlberg and Cosgrove, 1997*a*)
	0.9 cm s^{-1}	AP upon ice shock	*Vitis discolor*	(Houwink, 1935)
	0.1-0.2 cm s^{-1}	SWP caused by inflammation	*Populus trichocarpa* cv. Trichobel; *Populus tremula* x *P. tremuloides* Michx	(Lautner *et al.*, 2005)
	0.3-0.5 cm s^{-1}	SWP preceded by hydraulic signals (positive pressure steps)	*Pisum sativum* L.	(Stahlberg and Cosgrove, 1997*b*)

0.4 cm s^{-1}	Electrically induced AP	*Drosera rotundifolia*	(Pickard, 1973)
0.4-0.8 cm s^{-1}	AP caused by cooling	*Populus trichocarpa* cv. Trichobel; *Populus tremula; P.* tremuloides Michx	(Lautner *et al.*, 2005)
0.5-0.6 cm s^{-1}	SWP upon cutting	*Mimosa pudica*	(Fromm and Lautner, 2007)
1-2 cm s^{-1}	/	Most plants	(Fromm, 2006)
2 cm s^{-1}	AP upon ice shock	*Mimosa pudica*	(Houwink, 1935)
2-3 cm s^{-1}	AP upon ice shock or touching	*Mimosa pudica*	(Fromm and Lautner, 2007)
at least10 cm s^{-1}	SWP upon inflaming	*Triticum durum* Desf. cv. Iva	(Malone, 1992)
20 cm s^{-1}	AP during leaf closing	*Dionaea muscipula* Ellis	(Sanderson, 1888)
up to 4000 cm s^{-1}	AP upon the uncoupler carbonyl cyanide-p-trifluoromethoxyphenyl hydrazone (FCCP)	*Glycine max* (L.) Merrill	(Volkov, 2000)

*Inconclusive results. Authors could not determine signal pathway leading to the increase in JA.

For example, ABA is highly correlated with stomatal closure during drought stress (Zhang and Davies, 1989; Loewenstein and Pallardy, 1998; Davies *et al.,* 2002). However, given xylem's sluggish transport rate of 0.056 cm s^{-1} (Zimmermann and Brown, 1971), it is unlikely that root sourced ABA accounts for the rapid initiation of stomatal closure during drought events, strongly suggesting the existence of alternative and/or an additional long-distance signaling pathway (Zhang and Davies, 1991; Saliendra *et al.*, 1995; Whitehead *et al.*, 1996; Whitehead, 1998). These inferences are reinforced by experiments that failed to detect root sourced ABA as a mechanism for stomatal closure in grafted tomato (Holbrook *et al.*, 2002) and ABA deficient Arabidopsis plants (Christmann *et al.*, 2007). Reciprocal grafting could provide a means to study long-distance communication between the rootstock and the scion, which would help evaluate the significance of root hormone synthesis on shoot performance under stress conditions (Albacete et al., 2015).

The uncertainty of chemical long-distance signals initiating rapid physiological plant responses is also confirmed for jasmonic acid (JA) and salicylic acid (SA) (Vernooij *et al.*, 1994; Stratmann, 2003, respectively). Jasmonic acid is an important hormone in activating systemic acquired resistance, a nonspecific resistance response upon biotic attack, and long thought to be the long-distance signal activating these responses. Likewise, salicylic acid has also been considered a long-distance wound response. However, in both cases, even though JA and SA are important for triggering wound responses, they are not long-distance communicators but rather synthesized locally.

It is important to stress, that chemcial signals can indeed act as long-distance

signals in gradual metabolic responses, for example, in the integration of the external and internal nitrogen status of plants in which nitrate or the phytohormon cytokinin act as comminucators throughout the whole plant (Sakakibara et al., 2006). Additionally, major plant hormones like ABA, JA, SA ethylene, auxin, and cytokinins are highly discussed in terms of plant stress resistance/susceptibility to biotic and abiotic stressors, including their interaction and overlapping pathway utilization (Bostock, 2005).

Volatiles are also highly discussed in the literature as a systemic long-distance signal both between and within plants in response to herbivore or pathogen attacks. They can induce systemic defense responses in distant parts of plants which lack vascular connectivity (Frost et al., 2007) within hours (Howe and Jander, 2008) after insect attack, and are therefore a good mechanism for long-distance signaling. Their chemical diversity, mode of action, and their role in plant defense is nicely summarized in several reviews (Arimura et al., 2011; Dudareva et al., 2006; Howe and Jander, 2008; Kessler and Baldwin, 2001, 2002; Mithöfer and Boland, 2012; Wortemann et al., 2011; Zimmermann et al., 2009).

Despite the unlikelihood of chemical signals in rapid long-distance signaling, reactive oxygen species (ROS) were recently identified as possible auto-propagation chemical signals suited for traveling longer distances by which the signal travels from cell to cell (Miller *et al.*, 2009; Mittler *et al.*, 2011). Their fast propagation speed (up to 0.14 cm s^{-1}), their ability to spread to the entire plant from the site of initiation (root, stem, leaf) (Miller et al., 2009), and their potential interconnectivity with other signaling pathways (electrical, calcium waves, plant hormones, and hydraulic waves

(Mittler and Blumwald, 2015), makes them suitable biotic or abiotic stress communicators. ROS are mainly known as toxic byproducts of aerobic metabolism which harms plant tissue. However, through evolution, plants acquired detoxifying/scavenging enzymes and several antioxidants to handle the toxic effect of ROS, before ROS developed as a signaling mechanism. The ROS signaling mechanism is mainly based on a balance between ROS producing and ROS scavenging which occurs concurrently in plants, to maintain a balanced intercellular ROS concentration. Despite research demonstrating the suitability of ROS as signaling molecules, there are many unanswered questions regarding the signal specificity, transport, and sensing mechanisms (Mittler et al., 2011).

2.2.3 Electrical signals

Electrical signals were first recorded in venus fly trap *(Dionaea muscipula)* (Haberland, 1890) and Mimosa *(Mimosa pudica)* (Applewhite, 1972), so called "sensitive" plants. For a long time, scientists found it hard to believe that electrical signals could also manifest in "silent" plants, *i.e.* plants with no outward movement in response to a stimulus. This misconception hindered the early establishment of electrical signals in the literature as a common long-distance signal (Stahlberg *et al.*, 2006). Nowadays, electrical signals in plants are established as a rapidly propagated signal in response to both biotic and abiotic stimuli (Maffei and Bossi, 2006), and are defined as an ion imbalance across the plasma membrane leading to a voltage transient. The voltage transient's shape is dependent on the stimulus type and the resulting ion/anion fluxes. In general, four different kinds of electrical signals are

recognized in plants: action potentials (AP), slow wave potentials (SWP), also called variation potentials (VP), wound potentials (WP) and system potentials (SP) (Fig. 2.3).

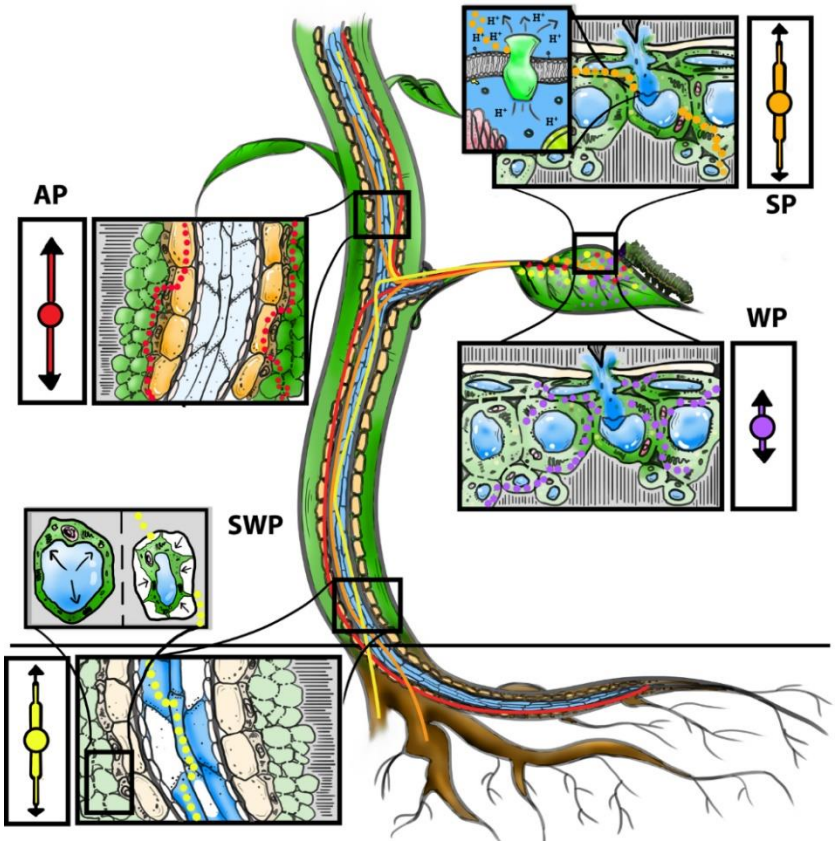

Figure 2.3: Illustrated representation of electrical signals in plants. Action potentials (AP), slow wave potentials (SWP), system potentials (SP) and wound potentials (WP) are common electrical signals in plants. Expanded black boxes show the path of travel for each respective signal type, i.e. AP (red dots) are propagated in the phloem, SWP (yellow dots) through functional xylem (blue xylem are water filled and white xylem are air filled), SP (orange dots) are propagated in the apoplast upon wounding, and WP (purple dots) are propagated through cell turgor changes initiating the depolarization of the plasma membrane. SWP are preceded and closely linked to hydraulic signals in the xylem tissue caused by either cavitation events (white xylem elements) or changes turgor changes (represented by swollen/plasmolysed cell). Red, yellow, orange, and purple circles represent the point of signal origin. Arrow length represents signal transmission ability. Short arrows indicate the inability of the signal to act as a long-distant signal. Arrow diameter represents signal strength intensity during signal propagation and transport. Original artwork by Alex Paya.

Action potentials are propagated in the phloem, characterized by a rapid depolarization phase of the membrane potential followed by a rapid repolarization phase, and are elicited by non-invasive stimuli including electrical stimuli, acid rain, irradiation, and cold shock, (Stankovic *et al.*, 1998; Shvetsova *et al.*, 2002; Volkov *et al.*, 2004; Trebacz *et al.*, 2006; Fromm and Lautner, 2007). The ionic initiation of the depolarization phase is initiated by voltage gated Ca^{+} channels which release Ca from internal (mitochondria, vacuole and ER) and external (apoplast) storage into the cytoplasm (Reddy *et al.*, 2011). In response to the Calcium influx, Cl^{-} channels open and Cl^{-} ions diffuse down an electrochemical gradient out of the cell (Lunevsky *et al.*, 1983) until voltage gated K^{+} channels are activated and K^{+} efflux occurs (repolarization phase) (Trebacz *et al.*, 2006). All stimuli triggering AP must meet a critical intensity in order to reach a pivotal threshold to trigger the AP. As soon as the threshold is reached (all-or-nothing rule), the signal is self-perpetuated through plasmodesmata of adjacent parenchyma cells or sieve pores in phloem cells (Trebacz et al., 2006). AP can be propagated with a constant amplitude and velocity. Average AP propagation speeds range from 1-2 cm s^{-1} (Fromm, 2006), but can also reach faster velocities up to 3000 cm s^{-1} as found in soybean (Volkov *et al.*, 2000) (Fig. 2.2).

Slow wave potentials are characterized by an initial rapid depolarization phase and followed by a longer-lasting and varying repolarization phase compared to AP. SWPs are mainly elicited by interfering abiotic and biotic stimuli like mechanical wounding, tissue burning or herbivore attack (Stankovic *et al.*, 1998; Maffei and Bossi, 2006; Gallé *et al.*, 2015). While the depolarization phase is caused by the same ionic mechanism as AP, the slow repolarization phase is initiated by a transient shut down

of H^+ pumps causing the repolarization phase to last up to 30 min (Stahlberg *et al.*, 2006). SWP differ from AP in that they are propagated in the xylem and therefore can be transmitted through dead tissue (Stahlberg and Cosgrove, 1996), they do not follow an all-or-nothing rule, and their propagation speed and amplitude attenuates 2.5% per cm, Stahlberg *et al.*, 2005) the farther the signal travels from the stimulus location (Oyarce and Gurovich, 2011) resulting in a range of different SWP intensities (Maffei and Bossi, 2006). It is important to mention here, that SWP are not self-perpetuating like AP because they are always preceded by a positive hydraulic pressure change and therefore their depolarization is hydraulically induced (Stahlberg and Cosgrove, 1996, 1997*b*). For example, positive pressure steps are followed by a SWP in pea epicotyls (*Pisum staivum*), and depending on the applied pressure, can delay SWP. However, if the hydraulic signal, in the form of positive pressure, reaches 80 kPa or higher, then the electrical and hydraulic signals will occur simultaneously (Stahlberg and Cosgrove, 1997*b*). The preceding hydraulic signal is the primary cause for SWP attenuation; water can travel radially from the xylem vessel into epidermal cells, resulting in hydraulic signal attenuation and, consequently, also the intensity of the SWP (Westgate and Boyer, 1984). This interconnection between the hydraulic signal and SWP was demonstrated in pea that ceased to elicit a SWP response upon submerging the epicotyls under water (Mancuso, 1999). The range of SWP intensities, allow substantially more information about the intensity of the injury compared to AP, enabling plants to decipher the distance of the wounding source from the small differences in pressure, shape, and intensity of the signal (Stahlberg *et al.*, 2006).

Wound potentials are similar to SWP in their ionic mechanisms inducing the

depolarization and repolarization phases, resulting in a similar signal shape (Stahlberg *et al.*, 2006). Clearly, their name is derived from the stressor (wounding) commonly initiating the potentials. Wounding, whether caused by biotic or abiotic stressors, is propagated through cell turgor changes initiating the depolarization of the plasma membrane (Shimmen, 2001). Therefore, WP like SWP, are not self-perpetuating (Zebelo and Maffei, 2012) and always follow pressure changes. However, unlike SWP, it is unclear if WP should be formally considered long-distance signals since to date they have only been recorded in the vicinity of injured cells (1.0-40.0 mm from the injured or dead cell) (Stahlberg and Cosgrove, 1994).

System Potentials are a recently suggested fourth electrical potential type (Zimmermann *et al.*, 2009) that are propagated in the apoplast upon wounding. SP can be distinguished from other electrical signals in their mode of action. While AP, SWP, and WP are caused by calcium streaming across the plasma membrane, SP signals are initiated by the activation of H^+ pumps (K^+, Cl^-, and Ca^{2+} streaming are initiated through SP). The advantage of the self-propagating SP is that they do not follow an all-or-nothing rule. Therefore, SP intensity can be modulated in order to carry information about wounding severity (Zimmermann *et al.*, 2009).

2.3 Hydraulic, chemical, and electrical signal integration: Understanding signal speed

Appropriate physiological plant responses to stressors require the rapid relay of information between distant plant organs. While we have discussed three individual signal pathways above, it seems likely that signal pathway integration is necessary for

a response to multiple concurrent stresses (Fig. 2.1). Nonetheless, decoding all three signal types to coordinate and activate plant defense mechanisms has yet to be fully understood. Reaching a consensus on which signal type relays primary information is inherently difficult, largely a result of the unresolved discrepancy around *in situ* long-distance signaling speeds and by the relatively few experiments that have measured all three major signaling pathways concurrently as a mean to establish the influence of each pathway on the final response

Hydraulic and electrical signals are unequivocal in their ability to transmit long-distance signals for rapid plant response to short-term environmental perturbations by virtue of their fast propagation (Christmann *et al.*, 2013; Gallé *et al.*, 2015), however longer time periods these effects may be negated by other signaling mechanisms (Munns, 2000). Hydraulic pressure waves caused by biotic as well as abiotic stressors can be propagated in water almost instantaneously and travel up to 150000 cm s^{-1} (the speed of sound) (Malone, 1993) while hydraulic mass flow, caused by wounding events, are estimated to travel on average 20 cm s^{-1} in herbaceous plants (Boari and Malone, 1993). It is important to note, that hydraulic signals are two component signals: a rapidly propagated pressure wave followed by xylem mass flow (Boari and Malone, 1993). Unfortunately, the literature does not distinguish between the two components and instead reports only hydraulic mass flow determined with a pressure transducer and recorded via leaf swelling, *e.g.* fluid translocation, and not the preceding pressure wave. The variation in recorded speeds may result from the measurement technique as well as other factors including plant size/age.

A lack of information on hydraulic signaling events makes it challenging to

integrate hydraulic signals into the plant response signaling pathway timeline. Additionally, it is unclear to what degree information about the stress intensity is carried through hydraulic signals. We do know that through the wounding process, cell turgor pressure decreases and pressure waves are elicited (Malone *et al.*, 1994). In fact, Alarcon and Malone (1994) showed that small feeding bouts of Spodoptera caterpillars at the base of tomato (*Lycopersicon esculentum*) leaflets induced a significant hydraulic signal, measured as an increase in distal leaflet thickness. Moreover, when petioles were girdled with heat, the signal could still be recorded in the distal leaf, indicating that a functioning membrane is not required and therefore hydraulic signals are responsible for proteinase inhibitor activation (Malone *et al.*, 1994). However, we know that hydraulic signals precede SWP, and thus electrical signals could also activate proteinase inhibitors. Therefore, despite evidence that both signal types exist, it remains elusive which signal type carries the critical information at a threshold required to elicit a particular plant response.

Chemical signals are often considered the slowest long-distance signal in plants (Baydoun and Fry, 1985) and are therefore not favored as the fundamental initial long-distance signaling mechanism. However further consideration is warranted, because depending on the transportation pathway, (xylem vs. phloem), the transmission velocity can differ widely. For example, carbon isotope labeling of mature tree canopies have shown photosynthate transportation speeds from leaves to the roots within the phloem takes on average 1-5 days (Mikan *et al.*, 2000; Johnson *et al.*, 2002; Steinmann *et al.*, 2004), too moderate a velocity to support chemical signals for primary long-distance information transmission. However, considerably higher

propagation speeds have been recorded in the xylem during leaf transpiration, 25 cm s^{-1} in wheat (Passioura, 1972). Nonetheless, during the night and under stress conditions, when stomata are closed, these propagation speeds decrease dramatically.

Water translocation occurs very rapidly (see above) and is a suitable medium for carrying wound signals throughout the entire plant (Boari and Malone, 1993). Chemical signal transport from a wounding site can quickly travel systemically through the plant via hydraulic signals as long as the wound signals can be produced in, or released into, the xylem sap within the time interval of the hydraulic signal propagation. Coupled hydraulic and chemical signaling within plants indicates that the integration of two signaling pathways might favor the faster pathway and thus the faster plant response. Nevertheless, it remains unknown if crucial chemical signals, utilized for plant stress responses, are indeed able to travel over longer distances. Glauser *et al.* (2008) demonstrated in Arabidopsis that the mechanical wounding signal leading to a systemic increase in JA must be propagated with a velocity of at least 0.05 cm s^{-1}. However, considering the phloem propagation speed of 0.01 cm s^{-1} for small molecules (Fisher, 1990), it is not likely that JA is transported throughout the plant via the phloem but rather was synthesized in the non-mechanically wounded leaves in response to a systemic signal. Proteinase inhibitor genes are activated through chemical signaling pathways (Farmer and Ryan, 1990). Yet, research shows that hydraulic as well as electrical signals are able to initiate proteinase inhibitor induction in tomato plants before an increase in proteinase inhibitor genes could be recorded (Stanković and Davies, 1996, 1997). Despite the debate on the suitability of chemical signals for long-distance transport, chemical signals are certainly part of the

first signaling cascades occurring in plant-herbivore interactions (Maffei *et al.*, 2007*a*; Bruce, 2015).

Electrical signals in plants can have a range of propagation speeds depending on the type of signal deployed (AP or SWP) (Fig. 2.2). Some experiments have found the propagation speed of AP is similar to hydraulic signals. For example, poplar trees exposed to a cold shock elicited propagation speeds of 0.4-0.8 cm s^{-1} (Fromm and Lautner, 2007), higher speeds up to 4000 cm s^{-1} were found in soybean after treatment with uncoupling agents, impacting oxidative phosphorylation (Volkov, 2000; Volkov *et al.*, 2000) and velocities of 2-3 cm s^{-1} were recorded in *M. pudica* during leaf closure in response to cold or touch stimulation (Fromm and Lautner, 2007).

The propagation speeds of SWPs elicited through leaf burning on poplar trees fell in the range of 0.1-0.2 cm s^{-1} (Lautner et al., 2005) whereas cutting leaflets in *M. pudica* resulted speeds of only 0.5-0.6 cm s^{-1} (Fromm and Lautner, 2007). This diversity in SWP propagation speed demonstrates the impact of the stressor as well as the plant species on the velocity of the electrical signal and therefore carries more information than AP. Additionally, SWPs are closely connected to, and in this case preceded by, hydraulic signals making SWPs, in combination with hydraulic signals, a suitable candidate for information propagation over longer distances.

Electrical signals have been elucidated as one of the primary responses to plant biotic attack, occurring within seconds to minutes after biotic wounding events, followed by a chemical signaling cascade (for review see: Maffei *et al.*, 2007*b*; Zebelo and Maffei, 2015). In the course of the membrane potential elicitation, secondary messengers are initiated leading to a downstream signaling cascade that terminates in

the production of phytohormones and changes in plant metabolism, a process which can take anywhere from hours to days (Maffei *et al.*, 2007*a*). During these cascades, calcium signaling is initiated (Reddy *et al.*, 2011), along with the production of Nitric Oxide (NO) and its derivatives (Leitner *et al.*, 2009), ROS (Mittler, 2006), and rises in JA, SA, and ethylene hormone production (Bari and Jones, 2009). However, the initiation of a calcium signal must precede other signals since it initiates the ion fluxes responsible for electrical signals (Zebelo and Maffei, 2012). Maffei *et al.* (2004 and 2006) showed that a thin layer of calcium signaling was recorded after lima bean (*Phaseolus lunatus* L.) leaves were wounded by the climbing cutworm (*Spodoptera littoralis*). Interestingly, calcium signaling was only initiated as a response to biotrophic wounding and could not be recorded after artificial mechanical wounding (Bricchi *et al.*, 2010).

Calcium is not the only secondary messenger involved in fast signaling responses. Recently ROS species have also been correlated with electrical signals. ROS signals can travel in the xylem up to 0.14 cm s^{-1} (Miller *et al.*, 2009), comparable to electrical signal propagation speeds. Therefore, current hypotheses support a close connection between ROS and electrical signals. Although, if ROS activate or increase the signal intensity has yet to be discovered. The application of a calcium channel blocker does not hinder ROS's ability to travel through the plant, indicating that Ca^{2+} is not required for fast signal propagation (Miller *et al.*, 2009) a surprising result considering ROS are integrated with calcium networks (Kobayashi *et al.*, 2007; Ogasawara *et al.*, 2008). The ROS signaling pathway is initiated by several stressors indicating that ROS is a general signaling molecule and diversity in its oscillations (frequency and amplitude)

allow the plant to decipher signals (Mittler *et al.*, 2011) in the same way distinct calcium oscillation signatures are deciphered in response to stimuli (Evans *et al.*, 2001).

There is distinct evidence that plants have several closely interconnected signaling pathways. However, we lack information on the integrated timing of hydraulic, electrical, and chemical signaling pathways, and the importance of each pathway for information transmission.

For example, while chemical signals are necessary for the initiation of metabolic responses, the long-distance communication signal has to be either electrical or hydraulic in nature (Stratmann and Ryan, 1997). Conversely, some evidence supports hydraulic signals as essential for signal propagation, even though, in some cases, they are not able to initiate chemical signaling cascades independently (Malone et al., 1994).

Furthermore, the connectivity among signaling pathways is shown by the inseparable connectivity of hydraulic signals and SWP. Additionally, electrical signals can initiate chemical signals and chemical signals in turn can intensify hydraulic signals resulting in essentially a feedback loop of signal types. A perfect example of this cascade is found in ABA's amplified decline in cell turgor pressure by downregulating permeability of the leaf hydraulic tissue (Pantin *et al.*, 2013) which in turn intensifies ABA production.

2.4 Combined stressors: How do simultaneous stressors affect plant stress/defense responses?

2.4.1 Distinguishing between different stressors

Plants are able to differentiate between both biotic and abiotic stressors and orchestrate signaling pathways despite very similar stress responses. A plant's ability to distinguish between specific biotic stressor types is frequently based on the chemical component of the attack mechanism. For example, herbivores, sucking insects, and pathogens have unique chemicals within their saliva, regurgitates, or exudates through which many plants are able to detect the identity of attacker. Bricchi *et al.*, (2010) wounded lima beans (*P. lunatus*) in three ways: single mechanical wounding event, multiple mechanical wounding events by a robotic worm, and by the herbivore (*S. littoralis*). After wounding, only an increase in volatile compound emission in response to multiple wounding by the robotic worm and herbivore was recorded, pinpointing that the repetition of wounding might be a trigger for stress response. The compound fraction of emitted volatiles unveiled a difference between the robotic worm and the herbivore indicating that the plants were able to differentiate between different wounding effects (Bricchi *et al.*, 2010). Further investigation revealed that only the saliva of *S. littoralis*, and not artificial, single, or multiple wounding events were able to induce calcium signaling and membrane polarization. Interestingly, these results suggest that more than one signaling pathway leading to volatile emissions exists in plants. However, experiments focused on plant wounding by different herbivores (caterpillar *S. littoralis* and snail *Cepaea hortensis*) found that lima beans released very similar compositions of volatiles regardless of herbivore type

(Mithöfer *et al.*, 2005). Wounding by three different biotic stressors (caterpillar: *S. littoralis,* aphid: *Myzus persicae,* and pathogen: *Pseudomonas syringae*) were directly correlated to the amount of damage caused (Bricchi *et al.* 2012) with membrane depolarization occurring 30 min to 2 hours after feeding by *S. littoralis*, 4-6 hours after feeding by *M. persicae* and 16 hours after infection of *P. syringae*. Interestingly, despite the same intensity of the membrane potential change, the plant deciphered the pathogen/herbivore causing the damage as exhibited in their gene expression. *M. persicae* regulated a ten-fold higher number of genes than *S. littoralis*, but had higher levels of suppressed gene expression compared to *P. syringae* (Bricchi *et al.*, 2012). These findings emphasize the ability of plants not only to identify the nature of the stressor, but also to fine tune the stress response and match the intensity of the response with the inflicted stress intensity.

Plants are able to distinguish between abiotic stresses despite a range of overlapping signal cascades. Among an array of abiotic stressors, cold, salt, and drought stress elicit similar responses by altering plant water relations thus affecting the osmotic potential (Shinozaki and Yamaguchi-Shinozaki, 1997; Mahajan and Tuteja, 2005). Based on the osmotic component, plants respond with overlapping signal cascades such as calcium signaling (Sanders *et al.*, 2002), ROS production (Hasegawa *et al.*, 2000), or MAPK (mitogen-activated protein kinase) activation (Wu and Zong, 2011). One example of cross-talk between signaling pathways is the induction of ABA in response to drought and/or salinity. Interestingly, it is thought that ABA induction is due to changes in water potential caused by each stressor, and not the high salt concentrations occurring during salinity (Zhang *et al.*, 2006).

However, salt stress has an additional ionic component which often leads to ion toxicity and thus initiation of a special signaling cascade, SOS (salt overly sensitive) (Mahajan *et al.*, 2008). Cold stress is unique due to the low temperature initiation of the ICE-CBF-COR signaling cascade, important for the up-regulation of cold responsive genes (Huang *et al.*, 2012). The receptors for the stress perception have not been identified; however, the plasma membrane plays a key role in the perception and transmission of stress responses and the cell wall participates in the triggering process because of its role in regulating tension of the plasma membrane (Jia *et al.*, 2001).

2.4.2 Stress combinations

The study of combinatory stresses is inherently difficult in that plants can respond in a number of ways including, a response characteristic to only one stress, an increased response intensity, or a unique response unlike any elicited by individual stressors (Rizhsky *et al.*, 2002). Generally speaking, we can look to results from gene expression studies as an indicator of typical plant responses to multiple stressors. Gene level responses can be , 1) additive, 2) synergistic (more than the sum of individual stresses), 3) idiosyncratic (completely different from the single stress responses), 4) dominant (response very close to one of the stressors) (Prasch and Sonnewald, 2015), or even antagonisitc (Bostock, 2005). Below we outline common stress interactions and examine typical plant responses.

2.4.2.1 Abiotic-Abiotic

Abiotic stressors are inherently tightly linked in the natural environment. Heat stress, one of the most observed stress factors, has been examined extensively, mainly in

light of predicted future climatic temperature increases (Meehl *et al.*, 2007) and its subsequent impact on plant productivity (Schlenker and Roberts, 2009). Elevated temperatures in combination with drought stress have a significantly greater detrimental effect on the growth and productivity of field crops compared to only elevated temperature or water shortage alone (Heyne and Brunson, 1940; Craufurd and Peacock, 1993; Savin and Nicolas, 1996; Jagtap *et al.*, 1998; Mittler, 2006). Likewise, in turf grasses high temperature and drought drastically impact plant health due to a decline in the activity of stress antioxidant enzyme activity (Jiang and Huang, 2001).

It is important to note that xylem sap hormone concentrations can differ from that found within roots or leaves and may provide a more informative measurement when deciphering the effects of single versus combined stresses. The difficulty arises when the stressor alters the plant response in a manner that contradicts the typical trend. Examples include, mitigation of negative drought and salt stress effects when CO_2 concentrations are increased resulting in elevated plant gas exchange, plant growth and plant nutrition (Piñero et al., 2014; Qaderi et al., 2006), increased leaf NO_3^- concentration in pepper plants (*Capsicum annuum*) exposed to elevated CO_2 and decreased Cl^- levels under ambient CO_2 concentrations, a finding that contradicts the prevailing trend found in plant leaves (Del Amor and Cuadra-Crespo, 2012; Tuna et al., 2008). In addition, roots exposed to salt stress and elevated CO_2 had decreased ABA levels in their roots in comparison to when roots were exposed to salt stress and ambient CO_2 (Piñero et al., 2014). It is important to consider that in these cases the plants were exposed to the treatment (drought, temperature, CO_2) for 11 days (Qaderi

et al., 2006) and 30 days (Piñero et al., 2014) before sampling, making it difficult to determine what role hydraulic and chemical signals played in the acclimation process.

In trees, increased temperature in combination with drought stress weakens tree defense mechanisms, resulting in a reduction in stored sugars and starch and consequently increased tree susceptibility to herbivore attack (Zvereva and Kozlov, 2006). Furthermore, the shortage of water supply, limits the transportation of defense compounds to the wounding site only compounding the tree's vulnerability to decline (Guerard *et al.*, 2007). From a whole plant perspective, Niinemets and Valladares (2006) studied 806 North American, European, and West Asian temperate tree and shrub species. The authors examined waterlogging, shade, and drought tolerance, and found that only 2.6–10.3% of the species were tolerant to two simultaneous environmental stresses, and only three tree species were tolerant to all three stresses, suggesting woody plants might be limited in their adaptability to environmental stressors. Likewise, Hallik identified leaf physiological characteristics of several temperate broadleaf tree species based on their shade and drought tolerance and demonstrated that the combination of drought and shade has opposing effects of foliar traits (Hallik *et al.*, 2009).

Interestingly, while other researchers found similar conclusions to the cross-continental observations like those of Niimentes and Vaaladares (2006) in carefully controlled experiments comparing gene transcription patterns between single and combined stressors (Rizhsky *et al.*, 2002, 2004; Hewezi *et al.*, 2008; Rasmussen *et al.*, 2013; Prasch and Sonnewald, 2015). Results to date reveal an anticipated distinct set of stress responses produced by coinciding stresses. For example, sunflowers exposed

to high light intensity, elevated temperature, and the combination of both expressed 129 genes after exposure to the combination treatment while only nine of them were expressed upon exposure to a single stress (Hewezi *et al.*, 2008). Arabidopsis exposure to elevated temperature, salt, and osmotic stress, or the combination of these stresses induced a total of 967 genes of which only about half were also induced by each stress individually (51, 42, 57% to salt, osmotic, heat stress, respectively), demonstrating that the stress combinations activated more genes. However, the number of genes which were down regulated during multiple stressor exposure repressed 719 genes whereby 25, 22, and 66% were also reduced by salt, osmotic and heat stress individually, emphasizing the variable response of plants under different stress conditions. Despite the detailed transcription analysis of genes in response to different/multiple stressors, the spatial component of this analysis is missing. According to our knowledge, we are lacking information on how the transcription level of genes in roots versus the shoot differ in response to multiple stressors.

2.4.2.2 Abiotic-biotic

The effect of abiotic and biotic stress combinations is well summarized (Prasch and Sonnewald, 2015). However, we would like to highlight general observed trends that emphasize simultaneous abiotic and biotic stress occurrences may result in either synergistic or antagonistic interactions. Most interesting perhaps is the plants increased susceptibility to pathogens when preceded by mild episodic stress (Bostock, 2014). For example, abiotic factors such as increased temperature benefits viruses as well as bacterial growth conditions, promoting the abundance of the bacterium *P. syringe* in tobacco (*Nicotiana tabacum* L.) and Arabidopsis (Wang *et al.*, 2009). In

addition, tobacco plants infected with the tobacco mosaic virus have reduce resistance when exposed to temperatures over 28 ºC through reduced R-gene mediated resistance (Király *et al.*, 2008). Furthermore, plant viruses benefit from elevated temperatures by enhanced virus survival and spread, an increased availability of insect vectors, and possibly suppressed host resistance (Moury *et al.*, 1998; Király *et al.*, 2008).

Elevated temperatures can also cause protein denaturation or aggregation leading to a lower affinity between interacting factors affecting the recognition of pathogen molecules (Fraire-Velázquez *et al.*, 2012). However, high temperatures can also increase plant defense response. For example, the rice blast Pib resistance gene is upregulated in plants grown under 25 ºC (Wang *et al.*, 2001). Likewise, sunflowers become more resistant to parasitic herbaceous plants (*Orobanche cumana* and *O. aegyptiaca*) under elevated temperatures through the increased ability to denature the parasitic tissue in their roots (Eizenberg, 2003). Determining the effects of temperature becomes even more challenging when changes in plant resistance are recorded on a genotype level. Twenty-seven lines of wheat (*Triticum aestivum*) were exposed to a range of temperatures and the plant resistance to leaf rust (*Puccinia recondita*) was highly dependent on the plant line with both increases and decreases with changes in temperature (Dyck and Johnson, 1983). Similarly, drought stress can also affect pathogen infection both positively and negatively. Mohr and Cahill (2003) demonstrated that Arabidopsis resistance to the bacterium *P. syringae* decreased when the root system was exposed to air drying , whereas the plant's resistance to the oomycete *Peronospora parasitica* did not change. However, in tomato three cycles of drought stress (fully hydrated until plant was wilted) with alternating recovery periods,

showed subsequent enhanced inoculation resistance to the fungus *Botrytis cinerea* in tomato plants (Achuo *et al.*, 2006) indicating that there is often an abiotic-biotic stress relationship.

Interestingly, biotic factors can also affect plant resistance to abiotic stressors like drought and freezing tolerance (Xu *et al.*, 2008). Several vegetable seedlings infected with four different viruses had improved drought and freezing tolerance, suggesting that infection with viruses can actually aid the plant in retaining water (Xu *et al.*, 2008). Viruses can form mutualistic relationships with plants under extreme stress conditions, even though viruses are considered parasitic symbionts under normal conditions. Under stress conditions virus infected plants show higher above ground water content as well as higher water retention abilities (Xu et al., 2008) which can correlate with lower transpiration rates leading to less water loss by these plants (Keller et al., 1989). Additionally, Virus infected plants showed increased salicylic acid content as well as increased levels of osmoprotectants and antioxidants which serve as defense mediators (Xu et al., 2008). Considering the contrasting effect of stressors on plants, in a recently published review, the authors caution against the generalization of abiotic stress factors including high temperature, humidity, drought, and salinity in weakening plant defenses (Sharma *et al.*, 2013) despite other studies having found increased pathogen susceptibility during periods of abiotic stress (Mohr and Cahill, 2003; Koga *et al.*, 2004).

2.4.2.3 Biotic-biotic

As with other stress combinations, plants are often attacked by multiple herbivores and are capable of producing an integrated response (Bostock, 1999; Bruxelles *et al.*,

2001). The simultaneous plant intrusion by the beet armyworm (BAW) *Spodoptera exigua* Hübner and the phloem feeder silverleaf whitefly *Bemisia tabaci* Gennadius reduced plant volatile emission by 60 % compared to those damaged by BAW alone (Rodriguez-Saona *et al.*, 2003). The authors hypothesize that the reduction in volatiles can weaken the plant's attractiveness to parasitoids. This kind of plant signal integration can not only occur during simultaneous biotic stressor encounters but is also evident when biotic stressors are temporally separated. In other words, individual biotic agents can induce a signaling cascade in favor of future stressors. When the mold fungus (*Sclerotium rolfsii* Saccodes) infects peanut plants, the plants change their volatile compound signature to increase their attractiveness to BAW thus making the plants more attractive to BAW larval parasitoids (*Cotesia marginiventris*) as well. Additionally, previously attacked plants were able to alter their resistance in subsequent attacks to other similar stressors (Bruce and Pickett, 2007). Rice plants damaged by the white-backed plant hopper (*Sogatella furicifera*) increased resistance to the fungus causing rice blast (*Magnaporthe grises*) only when the plants were previously exposed to the hopper (Kanno and Fujita, 2003; Kanno *et al.*, 2005). Clearly, it is difficult to generalize plant defense response(s) because the regulation of plant defense to different biotic agents depends on the plant-pathogen/herbivore interaction and is highly specific (Stout *et al.*, 1999). Pest resistance to three different biotic agents on tomato plants found that depending on the agent combination, pest resistance could increase or impair the development of other pathogens (Stout *et al.*, 1999), stressing the importance and need for empirical research focusing on multiple combined biotic stresses on plants to determine the patterns in plant signal integration

and to enable future predictions of plant responses and their resistance to biotic stresses in the field.

2.5 Other factors influencing stress response interaction

Even though the combination of stressors can determine overall stress susceptibility (Atkinson and Urwin, 2012), it is important to recognize there are several other physiological factors influencing plant stress responses. Plant nutritional state, plant age, the time of the day the plants are stressed, can influence, enhance, or dampen stress responses in plants.

2.5.1 Plant size and age

Plant developmental stage can partially dictate a plant's propensity to particular stresses (Niinemets, 2010). The shallow root systems of tree saplings are restricted to the upper soil layers and therefore have a higher dependence on precipitation events. Older, larger trees, on the other hand, have deeper root systems allowing access to deeper ground water and a greater uncoupling from minor drought events (Dawson, 1996; Drake *et al.*, 2009). However, as trees grow and gain in height, greater light interception leads to higher leaf temperatures and potential photoinhibition (Niinemets and Valladares, 2004 for review). Consequently, leaf cooling through transpiration is increased, requiring more water, a decrease in leaf water potential, and likely an increase in cavitation events if the water supply is not sufficient. Trees within distinct ontogenic stages are therefore prone to different stress combinations. The simultaneous occurrence of drought, photoinhibition, heat stress, and nutrient

limitation is expected to increase with increasing plant size, while shading and drought stress interactions are expected to be more prevalent in seedlings and saplings (Valladares and Pearcy, 1997, 2002; Niinemets and Valladares, 2004; Niinemets, 2010).

2.5.2 Nutrients

The effect of nutrients on plant signaling pertains to their role in supporting enzyme production and functioning (Ranieri *et al.*, 2001). The composition of herbivore-induced volatiles strongly depends on other abiotic environmental factors, such as nitrogen and phosphorous availability (Schmelz *et al.*, 2003), soil salinity and pH, and air humidity (Vallat *et al.*, 2005). However, in addition to the chemical stress response, nutrients can have a contrary effect on the plant defense status. Predicting the plant susceptibility to different pathogens remains challenging, because plant stress resistance is dependent on several factors including plant-pathogen interaction, environmental conditions, plant developmental stage as well as nutrient availability, whereby each nutrient element can impact the plant differently (Dordas, 2009; Huber and Haneklaus, 2007). Additionally, land management practices can affect nutrient availability for both the plant as well as the pathogen thus affecting plant disease severity (Huber and Graham, 1999).

A recent meta-analysis comparing the severity of fungal-pathogen infection relative to the addition of commercial fertilizer in herbaceous plants, revealed that in general, the addition of N fertilizer increased the severity of fungal-pathogen infection suggesting that a slightly depleted nutrient status would benefit plants. However,

species-specific differences exist and there are some plants, e.g. potato (*Solanum spp.*) which show decreased fungal infection levels in response to N fertilizer (Veresoglou et al., 2013).

A compilation of several studies has shown that an adequate K^+ nutrient status in plants tends to decrease aphid, herbivore, virus, and bacteria susceptibility (Prabhu *et al.*, 2007; Amtmann *et al.*, 2008). This is most likely a result of K^+ affecting the membrane potentials due to high K^+ permeability. Additionally, K^+ also plays a role in electrical signaling (Amtmann *et al.*, 2005) and can differentially affect hormone pathways (see review: Amtmann *et al.*, 2008). Despite advancement in our knowledge of K^+'s effect on signaling cascades as well as how other nutrients influence metabolic pathways, it still remains unknown how the plant's nutrient status fine tunes the signaling cascades leading to lower or higher susceptibility to stressors.

2.5.3 Circadian clock

A less explored field in plant signaling and stress response is the influence of the circadian rhythm on plants (Piechulla, 1993). The circadian clock is involved in a multitude of physiological processes, stomatal conductance, photosynthesis, stem elongation, flowering time, leaf movement, pathogen and herbivore resistance, response to abiotic stress, and plant immunity (Zhang *et al.*, 2013; for review see: Hsu and Harmer, 2014). Covington et al. (2008) integrated information from microarray experiments to find one third of Arabidopsis genes are controlled by the circadian clock. Furthermore, plant hormones are also up- or down-regulated depending on the time of day. For example, 40% of the genes responsible for ABA production are up-

regulated in the morning. The authors speculate that the difference in transcriptome abundance over the course of the day reflects the plant ABA level and therefore also the activity of the ABA signaling pathway.

The rhythm of gene expression can be highly affected by temperature. The expression of bPRP (soybean proline-rich Protein) in soybeans (*Glycine max* (L.) Merr. is enhanced by several factors including drought, salt, plant hormones and viruses. Under non-stressed condition bPRP expression follows a circadian rhythm, which becomes disturbed during low temperatures demonstrating that stress can affect the circadian rhythm of gene expression. Regulation of gene transcription patterns according to a circadian rhythm helps optimize the plant's resources and increases plant resistance to stressful environmental conditions when needed. This regulation has been shown for oxidative stress, and freezing tolerance in Arabidopsis plants (Nakamichi *et al.*, 2009; Dong *et al.*, 2011; Lai *et al.*, 2012) and heat shock resistance in cotton plants (*Gossypium hirsutum* L.cv. Deltapine 50) (Rikin, 1992). These experiments collectively show that plants use their resources efficiently by limiting signaling pathways at certain times of the day emphasizing the importance of including different time points in experiments focusing on plant stress responses (Rienth *et al.*, 2014).

2.6 Future directions

Undoubtedly, plants respond rapidly and distinctly to changing environmental conditions and biotic assaults despite their sessile life style. Here, we presented the mode of action of each signaling pathway, the signaling speed, and potential

interconnections between signaling pathways. And yet, many unknowns remain regarding signaling pathways, ranging from the importance of each pathway individually to the integration of signals. Specifically, hydraulic signals seem to play an important role in information transmission (Malone *et al.*, 1994). However, the lack of information on hydraulic signaling events makes integration of hydraulic signals into the plant response signaling pathway timeline challenging.

Even though there is still a debate if chemical signals are suitable as long-distance signaling pathways, the importance and presence of hydraulic, electric, and chemical pathways is beyond dispute. Additional investigation into the integration of all three signaling pathways along with deciphering the role of each signal type in information transfer remains an area in great need of future attention. Furthermore, it is important to include environmental variation and a more diverse spectrum of plant species into experimental design in order to account for unique species responses to changing environmental conditions. High variability of stress resistance to abiotic stressors exists even within lines from the same species (Dyck and Johnson, 1983), and susceptibility towards different stressors can vary depending on the ontogenetic stage of plants (Niinemets, 2010).

In the field, plants are rarely exposed to a single stressor, but instead face a combination of stressors that likely vary in intensity. Gene transcription analysis have emphasized the uniqueness of stress responses to combined stressors. Therefore, we call for research that moves beyond highly controlled settings and examines stress/defense responses of field grown plants. Finally, the severe lack of information on combined stressors hinders our ability to predict stress responses under changing

environmental conditions. The future of efficient crop production is highly dependent on our ability to predict stresses accurately. Therefore, addressing plant responses to different stress combinations will help researchers and farmers manage plant responses in order to minimize resource outputs and maximize productivity.

2.7 References

Achuo EA, Prinsen E, Hofte M. 2006. Influence of drought, salt stress and abscisic acid on the resistance of tomato to *Botrytis cinerea* and *Oidium neolycopersici*. Plant Pathology **55**, 178–186.

Alarcon J, Malone M. 1994. Substantial hydraulic signals are triggered by leaf-biting insects in tomato. Journal of Experimental Botany **45**, 953–957.

Albacete A, Martínez-Andújar C, Martínez-Pérez A, Thompson AJ, Dodd IC, Pérez-Alfocea F. 2015. Unravelling rootstock×scion interactions to improve food security. Journal of Experimental Botany **66**, 2211–2226.

Del Amor FM, Cuadra-Crespo P. 2012. Plant growth-promoting bacteria as a tool to improve salinity tolerance in sweet pepper. Functional Plant Biology **39**, 82–90.

Amtmann A, Hammond JP, Armengaud P, White PJ. 2005. Nutrient sensing and signalling in plants: potassium and phosphorus. Advances in Botanical Research **43**, 209–257.

Amtmann A, Troufflard S, Armengaud P. 2008. The effect of potassium nutrition on pest and disease resistance in plants. Physiologia Plantarum **133**, 682–691.

Applewhite PB. 1972. Behavioral plasticity in the sensitive plant, Mimosa. Behavioral Biology **7**, 47–53.

Arimura G-I, Ozawa R, Maffei ME. 2011. Recent advances in plant early signaling in response to herbivory. International Journal of Molecular Sciences **12**, 3723–3739.

Árnadóttir J, Chalfie M. 2010. Eukaryotic mechanosensitive channels. Annual Reviews of Biophysics **39**, 111–137.

Atkinson NJ, Urwin PE. 2012. The interaction of plant biotic and abiotic stresses: from genes to the field. Journal of Experimental Botany **63**, 3523–3544.

Baldwin IT. 2006. Volatile signaling in plant-plant interactions: 'talking trees' in the genomics era. Science **311**, 812–815.

Bale JS, Masters GJ, Hodkinson ID, *et al.* 2002. Herbivory in global climate change research: direct effects of rising temperature on insect herbivores. Global Change Biology **8**, 1–16.

Barber VA, Juday GP, Finney BP. 2000. Reduced growth of Alaskan white spruce in the twentieth century from temperature-induced drought stress. Nature **405**, 668–673.

Bari R, Jones JDG. 2009. Role of plant hormones in plant defence responses. Plant Molecular Biology **69**, 473–88.

Bauer H, Ache P, Lautner S, *et al.* 2013. The stomatal response to reduced relative humidity requires guard cell-autonomous ABA synthesis. Current Biology **23**, 53–57.

Baydoun EA, Fry SC. 1985. The immobility of pectic substances in injured tomato leaves and its bearing on the identity of the wound hormone. Planta **165**, 269–276.

Boari F, Malone M. 1993. Wound-induced hydraulic signals: survey of occurrence in a range of species. Journal of Experimental Botany **44**, 741–746.

Bonaventure G, VanDoorn A, Baldwin IT. 2011. Herbivore-associated elicitors: FAC signaling and metabolism. Trends in Plant Science **16**, 294–299.

Bostock RM. 2005. Signal crosstalk and induced resistance: straddling the line between cost and benefit. Annual Review of phytopathology **43**, 545–580.

Bostock R. 1999. Signal conflicts and synergies in induced resistance to multiple attackers. Physiological and Molecular Plant Pathology **55**, 99–109.

Bouchabké O, Tardieu F, Simonneau T. 2006. Leaf growth and turgor in growing cells of maize (*Zea mays* L.) respond to evaporative demand under moderate irrigation but not in water-saturated soil. Plant, Cell and Environment **29**, 1138–1148.

Bramley H, Turner NC, Turner DW, Tyerman SD. 2007. Comparison between gradient-dependent hydraulic conductivities of roots using the root pressure probe: the role of pressure propagations and implications for the relative roles of parallel radial pathways. Plant, Cell and Environment **30**, 861–874.

Bray EA, Bailey-Serres J, Weretilnyk E. 2000. Responses to abiotic stresses. In: Gruissem W, Buchannan B, Jones R. eds. Biochemistry and molecular biology of plants. Rockeville, MD: American Society of Plant Physiologists, 1158–1249.

Bréda N, Bréda N, Huc R, Granier A, Dreyer E. 2006. Temperate forest tree and stands under sever drought: a review of ecophysiological responses, adaptation processes and long-term consequences. Annales des Sciences Forestières **63**,

625–644.

Bricchi I, Bertea CM, Occhipinti A, Paponov IA, Maffei ME. 2012. Dynamics of membrane potential variation and gene expression induced by *Spodoptera littoralis*, *Myzus persicae*, and *Pseudomonas syringae* in Arabidopsis. PLoS ONE **7**, 1-20.

Bricchi I, Leitner M, Foti M, Mithöfer A, Boland W, Maffei ME. 2010. Robotic mechanical wounding (MecWorm) versus herbivore-induced responses: early signaling and volatile emission in Lima bean (*Phaseolus lunatus* L.). Planta **232**, 719–729.

Bruce TJA. 2015. Interplay between insects and plants: dynamic and complex interactions that have coevolved over millions of years but act in milliseconds. Journal of Experimental Botany **66**, 455–465.

Bruce TJ, Pickett JA. 2007. Plant defence signalling induced by biotic attacks. Current Opinion in Plant Biology **10**, 387–392.

Bruxelles D, Guy L, Roberts MR. 2001. Signals regulating multiple responses to wounding and herbivores. Critical Reviews in Plant Sciences **20**, 37–41.

Sanderson, JB. 1888. On the electromotive properties of the leaf of Dionaea in the excited and unexcited states. Philosophical Transactions of the Royal Society of London **179**, 417–449.

Choi WG, Toyota M, Kim SH, Hilleary R, Gilroy S. 2014. Salt stress-induced Ca^{2+} waves are associated with rapid, long-distance root-to-shoot signaling in plants. Proceedings of the National Academy of Sciences **111**, 6497–6502.

Christmann A, Grill E, Huang J. 2013. Hydraulic signals in long-distance signaling.

Current Opinion in Plant Biology **16**, 293–300.

Christmann A, Weiler EW, Steudle E, Grill E. 2007. A hydraulic signal in root-to-shoot signalling of water shortage. The Plant Journal : for cell and molecular biology **52**, 167–174.

Cochard H, Froux F, Mayr S, Coutand C. 2004. Xylem wall collapse in water-stressed pine needles. Plant Physiology, 401–408.

Cochard H, Bréda N, Granier A. 1996. Whole tree hydraulic conductance and water loss regulation in Quercus during drought : evidence for stomatal control of embolism ? Annals of Forest Science, 197–207.

Comstock JP. 2002. Hydraulic and chemical signalling in the control of stomatal conductance and transpiration. Journal of Experimental Botany **53**, 195–200.

Covington MF, Maloof JN, Straume M, Kay SA, Harmer SL. 2008. Global transcriptome analysis reveals circadian regulation of key pathways in plant growth and development. Genome Biology **9**, 1–18.

Craufurd PQ, Peacock JM. 1993. Effect of heat and drought stress on sorghum (*Sorghum bicolor*). II. Grain yield. Experimental Agriculture **29**, 77–86.

Davies WJ, Wilkinson S, Loveys B. 2002. Stomatal control by chemical signalling and the exploitation of this mechanism to increase water use efficiency in agriculture. New Phytologist **153**, 449–460.

Davies WJ, Zhang J. 1991. Root signals and the regulation of growth and development of plants in drying soil. Annual Review of Plant Physiology and Molecular Biology **42**, 55–76.

Dawson TE. 1996. Determining water use by trees and forests from isotopic, energy

balance and transpiration analyses: the roles of tree size and hydraulic lift. Tree Physiology **16**, 263–272.

Dicke M, Baldwin IT. 2010. The evolutionary context for herbivore-induced plant volatiles: beyond the 'cry for help'. Trends in Plant Science **15**, 167–175.

Dixon MAA, Grace J, Tyree MT. 1984. Concurrent measurements of stem density, leaf and stem water potential, stomatal conductance and cavitation on a sapling of *Thuja occidentalis* L. Plant, Cell and Environment **7**, 615–618.

Dong MA, Farre EM, Thomashow MF. 2011. CIRCADIAN CLOCK-ASSOCIATED 1 and LATE ELONGATED HYPOCOTYL regulate expression of the C-REPEAT BINDING FACTOR (CBF) pathway in Arabidopsis. Proceedings of the National Academy of Sciences **108**, 7241–7246.

Drake PL, Mendham DS, White DA, Ogden GN. 2009. A comparison of growth, photosynthetic capacity and water stress in *Eucalyptus globulus* coppice regrowth and seedlings during early development. Tree Physiology **29**, 663–674.

Dyck PL, Johnson R. 1983. Temperature sensitivity of genes for resistance in wheat to *Puccinia recondita*. Canadian Journal of Plant Pathology **5**, 229–234.

Dordas C. 2009. Role of nutrients in controlling plant diseases in sustainable agriculture: a review. Sustainable agriculture. Netherlands: Springer, 443–460.

Dudareva N, Negre F, Nagegowda DA, Orlova I. 2006. Plant volatiles: recent advances and future perspectives. Critical Reviews in Plant Sciences **25**, 417–440.

Egilla JN, Davies FT, Drew MC. 2001. Effect of potassium on drought resistance of *Hibiscus rosa-sinensis* cv. Leprechaun: plant growth, leaf macro- and micronutrient content and root longevity. Plant and Soil **229**, 213–224.

Eizenberg H. 2003. Resistance to broomrape (*Orobanche spp.)* in sunflower (*Helianthus annuus* L.) is temperature dependent. Journal of Experimental Botany **54**, 1305–1311.

Endo A, Sawada Y, Takahashi H, *et al.* 2008. Drought induction of Arabidopsis 9-cis-epoxycarotenoid dioxygenase occurs in vascular parenchyma cells. Plant Physiology **147**, 1984–1993.

Evans NH, McAinsh MR, Hetherington AM. 2001. Calcium oscillations in higher plants. Current Opinion in Plant Biology **4**, 415–420.

Ewers FW, Fisher JB. 1989. Variation in vessel length and diameter in stems of six tropical and subtropical lianas. American Journal of Botany **76**, 1452–1459.

Farmer EE, Ryan CA. 1990. Interplant cmmuniction: airborn methyl jasmonate induces synthesis of proteinase inhibitors in plant leaves. Proceedings of the National Academy of Sciences, USA **87**, 7713-7716.

Fisher DB. 1990. Measurement of phloem transport rates by an indicator-dilution technique. Plant Physiology **94**, 455–462.

Fraire-Velázquez S, Sánchez-Calderón L, Guzmán-Gonzáles S. 2012. Abiotic stress responses in plants: integrative genetic pathways and overlapping reactions between abiotic and biotic stress responses. In: Haryana N, Punj S. eds. Abiotic stress: new research. Hauppauge, NY: NOVA Science Publisher, 133–150.

Fromm J. 2006. Long-distance electrical signaling and physiological functions in higher plants. In: Volkov AG. ed. Plant electrophysiology - theory and methods. Berlin Heidelberg: Springer-Verlag, 269–285.

Fromm J, Lautner S. 2007. Electrical signals and their physiological significance in plants. Plant, Cell and Environment **30**, 249–257.

Frost CJ, Appel HM, Carlson JE, De Moraes CM, Mescher MC, Schultz JC. 2007. Within-plant signalling via volatiles overcomes vascular constraints on systemic signalling and primes responses against herbivores. Ecology Letters **10**, 490–498.

Fuchs WH, Grossmann F. 1972. Ernährung und Resistenz von Kulturpflanzen gegenüber Krankheitserregern und Schädlingen. In: Scharrer K, Linser H. eds. Handbuch der Pflanzenernährung und Düngung. Vienna: Springer Verlag, 1007–1107.

Fujita M, Fujita Y, Noutoshi Y, Takahashi F, Narusaka Y, Yamaguchi-Shinozaki K, Shinozaki K. 2006. Crosstalk between abiotic and biotic stress responses: a current view from the points of convergence in the stress signaling networks. Current Opinion in Plant Biology **9**, 436–442.

Gallé A, Lautner S, Flexas J, Fromm J. 2015. Environmental stimuli and physiological responses: the current view on electrical signalling. Environmental and Experimental Botany **114**, 15–21.

Garcia-Brugger A, Lamotte O, Vandelle E, Bourque S, Lecourieux D, Poinssot B, Wendehenne D, Pugin A. 2006. Early signaling events induced by elicitors of plant defenses. Molecular Plant-microbe Interactions **19**, 711–724.

Gilroy S, Suzuki N, Miller G, Choi WG, Toyota M, Devireddy AR, Mittler R. 2014. A tidal wave of signals: calcium and ROS at the forefront of rapid s ystemic signaling. Trends in Plant Science **19**, 623–630.

Glauser G, Grata E, Dubugnon L, Rudaz S, Farmer EE, Wolfender JL. 2008. Spatial and temporal dynamics of jasmonate synthesis and accumulation in Arabidopsis in response to wounding. Journal of Biological Chemistry **283**, 16400–16407.

Gollan T, Passioura JB, Munn R. 1986. Soil water status affects the stomatal conductance of fully turgid wheat and sunflower leaves. Australian Journal of Plant Physiology **13**, 459–464.

Gowing DJG, Davies WJ, Jones HG. 1990. A positive root-sourced signal as an indicator of soil drying in apple, *Malus x domestica* Borkh. Journal of Experimental Botany **41**, 1535–1540.

Guerard N, Pascale M, Claude B, Lieutier F, Erwin D. 2007. Do trees use reserve or newly assimilated carbon for their defense reactions? A ^{13}C labeling approach with young Scots pines inoculated with a bark-beetle-associated fungus (*Ophiostoma brunneo ciliatum*). Annals of Forest Science **64**, 601–608.

Haberland G. 1890. *Das Reizleitende Gewebesystem der Sinnpflanze*. Leipzig: Engelmann-Verlag.

Hacke UG, Stiller V, Sperry JS, Pittermann J, McCulloh KA. 2001. Cavitation fatigue: embolism and refilling cycles can weaken the cavitation resistance of xylem. Plant Physiology **125**, 779–786.

Hallik L, Niinemets Ü, Wright IJ. 2009. Are species shade and drought tolerance reflected in leaf-level structural and functional differentiation in Northern Hemisphere temperate woody flora? New Phytologist **184**, 257–274.

Hasegawa PM, Bressan RA, Zhu JK, Bohnert HJ. 2000. Plant cellular and molecular responses to high salinity. Annual Review of Plant Physiology and Plant Molecular Biology **51**, 463–499.

Heil M, Ton J. 2008. Long-distance signalling in plant defence. Trends in Plant Science **13**, 264–272.

Hewezi T, Léger M, Gentzbittel L. 2008. A comprehensive analysis of the combined effects of high light and high temperature stresses on gene expression in sunflower. Annals of Botany **102**, 127–140.

Heyne EG, Brunson AM. 1940. Genetic studies of heat and drought tolerance im maize. Journal of the American Society of Agronomy **32**, 803–814.

Holbrook NM, Shashidhar VR, James RA, Munns R. 2002. Stomatal control in tomato with ABA-deficient roots: response of grafted plants to soil drying. Journal of Experimental Botany **53**, 1503–1514.

Holopainen JK. 2004. Multiple functions of inducible plant volatiles. Trends in Plant Science **9**, 529–533.

Houwink AL. 1935. The condution of excitation in *Mimosa pudica*. Recuril des Tavaux Botaniques Neerlaandais **32**, 51–91.

Howe G, Jander G. 2008. Plant immunity to insect herbivores. Annual Review of Plant Biology **59**, 41–66.

Hsu PY, Harmer SL. 2014. Wheels within wheels: the plant circadian system. Trends

in Plant Science **19**, 240–249.

Huang GT, Ma SL, Bai LP, Zhang L, Ma H, Jia P, Liu J, Zhong M, Guo ZF. 2012. Signal transduction during cold, salt, and drought stresses in plants. Molecular Biology Reports **39**, 969–987.

Huber DM, Graham R. 1999. The role of nutrition in crop resistance and tolerance. In: Rengel Z, ed. Mineral Nutrition of Crops Fundamental Mechanisms and Implications. New York: Food Product Press, 205–226.

Huber DM, Haneklaus S. 2007. Managing nutrition to control plant disease. Landbauforschung Völkenrode **57**, 313–322.

Jagtap V, Bhargava S, Streb P, Feierabend J. 1998. Comparative effect of water , heat and light stresses on photosynthetic reactions in *Sorghum bicolor* (L.) Moench. Journal of Experimental Botany **49**, 1715–1721.

Jia W, Davies WJ. 2007. Modification of leaf apoplastic pH in relation to stomatal sensitivity to root-sourced abscisic acid signals. Plant Physiology **143**, 68–77.

Jia W, Zhang J, Liang J. 2001. Initiation and regulation of water deficit-induced abscisic acid accumulation in maize leaves and roots: cellular volume and water relations. Journal of Experimental Botany **52**, 295–300.

Jiang Y, Huang B. 2001. Drought and heat stress injury to two cool-season turfgrasses in relation to antioxidant metabolism and lipid peroxidation. Crop Science **41**, 436.

Johnson D, Leake JR, Ostle N, Ineson P, Read DJ. 2002. In situ $^{13}CO_2$ pulse-labelling of upland grassland demonstrates a rapid pathway of carbon flux from arbuscular mycorrhizal mycelia to the soil. New Phytologist **153**, 327–

334.

Kanno H, Fujita Y. 2003. Induced systemic resistance to rice blast fungus in rice plants infested by white-backed planthopper. Entomologia Experimentalis et Applicata **107**, 155–158.

Kanno H, Satoh M, Kimura T, Fujita Y. 2005. Some aspects of induced resistance to rice blast fungus, *Magnaporthe grisea*, in rice plant infested by white-backed planthopper, *Sogatella furcifera*. Applied Entomology and Zoology **40**, 91–97.

Keller P, Lüttge U, Wang XC, Büttner G. 1989. Influence of rhizomania disease on gas exchange and water relations of a susceptible and a tolerant sugar beet variety. Physiological and Molecular Plant Pathology **34**, 379–392.

Kessler A, Baldwin I. 2001. Defensive function of herbivore-induced plant volatile emissions in nature. Science (New York, N.Y.) **291**, 2141–2144.

Kessler A, Baldwin IT. 2002. Plant responses to insect herbivory: the emerging molecular analysis. Annual review of plant biology **53**, 299–328.

Kim SH, Shackel KA, Lieth JH. 2004. Bending alters water balance and reduces photosynthesis of rose shoots. Journal of the American Society of Hortorticultural Science **129**, 896–901.

Király L, Hafez YM, Fodor J, Király Z. 2008. Suppression of tobacco mosaic virus-induced hypersensitive-type necrotization in tobacco at high temperature is associated with downregulation of NADPH oxidase and superoxide and stimulation of dehydroascorbate reductase. Journal of General Virology **89**, 799–808.

Kobayashi M, Ohura I, Kawakita K, Yokota N, Fujiwara M, Shimamoto K, Doke N, Yoshioka H. 2007. Calcium-dependent protein kinases regulate the production of reactive oxygen species by potato NADPH oxidase. The Plant Cell **19**, 1065–1080.

Koga H, Dohi K, Mori M. 2004. Abscisic acid and low temperatures suppress the whole plant-specific resistance reaction of rice plants to the infection of *Magnaporthe grisea*. Physiological and Molecular Plant Pathology **65**, 3–9.

Kunkel BN, Brooks DM. 2002. Cross talk between signaling pathways in pathogen defense. Current Opinion in Plant Biology **5**, 325–331.

Lai AG, Doherty CJ, Mueller-Roeber B, Kay SA, Schippers JHM, Dijkwel PP. 2012. CIRCADIAN CLOCK-ASSOCIATED 1 regulates ROS homeostasis and oxidative stress responses. Proceedings of the National Academy of Sciences **109**, 17129–17134.

Laloi C, Stachowiak M, Pers-Kamczyc E, Warzych E, Murgia I, Apel K. 2007. Cross-talk between singlet oxygen- and hydrogen peroxide-dependent signaling of stress responses in *Arabidopsis thaliana*. Proceedings of the National Academy of Sciences **104**, 672–677.

Lautner S, Grams TEE, Matyssek R, Fromm J. 2005. Characteristics of electrical signals in poplar and responses in photosynthesis. Plant Physiology **138**, 2200–2209.

Leitner M, Vandelle E, Gaupels F, Bellin D, Delledonne M. 2009. NO signals in the haze. Nitric oxide signalling in plant defence. Current Opinion in Plant Biology **12**, 451–458.

Lindhauer MG. 1985. Influence of K nutrition and drought on water relations and growth of sunflower (*Helianthus annuus* L.). Zeitschrift für Pflanzenernährung und Bodenkunde **148**, 654–669.

Loewenstein NJ, Pallardy SG. 1998. Drought tolerance, xylem sap abscisic acid and stomatal conductance during soil drying: a comparison of canopy trees of three temperate deciduous angiosperms. Tree Physiology **18**, 431–439.

Lopez R, Badel E, Peraudeau S, Beaujard F. 2014. Tree shoot bending generates hydraulic pressure pulses: a new long-distance signal ? Journal of Experimental Botany **65**, 1997–2008.

Lunevsky VZ, Zherelova OM, Vostrikov IY, Berestovsky GN. 1983. Excitation of Characeae cell membranes as a result of activation of calcium and chlorid channels. Journal of Membrane Biology **58**, 43–58.

Maffei EM, Bossi S. 2006. Electrophysiology and plant responses to biotic stress. In: Volkov A. ed. Plant Electrophysiology. Theory and Methods. Berlin: Srpinger, 461–481.

Maffei M, Bossi S, Spiteller D, Mitho A, Boland W. 2004. Effects of feeding *Spodoptera littoralis* on lima bean leaves. I. Membrane potentials, intracellular calcium variations, oral secretions, and regurgitate components. Plant Physiology **134**, 1752–1762.

Maffei ME, Mithöfer A, Boland W. 2007*a*. Before gene expression: early events in plant-insect interaction. Trends in Plant Science **12**, 310–316.

Maffei ME, Mithöfer A, Boland W. 2007*b*. Insects feeding on plants: rapid signals and responses preceding the induction of phytochemical release.

Phytochemistry **68**, 2946–2959.

Mahajan S, Pandey GK, Tuteja N. 2008. Calcium- and salt-stress signaling in plants: shedding light on SOS pathway. Archives of Biochemistry and Biophysics **471**, 146–158.

Mahajan S, Tuteja N. 2005. Cold, salinity and drought stresses: an overview. Archives of Biochemistry and Biophysics **444**, 139–158.

Malone M. 1992. Kinetics of wound-induced hydraulic signals and variation potentials in wheat seedlings. Planta **187**, 505–510.

Malone M. 1993. Hydraulic signals. Philosophical Transactions of the Royal Society B: Biological Sciences **341**, 33–39.

Malone M, Alarcon J-J, Palumbo L. 1994. An hydraulic interpretation of rapid, long-distance wound signalling in tomato. Planta **193**, 181–185.

Mancuso S. 1999. Hydaulic and elecrical transmission of wound-induced signals in *Vitis vinifera*. Australian Journal of Plant Physiology **26**, 55–61.

Maule A, Faulkner C, Benitez-Alfonso Y. 2012. Plasmodesmata 'in communicado'. Frontiers in Plant Science **3**, 1–5.

Medvedev SS. 2005. Calcium signaling system in plants. Russian Journal of Plant Physiology **52**, 249–270.

Meehl GA, Arblaster JM, Tebaldi C. 2007. Contributions of natural and anthropogenic forcing to changes in temperature extremes over the United States. Geophysical Research Letters **34**, 1-5.

Mikan CJ, Zak DR, Kubiske ME, Pregitzer KS. 2000. Combined effects of atmospheric CO_2 and N availability on the belowground carbon and nitrogen

dynamics of aspen mesocosms. Oecologia **124**, 432–445.

Miller G, Schlauch K, Tam R, Cortes D, Torres MA, Shulaev V, Dangl JL, Mittler R. 2009. The plant NADPH oxidase RBOHD mediates rapid systemic signaling in response to diverse stimuli. Science Signaling **2**, 1–10.

Mithöfer A, Boland W. 2012. Plant Defense against Herbivores: Chemical Aspects. Annual Review of Plant Biology **63**, 431–450.

Mithöfer A, Wanner G, Boland W. 2005. Effects of feeding *Spodoptera littoralis* on lima bean leaves. II. Continuous mechanical wounding resembling insect feeding is sufficient to elicit herbivory-related volatile emission. Plant Physiology **137**, 1160–1168.

Mittler R. 2006. Abiotic stress, the field environment and stress combination. Trends in Plant Science **11**, 15–19.

Mittler R, Blumwald E. 2015. The Roles of ROS and ABA in systemic acquired acclimation. The Plant Cell Online **27**, 64–70.

Mittler R, Vanderauwera S, Suzuki N, Miller G, Tognetti VB, Vandepoele K, Gollery M, Shulaev V, Van Breusegem F. 2011. ROS signaling: the new wave? Trends in Plant Science **16**, 300–309.

Mohr PG, Cahill DM. 2003. Abscisic acid influences the susceptibility of *Arabidopsis thaliana* to *Pseudomonas syringae* pv. *tomato* and *Peronospora parasitica*. Functional Plant Biology **30**, 461–469.

Moury B, Selassie KG, Marchoux G, Daubeze AM, Palloix A. 1998. High-temperature effects on hypersensitive resistance to tomato spotted wilt tospovirus (Tswv) in pepper (*Capsicum-Chinense* Jacq.). European Journal of

Plant Pathology **104**, 489–498.

Nakagami H, Pitzschke A, Hirt H. 2005. Emerging MAP kinase pathways in plant stress signalling. Trends in Plant Science **10**, 339–346.

Nakamichi N, Kusano M, Fukushima A, Kita M, Ito S, Yamashino T, Saito K, Sakakibara H, Mizuno T. 2009. Transcript profiling of an Arabidopsis PSEUDO RESPONSE REGULATOR arrhythmic triple mutant reveals a role for the circadian clock in cold stress response. Plant and Cell Physiology **50**, 447–462.

Neumann PM, Van Volkenburgh E, Cleland RE. 1988. Salinity stress inhibits bean leaf expansion by reducing turgor, not wall extensibility. Plant Physiology **88**, 233–237.

Niinemets Ü. 2010. Responses of forest trees to single and multiple environmental stresses from seedlings to mature plants: past stress history, stress interactions, tolerance and acclimation. Forest Ecology and Management **260**, 1623–1639.

Niinemets Ü, Valladares F. 2004. Photosynthetic acclimation to simultaneous and interacting environmental stresses along natural light gradients: optimality and constraints. Plant Biology **6**, 254–268.

Niinemets Ü, Valladares F. 2006. Tolerance to shade, drought, and waterlogging of temperate northern hemisphere trees and shrubs. Ecological Monographs **76**, 521–547.

Ogasawara Y, Kaya H, Hiraoka G, *et al.* 2008. Synergistic activation of the Arabidopsis NADPH oxidase AtrbohD by Ca^{2+} and phosphorylation. Journal of Biological Chemistry **283**, 8885–8892.

Oyarce P, Gurovich L. 2011. Evidence for the transmission of information through electric potentials in injured avocado trees. Journal of Plant Physiology **168**, 103–108.

Pandey S, Upadhyaya KC, Sopory SK. 2000. Calcium signaling: linking environmental signals to cellular functions. Critical Reviews in Plant Sciences **19**, 291–318.

Pantin F, Monnet F, Jannaud D, Costa JM, Renaud J, Muller B, Simonneau T, Genty B. 2013. The dual effect of abscisic acid on stomata. New Phytologist **197**, 65–72.

Passioura JB. 1972. The effect of root geometry on the yield of wheat growing on stored water. Australian Journal of Agricultural Research **23**, 745–752.

Piechulla B. 1993. 'Circadian clock' directs the expression of plant genes. Plant Molecular Biology **22**, 533–542.

Piñero MC, Houdusse F, Garcia-Mina JM, Garnica M, del Amor FM. 2014. Regulation of hormonal responses of sweet pepper as affected by salinity and elevated CO_2 concentration. Physiologia Plantarum **151**, 375–389.

Prabhu AS, Fageria NK, Uber DM, Rodrigues FA, Thompson A. 2007. Potassium nutrition and plant diseases. In: Datnoff LE, Elmer WH, Huber DM. eds. Potassium and plant diesease. Saint Paul: The American Phytopathological Society Press, 57–78.

Prasch CM, Sonnewald U. 2015. Signaling events in plants: stress factors in combination change the picture. Environmental and Experimental Botany **114**, 4–14.

Qaderi MM, Kurepin L V., Reid DM. 2006. Growth and physiological responses of canola (Brassica napus) to three components of global climate change: Temperature, carbon dioxide and drought. Physiologia Plantarum **128**, 710–721.

Ranieri A, Castagna A, Baldan B, Soldatini GF. 2001. Iron deficiency differently affects peroxidase isoforms in sunflower. Journal of Experimental Botany **52**, 25–35.

Rasmussen S, Barah P, Suarez-Rodriguez MC, Bressendorff S, Friis P, Costantino P, Bones AM, Nielsen HB, Mundy J. 2013. Transcriptome Responses to combinations of stresses in Arabidopsis. Plant Physiology **161**, 1783–1794.

Reddy ASN, Ali GS, Celesnik H, Day IS. 2011. Coping with stresses: roles of calcium- and calcium/calmodulin-regulated gene expression. The Plant Cell **23**, 2010–2032.

Reymond P, Farmer EE. 1998. Jasmonate and salicylate as global signals for defense gene expression. Current Opinion in Plant Biology **1**, 404–411.

Rienth M, Torregrosa L, Luchaire N, Chatbanyong R, Lecourieux D, Kelly MT, Romieu C. 2014. Day and night heat stress trigger different transcriptomic responses in green and ripening grapevine (*Vitis vinifera*) fruit. BMC Plant Biology **14**, 1–18.

Rikin A. 1992. Circadian rhythm of heat resistance in cotton seedlings sysnthesis of heat shock proteins. European Journal of Cell Biology **59**, 160–165.

Rizhsky L, Liang H, Mittler R. 2002. The combined effect of drought stress and heat shock on gene expression in tobacco. Plant Physiology **130**, 1143–1151.

Rizhsky L, Liang H, Shuman J, *et al.* 2004. When defense pathways collide: the response of Arabidopsis to a combination of drought and heat stress. Plant Physiology **134**, 1683–1696.

Rodriguez-Saona C, Crafts-Brandner SJ, Cañas LA. 2003. Volatile emissions triggered by multiple herbivore damage: beet armyworm and whitefly feeding on cotton plants. Journal of Chemical Ecology **29**, 2539–2550.

Ryals JA, Neuenschwander UH, Willits MG, Molina A, Steiner HY, Hunt MD. 1996. Systemic acquired resistance. The Plant Cell **8**, 1809–1819.

Sakakibara H, Takei K, Hirose N. 2006. Interactions between nitrogen and cytokinin in the regulation of metabolism and development. Trends in Plant Science **11**, 440–448.

Saliendra N, Sperry J, Comstock J. 1995. Influence of leaf water status on stomatal response to humidity, hydraulic conductance, and soil drought in *Betula occidentalis*. Planta **196**, 357–366.

Salleo S, Lo Gullo MA, Raimondo F, Nardini A. 2001. Vulnerability to cavitation of leaf minor veins: any impact on leaf gas exchange? Plant, Cell and Environment **24**, 851–859.

Sanders D, Pelloux J, Brownlee C, Harper JF. 2002. Calcium at the crossroads of signaling. The Plant Cell **14 Suppl**, S401–S417.

Sathyanarayanan PV, Poovaiah BW. 2004. Decoding Ca^{2+} signals in plants. Critical Reviews in Plant Sciences **23**, 1–11.

Savin R, Nicolas M. 1996. Effects of short periods of drought and high temperature on grain growth and starch accumulation of two malting barley cultivars.

Australian Journal of Plant Physiology **23**, 201–210.

Schlenker W, Roberts MJ. 2009. Nonlinear temperature effects indicate severe damages to U.S. crop yields under climate change. Proceedings of the National Academy of Sciences **106**, 15594–15598.

Schmelz EA, Engelberth J, Alborn HT, O'Donnell P, Sammons M, Toshima H, Tumlinson JH. 2003. Simultaneous analysis of phytohormones, phytotoxins, and volatile organic compounds in plants. Proceedings of the National Academy of Sciences **100**, 10552–10557.

Sharma R, De Vleesschauwer D, Sharma MK, Ronald PC. 2013. Recent advances in dissecting stress-regulatory crosstalk in rice. Molecular Plant **6**, 250–260.

Shimmen T. 2001. Electrical perception of 'death message' in Chara: involvement of turgor pressure. Plant Cell Physiology **42**, 366–373.

Shinozaki K, Yamaguchi-Shinozaki K. 1997. Gene expression and signal transduction in water-stress response. Plant Physiology **115**, 327–334.

Shvetsova T, Mwesigwa J, Labady A, Kelly S, Thomas D, Lewis K, Volkov AG. 2002. Soybean electrophysiology: effects of acid rain. Plant Science **162**, 723–731.

Stahlberg R, Cleland RE, Van Volkenburgh E. 2006. Slow wave potentials - a propagating electrical signal unique to higher plants. In: Baluška F, Mancuso S, Volkmann D, eds. Communication in plants - neuronal aspects of plant life. Berlin, Germany: Springer-Verlag, 291–308.

Stahlberg R, Cleland RE, Van Volkenburgh E. 2005. Decrement and amplification of slow wave potentials during their propagation in Helianthus annuus L. shoots.

Planta **220**, 550–558.

Stahlberg R, Cosgrove DJ. 1994. Comparison of electric and growth responses to excision in cucumber and pea seedlings. I. Short-distance effects are a result of wounding. Plant, Cell and Environment **17**, 1143–51.

Stahlberg R, Cosgrove DJ. 1996. Induction and ionic basis of slow wave potentials in seedlings of *Pisum sativum* L. Planta **200**, 416–425.

Stahlberg R, Cosgrove DJ. 1997*a*. Slow wave potentials in cucumber differ in form and growth effect from those in pea seedlings. Physiologia Plantarum **101**, 379–388.

Stahlberg R, Cosgrove DJ. 1997*b*. The propagation of slow wave potentials in pea epicotyls. Plant Physiology **113**, 209–217.

Stanković B, Davies E. 1996. Both action potentials and variation potentials induce proteinase inhibitor gene expression in tomato. FEBS letters **390**, 275–279.

Stanković B, Davies E. 1997. Intercellular communication in plants: electrical stimulation of proteinase inhibitor gene expression in tomato. Planta **202**, 402–406.

Stankovic B, Witters DL, Zawadzki T, Davies E. 1998. Action potentials and variation potentials in sunflower: an analysis of their relationships and distinguishing characteristics. Physiologia Plantarum **103**, 51–58.

Steinmann K, Siegwolf RTW, Saurer M, Körner C. 2004. Carbon fluxes to the soil in a mature temperate forest assessed by ^{13}C isotope tracing. Oecologia **141**, 489–501.

Steudle E. 2001. The cohesion-tension mechanism and the acquisition of water by

plant roots. Annual Review of Plant Biology **52**, 847–875.

Stout MJ, Fidantsef AL, Duffey SS, Bostock RM. 1999. Signal interactions in pathogen and insect attack: systemic plant-mediated interactions between pathogens and herbivores of the tomato, *Lycopersicon esculentum*. Physiological and Molecular Plant Pathology **54**, 115–130.

Stratmann JW. 2003. Long distance run in the wound response – jasmonic acid is pulling ahead. Trends in Plant Science **8**, 247–250.

Stratmann JW, Ryan CA. 1997. Myelin basic protein kinase activity in tomato leaves is induced systemically by wounding and increases in response to systemin and oligosaccharide elicitors. Proceedings of the National Academy of Sciences **94**, 11085–11089.

Taiz L. 1984. Regulation of cell wall mechanical properties. Annual Review of Plant Physiology **35**, 585–657.

Tang A, Boyer JS. 2002. Growth-induced water potentials and the growth of maize leaves. Journal of Experimental Botany **53**, 489–503.

Tang AC, Boyer JS. 2003. Root pressurization affects growth-induced water potentials and growth in dehydrated maize leaves. Journal of Experimental Botany **54**, 2479–2488.

Tombesi S, Nardini A, Frioni T, Soccolini M, Zadra C, Farinelli D, Poni S, Palliotti A. 2015. Stomatal closure is induced by hydraulic signals and maintained by ABA in drought-stressed grapevine. Scientific Reports 5, 1-12.

Torres-Ruiz JM, Diaz-Espejo A, Perez-Martin A, Hernandez-Santana V. 2015. Role of hydraulic and chemical signals in leaves, stems and roots in the

stomatal behaviour of olive trees under water stress and recovery conditions. Tree Physiology **35,** 415-424.

Trebacz K, Dziubinska H, Krol E. 2006. Electrical signals in long-distance communication in plants. In: Baluska F, Mancuso S,Volkmann D, eds. Communication in plants – neuronal aspects of plant life. Heidelberg. Berlin: Springer -Verlag, 277–290.

Tuna AL, Kaya C, Dikilitas M, Higgs D. 2008. The combined effects of gibberellic acid and salinity on some antioxidant enzyme activities, plant growth parameters and nutritional status in maize plants. Environmental and Experimental Botany **62**, 1–9.

Tuteja N, Sopory SK. 2008. Chemical signaling under abiotic stress environment in plants. Plant Signaling and Behavior **3**, 525–536.

Tyree MT, Yang S. 1990. Water-storage capacity of Thuja, Tsuga and Acer stems measured by dehydration isotherms. The contribution of capillary water and cavitation. Planta **182**, 420–426.

Valladares F, Pearcy RW. 1997. Interactions between water stress, sun-shade acclimation, heat tolerance and photoinhibition in the sclerophyll *Heteromeles arbutifolia*. Plant, Cell and Environment **20**, 25–36.

Valladares F, Pearcy RW. 2002. Drought can be more critical in the shade than in the sun: a field study of carbon gain and photo-inhibition in a Californian shrub during a dry El Nino year. Plant, Cell and Environment **25**, 749–759.

Vallat A, Gu H, Dorn S. 2005. How rainfall, relative humidity and temperature influence volatile emissions from apple trees in situ. Phytochemistry **66**, 1540–

1550.

Vandeleur RK, Sullivan W, Athman A, Jordans C, Gilliham M, Kaiser BN, Tyerman SD. 2014. Rapid shoot-to-root signalling regulates root hydraulic conductance via aquaporins. Plant, Cell and Environment **37**, 520–538.

Veresoglou SD, Barto EK, Menexes G, Rillig MC. 2013. Fertilization affects severity of disease caused by fungal plant pathogens. Plant Pathology **62**, 961–969.

Vernooij B, Friedrich L, Morse A, Reist R, Kolditz-Jawhar R, Ward E, Uknes S, Kessmann H, Ryals J. 1994. Salicylic acid is not the translocated signal responsible for inducing systemic acquired resistance but is required in signal transduction. Plant Cell **6**, 959–965.

Volkov AG. 2000. Green plants: electrochemical interfaces. Journal of Electroanalytical Chemistry **483**, 150–156.

Volkov AG, Collins DJ, Mwesigwa J. 2000. Plant electrophysiology: pentachlorophenol induces fast action potentials in soybean. Plant Science **153**, 185–190.

Volkov AG, Dunkley TC, Morgan SA, Ruff D, Boyce YL, Labady AJ. 2004. Bioelectrochemical signaling in green plants induced by photosensory systems. Bioelectrochemistry **63**, 91–94.

Wang Y, Bao Z, Zhu Y, Hua J. 2009. Analysis of temperature modulation of plant defense against biotrophic microbes. Molecular Plant-Microbe Interactions **22**, 498–506.

Wang W, Vinocur B, Altman A. 2003. Plant responses to drought, salinity and extreme temperatures: towards genetic engineering for stress tolerance. Planta

218, 1–14.

Wang WX, Vinocur B, Shoseyov O, Altman A. 2001. Biotechnology of plant osmotic stress tolerance: physiological and molecular considerations. Acta Horticulturae **560**, 285–292.

Westgate ME, Boyer JS. 1984. Transpiration - and growth-induced water potentials in maize. Plant Physiology **74**, 882–889.

Whitehead D. 1998. Regulation of stomatal conductance and transpiration in forest canopies. Tree Physiology **18**, 633–644.

Whitehead D, Livingston NJ, Kelliher FM, Hogan KP, Pepin S, McSeveny TM, Byers JN. 1996. Response of transpiration and photosynthesis to a transient change in illuminated foliage area for a *Pinus radiata* D. Don tree. Plant, Cell and Environment **19**, 949–957.

Wortemann R, Herbette S, Barigah TS, Fumanal B, Alia R, Ducousso A, Gomory D, Roeckel-Drevet P, Cochard H. 2011. Genotypic variability and phenotypic plasticity of cavitation resistance in Fagus sylvatica L. across Europe. Tree Physiology **31**, 1175–1182.

Wu T, Zong XKX. 2011. Expression analysis of five maize MAP kinase genes in response to various abiotic stresses and signal molecules. Molecular Biology Reports **38**, 3967–3975.

Xiong L, Zhu J. 2003. Regulation of abscisic acid biosynthesis. Plant Physiology **133**, 29–36.

Xu P, Chen F, Mannas JP, Feldman T, Sumner LW, Roossinck MJ. 2008. Virus infection improves drought tolerance. New Phytologist **180**, 911–921.

Yao C, Moreshet S, Aloni B. 2001. Water relations and hydraulic control of stomatal behaviour in bell pepper plant in partial soil drying. Plant, Cell and Environment **24**, 227–235.

Zebelo SA, Maffei EM. 2012. Signal transduction in plant-insect interactions: from membrane potential variations to metabolomics. In: Volkov AG, ed. Plant electrophysiology. Berlin, Germany, 33–63.

Zebelo SA, Maffei ME. 2015. Role of early signalling events in plant-insect interactions. Journal of Experimental Botany **66**, 435–448.

Zhang J, Davies WJ. 1989. Abscisic acid produced in dehydrating roots may enable the plant to measure the water status of the soil. Plant, Cell and Environment **12**, 73–81.

Zhang J, Davies WJ. 1991. Antitranspirant activity in xylem sap of maize plants. Journal of Experimental Botany **42**, 317–321.

Zhang J, Jia W, Yang J, Ismail AM. 2006. Role of ABA in integrating plant responses to drought and salt stresses. Field Crops Research **97**, 111–119.

Zhang C, Xie Q, Anderson RG, *et al.* 2013. Crosstalk between the circadian clock and innate immunity in Arabidopsis. PLoS Pathogens **9**, 1–14.

Zhu JK. 2001. Cell signaling under salt, water and cold stresses. Current Opinion in Plant Biology **4**, 401–406.

Zimmermann MH. 1983. Xylem Structure and the Ascent of Sap. New York: Springer Verlag.

Zimmermann MH, Brown C. 1971. Trees: strucutre and function. Berlin, New York: Springer-Verlag.

Zimmermann MR, Maischak H, Mithoefer A, Boland W, Felle HH. 2009. System potentials, a novel electrical long-distance apoplastic signal in plants, induced by wounding. Plant Physiology **149**, 1593–1600.

Zvereva EL, Kozlov M V. 2006. Consequences of simultaneous elevation of carbon dioxide and temperature for plant-herbivore interactions: a metaanalysis. Global Change Biology **12**, 27–41.

CHAPTER 3

SIGNAL COORDINATION BEFORE, DURING, AND AFTER STOMATAL CLOSURE IN RESPONSE TO DROUGHT STRESS

3.1 Introduction

Plant survival during periods of drought stress is contingent upon multiple mechanisms that aid the plant in reducing water loss and accessing water resources. As a result, plants have developed a plethora of physiological and anatomical adaptations that enable them to respond to changes in water availability. Among these adaptations, stomata retain a very important role in regulating leaf-level water loss to the atmosphere thus impacting whole plant water balance (Franks *et al.*, 2007). Plant stomatal regulation entails the opening of the stomata to maximize photosynthetic capacity (Farquhar & Sharkey, 1982) and the closing of stomata to minimize water loss through transpiration (Sperry *et al.*, 2017). Therefore, stomatal control contributes to xylem water column maintenance and is the foundation for optimizing rates of transpiration (Tyree & Sperry, 1989). On a cellular level, stomatal response has been examined in detail and is well reviewed (Roelfsema & Hedrich, 2005; Kollist *et al.*, 2014). However, on a whole plant level, the underlying coordination of signal types preceding stomatal closure remains unclear, as is the contribution of each signal type and its interactions with stomatal conductance during drought stress of varying intensities.

Three types of plant signals (chemical, hydraulic, and electrical) are known to regulate stomatal behavior in response to internal and external stimuli such as changes

in atmospheric relative humidity and soil moisture, yet signal integration is highly complex and not well understood (e.g. Huber & Bauerle 2016). In various systems, each of these three signal types has been proposed as the primary contributor to stomatal closure (Zhang & Davies, 1989; Fromm & Eschrich, 1993; Christmann *et al.*, 2007). The involvement of chemical signals in stomatal closure has been studied extensively (e.g. Medvedev, 2005; Murata et al., 2015; Urano et al., 2017). In addition to a variety of different chemical agents (Schachtman & Goodger, 2008), the plant hormone abscisic acid (ABA) plays a dominant role in stomatal control (Munemasa *et al.*, 2015). In many studies, leaf level ABA has been associated with the initiation of stomatal closure in response to water shortages (Mittelheuser & Steveninck, 1969; Schroeder *et al.*, 2001; Holbrook *et al.*, 2002; Geiger *et al.*, 2009). The quick upregulation of ABA biosynthesis upon changes in leaf-to-air vapor pressure deficit (VPD) and drought stress, makes ABA a suitable candidate for actively initiating stomatal closure (McAdam *et al.*, 2016; Sussmilch *et al.*, 2017; Zhang *et al.*, 2018). Yet, the sensed property that initiates ABA synthesis, and the possibility of other signaling pathways controlling stomatal closure is suggested by a few studies that recorded stomatal closure prior to an increase in leaf level ABA concertation (Trejo & Davies, 1991; Tombesi *et al.*, 2015). Hydraulic signals in the form of turgor changes have also been proposed to passively control stomatal aperture. Indeed, research suggests that the hormonal stomatal control mechanism has evolved from a passive hydraulic control mechanism (McAdam & Brodribb, 2015). McAdam and Brodribb (2012) showed that stomatal aperture of ferns and lycophytes (an ancient lineage of land plants) is controlled by hydraulic signals, while the stomatal aperture of more

recently evolved seed plants is governed by the hormonal ABA signal (McAdam & Brodribb, 2012). In general, hydraulic signals, such as leaf turgor changes and cavitation events, have been increasingly recognized for their effect on stomatal response to drought (Salleo *et al.*, 2001; Tombesi *et al.*, 2015; Scoffoni *et al.*, 2017); the hydraulic state of the leaf, including leaf water potential and the loss of leaf turgor, have also been correlated with stomatal closure (Brodribb, 2003). However, none of these signal types and hydraulic parameters have been exclusively identified as the driving factor for stomatal closure, mainly a result of the lack of experimentation on all signal types cohesively.

Electrical signals in plants are the most understudied signal type in stomatal biology, even though they have been shown to play a significant role in coordinating various physiological processes (Fromm & Lautner, 2007). The role of electrical signals in stomatal control has been investigated in only a few studies. However, these studies primarily focused on stomatal response after rewatering (Grams *et al.*, 2007) or on stomatal response to heat-induced electrical signals (Kaiser & Grams, 2006). Thus, electrical signals have not been reported in intact plants during the onset of stomatal closure in response to drought stress. A possible interaction between different signal types is shown by studies in which embolism events stimulated electrical signals, and electrical signals were always preceded by hydraulic signals independent of the stressor (Stahlberg & Cosgrove, 1996, 1997). This ‘cross-talk’ between the two signals demonstrates the coordination across signal types and emphasizes the possibility that mechanistically different signals may work collectively to initiate stomatal responses.

Not only is little known about the underlying mechanism(s) of initiation, transduction, and interactions driving the different signal types (Christmann *et al.*, 2013), but it is also unclear if the drought stress magnitude affects the type of signal response within the plant (Correia & Pereira, 1995). For example, chemical signals have been implicated under more moderate drought events (Schachtman & Goodger, 2008), while hydraulic signals dominate under severe drought stresses (Christmann *et al.*, 2007). However, care should be taken in interpreting these results as they were inferred by experiments that sampled only one data point per day and therefore the signal(s) responsible for the onset of stomatal closure, and their interactions, if any, were never directly recorded.

Teasing out the signal interactions that may exist between signal types remains a challenge without a single experiment in which all three signal types are concurrently measured. In this study, we exposed sunflowers to two different drought stress treatments that differed in their intensity, while concurrently measuring chemical, hydraulic, and electrical signals *in situ*. Our aim was to simultaneously measure all three signal types in sunflower plants under two different drought stress intensities in order to investigate the timeline of the appearance and development of the different signal types possibly involved in the onset of stomatal closure. We hypothesized that rapidly induced drought stress magnifies hydraulic signals in the signaling cascade prior to stomatal closure, while the implementation of gradual drought increases hormonal concentrations prior to stomatal closure in sunflower plants.

3.2 Materials and Methods

Plant material:

Sunflower seeds (*Helianthus annuus*, Sunrich Orange (F1) Johnny's Selected Seed, Winslow, ME) were germinated and grown in a baked clay particulate medium (Turface® Athletics MVP Profile, Products, LLC; Buffalo Grove, IL) in 10 cm diameter, 8.4 cm deep pots (volume 400 ml) for 10 weeks under controlled conditions with a day/night regimen of 16/8 hrs. The plants were fertilized twice a week with Jack's 15-5-15 Fertilizer (JR Peters Inc, Allentown, PA), and watered twice a day (9 am and 3 pm) to keep them well hydrated. At the time of the experiment, sunflowers were on average 40 cm tall and had on average 15 leaves with an average leaf area of 750 cm^2 and basal area of 3 cm^2.

Experimental setup and treatments:

Prior to the experiment, sunflowers were watered to ensure that plants were fully hydrated. Then, hydrated potted sunflower plants were placed inside a custom-built Faraday cage to shield and eliminate electrostatic and electromagnetic extraneous noise. A high-pressure sodium lamp (LU 1000 Watt) was used as an artificial light source to ensure the same lighting conditions as in the greenhouse. Plants, in the cage, were kept an adequate distance from the light source to prevent the overheating of leaves. Environmental parameters at the top of the leaf were 28°C, vapor pressure deficit (VPD) 29 mb, and photosynthetic photon flux density (PPFD, 400-700 nm) of 430 μmol m^2 s^{-1}. After attaching all sensors, plants were equilibrated for 1-2 hrs, with the exception of the turgor pressure sensor (due to space limitations) (Fig. 3.1).

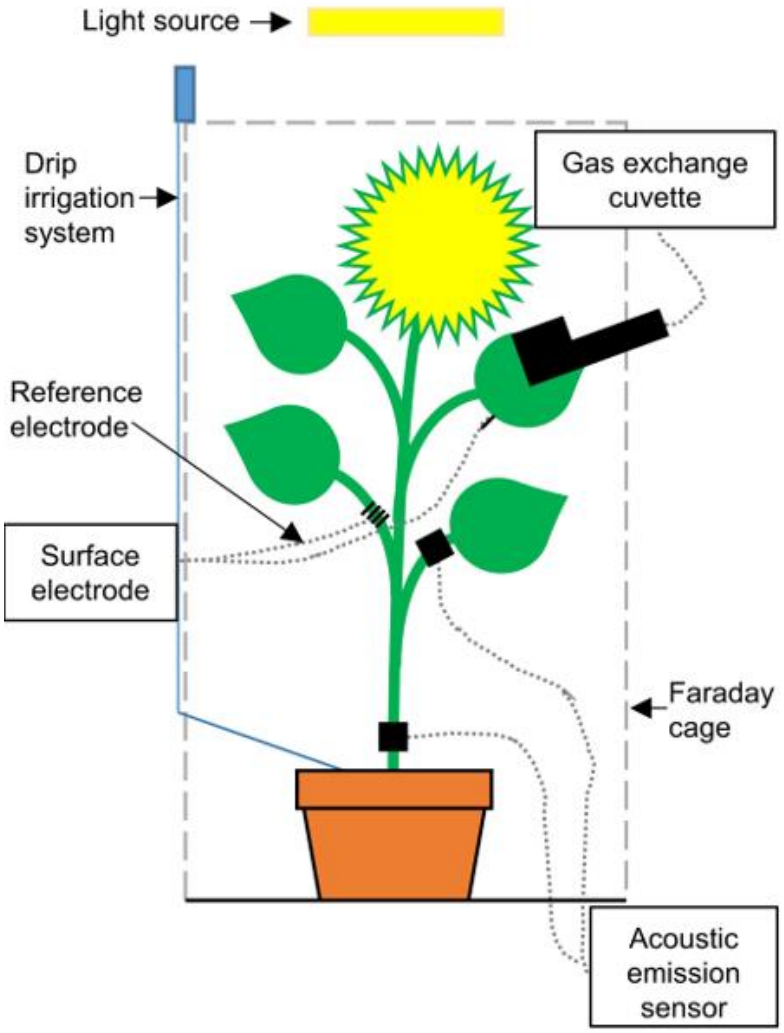

Figure 3.1: Schematic of the experimental setup. For each experimental run, a sunflower plant was placed inside a Faraday cage (dashed gray line) and had various sensors attached to healthy, mature leaves located in the upper-crown, so that simultaneous gas exchange, leaf surface potentials, and acoustic emissions measurements could be made (only leaves with attached sensors are shown in the figure). Using a drip irrigation system, each plant was either a) kept well-hydrated (control), b) exposed to a slow dehydration (NAT), or c) exposed to a rapid water stress treatment by applying a PEG solution to the roots.

Data collection started between 9 am and10 am. All experiments were conducted at ca.

25°C. After the equilibration time, individual plants were exposed to one of the

following three treatments to test if drought stress severity has an effect on the signaling cascade prior to stomatal closure: 1) plants were kept well-hydrated throughout the experiment (control; n=5), 2) a Polyethyleneglycol$_{8000}$ solution (PEG 8000 at 510 g/kg H_2O, equivalent to a -3.0 MPa water potential stress) was added to the plant pot (PEG treatment; n=8), or 3) water was withheld from the roots (NAT treatment; n=8). In the control and the PEG treatments, water or PEG solution was added to the roots at a flow rate of 7 ml/min for ca. 25 min using a custom-built drip irrigation system. PEG 8000 is a polymer that does not penetrate plant roots and therefore used as an osmoticum to induce drought stress in plants (Kaufmann & Eckard, 1971). Continuous measurements were recorded until stomatal conductance decreased to values less than 10 mmol H_2O m^{-2} s^{-1}. Each control experiment was stopped after 4 hours of continuous measurements. To prevent interference with the electrical measurements, all destructive measurements (anatomical, water potential, chemical and conductance loss) were performed on additional sets of sunflowers; one set for Ψ_{leaf} during the experiment, and one set for Ψ_{root}, Ψ_{stem}, and Ψ_{leaf} at the beginning and end of the experiments (n =5 sunflowers per set). Sunflowers in these additional sets were exposed to identical conditions.

Gas exchange measurements:

Stomatal conductance (gs) and photosynthesis (Pn) measurements were measured on an upper canopy fully developed leaf with a portable photosynthesis system (CIRAS-2, PP Systems, Amesbury, MA). The chamber environment was kept constant with the following settings: reference CO_2 of 400 ppm (400 µL/L), ambient VPD (18-23 mb),

flow rate of 200 ml min^{-1}, and PPFD of 1200 μmol m^2 s^{-1}. Gas exchange parameters were recorded every 60 s and running averages over 4-min time intervals were used in the analysis. This time interval reduced the noise of the signal but preserved the signal pattern. The derivative of the data with respect to time was calculated, and the onset of stomatal closure was characterized by three time points (Fig. 3.2), based on the second derivative: 1) time of transient increase in gs and Pn ($I1_{gs\&Pn}$), 2) time of peak gs and Pn ($I2_{gs\&Pn}$), and 3) the subsequent decay of gs and Pn. Gas exchange parameters were stable before the onset of stomatal closure. Therefore, the time at which gs and Pn were equal to the initial value was noted ($I3_{gs\&Pn}$). The decrease in g_S was determined by calculating the half-time required to reach a 50% decrease in gs relative to the maximum gs peak. The length of the transient increase, the time span from $I1_{gs}$ to $I3_{gs}$, was determined as the relative and absolute magnitude change in g_S and Pn between $I1_{gs}$ up to $I2_{gs}$. Gas exchange parameters were normalized among replicates by dividing all signal values within each data set by the maximum signal value within that set (original data see Appendix 1).

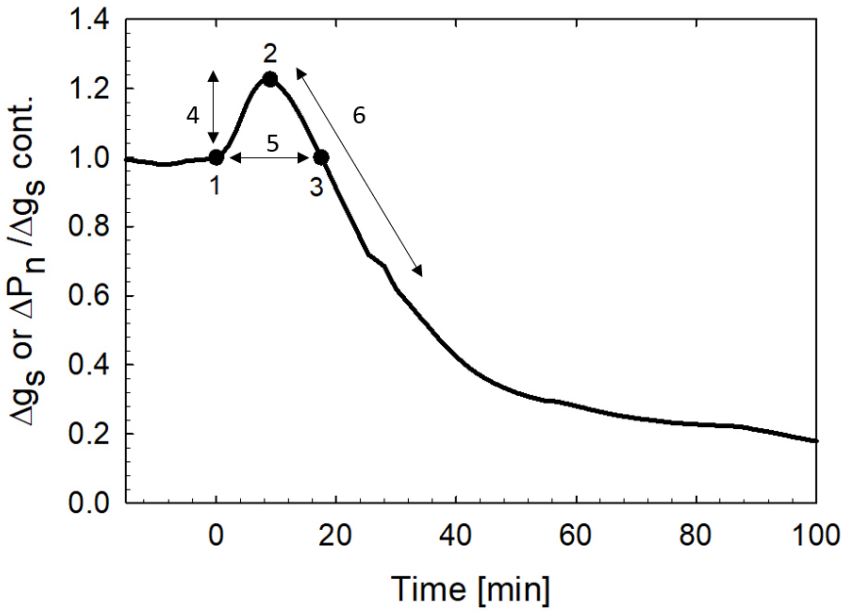

Figure 3.2 Reference points used from stomatal conductance (gs) and photosynthesis (Pn) response during a dry-down period. Changes in gs and Pn (Δgs or ΔPn) relative to control values (Δgs cont.). Stomatal conductance and Pn followed a transient increase before a continual decline. The transient increase is characterized by (1) time of gs and Pn increase ($I1_{gs\&Pn}$), (2) time of peak gs and Pn ($I2_{gs\&Pn}$), (3) time gs and Pn is equal to gs and Pn values before $I1_{gs}$ ($I3_{gs\&Pn}$), (4) the relative and absolute increase of gs and Pn, (5) the length of the Iwanoff Effect, and (6) the decay ½ time of gs and Pn.

Acoustic emission events:

Acoustic emission events (AE) of 1) a fully developed petiole on a leaf subtending the gs measurement leaf, and 2) the base of the main plant stem were recorded over a standard frequency range of 50-200 kHz and analyzed with AE WIN® software (150 kHz R14C transducer; Physical Acoustics, Princeton, NJ). To assure contact between the plant organ and the acoustic sensor, the epidermis of the underside of the petiole and the stem base were gently abraded with a fresh razor blade. A lubricating compound (Sil-Glyde AGS SG-2, American Grease Stick Company, Muskegon, MI) was applied between the plant organ and the sensor. Transducers were connected to

the portable Pocket AE-Power^{TM} system (Physical Acoustics, Princeton Jct, NJ) with an internal amplifier. Events were acquired at a 35 dB threshold. Peak definition time, hit definition time, and sample rate were set to 200 µs and 300 µs, respectively. Settings were adopted from Nolf *et al.* (2015). Data were smoothed using a Butterworth filter (Matlab2010b, The MathWorks, Inc., Natick, Massachusetts, USA) to reduce noise in the data set. AE event activity was calculated by computing the AE rate (AE events min^{-1}). To determine abrupt changes in the AE rate pattern, the increase in AE rate (I_{AE}), the peak AE rate (P_{AE}), and the alleviation of AE (A_{AE}) were calculated based on the second derivative. On a subset of plants, exposed to PEG and NAT treatments, we attached the acoustic sensor to the roots. However, we did not record any AE events in roots during the dry-down treatments.

Organ water potential:

To monitor changes in plant water status throughout the experiment, covered leaf water potential (Ψ_{leaf}) was measured before and after stress imposition at various time points. At each measuring time point, one bagged leaf (equilibrated for 2 hours) per sunflower (n =5), was excised from the plant with a razor blade, and inserted into a water status console (Soilmoisture Equipment Corp., Goleta, CA) (n=5). The pressure was gradually increased (100 kPa min^{-1}) until the balancing pressure was reached. Because the measurement time points did not always exactly coincide with the onset of stomatal closure, Ψ_{leaf} at the onset of stomatal closure was determined by linear interpolation between the closest measurement points (Ψ_{leaf} over time please see appendix 2). Additionally, Ψ_{leaf}, stem water potential (Ψ_{stem}) and root water potential

of the woody root (Ψ_{root}) were measured with a water status console on an additional set of plants (n =5) at the beginning and the end of each treatment to characterize changes in whole plant Ψ. Ψ_{stem} was measured on a 20 cm long shoot segment (cutting locations 2 cm and 22 cm above the soil) and Ψ_{root} was measured on one woody root per plant.

Indirect changes in leaf bulk turgor pressure:

On a subset of sunflower plants, we noninvasively and continuously monitored changes in leaf turgor pressure by measuring the pressure transfer function (P_p) through a leaf patch (area 4 x 2.5 cm^2) of an intact leaf (ZIM probes, ZIM Plant Technology GmbH, Henningsdorf Germany). P_p is inversely correlated to the leaf turgor pressure (Zimmermann et al. 2008 and 2010), thus changes in P_p, indirectly measures relative changes in leaf turgor. After placing the probes gently onto one fully developed leaf of a well-hydrated sunflower plant (n=5), sunflowers were equilibrated for ~2 hours before applying the PEG solution. The probe output pressure was recorded every 30 seconds. Gas exchange was measured simultaneously to correlate the onset of P_p to the onset of stomatal closure. P_p recordings and gas exchange measurements were analyzed by first smoothing the data (applying a 4-minute running average), then identifying the time at which sudden signal changes occurred (the second derivative of each data set). Finally, P_p change time points and the time of gs increase were averaged among replicates.

Hydraulic conductivity loss:

Hydraulic vulnerability curves (percent loss in conductivity, PLC curves) were calculated to examine the relationship between hydraulic conductivity loss in stems and decreasing water potential (increasing drought stress) according to the static centrifuge technique (Pockman *et al.*, 1995; Alder, 1997). Several studies have shown that this methodology is not prone to the open vessel artifact (Jacobsen & Pratt, 2012; Sperry *et al.*, 2012; Hacke *et al.*, 2014). Therefore, this technique was chosen since maximum vessel length of sunflower stems (23 cm, Ahmad *et al.*, 2018) exceeded the sample length that was examined in this study. Fourteen-cm-long stem segments of well-watered sunflowers were cut under water and fixed in a custom-made centrifuge rotor (Sorvall RC-5C; Thermo Fisher Scientific, Waltman, MA, USA). Stems were spun from -0.5 MPa to -5.5 MPa in 0.5 MPa increment steps for 4 min each. Between the centrifugation steps, the hydraulic flow rate was measured with a custom-built low-pressure flow meter (Melcher *et al.*, 2012). Both ends of each stem segment were attached to the hydraulic apparatus using thick-walled platinum coated silicon tubing. Samples were perfused with (0.1 µm) filtered 20 mM KCl solution. Hydraulic conductance was measured using a hydraulic pressure difference across the sample of 3kPa and the flow rate was measured every 10 s with an analytical balance (HR-200, A&D, Elk Grove, Il) interfaced to a computer. Measurements were stopped when the flow rate (F, kg s^{-1}) was stabilized. Hydraulic conductivity (K_h) was determined by:

$$K_h = F*L / \Delta P \qquad \text{(Eqn 3.1)}$$

where, L is the length of the sample, and ΔP is the hydraulic pressure gradient (Melcher *et al.*, 2012). PLC was calculated by:

$$PLC = 100 \times (1-(K_h/K_{in})) \quad \text{(Eqn 3.2)}$$

Where K_{in} is the initial hydraulic conductivity. The value that reduced K_h by 50% (P_{50} value), was determined from vulnerability curves following the protocol detailed in (Sparks & Black, 1999; Domec & Gartner, 2001).

An additional PLC curve based on the staining of functional xylem vessels was performed to confirm the absence of an open vessel artifact. Stem segments (20 cm-long) of well-watered, equilibrated sunflowers (bagged for 12 hours), were cut under water and centrifuged to steps of defined water potentials (see above, n=4). Stems were then perfused at 3 kPa with pre-filtered (0.1 μm) safranin (w/v) solution (Saint-Gobain [Formerly ZenPure], Manassas, VA) for 3 min using a hydraulic apparatus (described above). After 3 mins, 7 cm of the infusion end of the stems were removed, and the remaining stained stem segments were sliced at a 40 μm cutting distance with a sliding microtome (American Optical, 680 sliding microtome). Digital images of cross-sections were taken (Olympus Imaging Corp, Tokyo, Japan) at 100x magnification using a compound light microscope (Carl Zeiss Microscopy, Axioskop 2 plus Zeiss, Thornwood, NY, USA). Stained and unstained vessels and vessel perimeters were measured (ImageJ 1.48v, National Institute of Health, Bethesda, MD, USA). Vessel count data was fitted with an exponential sigmoidal equation (see below) and the corresponding P_{50} calculated. Hydraulic weighted diameter (Hagen-Poiseuille law, Zimmermann, 1983) was calculated by assuming that vessels were circular, and the area (A) was converted into diameter (D) using the following relationship (as described in (Cai & Tyree, 2010))

$$D = \sqrt{(A}/4\pi). \quad \text{(Eqn 3.3)}$$

Vulnerability Curve fitting

Vulnerability curves were constructed by either plotting PLC, or the percent of stained vessels/ diameter of hydraulic weighted vessels against tissue water potential, respectively. The data was fitted with an exponential sigmoidal equation of:

$$PLC = 100/ (1 + \exp(a(\Psi - b))) \quad \text{(Eqn 3.4)}$$

Where, a and b are fitting parameters, whereby a describes the slope of the curve and b represents the position of the curve on the x-axis at 50% PLC (Pammenter & Van der Willigen, 1998).

Air-seeding pressure of root, stem, and leaf organs:

Roots and petioles were too short to perform PLC curves with the centrifuge technique. Therefore, we determined the air-seeding threshold, the required pressure to press gas across bordered pit membranes, to identify the organ specific water potential that induces massive cavitation events. These thresholds were then compared to recorded AE events in petioles and stems. Single-vessel air injection pressure threshold of roots (n=16), petiole-leaf veins (n=10), and stems (n=13) was determined using the single vessel injection technique (Melcher *et al.*, 2003). Well-watered sunflowers were double bagged with a wet paper towel and equilibrated overnight. Organ segments were excised under water using a razor blade. Thick walled glass microcapillary tubes (Item# 1B150F-6 World Precision Instruments, Inc Sarasota, CA) were randomly inserted into an open vessel lumen of medium to large xylem vessels via a micromanipulator and 50x stereo microscope (SZ-STB2, Olympus Tokyo) and glued to the segment using a fast-setting cyanoacrylic glue (Locolite superbonder 409,

Locolite Corp., Rocky Hill, CA) and an accelerator (Locolite 712, Locolite Corp., Rocky Hill, CA).

To measure the pressure threshold required to force compressed nitrogen gas across inter-vessel bordered pit membranes, the capillary end that was not connected to the plant segment was attached to HPLC tubing using compression fittings and attached to a pressure chamber system (Model 1000, PMS Instrument Company, Corvallis, OR). The glass tube and sample were placed under water and pressure was applied (100 kPA min^{-1}) until tiny bubbles were observed exiting the downstream end of the sample. Measurements of air seeding pressures lower than 100 kPa were discarded. Vessels with such low air pressure are most likely lacking pit membranes throughout the length of the organ segment. Different vessel lumen diameters were probed to eliminate large-vessel bias and ensure that measurements were made across vessels of different diameters

Electrical Signal

Electrical surface potentials of fully developed leaves were recorded relative to a reference electrode, positioned at a subtending petiole of the measurement leaf. The Ag/AgCl silver wires (0.5mm diameter; World Precision instruments, Inc., Sarasota, Fl) were connected to the head stages, which were in turn connected to a high impedance dual channel differential electrometer (Electrometer model FD 223, World Precision Instruments, Sarasota, FL). The connection between leaf surface and AgCl wire was secured by a neurodiagnostic electrode paste (Ten20 conductive, Weaver and Company, Aurora, CO). Data sampling was performed via Minidigi 1A at a sampling

interval of 10 ms. Data acquisition and analysis was performed with PClamp 10.3 (Molecular devices, Sunnyvale, CA). Changes in the data pattern was determined based on the second derivative.

Leaf Abscisic Acid:

At time intervals matching those for Ψ_{organ} measurements, two 0.5 cm^3 leaf punches were taken from different leaves and submerged in 1.5 ml of 80% ice cold ethanol and stored at -30°C. Before analyzing, the sample disk-ethanol solution was well mixed at room temperature for 2 hours, and an aliquot of 300 µm was transferred into a 96 well plate and dried at 40°C. Samples were redissolved in 30% methanol and cleaned using reverse-phase chromatography in columns packed with 25 mg of 40 µm C_{18}-silica material (Supelco Discovery® DSC-18 SPE, Millipore Sigma, Darmstadt, Germany). Samples were analyzed with an enzyme-linked immunosorbent assay (ELISA) (Setter & Parra, 2010; Setter, 2012). In this method, the ABA concentration of the sample was determined by an inverse relationship between the [ABA] in the sample and a known concentration of immobile antibody-ABA complex. Wells in a microplate were coated with a constant amount of protein-ABA conjugate, while the sample with an unknown [ABA] was dissolved in the wells. An Anti—ABA primary antibody (mouse monoclonal antibody) was added to the wells to competitively bind to the immobilized protein-ABA conjugates as well as the dissolved ABA. After washing the dissolved ABA from the wells, a secondary antibody that targets the mouse antibody tagged with an enzyme (alkaline phosphatase) was added to the wells. The secondary antibody-enzyme complex reactions resulted in a color change that was quantified

with an optical plate reader. To improve accuracy, we performed two ELISA technical replicates for each sample and used their averages for ANOVA

Statistical analysis:

Statistical differences between organ water potentials and treatments were tested with a two-way ANOVA using treatment, organ, and organ x tissue as fixed effects, and sunflower as a random effect. The air seeding threshold of the plant organs was compared using a one-way ANOVA with organ (root, stem, petiole) as a fixed effect. Post-hoc comparisons between groups for organ potentials as well as the air seeding threshold data set were made using Tukey's HSD to control for multiple comparisons. Due to the small sample size, comparisons between signal time points (gs and Pn) were made with the nonparametric Wilcoxson rank test. Differences in leaf ABA levels between treatments by time were calculated in a linear mixed effect model with fixed effects of time, treatment, and time x treatment and a random plant as well as random plant x time effect. Comparisons between treatments were made at each time point using the Holm adjustment for multiple comparisons or Bonferroni adjustment. A log transformation was applied for ABA data in the NAT treatment to fulfill the model assumptions. However, data is presented in the non-transformed version. Statistical analysis was performed in JMP Pro 12 (SAS Institute Inc., Cary, NC) for all but the ABA analysis which was performed in R version 3.3.1 (R Core Team, 2006) with the packages: lsmeans, dplyr, lme4, and lmerTest. All tests were performed with a probability level of $P < 0.05$).

3.3 Results

Gas exchange parameters:

Under well-watered conditions (control), sunflower stomatal conductance (gs) and net photosynthesis (Pn) remained stable for the duration of the experiment (i.e. up to about 3 hours) (Fig. 3.3a). In contrast, in both the fast (PEG) and slow (NAT) drought stress treatments, sunflower stomatal conductance (gs) initially increased prior to showing a steady decline, thereby displaying a transient response commonly referred to as the Iwanoff or Wrong Way Effect (Iwanoff 1928; Fig. 3.3b-e). The time at which gs and Pn increased ($I1_{gs\ \&Pn}$), peaked ($I2_{gs\&Pn}$), and returned to the original value ($I3_{gs\&Pn}$), occurred significantly earlier in the PEG than in the NAT treatment ($P < 0.0001$ for each time point). Yet, gs and Pn changed in parallel within each treatment (Fig. 3.3b-e). In the fast dry-down treatment, $I1_{gs}$ occurred 4.9 ± 1.8 min after the addition of PEG. The time span from the beginning to the end of the Iwanoff effect ($I1_{gs}$ until $I3_{gs}$) was significantly shorter in the PEG (18.4 ± 1.1 min) compared to the NAT (32.0 ± 5.0 min) treatment ($P = 0.023$). The relative increase in gs within the PEG treatment was double that of the NAT treatment ($P = 0.007$), despite occurring in half the time. The duration between $I2_{gs}$ to $I3_{gs}$ did not differ between the treatments. However, the duration to reach a 50% decline in gs relative to $I2_{gs}$ was half that of the PEG treatment (23.2 ± 4.4 min) in comparison to the NAT treatment (49.4 ± 7.3 min; $P = 0.023$).

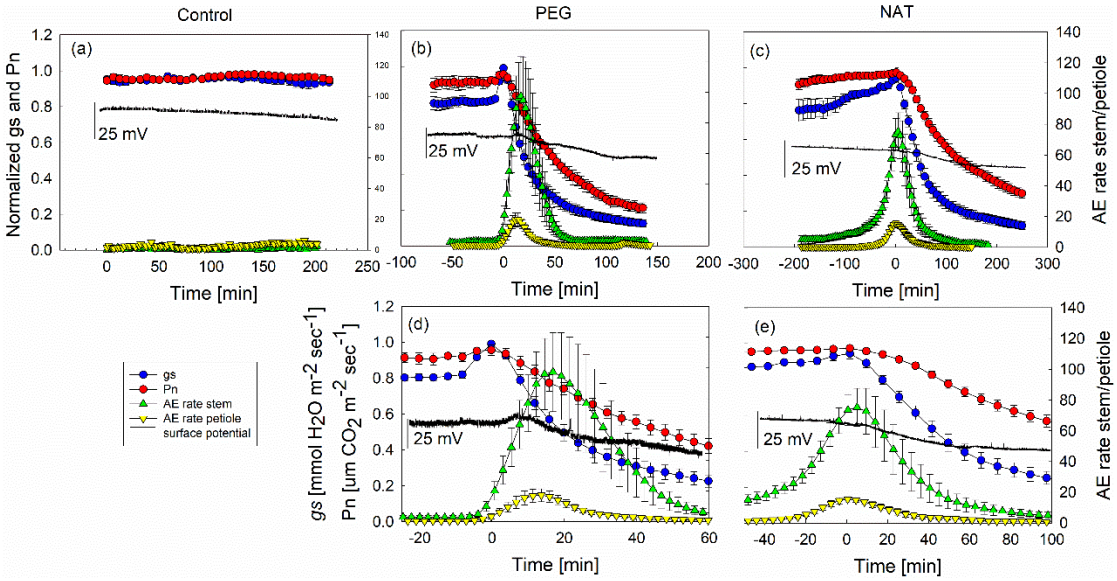

Figure 3.3: Mean and SE of stomatal conductance (gs; blue circles), photosynthesis (Pn; red circles), acoustic emission rates (AE rates) of stem (green triangles) and petioles (yellow inverted triangles), and surface electrical potential changes (black line) measured on sunflower stems and petioles. Well-hydrated control plants (n=5), panel (a), panels (b) and (d) are the fast dry-down PEG treatment (n=8), and natural dry-down treatment (NAT) panels (c) and (e) (n = 8). Measurements for the entire duration of the experiment are shown in panels (a), (b), and (c). Panels (d) and (e) are the same data but zoomed into the period in time when the stomata were responding. For clarity, only one representative surface electrical potential response is shown on each graph (solid line). The timeline for all experiments was adjusted so that the peak of gs was arbitrarily set to 0.

Hydraulic signal:

The sudden increase (I_{AE}) in the acoustic emission rate (AE rate), the peak of AE rate (P_{AE}), and the sudden alleviation of the AE rate (A_{AE}) in petioles and stems did not vary significantly within each treatment (Fig. 3.3b-e). The AE rate increased ca. 13 min before $I1_{gs}$ in the PEG treatment and between 40-70 min before $I1_{gs}$ in the NAT treatment ($P < 0.0001$). After I_{AE}, the AE rates of both the petiole and stem increased continuously until they peaked concurrently with $I2_{gs}$. The stem AE rates were significantly higher than in the petiole at P_{AE} for both dry-down treatments (P =

0.0002). After AE rates of both the petiole and stem peaked, they continuously decreased and leveled off around the same time (ca 40 min).

Electrical signals:

There was no difference between $I1_{gs}$ and the fast decline of the surface potential in both dry-down treatments (Fig. 3.3b-e). The signal pattern of the surface potential during the dry-down treatments could be distinguished into two declining phases, a fast declining phase, followed by a slow declining phase. The fast declining phase (121.59 ± 21.76 min) in the NAT treatment took twice as long as in the PEG treatment (57.85 ± 6.81 min, $P = 0.014$). However, despite this time difference, the total shift of the surface potential (around 14 mV) did not differ between the two dry-down treatments. The shift from the fast declining to the slow declining phase was recorded 49.19 ± 8.65 minutes after $I2_{gs}$ for the PEG treatment and 99.79 ± 24.50 min after $I2_{gs}$ for the NAT treatment ($P = 0.033$).

Organ water potential, turgor loss point, and indirect changes in leaf bulk turgor pressure:

When gs peaked ($I2_{gs}$), plants from both drought treatments displayed a significant drop in Ψ_{leaf} compared to Ψ_{leaf} under well-hydrated conditions (Table 3.1). After $I2_{gs}$, only Ψ_{leaf} of the PEG treatment continued to decrease until $I3_{gs}$ (Table 3.1). Thus, Ψ_{leaf} at $I3_{gs}$ was significantly different between the two dry-down treatments (P =0.007).

Table 3.1: Leaf water potentials (Ψ_{leaf}) at the onset of stomatal closure for a fast dry-down treatment using a PEG solution (PEG) versus a natural dry-down treatment (NAT; n=5, respectively). Letters indicate significance level ($P \leq 0.05$). The timing of the transient increase in stomatal conductance (gs) followed by its continual decline was monitored in both dry-down treatments. The time length of the increase and decline in gs was calculated based on three different time points: 1) time of gs increase ($I1_{gs}$), 2) time of peak gs ($I2_{gs}$), 3) time gs is equal to gs values before $I1_{gs}$ ($I3_{gs}$). The time is the amount of time that passed between two consecutive measurement points between $I1_{gs}$ and $I2_{gs}$, and $I2_{gs}$ and $I3_{gs}$.

	Treatment			
	PEG		**NAT**	
	Ψ_{leaf} (MPa)	Time (min)	Ψ_{leaf} (MPa)	Time (min)
$I1_{gs}$	-0.38 ± 0.02 [c]		-0.41 ± 0.03[c]	
		9.3 ± 0.7		18.3 ± 2.3
$I2_{gs}$	-0.64 ± 0.02 [b]		-0.56 ± 0.03[b]	
		9.0 ± 0.6		13.4 ± 3.6
$I3_{gs}$	-0.75 ± 0.02 [a]		-0.59 ± 0.04[b]	

Organ water potentials at the end of the experiment differed significantly within both treatments (Fig. 3.4). In the PEG treatment, Ψ_{leaf} (-0.97 ± 0.01 MPa) was seven-fold more negative than Ψ_{stem} (-0.15 ± 0.03 MPa) and 8.8-fold more negative than Ψ_{root} (-0.12 ± -0.02 MPa) ($P < 0.0001$ respectively). In the NAT treatment Ψ_{leaf} (-1.35 ± 0.02 MPa) was 5.8-fold more negative than Ψ_{stem} (-0.24 ± 0.01 MPa) and 17.5-fold more negative than Ψ_{root} (-0.09 ± 0.018 MPa) ($P < 0.0001$ respectively). Ψ_{stem} and Ψ_{root} did not differ at the end of the experiment for either the control or the PEG treatment but were significantly different in the NAT treatment ($P = 0.0002$). Changes in the patch pressure (ΔP_p) in leaves of the PEG treatment were recorded 4.61 ± 1.15 min prior to $I1_{gs}$ ($P = 0.0159$). Shortly thereafter, gs increased and ΔP_p increased 0.82 ± 0.2 kPa (for data timeline see Appendix 3).

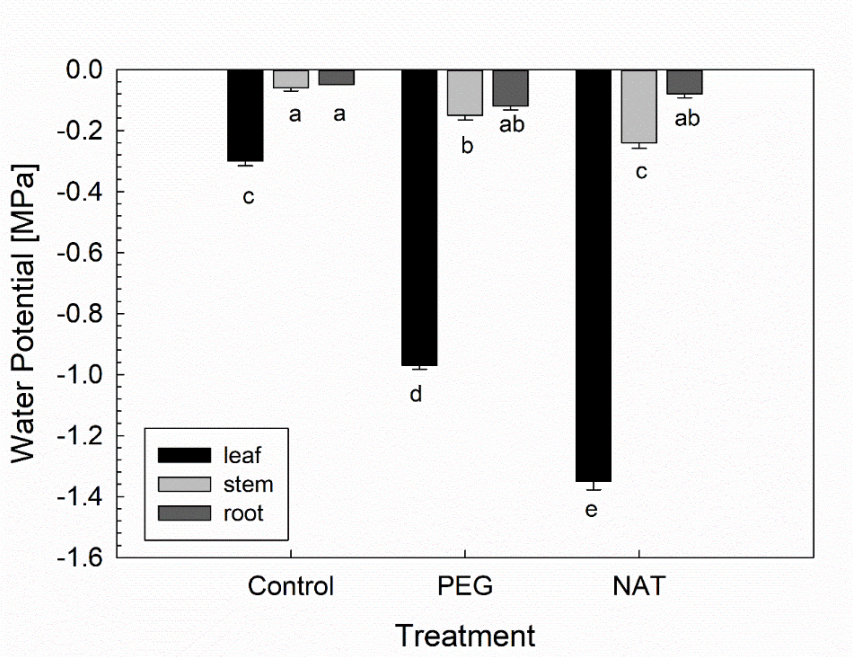

Figure 3.4: Mean and SE of root, stem, and covered leaf water potential (MPa), measured on sunflower plants (n = 5) at the end of a control treatment (well-hydrated) or at the end of the experiment of one of the following dry-down treatments: 1) fast dry-down treatment (PEG), or 2) natural dry-down treatment (NAT). Significant differences are indicated with letters ($P \leq 0.05$).

Hydraulic conductivity loss during drought stress intensities:

Comparison between Ψ_{stem} and PLC curves calculated based on hydraulic conductivity loss and from vessel staining methods indicated that the sunflower plants operated at around 95% of their full hydraulic capacity under well-watered conditions (Ψ_{leaf} = -0.35 MPa, Ψ_{stem} = -0.1 MPa; Fig. 3.4 and 3.5).

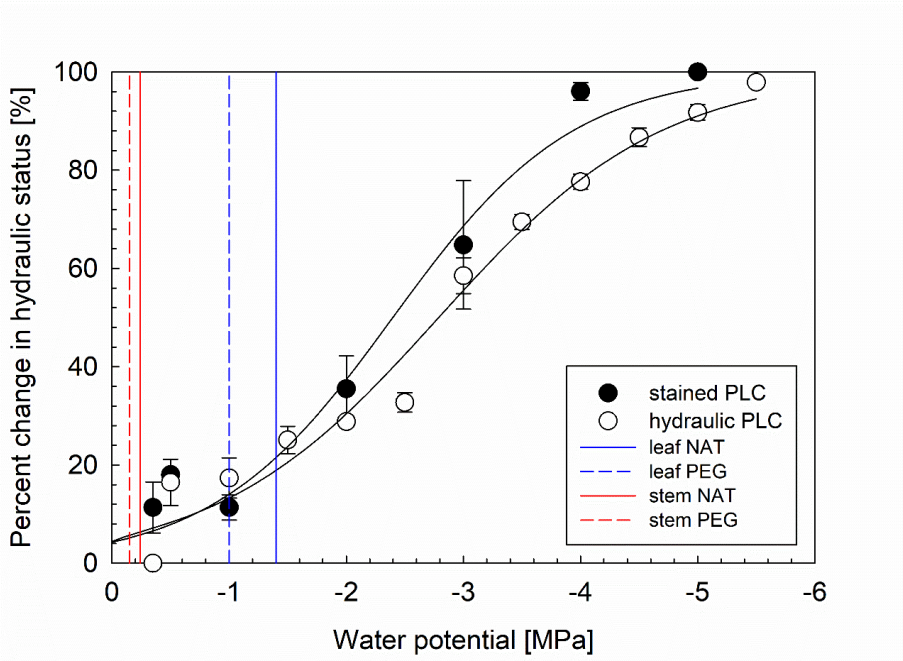

Figure 3.5: The mean and SE of percent loss in hydraulic conductance (PLC, open circles) and the number of embolized vessels, determined from visually counting embolism from staining methods (solid circles), are shown (n=5, respectively). The water potential values of leaves (blue vertical lines) and stems (red vertical lines) at the end of the NAT and the PEG treatments are shown for reference.

Furthermore, the comparison of Ψ_{stem} at the end of both dry-down treatments to PLC curves revealed that stems suffered only minimal hydraulic conductivity loss (~ 1%) during the entire experiment (Fig. 3.4 and 3.5). Finally, vessel vulnerability curves showed that sunflower stems would have sustained a 50% hydraulic conductance loss (P_{50}) between -2.5 MPa to -2.9 MPa (Fig. 3.5). However, sunflower stems in both dry-down experiments never reached the Ψ_{stem} required to induce P_{50} during the experiment.

Air seeding pressure:

Air-seeding threshold comparisons showed that sunflower stems could withstand a two-fold higher tension compared to roots and petioles ($P < 0.0001$) before embolisms would spread across bordered pit membranes (-2.3 ± 0.1 MPa). There were no observed significant differences between air-injection pressures required to spread embolisms across bordered pit membranes in roots and petioles (Fig. 3.6).

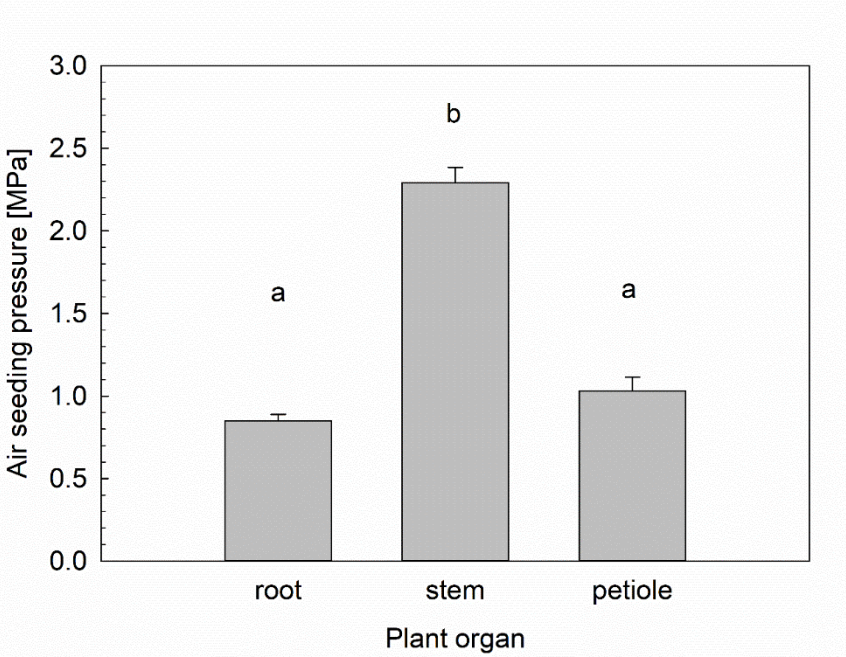

Figure 3.6: **:** Mean and SE pressure required to force gas across bordered pit membranes in the xylem of sunflower petioles, roots, and stems (n =10 for each organ system). Significant differences are represented by letters (ANOVA, $P \leq 0.05$).

Leaf Abscisic Acid:

The onset of stomatal closure occurred before any detectable increase in leaf [ABA] (Table 3.2 and 3.3). Comparison between well-watered sunflowers and sunflowers exposed to PEG showed an interaction between treatment and time ($P = 0.013$). Leaf

[ABA] at time points throughout the experiment were compared between sunflowers that were exposed to either drought treatment or the control (Controls were run parallel with drought treatment, respectively).

The leaf [ABA] of sunflowers in the PEG treatment was about two-fold higher than the control at 60 min ($P = 0.01$) and 120 min ($P = 0.043$) (Table 3.2). In the NAT treatment, leaf [ABA] increased about 2.5-fold 8 hours after the experiment start compared to the leaf [ABA] in the control ($P = 0.04$). Additionally, we did not find any differences between leaf [ABA] throughout the experiment compared to leaf [ABA] at the beginning of the experiment within either drought treatment.

Table 3.2: Mean and SE of leaf ABA (pmol cm^{-2}) in control (continuously watered) and water stressed (-3.0 MPa PEG solution added at time=0) sunflower plants (n=5, respectively). Pairwise comparisons between well-watered controls and PEG treatments at each time point, were calculated and adjusted using a Holm correction. Asterisks indicate significant ($P \leq 0.05$) differences between treatments at a given time point (ns, not significant).

.		Leaf level [ABA]		
Time point	Time (min)	Well-watered control	Drought (PEG)	Comparison (p-values)
0	-30	0.29 ± 0.06	0.43 ± 0.08	ns
1	0	0.29 ± 0.03	0.47 ± 0.05	ns
2	5	0.46 ± 0.07	0.36 ± 0.10	ns
3	20	0.46 ± 0.12	0.35 ± 0.09	ns
4	30	0.26 ± 0.05	0.37 ± 0.07	ns
5	60	0.29 ± 0.03	0.62 ± 0.09	0.010
6	120	0.33 ± 0.07	0.60 ± 0.05	0.043

Table 3.3: Mean and SE of leaf ABA (pmol cm^{-2}) in control (continuously watered) and naturally dried down sunflower plants (NAT) (n=5, respectively). Pairwise comparisons between treatments at each time point were calculated in a linear mixed effect model and adjusted using the Holm correction. Asterisks indicate significant ($P \leq 0.05$) differences between treatments at a given time point. P values were calculated with log-transformed data to satisfy model assumptions (ns, not significant).

Time point	Time (hr)	Leaf [ABA]		
		Well-watered control	Drought (NAT)	Comparison (p-values)
0	0	0.45 ± 0.10	0.67 ± 0.10	ns
1	1	0.70 ± 0.06	0.50 ± 0.07	ns
2	2	0.41 ± 0.08	0.40 ± 0.06	ns
3	3	0.57 ± 0.12	0.58 ± 0.09	ns
4	4	0.58 ± 0.12	0.43 ± 0.05	ns
5	5	0.65 ± 0.05	0.57 ± 0.13	ns
6	6	0.55 ± 0.09	0.55 ± 0.12	ns
7	7	0.50 ± 0.08	0.82 ± 0.07	ns
8*	8	0.57 ± 0.05	1.48 ± 0.30	0.04

3.4 Discussion

Signaling timeline at the onset of stomatal closure

Our simultaneous recording of hydraulic, chemical, and electrical signals revealed that AE rates in petioles and stems, and changes in the patch pressure (P_p) occurred prior to any change in stomatal conductance across treatments, suggesting that these properties may serve as signals driving stomatal closure. It is likely that the bulk leaf turgor decreased prior to stomatal closure. However, because bulk P_p was measured on a small leaf area, and because large water potential gradients can occur within leaves (Buckley *et al.*, 2015), localized regions and individual cells within the leaf with even lower turgor pressure are possible. We recognize that the observational nature of our

experiment does not permit a proven mechanistic linkage between signal types and stomatal closure. Therefore, bulk turgor changes should be considered as an indicator for leaf hydraulic changes and further investigated to quantify cellular turgor changes.

Similar to previous experiments, we found the first registered response in stomatal conductance to drought stress initiation in both dry-down treatments was a short-lived sudden increase (Wrong Way or Iwanoff effect) followed by a continual decline as drought conditions persisted (Iwanoff, 1928; Paoletti, 2005; Kaiser & Grams, 2006; Kaiser & Legner, 2006; Powles *et al.*, 2006; Hoshika *et al.*, 2013; Kaiser & Paoletti, 2014) (Fig. 3.2 and 3.3). Moreover, changes in surface potentials and the peak of stem and petiole AE events were concurrent with $I2_{gs}$, also demonstrating a close correlation with stomatal closure (Fig. 3b,c). The observed differences in stem and petiole AE rates might have been caused by tissue volume differences between the two organs. Stems contain greater biomass, including fibers and parenchyma cells, compared to the petioles and as a result, offer more potential sources of AE events.

Our measurements of AE events in roots did not detect any events in either dry-down treatment, most likely because roots remained hydrated (Fig. 3.4). Electrical signals occurred when AE rates and gs peaked (Fig. 3.3b,c), indicating a close connection between the two signal types and supporting previous findings that show a similar correlation (Stahlberg & Cosgrove, 1996, 1997). However, the temporal resolution of our data set, does not allow us to pinpoint what hydraulic threshold caused the shift in surface potentials, nor decipher if the shift was a result of increased AE rates or turgor changes. While outside the scope of this experiment, the precise connection between the shift in surface potential and peak gs also remains unknown.

However, stomatal closure itself is executed by fluxes of osmotically active solutes that lead to plasma membrane depolarization (Kollist *et al.*, 2014), which could have been elicited the surface potential shift that we observed, making the exact role of surface potential fluctuations unknown at this time.

The loss in bulk leaf turgor pressure, as indicated by P_p measurements, preceded stomatal closure, while increases in leaf ABA levels were not detected until after stomatal closure, or after the experiment ended (Fig. 3.3b,c, Table 3.2 and 3.3). The delayed increase in leaf ABA (after the onset of stomatal closure) could support the idea that ABA maintains stomatal closure instead of initiating it (Trejo & Davies, 1991; Tombesi *et al.*, 2015). Yet, we cannot rule out the potential role that ABA plays in stomatal regulation since we measured ABA in the bulk leaf rather than ABA in localized cells, and we did not directly measure ABA relocation within leaves (Zhang & Outlaw, 2001; Wilkinson & Davies, 2008). Moreover, recent studies have shown that ABA in leaves is synthesized de novo as opposed to relocated (McAdam *et al.*, 2016; Zhang *et al.*, 2018). It is possible that the use of bulk-leaf ABA extracts masks localized increases in ABA due to de novo synthesis at sites of evaporation in leaf mesophyll cells near guard cells where water potential and leaf turgor are the lowest. However,

The difference in drought stress intensity between the two treatments did not qualitatively affect the dynamics of the signal types measured during stomatal closure; although the stomatal response to PEG was quantitatively more drastic and rapid (half as long) (Fig. 3.3b,c). Despite this shorter time frame, the magnitude of the increase in gs was two-fold higher in the PEG treatment. We were unable to determine the

Turface® water potential in the NAT treatment at the onset of stomatal closure. However, the decline in plant water potential in the NAT treatment occurred gradually as water was depleted from the Turface® substrate and the matric component of water potential gradually decreased. In the PEG treatment, water potential decreased very rapidly due to the introduction of the PEG osmoticum. During the initial phases of these water deficit treatments, water potential across plant organs was a function of the rate of water flux through the soil-plant-atmosphere continuum and hydraulic resistance. Rapid turgor loss in epidermal cells compared to guard cells can result in a transient loss of guard cell lateral support and an increase in gs values (Iwanoff effect) (Kappen *et al.*, 1987; Franks *et al.*, 1998; Powles et al., 2006; Hoshika *et al.*, 2013). The higher Iwanoff effect amplitude in the PEG compared to the NAT treatment could have resulted from the rapid decline in water potential in the root zone, such that root water uptake and flux through the xylem was rapidly diminished, despite continued water loss by subsidiary cells leading to turgor loss and stomatal opening. In contrast, in the NAT treatment, the change in soil water potential was sufficiently gradual to limited the Iwanoff effect.

What are AE events?

Acoustic emission events during drought stress have been mainly attributed to cavitation events in xylem conduits (Milburn, 1973; Dixon *et al.*, 1984). It was surprising to observe increased levels of AE rates in the petioles during the beginning of drought before the onset of stomatal closure, since Ψ_{leaf} did not reach values that would result in xylem embolism formation until the end of the experiment (Fig. 3.4

and 3.6). This was also the case for Ψ_{stem} (Fig. 3.4, 3.5, and 3.6). It was also unexpected to observe a rapid decrease in AE rates after stomatal closure since the decrease in Ψ_{leaf} indicated that the tension on the water column increased. We originally speculated that this decline in AE events meant that the vessels had already embolized; however, conductance and anatomy measurements, showed that stems did not lose any meaningful hydraulic conductivity or vessel function during the point of stomatal closure for both dry-down treatments (Fig. 3.5) and the stem, contrary to the leaf, remained hydrated (above -0.25 MPa) throughout the entirety of the experiment for both drought intensities (Fig. 3.4). Consequently, the discrepancy between increased AE events and embolism threshold data of stems and petioles led us to conclude that AE events in both organs are not related to embolism events at least in sunflower plants and that stomatal closure occurs prior to embolism events (Manzoni *et al.*, 2014; Bartlett *et al.*, 2016; Martin-StPaul *et al.*, 2017). A recent examination of hydraulic integrity of sunflower leaf midribs did not detect any embolism events up to a leaf water potential of -1.0 MPa (Cardoso *et al.*, 2018). Furthermore, water potential data in combination with air seeding and PLC measurements suggest, that using PLC data solely measured at the stem-level as a proxy of embolism formation on whole plant functional traits, such as stomatal closure is misleading, at least in sunflower plants. Nevertheless, the disagreement between AE and embolism events raises the question as to what process underlies the recorded AE events.

Other studies have shown that AE events are not always caused by embolism events in xylem cells (Ritman & Milburn, 1991; Kikuta *et al.*, 1997; Rosner *et al.*, 2006; Ponomarenko *et al.*, 2014; Vergeynst *et al.*, 2015), but rather result from

cavitation in non-conducting tissue, e.g. sclerenchyma cells (Kikuta & Richter, 2003), fibers (Ritman & Milburn, 1988), bark tissues (Kikuta, 2003); tissue fractures (Wolkerstorfer *et al.*, 2012); dehydration and shrinkage processes (Hölttä *et al.*, 2005; Vergeynst *et al.*, 2015); and continuous cavitation refilling cycles (Kageyama *et al.*, 2007, 2009). AE events originating from the same vessels, caused by continual cavitation refilling cycles, could have limited our ability to measure a loss in hydraulically functional xylem vessels (Canny, 1997; Trifilò *et al.*, 2014). However, the wide range of reported refilling response times: from 10 to 30 minutes in *A. rubrum* (Melcher & Zwieniecki, 2013; Zwieniecki et al., 2013, respectively), 2 to 3 hours in *V. vinifera* (Holbrook, 2001), and up to 17 to 47 hours in *C. sativus* (Scheenen *et al.*, 2007) make it difficult to determine what level of refilling could have occurred or if any refilling occurred during the one hour of intense AE events that we measured during our experiment. It is also unlikely that embolism events in non-conducting tissues were the source of AE events because this type of embolism event has only been observed under severe drought conditions where xylem vessels are fully embolized (Hacke & Sauter, 1996; Kowalski & Smoczkiewicz, 2004; Wolkerstorfer *et al.*, 2012; Rosner, 2014). AE events that occur during early stages of drought stress have been attributed to early dehydration processes, such as turgor loss (Rodriguez-Dominguez *et al.*, 2016) and radial shrinkage, and not from xylem embolism formation (Hölttä *et al.*, 2009; Vergeynst *et al.*, 2015). Additionally, it has been found that water released from parenchyma cells could result in a release of turgor pressure and consequently cell wall shrinkage which could cause AE events early in dry-down experiments (Čunderlik *et al.*, 1996; Kowalski *et al.*, 2004; Vergeynst *et al.*, 2015).

Unfortunately, these studies did not investigate the relationship between AE events and changes in stomatal conductance. Nevertheless, we suspect that the recorded AE events in our experiment were caused by mechanical stress as evidenced by visible radial tissue shrinkage, in petioles and stems at the beginning of the drought stress treatments, and not from embolism formation since the air-seeding pressure of the leaf was not reached prior to stomatal closure (Fig. 3.6). The observed 7-fold and 5.8-fold gradient (NAT and PEG, respectively) between Ψ_{leaf} and Ψ_{stem} at the end of the experiment supports this hypothesis (Fig. 3.4). Although we did not measure changes in leaf hydraulic conductance during the experiment, it is likely a decrease in leaf hydraulic changes contributed to this result (Brodribb & Holbrook, 2006).

Root, the organ of drought stress origin?

While the PEG treatment lowered the water potential of the rooting medium via introduced osmoticum, root water potentials remained relatively unchanged at water potentials above xylem cavitation thresholds throughout the entire experiment. In contrast, the leaf water potentials declined shortly after drought stress induction and continued to decline significantly. The lack of a decrease in Ψ_{root} was surprising and could have been caused by several mechanisms: first, highly porous soils or growing medium such as Turface® are prone to root-soil air gaps that increase hydraulic resistance in the soil and prevent water flux from the drier soil to the root (Blizzard & Boyer, 1980; North & Nobel, 1997). In the NAT treatment, air gaps could have prevented flux to roots. Additionally, increased hydraulic resistance coupled with higher ion concentrations in the roots might have prevented the water potential from

decreasing (Blum, 2017).

What signal is driving stomatal closure?

Given the tight correlation of signal types during stomatal closure, it remains difficult to identify the individual signal responsible for initiating the process (Fig. 3.7).

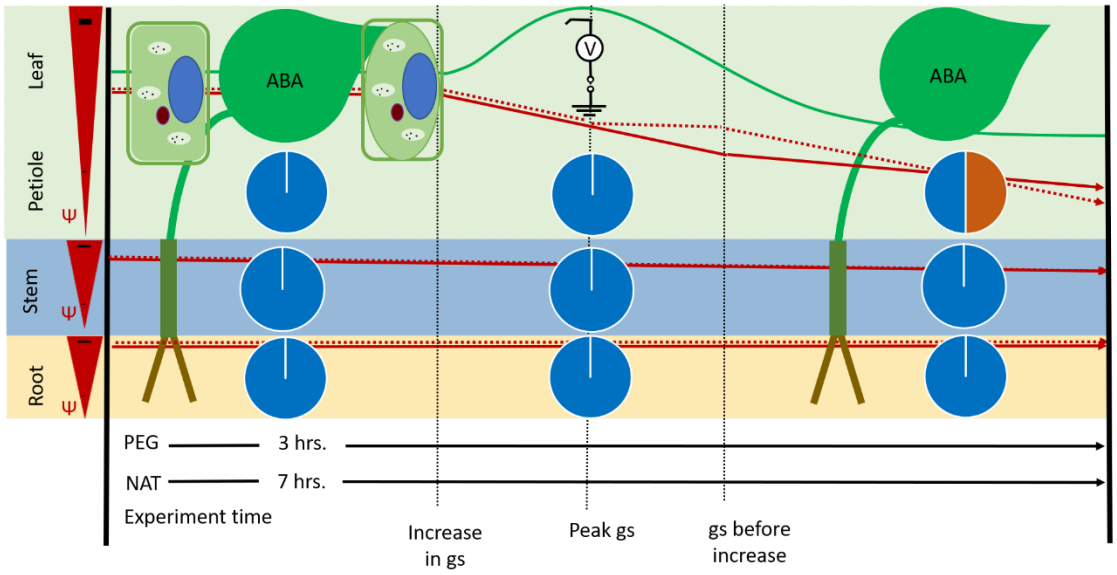

Figure 3.7: Timeline of signal types preceding and following the onset of stomatal closure during a natural and an induced dry-down treatment (NAT and PEG, respectively). Stomatal conductance (gs, green line) is characterized by a sudden increase in gs prior to a steady decline. Changes in leaf turgor pressure (flaccid cell) is the only signal type that preceded the increase in gs. Surface potentials started shifting at the peak of gs (electrical circuit). Leaf [ABA] did not change significantly throughout the experiment. Water potentials (Ψ) of roots and stems were high throughout the experiment (red triangles, relative scale of Ψ in the experiment), while Ψ_{leaf} decreased noticeably (NAT, dashed red line; PEG solid red line) and declined below the embolism threshold. Thus, the petiole was the only organ that experienced a significant loss in hydraulic conductance (orange area of pie chart).

Nevertheless, the late occurrence of electrical surface potential changes, and embolism events, do not provide evidence to implicate them as drivers of stomatal closure.

Conversely, the loss of leaf turgor pressure and AE events in stem and petiole closely preceded the onset of stomatal closure, indicating a close relationship between these variables and stomatal closure (Fig. 3.7). These findings agree with studies that indicate the decrease in leaf turgor pressure is the hydraulic signal most tightly linked to the increase in gs (Shackel & Brinckmann, 1985; Mott *et al.*, 1997; Mott & Franks, 2001; Dodd *et al.*, 2008; Rodriguez-Dominguez *et al.*, 2016).

AE events, which we attributed to tissue shrinkage processes, started to occur prior to measured turgor pressure changes and therefore cannot be ruled out as a possible driving factor for stomatal closure. Indeed, it is possible these events represented early stages of localized turgor loss, before bulk-leaf turgor decreases could be detected. The importance of plant organ water status in stomatal control is supported by Ψ_{leaf} measurements, that show the initiation of stomatal closure occurred at similar Ψ_{leaf} across treatments, despite significant differences in soil dry-down rates. This study provides an insight into the complexity and intricacy of signal coordination prior to, during, and after stomatal closure. Nevertheless, more research is needed to elucidate root-shoot signal coordination and clarify the cause-effect relationship between hydraulic factors and the coordination of secondary signals.

3.5 References

Ahmad HB, Lens F, Capdeville G, Burlett R, Lamarque LJ, Delzon S. 2018. Intraspecific variation in embolism resistance and stem anatomy across four sunflower (*Helianthus annuus* L.) accessions. Physiologia Plantarum **163**, 59–72.

Alder NN. 1997. Use of centrifugal force in the study of xylem cavitation. Journal of Experimental Botany **48**, 665–674.

Bartlett MK, Klein T, Jansen S, Choat B, Sack L. 2016. The correlations and sequence of plant stomatal, hydraulic, and wilting responses to drought. Proceedings of the National Academy of Sciences **113**, 13098–13103.

Blizzard WE, Boyer JS. 1980. Comparative resistance of the soil and the plant to water transport. Plant Physiology **66**, 809–814.

Blum A. 2017. Osmotic adjustment is a prime drought stress adaptive engine in support of plant production. Plant, Cell and Environment **40**, 4–10.

Brodribb TJ. 2003. Stomatal closure during leaf dehydration, correlation with other leaf physiological traits. Plant Physiology **132**, 2166–2173.

Brodribb TJ, Holbrook NM. 2006. Declining hydraulic efficiency as transpiring leaves desiccate: two types of response. Plant, Cell and Environment **29**, 2205–2215.

Brodribb TJ, Holbrook NM, Edwards EJ, Gutiérrez M V. 2003. Relations between stomatal closure, leaf turgor and xylem vulnerability in eight tropical dry forest trees. Plant, Cell and Environment **26**, 443–450.

Buckley TN, John GP, Scoffoni C, Sack L. 2015. How does leaf anatomy influence water transport outside the xylem? Plant Physiology **168**, 1616–1635.

Cai J, Tyree MT. 2010. The impact of vessel size on vulnerability curves: data and models for within-species variability in saplings of aspen, *Populus tremuloides* Michx. Plant, Cell and Environment **33**, 1059–69.

Canny MJ. 1997. Vessel contents during transpiration - embolisms and refilling.

American Journal of Botany **84**, 1223–1230.

Cardoso AA, Brodribb TJ, Lucani CJ, DaMatta FM, McAdam SAM. 2018. Coordinated plasticity maintains hydraulic safety in sunflower leaves. Plant Cell and Environment **41**, 2567–2576.

Christmann A, Grill E, Huang J. 2013. Hydraulic signals in long-distance signaling. Current Opinion in Plant Biology **16**, 293–300.

Christmann A, Weiler EW, Steudle E, Grill E. 2007. A hydraulic signal in root-to-shoot signalling of water shortage. The Plant Journal **52**, 167–174.

Correia MJ, Pereira JS. 1995. The control of leaf conductance of white lupin by xylem ABA concentration decreases with the severity of water deficits. Journal of Experimental Botany **46**, 101–110.

Čunderlik I, Moliński W, Raczkowski J. 1996. The monitoring of drying cracks in the tension and opposite wood by acoustic emission and scanning electron microscopy methods. Holzforschung-International Journal of the Biology, Chemistry, Physics and Technology of Wood **50**, 258–262.

Dixon MAA, Grace J, Tyree MT. 1984. Concurrent measurements of stem density, leaf and stem water potential, stomatal conductance and cavitation on a sapling of *Thuja occidentalis* L. Plant, Cell and Environment **7**, 615–618.

Dodd IC, Egea G, Davies WJ. 2008. Abscisic acid signalling when soil moisture is heterogeneous: decreased photoperiod sap flow from drying roots limits abscisic acid export to the shoots. Plant, Cell and Environment **31**, 1263–1274.

Domec J-C, Gartner BL. 2001. Cavitation and water storage capacity in bole xylem segments of mature and young Douglas-fir trees. Trees **15**, 204–214.

Farquhar GD, Sharkey TD. 1982. Stomatal conductance and photosynthesis. Annual Review of Plant Physiology **33**, 317–345.

Franks PJ, Cowan IR, Farquhar GD. 1998. A study of stomatal mechanics using the cell pressure probe. Plant, Cell and Environment **21**, 94–100.

Franks PJ, Drake PL, Froend RH. 2007. Anisohydric but isohydrodynamic: seasonally constant plant water potential gradient explained by a stomatal control mechanism incorporating variable plant hydraulic conductance. Plant, Cell and Environment **30**, 19–30.

Fromm J, Eschrich W. 1993. Electric signals released from roots of willow (*Salix viminalis* L.) change transpiration and photosynthesis. Journal of Plant Physiology **141**, 673–680.

Fromm J, Lautner S. 2007. Electrical signals and their physiological significance in plants. Plant, Cell and Environment **30**, 249–257.

Geiger D, Scherzer S, Mumm P, *et al.* 2009. Activity of guard cell anion channel SLAC1 is controlled by drought-stress signaling kinase-phosphatase pair. Proceedings of the National Academy of Sciences **106**, 21425–21430.

Grams TEE, Koziolek C, Lautner S, Matyssek R, Fromm J. 2007. Distinct roles of electric and hydraulic signals on the reaction of leaf gas exchange upon re-irrigation in *Zea mays* L. Plant, cell & environment **30**, 79–84.

Hacke U, Sauter JJ. 1996. Drought-induced xylem dysfunction in petioles, branches, and roots of *Populus balsamifera* L. and *Alnus glutinosa* (L.) Gaertn. Plant Physiology **111**, 413–417.

Hacke UG, Venturas MD, MacKinnon ED, Jacobsen AL, Sperry JS, Pratt RB.

2014. The standard centrifuge method accurately measures vulnerability curves of long-vesselled olive stems. New Phytologist **205**, 116–127.

Holbrook NM. 2001. In vivo observation of cavitation and embolism repair using magnetic resonance imaging. Plant Physiology **126**, 27–31.

Holbrook NM, Shashidhar VR, James R a, Munns R. 2002. Stomatal control in tomato with ABA-deficient roots: response of grafted plants to soil drying. Journal of experimental botany **53**, 1503–1514.

Hölttä T, Mencuccini M, Nikinmaa E. 2009. Linking phloem function to structure: analysis with a coupled xylem-phloem transport model. Journal of Theoretical Biology **259**, 325–37.

Hölttä T, Vesala T, Nikinmaa E, Perämäki M, Siivola E, Mencuccini M. 2005. Field measurements of ultrasonic acoustic emissions and stem diameter variations. New insight into the relationship between xylem tensions and embolism. Tree Physiology **25**, 237–243.

Hoshika Y, Omasa K, Paoletti E. 2013. Both ozone exposure and soil water stress are able to induce stomatal sluggishness. Environmental and Experimental Botany **88**, 19–23.

Huber AE, Bauerle TL. 2016. Long-distance plant signaling pathways in response to multiple stressors: the gap in knowledge. Journal of Experimental Botany **67**, 2063–2079.

Iwanoff L. 1928. Zur Methodik der Transpirationsbestimmung am Standort. Berichte der Deutschen Botanischen Gesellschaft **46**, 306–310.

Jacobsen AL, Pratt RB. 2012. No evidence for an open vessel effect in centrifuge-

based vulnerability curves of a long-vesselled liana (*Vitis vinifera*). New Phytologist **194**, 982–990.

Kageyama K, Inoue Y, Kato H. 2009. Estimation for embolism risk of tomato using acoustic emission response to increased drought stress. Environmental Control in Biology **47**, 127–136.

Kageyama K, Kaminaga M, Kato H. 2007. Correlation between acoustic emissions generated from cavitation in rubber tree leaf veins. Environmental Control in Biology **45**, 59–65.

Kaiser H, Grams TEE. 2006. Rapid hydropassive opening and subsequent active stomatal closure follow heat-induced electrical signals in *Mimosa pudica*. Journal of Experimental Botany **57**, 2087–2092.

Kaiser H, Legner N. 2006. Localization of mechanisms involved in hydropassive and hydroactive stomatal responses of *Sambucus nigra* to dry air. Plant Physiology **143**, 1068–1077.

Kaiser H, Paoletti E. 2014. Dynamic stomatal changes. In: Tausz M In: Grulke N, eds. Trees in a Changing Environment. Dordrecht: Springer Science+Business Media, 61–82.

Kappen L, Andresen G, Lösch R. 1987. In situ observations of stomatal movements. Journal of Experimental Botany **38**, 126–141.

Kaufmann MR, Eckard AN. 1971. Evaluation of water stress control with polyethylene glycols by analysis of guttation. Plant Physiology **47**, 453–456.

Kikuta SB. 2003. Ultrasound acoustic emissions from bark samples differing in anatomical characteristics. Phyton - Annales Rei Botanicae **43**, 161–178.

Kikuta SB, Lo Gullo MA, Nardini A, Richter H, Salleo S. 1997. Ultrasound acoustic emissions from dehydrating leaves of deciduous and evergreen trees. Plant, Cell and Environment **20**, 1381–1390.

Kikuta SB, Richter H. 2003. Ultrasound acoustic emissions from freezing xylem. Plant, Cell and Environment **26**, 383–388.

Kollist H, Nuhkat M, Roelfsema MRG. 2014. Closing gaps: linking elements that control stomatal movement. New Phytologist, 44–62.

Kowalski SJ, Moliński W, Musielak G. 2004. The identification of fracture in dried wood based on theoretical modelling and acoustic emission. Wood Science and Technology **38**, 35–52.

Kowalski SJ, Smoczkiewicz A. 2004. Acoustic emission in wood under drying. Folia Forestalia Polonica **35**, 59–71.

Manzoni S, Katul G, Proporato A. 2014. A dynamical system perspective on plant hydraulic failure. Water Resource Research **50**, 5170–5183.

Martin-StPaul N, Delzon S, Cochard H. 2017. Plant resistance to drought depends on timely stomatal closure. Ecology Letters **20**, 1437–1447.

McAdam SAM, Brodribb TJ. 2012. Fern and lycophyte guard cells do not respond to endogenous abscisic acid. The Plant Cell **24**, 1510–1521.

McAdam SAM, Brodribb TJ. 2015. The evolution of mechanisms driving the stomatal response to vapor pressure deficit. Plant Physiology **167**, 833–843.

McAdam SAM, Sussmilch FC, Brodribb TJ. 2016. Stomatal responses to vapour pressure deficit are regulated by high speed gene expression in angiosperms. Plant Cell and Environment **39**, 485–491.

Medvedev SS. 2005. Calcium signaling system in plants. Russian Journal of Plant Physiology **52**, 249–270.

Melcher PJ, Michele Holbrook N, Burns MJ, Zwieniecki MA, Cobb AR, Brodribb TJ, Choat B, Sack L. 2012. Measurements of stem xylem hydraulic conductivity in the laboratory and field. Methods in Ecology and Evolution **3**, 685–694.

Melcher PJ, Zwieniecki MA. 2013. Functional analysis of embolism induced by air injection in Acer rubrum and Salix nigra. Frontiers in Plant Science **4**, 1–10.

Melcher PJ, Zwieniecki MA, Holbrook NM. 2003. Vulnerability of xylem vessels to cavitation in sugar maple. Scaling from individual vessels to whole branches. Plant Physiology **131**, 1775–1780.

Milburn JA. 1973. Cavitation studies on whole *Ricinus* plants by acoustic detection. Planta **112**, 333–342.

Mittelheuser CJ, Steveninck RFM. 1969. Stomatal closure and inhibition of transpiration induced by (RS)-abscisic acid. Nature **221**, 281–282.

Mott KA, Denne F, Powell J. 1997. Interactions among stomata in response to perturbations in humidity. Plant, Cell and Environment **20**, 1098–1107.

Mott KA, Franks PJ. 2001. The role of epidermal turgor in stomatal interactions following a local perturbation in humidity. Plant, Cell and Environment **24**, 657–662.

Munemasa S, Hauser F, Park J, Waadt R, Brandt B, Schroeder JI. 2015. Mechanisms of abscisic acid-mediated control of stomatal aperture. Current Opinion in Plant Biology **28**, 154–162.

Murata Y, Mori IC, Munemasa S. 2015. Diverse stomatal signaling and the signal integration mechanism. Annual Review of Plant Biology **66**, 369–392.

Nolf M, Beikircher B, Rosner S, Nolf A, Mayr S. 2015. Xylem cavitation resistance can be estimated based on time-dependent rate of acoustic emissions. New Phytologist **208**, 625–632.

North GB, Nobel PS. 1997. Drought-induced changes in soil contact and hydraulic conductivity for roots of *Opuntia ficus-indica* with and without rhizosheaths. Plant and Soil **191**, 249–258.

Pammenter NW, Van der Willigen C. 1998. A mathematical and statistical analysis of the curves illustrating vulnerability of xylem to cavitation. Tree Physiology **18**, 589–593.

Paoletti E. 2005. Ozone slows stomatal response to light and leaf wounding in a Mediterranean evergreen broadleaf, Arbutus unedo. Environmental Pollution **134**, 439–445.

Pockman WT, Sperry JS, O'leary JW. 1995. Sustained and significant negative water pressure in xylem. Nature **378**, 715–716.

Ponomarenko A, Vincent O, Pietriga A, Cochard H, Badel É, Marmottant P. 2014. Ultrasonic emissions reveal individual cavitation bubbles in water-stressed wood. Journal of the Royal Society Interface **11**, 20140480.

Powles JE, Buckley TN, Nicotra AB, Farquhar GD. 2006. Dynamics of stomatal water relations following leaf excision. Plant, Cell and Environment **29**, 981–992.

Ritman KT, Milburn JA. 1988. Acoustic emissions from plants: ultrasonic and

audible compared. Journal of Experimental Botany **39**, 1237–1248.

Ritman KT, Milburn JA. 1991. Monitoring of ultrasonic and audible emissions from plants with or without vessels. Journal of Experimental Botany **42**, 123–130.

Rodriguez-Dominguez CM, Buckley TN, Egea G, de Cires A, Hernandez-Santana V, Martorell S, Diaz-Espejo A. 2016. Most stomatal closure in woody species under moderate drought can be explained by stomatal responses to leaf turgor. Plant, Cell and Environment **39**, 2014–2026.

Roelfsema MRG, Hedrich R. 2005. In the light of stomatal opening: new insights into 'the Watergate'. New Phytologist **167**, 665–691.

Rosner S. 2014. A new type of vulnerability curve: is there truth in vine? Tree Physiology **35**, 410–414.

Rosner S, Klein A, Wimmer R, Karlsson B. 2006. Extraction of features from ultrasound acoustic emissions: a tool to assess the hydraulic vulnerability of Norway spruce trunkwood? New Phytologist **171**, 105–116.

Salleo S, Lo Gullo MA, Raimondo F, Nardini A. 2001. Vulnerability to cavitation of leaf minor veins: any impact on leaf gas exchange? Plant, Cell and Environment **24**, 851–859.

Schachtman DP, Goodger JQD. 2008. Chemical root to shoot signaling under drought. Trends in Pant Science **13**, 281–287.

Scheenen TWJ, Vergeldt FJ, Heemskerk AM, Van As H. 2007. Intact plant magnetic resonance imaging to study dynamics in long-distance sap flow and flow-conducting surface area. Plant Physiology **144**, 1157–1165.

Schroeder JI, Kwak JM, Allen GJ. 2001. Guard cell abscisic acid signalling and

engineering drought hardiness in plants. Nature **410**, 327–330.

Scoffoni C, Albuquerque C, Brodersen CR, Townes S V., John GP, Bartlett MK, Buckley TN, McElrone AJ, Sack L. 2017. Outside-xylem vulnerability, not xylem embolism, controls leaf hydraulic decline during dehydration. Plant Physiology **173**, 1197–1210.

Setter TL. 2012. Analysis of constituents for phenotyping drought tolerance in crop improvement. Frontiers in Physiology **3**, 1–12.

Setter TL, Parra R. 2010. Relationship of carbohydrate and abscisic acid levels to kernel set in maize under postpollination water deficit. Crop Science **50**, 980–988.

Shackel KA, Brinckmann E. 1985. In situ measurement of epidermal cell turgor, leaf water potential, and gas exchange in *Tradescantia virginiana* L. Advances in Botanical Research **78**, 66–70.

Sparks JP, Black RA. 1999. Regulation of water loss in populations of *Populus trichocarpa*: the role of stomatal control in preventing xylem cavitation. Tree Physiology **19**, 453–459.

Sperry JS, Christman M a, Torres-Ruiz JM, Taneda H, Smith DD. 2012. Vulnerability curves by centrifugation: is there an open vessel artefact, and are 'r' shaped curves necessarily invalid? Plant, Cell and Environment **35**, 601–10.

Sperry JS, Venturas MD, Anderegg WRL, Mencuccini M, Mackay DS, Wang Y, Love DM. 2017. Predicting stomatal responses to the environment from the optimization of photosynthetic gain and hydraulic cost. Plant, Cell and Environment **40**, 816–830.

Stahlberg R, Cosgrove DJ. 1996. Induction and ionic basis of slow wave potentials in seedlings of Pisum sativum L. Planta **200**, 416–425.

Stahlberg R, Cosgrove DJ. 1997. The propagation of slow wave potentials in pea epicotyls. Plant Physiology **113**, 209–217.

Sussmilch FC, Brodribb TJ, McAdam SAM. 2017. Up-regulation of NCED3 and ABA biosynthesis occur within minutes of a decrease in leaf turgor but AHK1 is not required. Journal of Experimental Botany **68**, 2913–2918.

Tombesi S, Nardini A, Frioni T, Soccolini M, Zadra C, Farinelli D, Poni S, Palliotti A. 2015. Stomatal closure is induced by hydraulic signals and maintained by ABA in drought-stressed grapevine. Scientific Reports **5**, 1–12.

Trejo CL, Davies WJ. 1991. Drought-induced closure of *Phaseolus vulgaris* L. stomata precedes leaf water deficit and any increase in xylem ABA concentration. Journal of Experimental Botany **42**, 1507–1516.

Trifilò P, Raimondo F, Lo Gullo M a., Barbera PM, Salleo S, Nardini A. 2014. Relax and refill: xylem rehydration prior to hydraulic measurements favours embolism repair in stems and generates artificially low PLC values. Plant, Cell and Envrionment, 2491–2499.

Tyree MT, Sperry JS. 1989. Vulnerability of xylem to cavitation and embolism. Annual Review of Plant Physiology and Plant Molecular Biology **40**, 19–38.

Urano K, Maruyama K, Jikumaru Y, Kamiya Y, Yamaguchi-Shinozaki K, Shinozaki K. 2017. Analysis of plant hormone profiles in response to moderate dehydration stress. Plant Journal **90**, 17–36.

Vergeynst LL, Dierick M, Bogaerts JAN, Cnudde V, Steppe K. 2015. Cavitation:

A blessing in disguise? New method to establish vulnerability curves and assess hydraulic capacitance of woody tissues. Tree Physiology **35**, 400–409.

Wilkinson S, Davies WJ. 2008. Manipulation of the apoplastic pH of intact plants mimics stomatal and growth responses to water availability and microclimatic variation. Journal of Experimental Botany **59**, 619–631.

Wolkerstorfer S V, Rosner S, Hietz P. 2012. An improved method and data analysis for ultrasound acoustic emissions and xylem vulnerability in conifer wood. Physiologia plantarum **146**, 184–191.

Zhang J, Davies WJ. 1989. Abscisic acid produced in dehydrating roots may enable the plant to measure the water status of the soil. Plant, Cell and Environment **12**, 73–81.

Zhang SQ, Outlaw JR. 2001. The guard-cell apoplast as a site of abscisic acid accumulation in *Vicia faba* L . Plant, Cell and Environment **24**, 347–355.

Zhang FP, Sussmilch F, Nichols DS, Cardoso AA, Brodribb TJ, McAdam SAM. 2018. Leaves, not roots or floral tissue, are the main site of rapid, external pressure-induced ABA biosynthesis in angiosperms. Journal of Experimental Botany **69**, 1261–1267.

Zwieniecki MA, Melcher PJ, Ahrens ET. 2013. Analysis of spatial and temporal dynamics of xylem refilling in *Acer rubrum* L. using magnetic resonance imaging. Frontiers in Plant Science **4**, 1–8.

CHAPTER 4

HYDRAULIC INTEGRITY OF PLANT ORGANS DURING DROUGHT STRESS AND DROUGHT RECOVERY

4.1 Introduction

A popular method for characterizing plant drought tolerance and quantifying xylem vessel resistance to embolism (air bubble formation) is percent loss of conductivity curves (PLC curves), which plot the percent loss of hydraulic conductance against water potential (Lo Gullo *et al.*, 2003; Tyree, 2003; McDowell *et al.*, 2008). The water potential that corresponds with a 50% loss of hydraulic conductance (P_{50} value) has become a gold standard method for comparing drought resistance across plant species (Pockman and Sperry, 2000; Maherali *et al.*, 2004). Interestingly, PLC curves are often only calculated using stems, the most hydraulically resistant plant organ for embolism (Nardini *et al.*, 2003; Choat *et al.*, 2005; Jacobsen *et al.*, 2007; Bucci *et al.*, 2008; Hao *et al.*, 2008), which may overestimate drought stress tolerance on a whole-plant level. This overestimation could lead to errors in predicting how water stress impacts stomatal behavior (Brodribb *et al.*, 2003). For example, PLC response curves measured on *Acer rubrum* and *Salix nigra* cut stems via pneumatic pressurization showed that both species lost 100% conductivity at air-seeding pressures less than 5.5 MPa (Melcher and Zwieniecki 2013). While air-injection pressures of 5.5 MPa into the intact plant stems of *S. nigra* resulted in rapid stomatal closure, wilting and eventual plant death, this same treatment had no effect on stomatal conductance or any measurable change in plant functions in *A. rubrum.* This example demonstrates

the vast inconsistency between in stem-level PLC measurement interpretation of drought tolerance and changes in whole plant drought response.

Changes in xylem vessel hydraulic conductance is understood to be attributed to changes in the percent of embolized xylem conduits (Tyree and Sperry, 1988; Cochard *et al.*, 1992; Lobo *et al.*, 2018). However, there are other potential mechanisms that can alter a plant's hydraulic state, including changes in cell turgor pressures (Brodribb and Holbrook, 2006), the deformation of leaf mesophyll (Scoffoni *et al.*, 2014), and the collapse of tracheids or xylem vessels in leaves themselves, in the absence of embolism events (Cochard *et al.*, 2004; Zhang *et al.*, 2016). Further, a reduction in leaf hydraulic conductance (K_{leaf}) can result from the collapse of extra-xylary tissue (Brodribb and Holbrook, 2005), also known as transfusion tissue in gymnosperms (Gambles and Dengler, 1982). The collapse of extra-xylary tissue is thought to require less energy to return to non-stressed hydraulic state conditions in comparison to embolism refilling (Brodribb and Holbrook, 2005). Even though transfusion tissue, primarily constructed of tracheids, has only been described in conifers, the deformation/collapse of extra-xylary tissue (Charra-Vaskou *et al.*, 2012; Zhang *et al.*, 2016), and the collapse of the outermost leaf veins prior to cavitation events has also been observed in angiosperms (Cochard *et al.*, 2004; Brodribb and Holbrook, 2005; Zhang *et al.*, 2016). It is clear that we need a better understanding of how plants maintain hydraulic integrity within plant organs (root, stems, petioles) and how tissue collapse in response to drought affects stomatal function; both of which are crucial to provide a more complete model of plant drought stress behavior.

Studies continue to dispute whether roots (Sperry and Saliendra, 1994; Alder *et al.*,

1996; Hacke and Sauter, 1996; McElrone *et al.*, 1999; Pratt *et al.*, 2015; Johnson *et al.*, 2016) or leaves (Choat *et al.*, 2005; Rodriguez-Dominguez *et al.*, 2018) are more vulnerable to drought stress. From a drought survivorship perspective, both organs are equally critical in maintaining plant health. Roots are essential for providing plants with water during drought stress periods through deep root systems, extending lifespan of roots in dry soil zones and through internal water relocation (Bauerle *et al.*, 2008) while leaves are essential in maintaining a positive carbon balance (McDowell *et al.*, 2008). Furthermore, maintaining leaf health during drought stress periods ensures quick carbon fixation after drought stress periods (Chabot and Hicks, 1982). The underlying reason for this ongoing disparity on organ vulnerability is that very little research has compared xylem vulnerability across plant organs (Choat *et al.*, 2005; Rodriguez-Dominguez *et al.*, 2018). While this might seem surprisingly simple, in addition to the difficulty in accessing roots, the invasive nature of hydraulic conductance measurement techniques presents a challenge in determining root organ vulnerability (Choat *et al.*, 2005; Froux *et al.*, 2005). Disrupting the hydraulic state of plants sets the stage for multiple measurement mistakes (Martin-StPaul *et al.*, 2014; Rockwell *et al.*, 2014) and it was not until recently that noninvasive, visual measurement techniques were applied (Brodribb *et al.*, 2010; Brodersen *et al.*, 2013; Cuneo *et al.*, 2016; Scoffoni *et al.*, 2017; Rodriguez-Dominguez *et al.*, 2018) allowing for the simultaneous observation of root, stem, and petiole vulnerability within a single plant (Rodriguez-Dominguez *et al.*, 2018).

Recovery of the hydraulic continuum after drought stress is usually determined at the leaf level by comparing stomatal conductance recovery to pre-stress levels

(Blackman *et al.*, 2009; Brodribb and Cochard, 2009; Resco *et al.*, 2009; Skelton *et al.*, 2017). Research has shown that stomatal conductance recovery is highly correlated with the recovery of K_{leaf} (Lo Gullo *et al.*, 2003; Blackman *et al.*, 2009), varies between tree species (Melcher and Zwieniecki, 2013), and is dependent on drought intensity (Blackman *et al.*, 2009; Brodribb and Cochard, 2009). Skelton et al. (2017) documented the recovery of eight woody plant species after a drought stress period and observed that branch sap flow and leaf gas exchange recovered within one day after a heavy rainfall, unless critical K_{leaf} loss occurred due to embolism events resulting from drought stress. Hence, discrepancies in species recovery rate was attributed to whether or not embolisms were formed in the xylem vessels and how fast the tissues were able to recover (Skelton *et al.*, 2017). Several studies have observed embolism recovery within hours to days in petioles and stems (Bucci *et al.*, 2003; Salleo *et al.*, 2004; Melcher and Zwieniecki, 2013; Zwieniecki *et al.*, 2013), while collapsed extra-xylary parenchyma recovery can happen within minutes after rewatering (Zhang *et al.*, 2016), suggesting that the key to expedited leaf gas exchange recovery is the avoidance of embolism events (Skelton 2017).

While plants succumb to and refill embolism events on a daily basis (Melcher *et al.*, 2001; Hacke and Sperry, 2003; Taneda and Sperry, 2008), the embolized xylem vessel repair mechanism is still unclear, as are the plant traits and environmental conditions that enable this recovery. Identifying parameters associated with embolism repair is impeded by variability in species within the same genus and functional group differing in their ability to repair embolism events (Brodersen and McElrone, 2013). Nevertheless, embolism refilling has been observed in many plants, across species and

biomes (Klein *et al.*, 2018). The restoration of the hydraulic continuum has been observed to occur by the formation of new wood (Brodribb *et al.*, 2010; Christensen-Dalsgaard and Tyree, 2014) or by spontaneous bubble dissolution when xylem tension is relaxed which can occur under positive root pressure (Brodersen and McElrone, 2013). A third option is the restoration of embolisms under tension, which is referred to as novel refilling. However, its occurrence and process are still under debate (Brodersen and McElrone, 2013; Klein *et al.*, 2018). Given the uncertainty of how plants restore hydraulic conductance after drought, more research is needed to understand the role of embolism events in plant organs during drought stress periods and their effect on restoring leaf gas exchange after periods of water shortage.

To test the hypothesis that embolism formation in stems is not correlated with stomatal function, we measured the level of water stress that impacts the hydraulic status of plant xylem vessels in petioles, stems, and roots and correlated these findings with stomatal conductance. Measurements were made on *Helianthus annuus* and *Populus x canadensis* plants that were exposed to varying degrees of drought stress with a subsequent rewatering event. Additionally, four temperate tree species were also subjected to the same drought treatments to examine if the observed changes in organ specific hydraulic conductivity in *Populus x canadensis* followed similar patterns across other woody tree species.

4.2 Materials and Methods

Plant material

This experiment was conducted on one herbaceous: *Helianthus annuus* (Sunrich

Orange (F1) Johnny's Selected Seed, Winslow, ME), and five tree species: two-year-old *Populus x canadensis* "Imperial", *Acer saccharum, Acer saccharinum*, *Picea glauca* (Lawyer Nursery, Olympia, WA), and *Tsuga canadensis* seedlings (Saratoga Tree Nursery, Saratoga Springs, NY). *H. annuus* and *P. x canadensis* were chosen as model species based on previous data sets that revealed a discrepancy between predicted cavitation events and the onset of stomatal closure (A.E. Huber, P.J. Melcher, M.A. Piñeros, T.L. Setter, and T. L. Bauerle, unpublished *for H. annuus*). The remaining four tree species represent common tree species in Northeastern forests and were chosen to investigate if the data pattern we observed in the two model species is a common strategy across woody tree species.

All species were planted in a baked clay particulate medium (Turface® Athletics MVP, Profile, Buffalo Grove, IL) and grown under greenhouse conditions, day/night light ratio of 16/8 hours, from May to October 2017. To adapt plants to this medium, *H. annuus* plants were grown from seed in Turface®, while bare rooted tree seedlings and cuttings were planted in the Turface® medium in the beginning of the spring when the deciduous trees were still dormant. Plants were grown under optimal conditions until tree leaves were fully developed and *H. annuus* plants were ten-weeks-old. During this time, plants were watered two- to three-times a day and fertilized twice a week with Jack's 15-5-15 Fertilizer (JR Peters Inc, Allentown, PA).

Experimental procedure

At the start of the experiment, all plants were exposed to a reduced irrigation regime with a subsequent re-watering event. During the reduced irrigation regime, the soil

water content was reduced from 100% soil field capacity (FC) to 25% FC in 25% increment steps. Soil FCs were maintained by weighing each plant's pot in the morning and in the evening to determine evapotranspired water and then watered up to the respective FC. 100% FC was determined by weighing five fully hydrated and freely drained pots per plant species before the experiment started. Then, the Turface® was dried in an oven for 4 days at 60 °C and its dry weight determined. Other FCs were calculated based upon their fully saturated condition. The dry-down period between two FCs took 2-5 days. Physiological measurements were conducted for each FC on eight replicate plants at the end of every dry-down step. For the final measurements, pots were re-watered from 25% FC back to 100% FC. Stomatal conductance (gs), as well as leaf water potential (Ψ_{leaf}) measurements, were performed on all eight plants (n=8). The plants were subsequently divided into two groups. Plants from the first group were used for cryo-SEM analysis (n=4) and plants from the second group were used for destructive stem and root water potential measurements (n=4). Additionally, relative tissue water content and air seeding measurements were performed on each plant within the second group of the two-model species (*P. x canadensis* and *H. annuus*) to compare the dry-down behavior of one herbaceous and one woody plant species (n=4).

Stomatal conductance

Midday stomatal conductance (gs) of the two model species as well as the four temperate tree species was measured on each measurement day on two fully-developed, upper canopy leaves per plant with a portable photosynthesis system

(CIRAS-2, PP Systems, Amesbury, MA). The atmosphere in the gas exchange cuvette was kept constant with the following settings: reference CO_2 concentration of 400 ppm, reference H_2O 50% of ambient, flow 200 ml min^{-1}. An attached LED light unit (red and white LED) allowed for constant synthetically photoactive radiation (PAR, 400-700 nm) with a photon flux density of 1200 μmol m^{-2} s^{-1} within the cuvette. Stomatal conductance values were recorded after signal stabilization. Because conifer needles did not completely fill the chamber area during the measurements, they were harvested, and their projected leaf surface area determined with a leaf area meter (air-LI-3100, LI-COR, Lincoln, NE). Stomatal conductance values were calculated for the actual projected leaf area of conifer needles.

Additional gs measurements were recorded on an extra set of seven *P. x canadensis* plants to determine the relationship between Ψ_{leaf} and the onset of stomatal closure. These trees were dried down naturally, while gs was recorded every 60 seconds. During the dry-down period, Ψ_{leaf} measurements were taken at regular time intervals that were based on the change in gs. After the experiment, Ψ_{leaf} was correlated with decreasing gs.

Organ water potential

Two covered (Ψ_{CL}) and two uncovered (Ψ_{UCL}) leaf water potential measurements of fully developed canopy leaves of eight plants per plant species were taken on each measurement day at the same time as stomatal conductance. To allow for equilibration of leaves with the stem, Ψ_{CL} leaves were bagged two hours prior to measuring. Because there was no difference between Ψ_{CL} and Ψ_{UCL}, we do not distinguish

between them and refer only to leaf water potential (Ψ_{leaf}) from here forward (Appendix 4). After Ψ_{leaf} was measured, plants were divided into two groups. Plants of the second group were swiftly dissected and stem water potential (Ψ_{stem}; 15-20 cm long stem segments, cutting location 2 cm and 17- 22 cm above the ground) and woody root water potential (Ψ_{root}) (~ 20 cm in lengths, cut at the trunk -root junction; two measurements per plant) were determined via a water status console (Soilmoisture Equipment Corp., Goleta, CA) where the pressure was gradually increased (100 kPa min^{-1}) until the balancing pressure was reached. *P. glauca*, as well as *T. canadensis* needles, were too small to determine the balancing pressure accurately despite a magnifying glass. For this reason, we measured Ψ on one-year-old twigs (Ψ_{twig}).

Cryo-microscopy

Following Ψ_{leaf} measurements, four plants per species were brought to the lab, removed from the Turface® medium and immediately frozen by submerging the whole plant in a nitrogen slush (vacuum treated liquid nitrogen; Pathan et al. 2009). Plants were kept frozen, while 5-10 mm long samples of roots, stems, and petioles were dissected, put in small vials, and stored in liquid nitrogen. Samples were later mounted onto a cryo-microtome at -20 °C (Reichert 855 Histostat Cryostat Microtome, Reichert Histo Stat, MOC Inc, Valley Cottage, NY) and cut at a 25 µm dissecting distance. Finally, cyro-images were taken with a stereo light microscope (Mitutoyo 375, Mitutoyo America Corporation, Il, USA) with a 100x magnification. The objective of the microscope was mounted over a cryo chamber (Leica EM FCS (Leica Microsystems, Buffalo Grove, Il), which was cooled and maintained at -50 °C during

the imaging process. The plant samples were mounted in ultramicrotome chucks (Electron Microscopy Science, PA) and placed inside the cryo-chamber. Images were taken with a camera (Infinity 3-1, Lumenera Corporation, Ottawa, Ontario) attached to the microscope. An external high-intensity illuminator (Fiber-Lite Illuminators Model 181-1 lite, Dolan-Jenner, Boxborough, MA) was used to improve image brightness. To ensure the validity of the custom-built stage, additional images were taken with a cryo-scanning electron microscope (cryo-SEM) and vessel counts were performed to compare the two methods. However, xylem vessels of *H. annuus* roots were too small to image using the stereo microscope. Therefore, only cryo-SEM images were taken for *H. annuus* roots. For the cryo-SEM imaging analysis, frozen samples were inserted into a FEI Strata 400 STEM FIB (Thermo Fisher Scientific, Waltham, Ma). A cold stage attached to the preparation chamber (Quorum PP3010, Quorum Technologies Ltd, Lewes, East Sussex, UK) kept the samples frozen during the imaging process. After placing each sample into the preparation chamber, samples were sublimed from -165 °C to -90 °C for 7 minutes to remove ice contamination from the sample surface. Upon completion, samples were coated with gold-palladium for 20 seconds at a current of 10 mA. Images were recorded at a voltage of 5 kV and a beam current of 0.4 mA. During both imaging methods, the entire cross-section of xylem tissue was imaged, and liquid filled and cavitated vessels (vessels lacking water) were counted. The percentage of liquid filled vessels was calculated by dividing the number of liquid filled vessels by the total number of vessels. Three random samples per plant organ and replicate were then analyzed.

Air seeding pressure

Single-vessel air injection pressure thresholds of roots (n=10), petiole-leaf veins (n=10), and stems (n=10) of *P. x canadensis* were determined using the single vessel injection technique (Melcher *et al.*, 2003). Single-vessel air injection threshold measurements for *H. annuus* organs were performed as described in earlier work (A.E. Huber, P.J. Melcher, M.A. Piñeros, T.L. Setter, and T. L. Bauerle, unpublished). Organ segments were excised under water from well-watered, overnight-equilibrated *P. x canadensis* plants. Then, glass-microcapillary tubes were inserted into an open vessel lumen via a micromanipulator and 50x stereo microscope (SZ-STB2, Olympus Tokyo) and glued to the segment using a fast-setting cyanoacrylic glue (Locolite Super Bonder 409, Locolite Corp., Rocky Hill, CA) and an accelerator (Locolite 712, Locolite Corp., Rocky Hill, CA). Different vessel lumen diameters were probed to eliminate large-vessel bias and ensure that measurements were made across vessels of different diameters. The open end of the glass tube was attached to a pressure chamber system (Model 1000, PMS Instrument Company, Corvallis, OR) through HPLC tubing before the glass tube and sample were placed underwater (5-8 cm deep). Lastly, pressure was applied (100 kPA min^{-1}) until tiny bubbles were observed to exit the downstream end of the sample, which determined the pressure threshold required to force compressed nitrogen gas across inter-vessel bordered pit membranes. Measurements of air seeding pressures lower than 100 kPa were discarded. Vessels with such low air pressure are most likely lacking pit membranes throughout the length of the organ segment (Melcher *et al.*, 2003).

Relative water content

Relative water content (RWC) of woody roots, stems, petioles, and leaf blades of *H. annuus* and deciduous trees, and on woody roots, stems and needles of conifers was measured. On measurement days, organs were cut at noon (two random samples per plant), their fresh weight measured with an analytical balance (HR-200, A&D, Elk Grove, Il) and subsequently rehydrated by floating in tap water for three hours in the lab. After blotting off excess water, the plant organs were reweighed to determine the saturated weight (SW). Finally, plant organs were dried at 65 °C, to determine dry weight (DW). RWC was determined with the following equation

$$RWC = (FW-DW)/(SW-DW) \quad \text{(Eq. 4.1)}$$

Statistical analysis

Statistical analysis was performed in JMP pro 12 (SAS Institute Inc., Cary, NC.) All tests were performed with probability level $P < 0.05$. Changes in the dependent variable within organs were calculated using an ANOVA with FC as a fixed effect and replicates as a random effect. Multiple comparisons between treatments were made using the Tukey HSD test. Data were transformed for organ potential data and liquid filled vessel data to fulfill the model assumptions. However, data are presented in the non-transformed version. Additionally, organ potential data were also compared between organs at each soil field capacity level. For this model, organ, field capacity and organ x field capacity were used as a fixed effect.

4.3 Results

Stomatal conductance and organ potential

Stomatal closure was initiated in *H. annuus* and *P. x canadensis* between 100% and 75% FC steps (Fig. 4.1a,b). Stomatal closure in *H. annuus* occurred at a leaf water potential of -0.41 ± 0.03 MPa, whereas stomatal closure in *P. x canadensis* occurred at a two-fold lower water potential of -0.85 ± 0.03 MPa as shown by the comparison of FC to Ψ_{leaf} (Fig. 4.2a,b). The rate at which the stomatal conductance (gs) declined was different across the two model species: While *P. x canadensis* gs was near zero at 75% FC ($P > 0.0001$; Fig. 4.1b), *H. annuus* gs did not achieve similar values until 50% FC was reached (gs decline between 100 and 50% FC $P < 0.0001$; Fig. 4.1a).

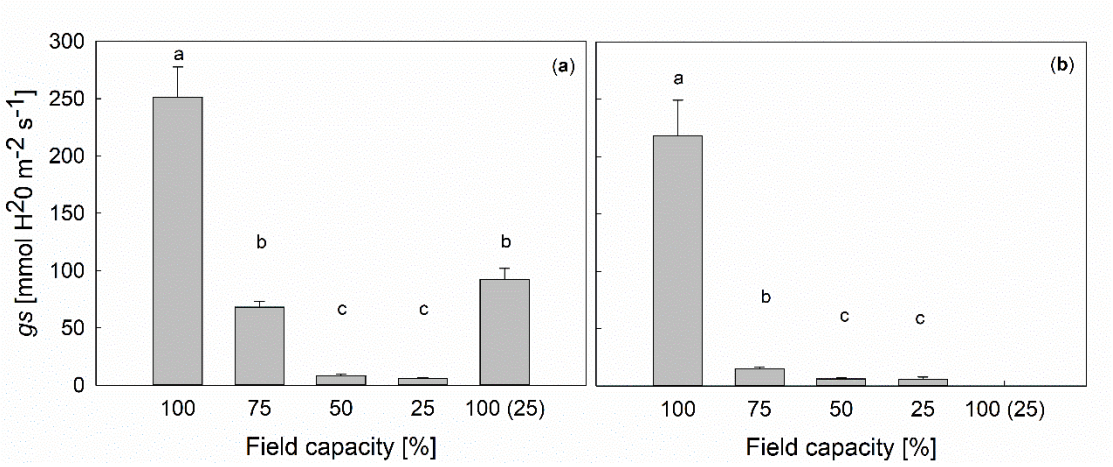

Figure 4.1: Mean (+/- SE) stomatal conductance (gs) of *H. annuus* (a) and *P. x canadensis* (b) measured at different field capacities (FC) that ranged from saturated (100% FC) to extreme drought (25% FC) followed by rewatering to saturation (100 (25)% FC) (n =8, respectively). Letters above columns represent significant differences ($P < 0.05$).

H. annuus and *P. x canadensis* exhibited very different organ-level Ψ responses to the changes in FC (Fig. 4.2a,c,e vs 4.2b,d,f). *H. annuus* Ψ_{leaf} decreased by a total of 2.0 MPa over the course of the experiment ($P < 0.0001$) compared to no observed changes in Ψ_{stem}, and only minimal changes in Ψ_{root} (0.2 MPa, $P < 0.0001$, Fig. 4.2a,c,e). In *P. x canadensis*, Ψ of all three plant organs declined by ca. 2.2 MPa in response to changes in FC ($P < 0.0001$, Fig. 4.2b,d,f). After rewatering, gs of *H. annuus* plants only recovered to values comparable to 75% FC (Fig. 4.1a), while Ψ_{leaf} and Ψ_{root} of *H. annuus* completely recovered to values comparable to 100% FC ($P < 0.0001$, and $P = 0.0005$ respectively). *P. x canadensis* leaf measurements were not possible because *P. x canadensis* shed its leaves after 25% FC. *P. x canadensis* Ψ_{root} recovered to initial values ($P < 0.0001$), while Ψ_{stem} only recovered to values comparable to 75% FC ($P < 0.0018$). Comparison of Ψ_{organ} within a soil moisture level revealed that despite stomatal closure, Ψ_{leaf} of *H. annuus* was never in equilibrium with Ψ_{stem} or Ψ_{root} ($P < 0.007$), while Ψ_{leaf} of *P. x canadensis* reached equilibrium with Ψ_{stem} and Ψ_{root} at 25% FC.

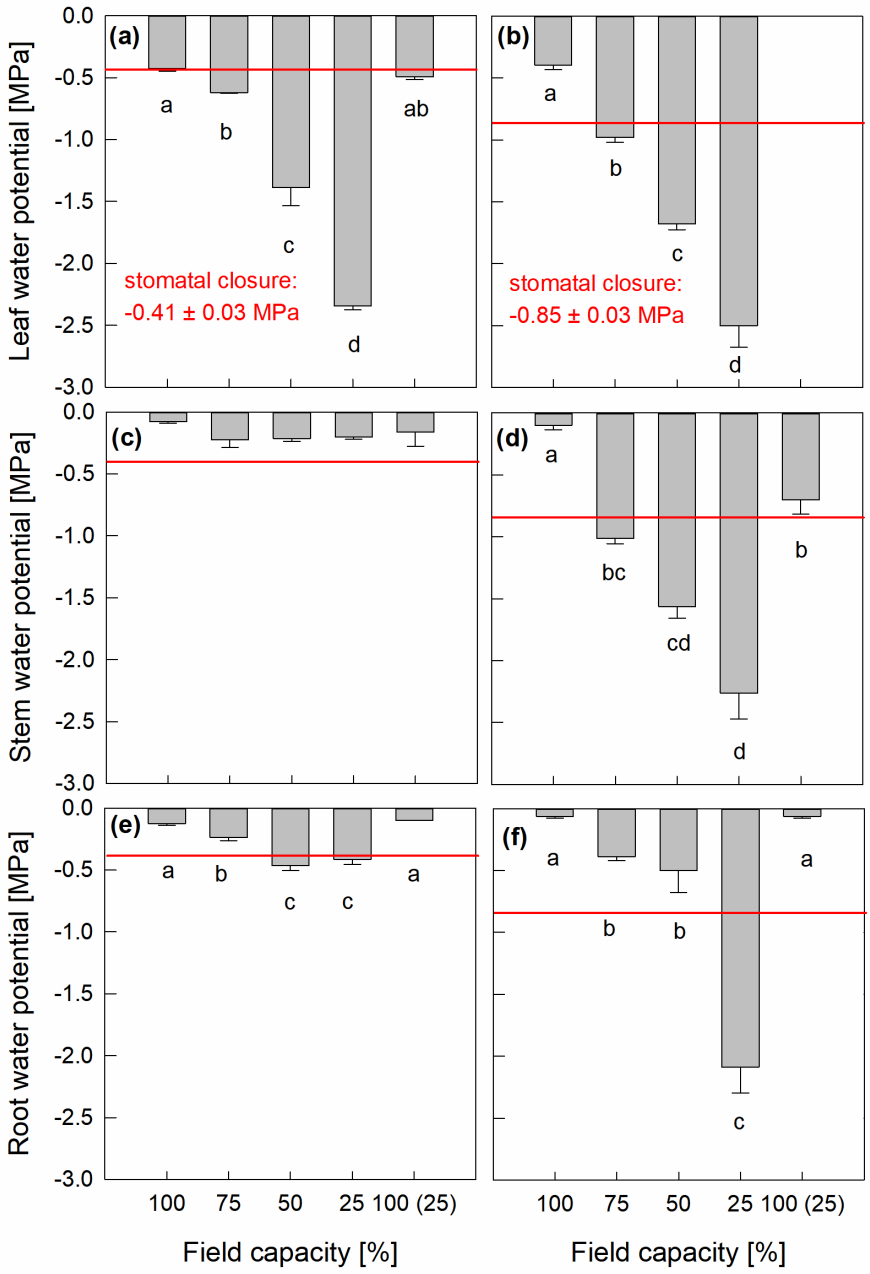

Figure 4.2: Mean (+/- SE) uncovered root, stem and leaf water potentials of *H. annuus* (a, c, e) and *P. x canadensis* (b, d, f) measured at different field capacities (FC) ranging from saturated (100% FC) to extreme drought (25% FC) and followed by rewatering to saturation (100 (25)% FC). The red line represents the mean leaf water potential at the point of stomatal closure. *P. x canadensis* leaf water potential at 100 (25)% FC was not measured due to leaf shedding after 25% FC. Letters below columns represent significant differences ($P < 0.05$).

In *A. saccharum*, *A. saccharinum*, and *T. canadensis* stomatal closure occurred between 75% and 50 % FC ($P < 0.0001$, respectively) (Fig. 4.8a,d,j), while *P. glauca* did not close its stomates until 25% FC ($P < 0.0001$) (Fig. 4.8g). Stem and leaf water potential of both *Acer* species declined continuously ~2.0 MPa during the entire dry-down period ($P < 0.0001$, respectively) (Fig. 4.8b,e). Roots of *A. saccharinum* showed a similar drop, while Ψ_{root} of *A. saccharum* only decreased ~1.5 MPa ($P < 0.0001$, respectively) (Fig. 4.8b,e). The organ potentials of the two conifer species decreased to -2.0 MPa in *P. glauca* and -1.8 MPa in *T. canadensis* (at 25% FC ($P < 0.0001$, respectively)) (Fig. 4.8h,k).

After rewatering, gs of *A. saccharinum* recovered significantly ($P = 0.0009$), although not to pre-drought levels. Stomatal conductance of *A. saccharum* remained low (Fig. 4.8a). All *Acer* organs recovered to pre-drought stress conditions ($P < 0.0001$) except for Ψ_{stem} of *A. saccharum* ($P = 0.1027$), even though Ψ_{stem} increased by approximately 1.5 MPa (Fig. 4.8b,e). Stomatal conductance of both conifer species recovered completely ($P < 0.0001$ respectively) (Fig. 4.8g,j). This recovery coincided with the significant increase in Ψ_{root}, Ψ_{stem}, and Ψ_{twig} in both conifer species, which recovered to values that were comparable to 100% FC after rewatering ($P < 0.0001$ respectively; Fig. 4.8h,k).

Embolism formation, embolism threshold, and embolism recovery measured in the three organ systems

At 25% FC, the proportion of embolized vessels in *H. annuus* petioles and stems increased to 60% in the petiole ($P = 0.0158$) and 28% in the stem compared to the

100% FC (P = 0.0432) (Fig. 4.3a). Xylem vessels of *H. annuus* roots showed the lowest proportion of embolized vessels during the dry-down period, even though embolized vessels were recorded at higher FCs than for the stems and the petioles. At 50% FC, we recorded a 10% increase of embolized root vessels (P = 0.0463). This proportion remained unchanged until the end of the dry-down treatment (Fig. 4.3a). After rewatering, the number of embolized xylem vessels decreased significantly in petioles (P = 0.0292) and roots (P = 0.0135) but not in the stem (Fig. 4.3a).

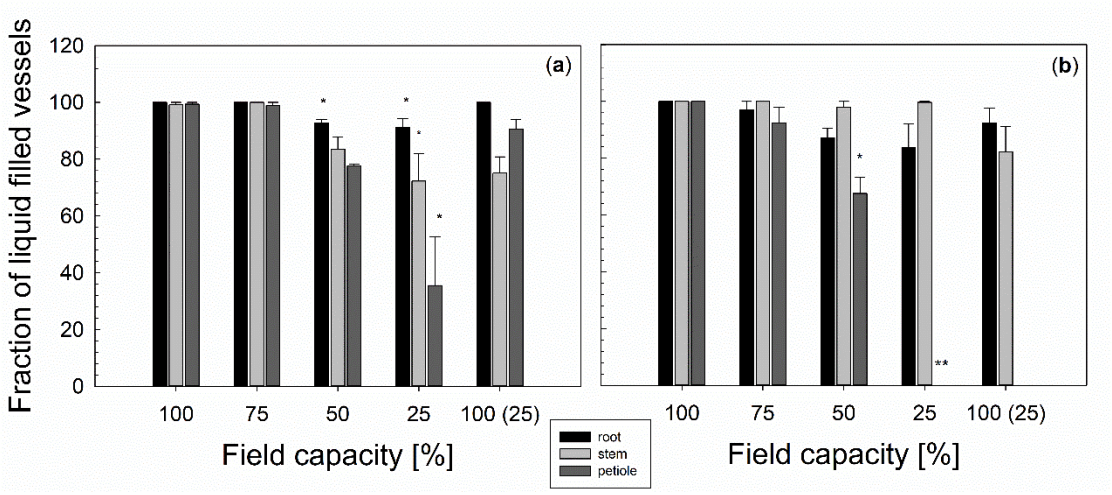

Figure 4.3: The mean fraction (+/-SE) of liquid filled vessels of *H. annuus* (a) and *P. x canadensis* (b) (n =4) exposed to changes in field capacities (FC) from 100% FC (saturated) to 25% FC (extreme drought) followed by rewatering to 100% FC (100 (25)% FC). 100% of the xylem vessels in *P. x canadensis* petioles lost their functionality at 25 % FC and did not recover after rewatering 100 (25)% FC. Columns with stars (*) denote significant differences (P < 0.05) at different FC within each plant organ system in comparison to 100% FC.

In *P. x canadensis*, petioles were the only tissues that had a significant increase in embolism formation (30% increase at a 50% FC (P < 0.0001)), with the proportion of embolisms continuing to increase until 100% of the vessels were embolized at 25%

FC ($P < 0.0012$). No significant increases in embolized vessels were observed in the stems or the roots (Fig. 4.3b). Embolism recovery was difficult to measure in *P. x canadensis* because the trees dropped most of their leaves after the 25% FC drought treatment.

P. x canadensis stems were the most cavitation resistant organ compared to the roots and the petioles as demonstrated through air seeding thresholds. The air seeding pressure was twice as negative as that measured in roots and petioles ($P < 0.0001$ respectively, Fig. 4.4).

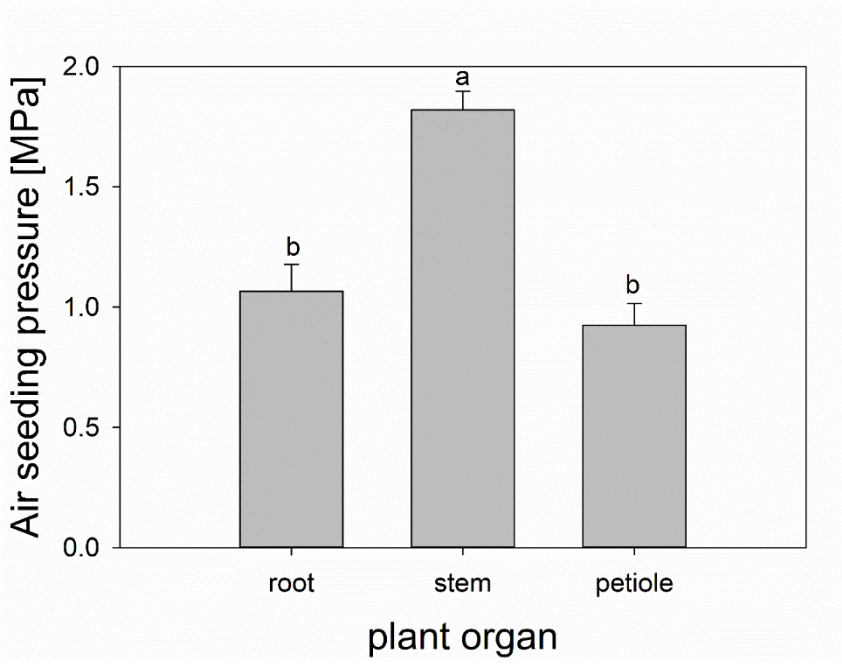

Figure 4.4: Mean (+/- SE) air seeding pressure of root, stem, and leaf of *P. x canadensis* (n = 10, respectively). Letters represent significant differences ($P < 0.05$).

In *A. saccharum* and *A. saccharinum*, the only plant organ that had an increase in embolized vessels during the dry-down period was the petiole ($P < 0.0001$ for *A. saccharum* and $P = 0.0007$ for *A. saccharinum*; Fig. 4.8c,f). The ~60% increase in the

number of embolized vessels in *A. saccharum* and *A. saccharinum* petioles occurred at 25% FC. Xylem vessels of stems and roots of both conifer species remained fully hydrated throughout the entire drought experiment (Fig. 4.8i,l).

The comparison of Ψ_{stem} and established PLC curves revealed that only *P x canadensis* and *A. saccharinum* reached Ψ_{stem} low enough to cause a 50% loss in hydraulic conductance (Table 4.1; Fig. 4.2c,d and 4.8b,e,h,k).

Table 4.1: P_{50} values of *A. saccharum*, *A. saccharinum*, *P. glauca*, *T. canadensis*, *P. x canadensis*, and *H. annuus* with respective references.

Tree species	**P_{50}-value (branch)**	**Reference**
Acer saccharum	-4.0 MPa	Tyree and Dixon, 1986 Tyree and Ewers, 1991
Acer saccharinum	-0.5 to -1.5 MPa	Tsuda and Tyree, 1997
Picea glauca	-3.8 MPa	Sperry *et al.*, 1994
	-4.5 MPa	Laur and Hacke, 2014
Tsuga canadensis	-8.0 MPa	Huggett *et al.*, 2018
Populus x canadensis	-0.69 MPa	A.E. Huber and T.L. Bauerle, pers. obs.
Helianthus annuus	-2.5 to 3.0 MPa	A.E. Huber, P.J. Melcher, M.A. Piñeros, T.L. Setter, and T. L. Bauerle, unpublished

After rewatering, the embolized xylem vessels in petioles of both *Acer* species recovered completely to pre-drought stress conditions ($P < 0.0001$ and $P = 0.001$ respectively) (Fig. 4.8c,f). The 30% change in the number of liquid filled vessels in the stems of *A. saccharum* after rewatering was statistically significant ($P = 0.0519$; Fig. 4.8c).

Relative water content of root, stem, petiole, and leaf blade

The relative water content (RWC) decreased significantly across all tissues in *H. annuus* from 100 to 25% FC ($P = 0.0294$ for root, $P < 0.0001$ for stems, petioles, and leaf blades respectively, Fig. 4.5a). The greatest reduction in RWC in *H. annuus* was approximately 20% across all tissues and occurred from the reduction of 75% FC to 50% FC. After rewatering, all tissues recovered to a RWC comparable to 100% FC ($P < 0.0001$ for all organs; Fig. 4.5a). On the contrary, *P. x canadensis* RWC did not change in leaves, stems, or roots at any of the drought and rewatering treatments; with the exception of the leaf blades which decreased by ca. 60% RWC after rewatering ($P < 0.0001$; Fig. 4.5b).

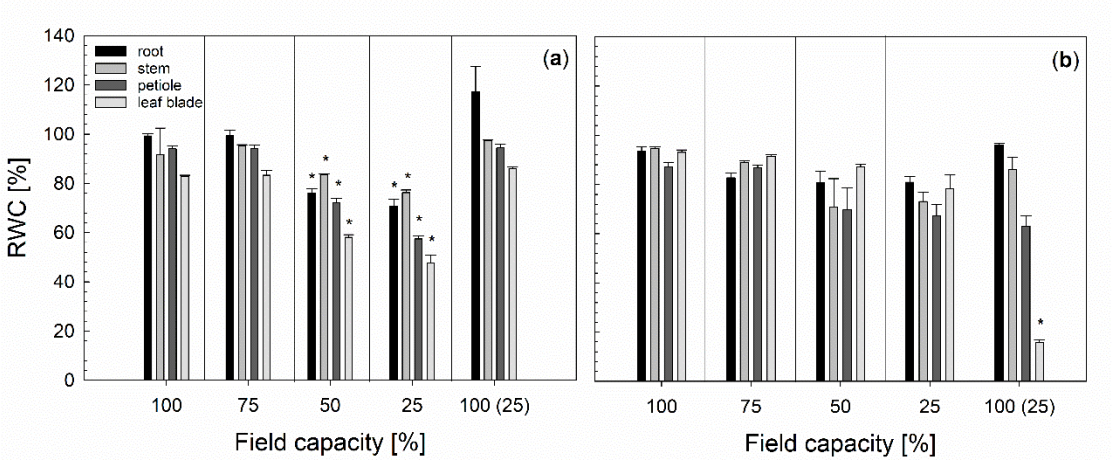

Figure 4.5: Mean +/-SE Relative Water Content (RWC) of roots, stems, petioles, and leaf blades of *H. annuus* (a) and *P. x canadensis* (b) (n =4, respectively) as field capacity (FC) changed from saturated (100% FC) to extreme drought (25% FC) followed by rewatering to saturating (100 (25)% FC). Columns with a star (*) are significantly different ($P < 0.05$) from columns at previous FC within one organ.

Extra cellular tissue deformation in *H. annuus* roots and petioles

Cryo-SEM images revealed that under fully hydrated conditions, parenchyma cells in the extra-xylary tissue of *H. annuus* petioles and roots were fully hydrated and turgid. Furthermore, we identified intercellular space between the parenchyma cells (Fig. 4.6a and 4.7a). During the dry-down period, the intercellular spaces were not present, and parenchyma cells were deformed, indicating that the tissue underwent cellular deformation during the dry-down period (Fig. 4.6b and 4.7b). After drought stress recovery, the cell deformation was reversed (Fig. 4.6c and 4.7c). In *P. x canadensis*, tissue deformation was not detected.

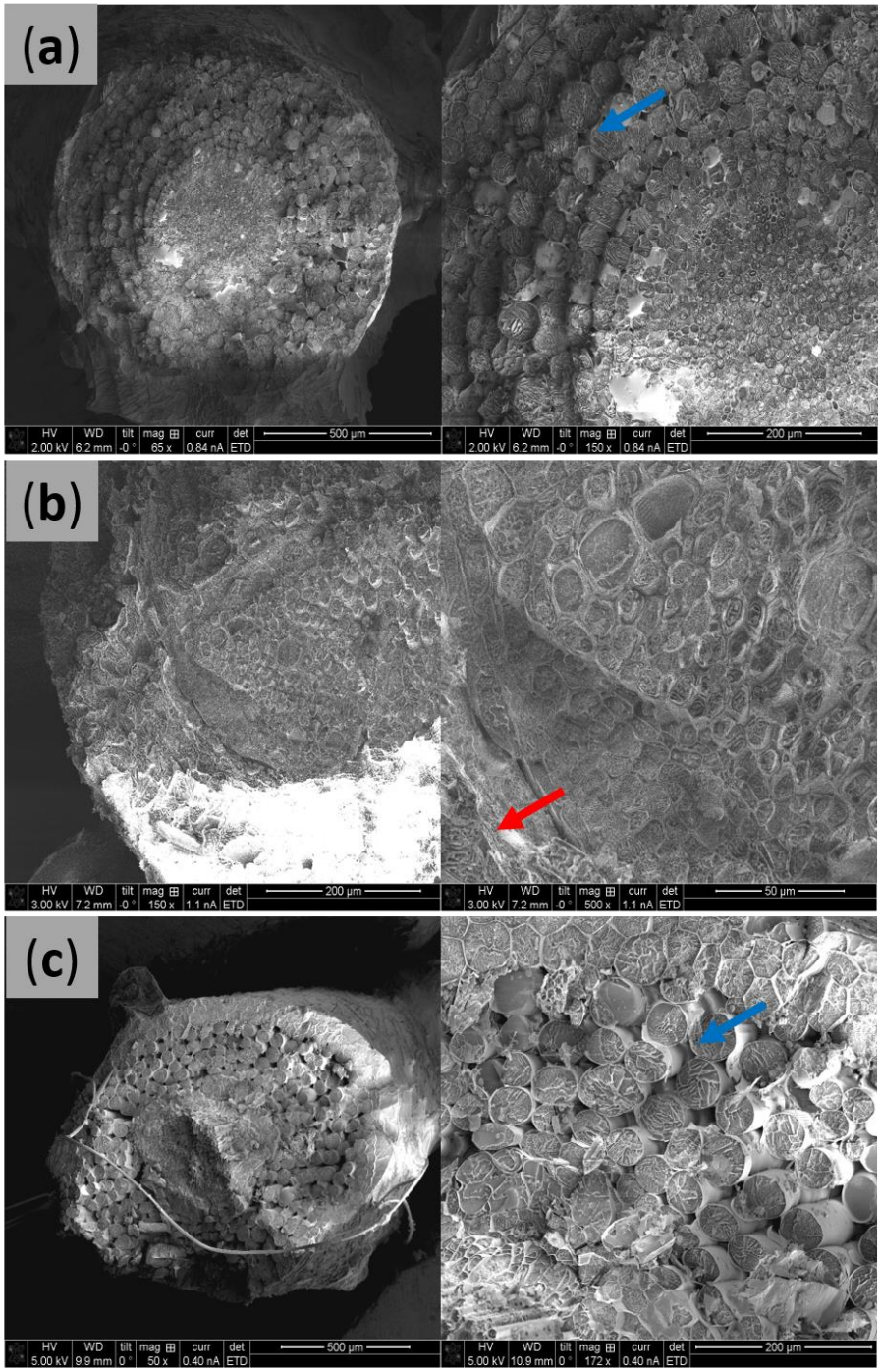

Figure 4.6: *H. annuus* root cross-sections at different field capacities (FC) ranging from saturated (a) (100% FC) to extreme drought (b) (25% FC) followed by rewatering to saturating (c) (100 (25)% FC). Right images are close-ups of the left images to show more detail. Under saturated conditions (a, c) the parenchyma cells of the cortex are turgid and intercellular space is visible (blue arrows). Under extreme drought (b) parenchyma cells are deformed and intercellular cavities are absent (blue arrow).

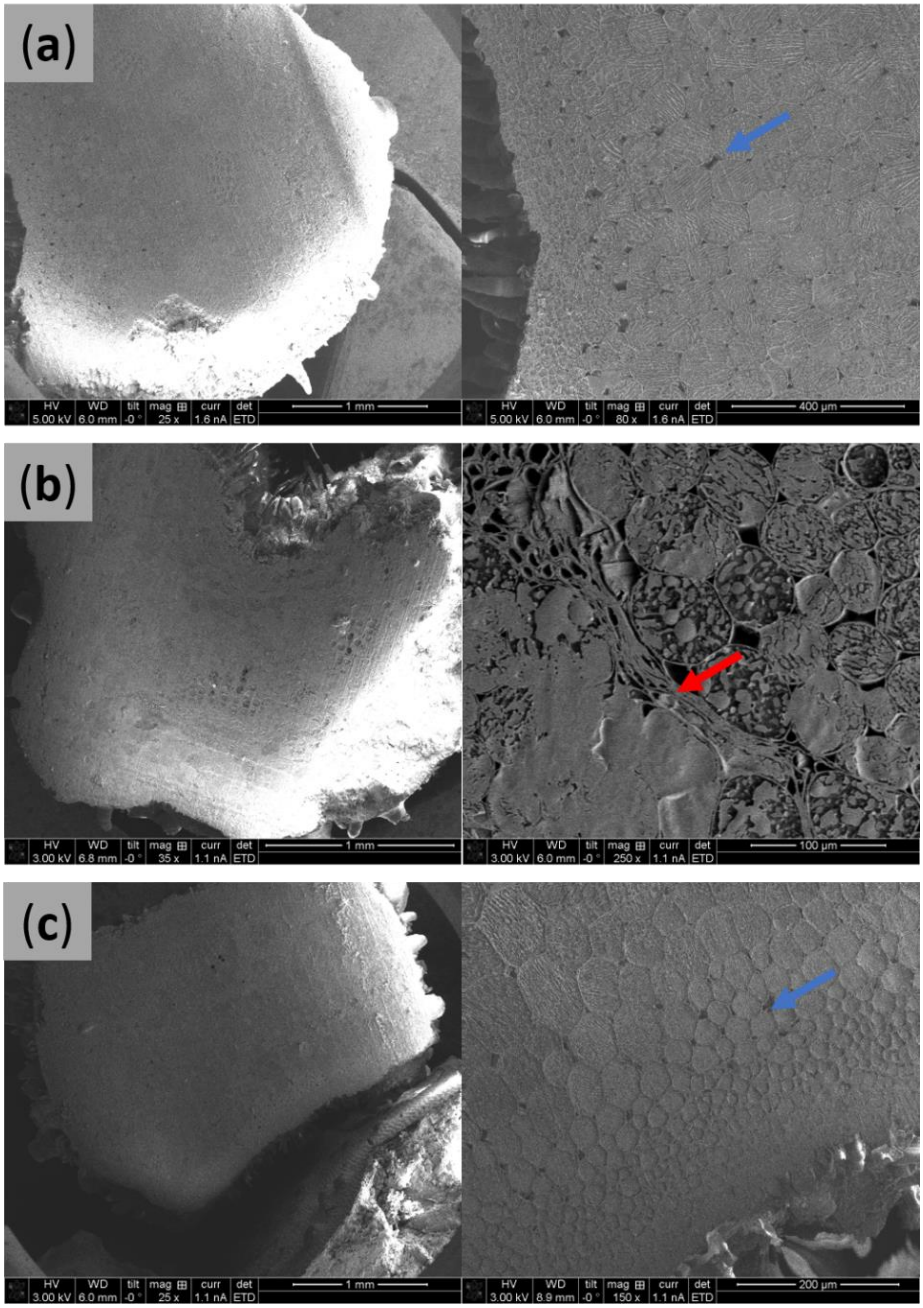

Figure 4.7: Different magnifications of *H. annuus* petiole cross-sections at different field capacities (FC) ranging from saturated (a) (100% FC) to moderate stress (b) (50% FC) followed by rewatering to saturating (c) (100 (25)% FC). Right images are close-ups of the left images to show more details. Under saturated conditions (a, c) the parenchyma cells of the cortex are turgid and intercellular space are visible (blue arrows). Under moderate stress conditions (b) parenchyma cells are deformed and intercellular cavities are absent (blue arrow).

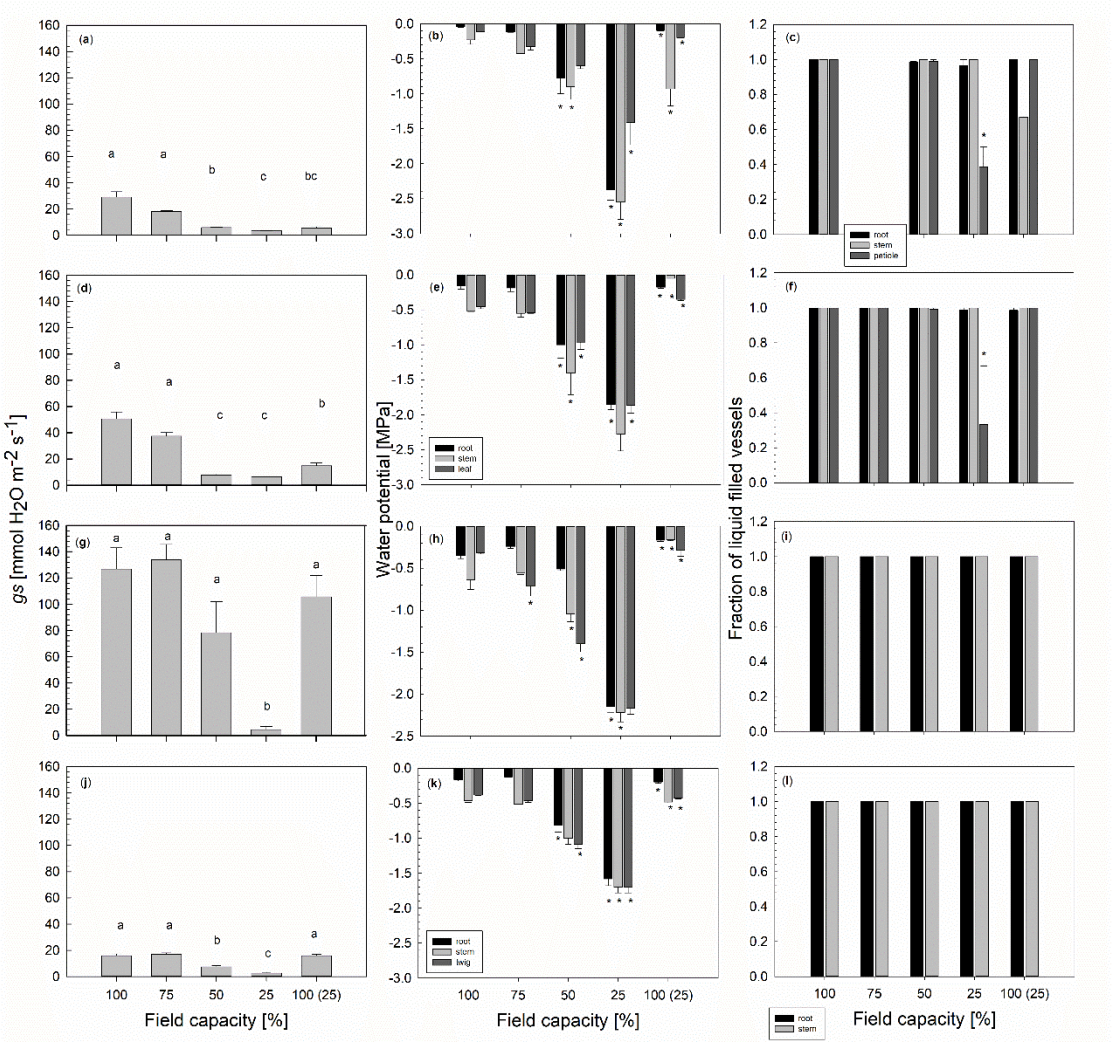

Figure 4.8: Mean (+/- SE) stomatal conductance (gs), organ water potential, and fraction of liquid filled vessels of *A. saccharum* (a, b, c), *A. saccharinum* (d, e, f), *P. glauca* (g, h, i), and *T. canadensis* (j, k, l) (n= 4, respectively) measured as field capacity (FC) changed from saturated (100% FC) to extreme drought (25% FC) followed by rewatering to saturating (100 (25)% FC). Columns with different letters are significantly different ($P < 0.05$). Columns with a star (*) are significantly different ($P < 0.05$) from columns at previous FC within one organ.

4.4 Discussion

Plant response at the beginning of the drought stress period:

For all species measured, we found that stomatal closure was closely correlated with the leaf and not with the root or the stem water status (Fig, 4.2a-f and

4.8a,b,d,e,g,h,j,k), supporting previous findings (Saliendra *et al.*, 1995; Cochard *et al.*, 1996; Salleo *et al.*, 2000; Brodribb *et al.*, 2003; Jacobsen *et al.*, 2008). *P. glauca* closed its stomata at lower field capacities compared to the other species, despite having the highest rate of stomatal conductance (Fig. 4.8a,d,g,j). As described in other studies, this may result from a high water capacitance that allowed *P. glauca* leaves to maintain open stomata longer when exposed to sustained drought stress conditions compared to species with lower capacitance (Holbrook and Sinclair, 1992; Scholz *et al.*, 2007).

Xylem vessels within all the plant organs for all six species remained liquid filled at the onset of stomatal closure (Fig. 4.3a,b and 4.8c,f,i,l), as determined from analysis of vessel content using cryo-scanning-microscopy (cryo-SEM). Vessels scored as liquid filled were considered to be functional (water conducting) in long-distance sap transport. It seems unlikely that the liquid filled xylem vessels within this study were hydraulically isolated (Mrad *et al.*, 2018) since we did not see any embolisms in any of the samples measured before the onset of stomatal closure. Thus, it is highly unlikely that there were embolisms upstream or downstream of the random cross-sections analyzed and it is unlikely that the water in the xylem originated from an ongoing embolism refilling process (Borghetti *et al.*, 1991; Brodersen *et al.*, 2010; Melcher and Zwieniecki, 2013; Zwieniecki *et al.*, 2013). Additionally, in the species tested in this study, our findings support the observation by Scoffoni *et al.* (2017) that mild drought conditions do not result in a massive number of embolisms and support our hypothesis that embolism is not tightly correlated to stomatal function in these species.

Plant response during drought stress:

Leaf water potentials and Ψ_{stem} of all tree species continually declined until 25% FC (Fig, 4.2b,d and 4.8b,e,h,k). Ψ_{root} and Ψ_{stem} of *H. annuus* however, did not significantly change throughout the entire drought treatment (Fig. 4.2c,e), suggesting that herbaceous and woody species have disparate organ-level responses to changes in water availability. For example, we observed deformation of extra-xylary tissue and the loss of intercellular spaces within *H. annuus* roots and petioles as drought intensity increased, although the deformation of extra-xylary tissue occurred at more negative Ψ_{leaf} compared to roots (Fig. 4.6a,b,c and Fig. 4.7a,b,c). We suspect that the large fraction of parenchyma cells, extra-xylary tissues, and the intercellular spaces within the organ systems of *H. annuus* provided a source of water to the xylem stream as the level of drought intensified. We calculated the amount of water in the sunflowers stems (height 40 cm, radius 1 cm) to be 120 ml under hydrated conditions, assuming that the stem is a cylinder. A reduction in the volume of the extra-xylary tissue by 13% would release around 12 ml of water into the xylem stream. Likewise, a 13 % shrinkage of extra xylary tissue in the petiole (length 5 cm, radius 0.3 cm) would release around 0.2 ml. Thus, a sunflower plant with 15 petioles would give the plant water resources for another 1.5 days, given that sunflower plants lost around 10 ml water a day, after stomatal closure. Reduction in xylem conducting area from tissue compression (Scoffoni *et al.*, 2017) has been shown to occur in leaf veins and may serve as a mechanism to reduce embolism formation in xylary tissue during drought (Brodribb and Holbrook, 2005; Scoffoni *et al.*, 2017). Our data support these findings, as we observed significant deformation of extra-xylary tissue within the roots at 25%

FC and yet, we observed that only 10% of the root vessels were embolized (Fig. 4.3a and 4.6b).

No tissue deformation occurred in either petioles or roots of *P. x canadensis* plants exposed to the varying soil moisture levels. We suspect that this tissue resilience might have been a result of the unaltered organ RWC throughout the experiment (Fig. 4.5b). As Ψ_{leaf} and Ψ_{stem} decreased with decreasing FCs, embolism formation varied across the organ systems. In *P. x canadensis*, the petiole xylem vessels were 100% embolized at the end of the dry-down period, compared to 0% embolized in the stem xylem vessels (Fig. 4.3b). Leaf shedding after the drought treatment in *P. x canadensis* most likely serves as a mechanism to reduce leaf area and evapotranspiration and may also protect the hydraulic continuum by isolating the stem hydraulic system from the leaves during drought (Wolfe *et al.*, 2016). Protecting the hydraulic integrity in stems through leaf shedding supports the hypothesis that deciduous leaves can be easily discarded during long periods of drought due to their inexpensive construction costs relative to stems (Chabot and Hicks, 1982). *P. x canadensis* Ψ_{root} remained significantly higher than Ψ_{leaf} and Ψ_{stem} until 50% FC (Fig. 4.2b,d,f). Since stomatal closure occurred between 100% and 75% FC and flowrates are minimized with stomatal closure, we would have expected Ψ to be equilibrated across plant organs. Our findings suggest a hydraulic resistance in the root that prevented Ψ_{root} from equilibrating with Ψ_{stem} and Ψ_{leaf} (Begg and Turner, 1970) demonstrating that Ψ_{root} cannot be determined by covered Ψ_{leaf} measurements. Moreover, in order to correlate the hydraulic status of plant organs to Ψ_{leaf}, one should make concurrent measurements of the Ψ of each organ system.

We found that the root and petiole xylem of *P. x canadensis* were equally vulnerable to drought stress and more vulnerable than stems (Fig. 4.4). However, drawing conclusions based on these measurements are misleading, because *P. x canadensis* petioles reach the air seeding pressure threshold at higher FCs than roots. Similar findings have shown that the air seeding thresholds measured in *H. annuus* roots and leaves were comparable to each other, but there was a large disparity in Ψ_{root} and Ψ_{leaf} measurements at different drought levels (A.E. Huber, P.J. Melcher, M.A. Piñeros, T.L. Setter, and T.L. Bauerle, unpublished). Furthermore, even though *H. annuus* Ψ_{leaf} reached values that would cause embolism formation in petioles and root xylem, the roots never reached Ψ values that would result in embolism formation (A.E. Huber, P.J. Melcher, M.A. Piñeros, T.L. Setter, and T.L. Bauerle, unpublished). These data suggest that the roots measured *in situ* were the most resistant to drought stress, followed by the stem, and then the leaf. In our study, the petiole xylem vessels were found to be the most vulnerable tissue to embolism formation and the only tissue that operated at Ψ near their embolism thresholds. Petioles, therefore, acted as a hydraulic isolation safety valve during times of drought stress, which supports the segmentation hypothesis (Zimmermann, 1983).

Here we show that xylem vessels remained liquid-filled even when Ψ levels were lower than the calculated values determined to result in 50% embolized vessels (found from air injection and P_{50} values), across all organ systems. It is possible that there is a method limitation that resulted in potential under- or overestimation of embolism formation. Cryo-methods have been criticized as artificially causing cavitation events to occur as a consequence of the tensions acting on the water column during the

freezing process (Cochard *et al.*, 2000). In this study, however, we observed no such artifacts, raising questions about the validity of these claims. For example, we found that only two plant species reached the predicted Ψ that would have caused a 50% loss of hydraulic conductance (P_{50} value), but we did not detect any embolized xylem vessels in these species at these Ψ (Table 4.1, Fig. 4.3a,b and 4.8c,f,i,l). Further, the cryo-method also showed that ~75% of the stem xylem vessels were liquid filled in *R. mangle* growing in seawater at maximum covered leaf water potentials of -3.2 MPa (Melcher *et al.*, 2001), suggesting that the cryo-method does not cause artificial embolism events.

The minimum native Ψ_{stem} that we measured during this experiment was -2.5 MPa. However, the predicted P_{50} values of four of the six examined species are at much lower water potentials (Table 4.1). These results confirm previous findings that show that embolism thresholds are far below the Ψ stress levels that plants would experience naturally (Melcher and Zwieniecki, 2013), and raise the question of the usefulness that P_{50} values have on predicting drought stress resistance of plants during drought scenarios (Lo Gullo *et al.*, 2003; Tyree, 2003; McDowell *et al.*, 2008). The value of using stem-level P_{50} values as a criterion to assess whole plant response to drought is not strongly grounded in biological relevance, for example: P_{50} values do not account for differences in plant organ vulnerabilities; they do not take into account if the Ψ across the organ-systems are near equilibrium at the time when transpiration is near zero and stomata are closed, and they ignore Ψ variation that may exist at the different organ-systems during drought exposure that would result in 50% embolism in the xylem outside of the stem. Thus, studies that rely only on assessing plant

drought response from measurements made on P_{50} values of stems are not ideal in predicting whole plant responses to drought stress.

Plant response after the rewatering event:

We observed varying recovery strategies across the different species during rehydration from drought. As expected, the root systems of all six species rehydrated to their full extent after rewatering (Fig. 4.2e,f and 4.8b,e,h,k). This response makes sense since one would expect root rehydration to take place prior to other plant organs (stems and leaves) since the roots are the major site of water uptake. Complete recovery in Ψ_{stem} was observed in *A. saccharinum* and the two conifer species (Fig. 4.8e,h,k), while Ψ_{stem} in *H. annuus*, *P. x canadensis*, and *A. saccharum*, only partly recovered (Fig. 4.2c,d and 4.8b), even after two days of rewatering. Embolized xylem vessels of *H. annuus* stems did not recover after rewatering, as determined by the fraction of empty xylem vessels in the cryo-image analysis (Fig. 4.3a). Additionally, after rewatering, we observed a 15% and 40% increase in embolized vessels in the stems of both *P. x canadensis* and *A. saccharum* trees, respectively (Fig. 4.3b and 4.8c). Although the increase in embolized vessels in *P. x canadensis* stems was not statistically significant after the correction for multiple comparisons, this observation was unexpected because one would not expect that rehydration would result in increased embolism formation in the stems. One possible explanation for this observation in *P. x canadensis* is that this tree species relies on stem-level photosynthesis which aids in the development of new xylem tissue growth after drought stress (Bloemen *et al.*, 2016). This investment in new growth may serve to

restore the hydraulic continuum rather than repairing cavitated xylem vessels (Brodribb *et al.*, 2010). Although we are unable to fully explain why cavitation events increased after rewatering, we speculate that the observed increase may have resulted from the mechanical expansion of xylem vessel conduits as the root cortex tissues were rehydrating. The swelling of the cortex would result in a minimal expansion of xylem vessels. This minimal expansion might have been enough to increase the water tension in the xylem vessels thus increasing tension in the water columns and increasing embolism formation in the xylem vessels along the hydraulic continuum, e.g., from root to stem xylem. Since this result was unexpected, we did not specifically design experiments to test these hypotheses; however, we did observe turgor changes during rehydration of the parenchyma cells in *H. annuus* petioles and roots (Fig. 4.6c and 4.7c) and found that the recovery of cell turgor occurred prior to stomatal opening (Fig. 4.1a). Clearly, further investigation is needed to clarify the underlying mechanism(s) causing xylem cavitation events after rewatering.

Leaf water potential recovered to values similar to initial pre-drought levels in all species, with the exception of *P. x canadensis* that shed its leaves. Furthermore, we observed recovery of cavitated xylem vessels in both *Acer* species, and *H. annuus* petioles after rewatering (Fig. 4.5 and 4.8c,f). The fact that refilling was not observed in stem xylem in *H. annuus*, *P. x canadensis*, and *A. saccharum*, suggests that restoring hydraulic continuity of the petiole is of higher priority for these plant species. In *A. saccharum* and *H. annuus*, many of the physiological and anatomical functions seemed to be fully restored in the leaf after rewatering (Fig. 4.3, 4.4, 4.6, 4.7 for *H. annuus*, and 4.8a,b,c for *A. saccharum*), with the exception of stomatal

conductance, which remained inhibited, or only partially recovered, indicating that the stem might play an important role in recovering processes after drought stress.

4.5 References

Alder NN, Sperry JS, Pockman WT. 1996. Root and stem xylem embolism, stomatal conductance, and leaf turgor in *Acer grandidentatum* populations along a soil moisture gradient. Oecologia **105**, 293–301.

Bauerle TL, Richards JH, Smart DR, Eissenstat DM. 2008. Importance of internal hydraulic redistribution for prolonging the lifespan of roots in dry soil. Plant, Cell and Environment **31**, 177–186.

Begg JE, Turner NC. 1970. Water potential gradients in field tobacco. Plant Physiology **46**, 343–346.

Blackman CJ, Brodribb TJ, Jordan GJ. 2009. Leaf hydraulics and drought stress: response, recovery and survivorship in four woody temperate plant species. Plant, Cell and Environment **32**, 1584–1595.

Bloemen J, Vergeynst LL, Overlaet-Michiels L, Steppe K. 2016. How important is woody tissue photosynthesis in poplar during drought stress? Trees **30**, 63–72.

Borghetti M, Edwards WRN, Grace J, Jarvis PG, Raschi A. 1991. The refilling of embolized xylem in *Pinus sylvestris* L. Plant, Cell and Environment **14**, 357–369.

Brodersen CR, McElrone AJ. 2013. Maintenance of xylem network transport capacity: a review of embolism repair in vascular plants. Frontiers in Plant Science **4**, 1–11.

Brodersen CR, McElrone AJ, Choat B, Lee EF, Shackel KA, Matthews MA. 2013. In vivo visualizations of drought-induced embolism spread in *Vitis vinifera*. Plant Physiology **161**, 1820–1829.

Brodersen CR, McElrone AJ, Choat B, Matthews MA, Shackel KA. 2010. The dynamics of embolism repair in xylem: in vivo visualizations using high-resolution computed tomography. Plant Physiology **154**, 1088–1095.

Brodribb TJ, Bowman DJMS, Nichols S, Delzon S, Burlett R. 2010. Xylem function and growth rate interact to determine recovery rates after exposure to extreme water deficit. New Phytologist **188**, 533–542.

Brodribb TJ, Cochard H. 2009. Hydraulic failure defines the recovery and point of death in water-stressed conifers. Plant Physiology **149**, 575–584.

Brodribb TJ, Holbrook NM. 2005. Water stress deforms tracheids peripheral to the leaf vein of a tropical conifer. Plant Physiology **137**, 1139–1146.

Brodribb TJ, Holbrook NM. 2006. Declining hydraulic efficiency as transpiring leaves desiccate: two types of response. Plant, Cell and Environment **29**, 2205–2215.

Brodribb TJ, Holbrook NM, Edwards EJ, Gutiérrez M V. 2003. Relations between stomatal closure, leaf turgor and xylem vulnerability in eight tropical dry forest trees. Plant, Cell and Environment **26**, 443–450.

Bucci SJ, Scholz FG, Goldstein G, Meinzer FC, Franco C, Zhang Y, Hao G. 2008. Water relations and hydraulic architecture in *Cerrado* trees : adjustments to seasonal changes in water availability and evaporative demand. Brazilian Journal of Plant Physiology **20**, 233–245.

Bucci SJ, Scholz FG, Goldstein G, Meinzer FC, Sternberg LDSL. 2003. Dynamic changes in hydraulic conductivity in petioles of two savanna tree species: Factors and mechanisms contributing to the refilling of embolized vessels. Plant, Cell and Environment **26**, 1633–1645.

Chabot BF, Hicks DJ. 1982. The Ecology of Leaf Life Spans. Annual Review of Ecology and Systematics **13**, 229–259.

Charra-Vaskou K, Badel E, Burlett R, Cochard H, Delzon S, Mayr S. 2012. Hydraulic efficiency and safety of vascular and non-vascular components in *Pinus pinaster* leaves. Tree Physiology **32**, 1161–1170.

Choat B, Lahr EC, Melcher PJ, Zwieniecki MA, Michele N. 2005. The spatial pattern of air seeding thresholds in mature sugar maple trees. Plant, Cell and Environment **28**, 1082–1089.

Christensen-Dalsgaard KK, Tyree MT. 2014. Frost fatigue and spring recovery of xylem vessels in three diffuse-porous trees in situ. Plant, Cell and Environment **37**, 1074–1085.

Cochard H, Bodet C, Améglio T, Cruiziat P. 2000. Cryo-SEM observations of vessel content during transpiration in walnut petioles: facts or artifacts? Plant Physiology **124**, 1191–1202.

Cochard H, Breda N, Grainer A, Aussenac G. 1992. Vulnerability to air embolism of three European species (*Quercus petraea* (Matt) Liebl, *Q pubescens* Wild, *Q robur* L). Annals of Forest Science, 225–233.

Cochard H, Bréda N, Granier A. 1996. Whole tree hydraulic conductance and water loss regulation in *Quercus* during drought: evidence for stomatal control of

embolism ? Annals of Forest Science, 197–207.

Cochard H, Foux F, Mayr S, Coutand C. 2004. Xylem wall collapse in water-stressed pine needles. Plant Physiology **134**, 401–408.

Cuneo IF, Knipfer T, Brodersen CR, McElrone AJ. 2016. Mechanical failure of fine root cortical cells initiates plant hydraulic decline during drought. Plant Physiology **172**, 1669–1678.

Froux F, Ducrey M, Dreyer E, Huc R. 2005. Vulnerability to embolism differs in roots and shoots and among three Mediterranean conifers: consequences for stomatal regulation of water loss? Trees **19**, 137–144.

Gambles RL, Dengler RE. 1982. The anatomy of the leaf or red pine, *Pinus resinosa*. II Vascular tissue. Canadian Journal of Botany **60**, 2804–2824.

Lo Gullo MA, Salleo S, Rosso R, Trifilò P. 2003. Drought resistance of 2-year-old saplings of Mediterranean forest trees in the field: relations between water relations, hydraulics and productivity. Plant and Soil **250**, 259–272.

Hacke U, Sauter JJ. 1996. Drought-induced xylem dysfunction in petioles, branches, and roots of *Populus balsamifera* L. and *Alnus glutinosa* (L.) Gaertn. Plant Physiology **111**, 413–417.

Hacke UG, Sperry JS. 2003. Limits to xylem refilling under negative pressure in *Laurus nobilis* and *Acer negundo*. Plant, Cell and Environment **26**, 303–311.

Hao GY, Hoffmann WA, Scholz FG, Bucci SJ, Meinzer FC, Franco AC, Cao KF, Goldstein G. 2008. Stem and leaf hydraulics of congeneric tree species from adjacent tropical savanna and forest ecosystems. Oecologia **155**, 405–415.

Holbrook NM, Sinclair TR. 1992. Water balance in the arborescent palm, *Sabal*

palmetto. II. Transpiration and stem water storage. Plant, Cell and Environment **15**, 401–409.

Huggett BA, Savage JA, Preisser EL, Hao G-Y, Holbrook NM. 2018. Impact of hemlock woolly adelgid (*Adelges tsugae*) infestation on xylem structure and function and leaf physiology in eastern hemlock (*Tsuga canadensis*). Functional Plant Biology **45**, 501.

Jacobsen AL, Agenbag L, Esler KJ, Pratt RB, Ewers FW, Davis SD. 2007. Xylem density, biomechanics and anatomical traits correlate with water stress in 17 evergreen shrub species of the Mediterranean-type climate region of South Africa. Journal of Ecology **95**, 171–183.

Jacobsen AL, Pratt RB, Davis SD, Ewers FW. 2008. Comparative community physiology: nonconvergence in water relations among three semi-arid shrub communities. New Phytologist **180**, 100–113.

Johnson DM, Wortemann R, McCulloh KA, Jordan-Meille L, Ward E, Warren JM, Palmroth S, Domec JC. 2016. A test of the hydraulic vulnerability segmentation hypothesis in angiosperm and conifer tree species. Tree Physiology **36**, 983–993.

Klein T, Zeppel MJB, Anderegg WRL, Bloemen J, De Kauwe MG, Hudson P, Ruehr NK, Powell TL, von Arx G, Nardini A. 2018. Xylem embolism refilling and resilience against drought-induced mortality in woody plants: processes and trade-offs. Ecological Research **33**, 839–855.

Laur J, Hacke UG. 2014. Exploring *Picea glauca* aquaporins in the context of needle water uptake and xylem refilling. New Phytologist **203**, 388–400.

Lobo A, Torres-Ruiz JM, Burlett R, *et al.* 2018. Assessing inter- and intraspecific variability of xylem vulnerability to embolism in oaks. Forest Ecology and Management **424**, 53–61.

Maherali H, Pockman W, Jackson RB. 2004. Adaptive variation in the vulnerability of woody plants to xylem cavitation. Ecology **85**, 2184–2199.

Martin-StPaul NK, Longepierre D, Huc R, Delzon S, Burlett R, Joffre R, Rambal S, Cochard H. 2014. How reliable are methods to assess xylem vulnerability to cavitation? The issue of 'open vessel' artifact in oaks. Tree Physiology **34**, 894–905.

McDowell N, Pockman WT, Allen CD, *et al.* 2008. Mechanisms of plant survival and mortality during drought: why do some plants survive while others succumb to drought? New Phytologist **178**, 719–739.

McElrone AJ, Pockman WT, Martínez-Vilalta J, Jackson RB. 2004. Variation in xylem structure and function in stems and roots of trees in 20 m depth. New Phytologist **163**, 507–517.

Melcher PJ, Goldstein G, Meinzer FC, Yount DE, Jones TJ, Holbrook NM, Huang CX. 2001. Water relations of coastal and estuarine *Rhizophora mangle*: xylem pressure potential and dynamics of embolism formation and repair. Oecologia **126**, 182–192.

Melcher PJ, Zwieniecki MA. 2013. Functional analysis of embolism induced by air injection in *Acer rubrum* and *Salix nigra*. Frontiers in Plant Science **4**, 1–10.

Melcher PJ, Zwieniecki MA, Holbrook NM. 2003. Vulnerability of xylem vessels to cavitation in sugar maple. Scaling from individual vessels to whole branches.

Plant Physiology **131**, 1775–1780.

Mrad A, Domec JC, Huang CW, Lens F, Katul G. 2018. A network model links wood anatomy to xylem tissue hydraulic behaviour and vulnerability to cavitation. Plant, Cell and Environment **41**, 2718–2730.

Nardini A, Salleo S, Raimondo F. 2003. Changes in leaf hydraulic conductance correlate with leaf vein embolism in *Cercis siliquastrum* L. Trees **17**, 529–534.

Pockman WT, Sperry JS. 2000. Vulnerability to xylem cavitation and the distribution of Sonoran desert vegetation. American Journal of Botany **87**, 1287–1299.

Pratt RB, MacKinnon ED, Venturas MD, Crous CJ, Jacobsen AL. 2015. Root resistance to cavitation is accurately measured using a centrifuge technique. Tree Physiology **35**, 185–196.

Resco V, Ewers BE, Sun W, Huxman TE, Weltzin JF, Williams DG. 2009. Drought-induced hydraulic limitations constrain leaf gas exchange recovery after precipitation pulses in the C3 woody legume, *Prosopis velutina*. New Phytologist **181**, 672–682.

Rockwell FE, Wheeler JK, Holbrook NM. 2014. Cavitation and its discontents: opportunities for resolving current controversies. Plant Physiology **164**, 1649–1660.

Rodriguez-Dominguez CM, Carins Murphy MR, Lucani C, Brodribb TJ. 2018. Mapping xylem failure in disparate organs of whole plants reveals extreme resistance in olive roots. New Phytologist **218**, 1025–1035.

Saliendra N, Sperry J, Comstock J. 1995. Influence of leaf water status on stomatal

response to humidity, hydraulic conductance, and soil drought in *Betula occidentalis*. Planta **196**, 357–366.

Salleo S, Lo Gullo MA, Trifilò P, Nardini A. 2004. New evidence for a role of vessel-associated cells and phloem in the rapid xylem refilling of cavitated stems of *Laurus nobilis* L. Plant, Cell and Environment **27**, 1065–1076.

Salleo S, Nardini A, Pitt F, Gullo MA. 2000. Xylem cavitation and hydraulic control of stomatal conductance in Laurel (*Laurus nobilis* L.). Plant, Cell and Environment **23**, 71–79.

Scholz FG, Bucci SJ, Goldstein G, Meinzer FC, Franco AC, Miralles-Wilhelm F. 2007. Biophysical properties and functional significance of stem water storage tissues in Neotropical savanna trees. Plant, Cell and Environment **30**, 236–248.

Scoffoni C, Albuquerque C, Brodersen CR, Townes S V., John GP, Bartlett MK, Buckley TN, McElrone AJ, Sack L. 2017. Outside-xylem vulnerability, not xylem embolism, controls leaf hydraulic decline during dehydration. Plant Physiology **173**, 1197–1210.

Scoffoni C, Vuong C, Diep S, Cochard H, Sack L. 2014. Leaf Shrinkage with Dehydration: coordination with hydraulic vulnerability and drought tolerance. Plant Physiology **164**, 1772–1788.

Skelton RP, Brodribb TJ, McAdam SAM, Mitchell PJ. 2017. Gas exchange recovery following natural drought is rapid unless limited by loss of leaf hydraulic conductance: evidence from an evergreen woodland. New Phytologist **215**, 1399–1412.

Sperry JS, Nichols KL, Sullivan JEM, Eastlack SE. 1994. Xylem embolism in ring-

porous, diffuse-porous, and coniferous trees of Northern Utah and Interior Alaska. Ecology **75**, 1736–1752.

Sperry JS, Saliendra NZ. 1994. Intra- and inter-plant variation in xylem cavitation in *Betula occidentalis*. Plant, Cell and Environment **17**, 1233–1241.

Taneda H, Sperry JS. 2008. A case-study of water transport in co-occurring ring- versus diffuse-porous trees: contrasts in water-status, conducting capacity, cavitation and vessel refilling. Tree physiology **28**, 1641–1651.

Tsuda M, Tyree MT. 1997. Whole-plant hydraulic resistance and vulnerability segmentation in *Acer saccharinum*. Tree Physiology **17**, 351–7.

Tyree MT, Dixon MA. 1986. Water stress induced cavitation and embolism in some woody plants. Physiologia Plantarum **66**, 397–405.

Tyree MT, Engelbrecht MJ, Vargas G, Kursar TA. 2003. Desiccation tolerance of five tropical seedlings in Panama. Relationship to a field assessment of drought performance. Plant Physiology **132**, 1439–1447.

Tyree MT, Ewers FW. 1991. Tansley Review No . 34 The hydraulic architecture of trees and other woody plants. New Phytologist **119**, 345–360.

Tyree MT, Sperry JS. 1988. Do woody plants operate near the point of catastrophic xylem dysfunction caused by dynamic water stress? Answers from a model. Plant Physiology **88**, 574–580.

Wolfe BT, Sperry JS, Kursar TA. 2016. Does leaf shedding protect stems from cavitation during seasonal droughts? A test of the hydraulic fuse hypothesis. New Phytologist **212**, 1007–1018.

Zhang Y-J, Rockwell FE, Graham AC, Alexander T, Holbrook NM. 2016.

Reversible leaf xylem collapse: a potential “circuit breaker” against cavitation. Plant Physiology **172**, 2261–2274.

Zimmermann MH. 1983. *Xylem structure and the ascent of sap*. New York: Springer Verlag.

Zwieniecki MA, Melcher PJ, Ahrens ET. 2013. Analysis of spatial and temporal dynamics of xylem refilling in *Acer rubrum* L. using magnetic resonance imaging. Frontiers in Plant Science **4**, 1–8.

CHAPTER 5

XYLEM NETWORK CHARACTERISTICS OF RING- AND DIFFUSE-POROUS TREES

This chapter was written in collaboration with Dr. Mohammad Haft-Jahaverian and Prof. Nozomi Nishimura, School of Medical Engineering, at Cornell University.

5.1 Introduction

With respect to biological fluid transport networks, the topology can impact the robustness, or vulnerability, of the system in response to stochastic events such as local fluid flow disruptions (Zimmermann, 1983). Therefore, the ability to accurately map biological networks into well-defined networks is a crucial step toward understanding the dynamics of these complex systems.

One network, whose dynamics are crucial for a reliable water transport in plants is the xylem network. The xylem network consists of water conducting, tube-shaped vessels, called xylem vessels, that are connected through intervessel pits, which form between two adjacent vessels. Pits are porous membranes with pore sizes ranging from 1-10 nm that are many-fold smaller than the diameters of xylem vessels, whose diameters range from 5-400 μm in trees (Sperry and Sullivan, 1992; Woodcock, 1989). However, irrespective of the difference in their size, both xylem vessels, and intervessel pit connections are important components of the water transport efficiency through xylem vessels, given that vessel diameter and intervessel connections are co-limiting the water flow through the xylem vessels (Sperry *et al.* , 2005).

Maintaining the integrity of the water column is essential for efficient water

transport in plants. Unlike most water transport systems, water in plants is transported along a gradient of negative pressure (tension) between the soil and subsaturated air (Zimmermann, 1983). However, during water shortages (drought), the tension in the water column can significantly increase. This increased tension can cause the micro air nuclei in the xylem sap to spontaneously expand (cavitation events) to form embolisms (Tyree and Dixon, 1986), which block water flow through xylem vessels. If the tension in the water column increases further, embolisms can spread across pits into adjoining xylem conduits by aspiration. Thus, embolism events have the potential to decrease the hydraulic conductivity of the xylem network and this diminishes the water supply to distal plant organs (Zimmermann, 1983). Embolism vulnerability of single vessels is well examined and can be attributed to anatomical traits such as vessel diameter, vessel wall thickness, secondary vessel wall thickening, membrane properties of pit connections, and vessel age (Melcher *et al*., 2003; Choat *et al.*, 2005; Jacobsen *et al*., 2005; Wheeler *et al.*, 2005; Jansen et *al.*, 2009). Additionally, larger volume vessels are more likely to embolize because, on average, they contain more pit membranes and larger pit pores, where larger pore sizes require less tension to aspire air (Wheeler *et al.*, 2005). Thus, vessel connectivity and vessel size are not only important anatomical characteristics for water transport efficiency but also embolism resistance. Yet, it is questionable if vessel length per se affects embolism resistance, given that no significant relationship has been identified between vessel length and hydraulic conductance loss (Wheeler *et al*., 2005). Consequently, drawing conclusions from xylem characteristics to the overall hydraulic efficiency or embolism resistance of xylem networks is unfeasible, because hydraulic efficiency and embolism resistance

of xylem networks are not only a function of the anatomical traits of single vessels, but also of vessel topology and xylem vessel connectivity.

The robustness of networks, the ability to withstand lesion or perturbations, can be tested by randomly eliminating vertices or edges, whereby the effect of the elimination on the network depends on its topology and organizational structure (Aerts *et al.*, 2016). There is an ongoing debate on how xylem vessel topology relates to drought tolerance and whether higher vessel connectivity leads to a xylem network with higher resistance to embolism or if the opposite is the case. Both hypotheses are reasonably argued and supported: Loepfe *et al.* 2007 suggested that higher xylem vessel connectivity impedes the network resistance to embolism because the risk of embolism spread through the xylem network increases with the amount of intervessel connections. Indirect support for Loepfe's results is given by an empirical study that showed that drought tolerant woody plants have less integrated xylem pathways, i.e. a fewer intervessel connections (Zanne *et al.,* 2006). Contrarily, interconnected xylem networks could be more resistant to drought stress because redirecting water flow around an embolism event is facilitated by a high number of interconnected xylem vessel. Thus, embolism events will have less impact on hydraulic conductance in a well-connected network. For example, high intervessel connectivity led to a more resistant xylem network across six species of Acer (Lens *et al.*, 2011). These two contrary arguments highlight the necessity for characterizing the architecture of xylem networks to identify network traits affecting embolism resistance. However, both vessel topology and vessel connections are difficult to map due to technical limitations and are therefore poorly understood. As a result, our understanding of how network

connectivity affects xylem network vulnerability to embolism is quite limited.

An established method for quantifying xylem network resistance to embolisms that overlooks anatomical trait characterization are hydraulic vulnerability curves (PLC curves) (Alder, 1997). Because these curves characterize the percent loss of hydraulic conductivity of a tissue segment as a function of the water potential within the tissue, there is an implicit assumption that the water potential within the tissue is correlated with the degree of embolism within the vessel network (Cochard *et al.,* 2013). The water potential corresponding to a 50% hydraulic conductance loss through the xylem is defined as the P_{50} value and is a commonly used metric to compare drought resistance across plants (e.g. Melcher *et al.,* 2001; Maherali *et al.*, 2004; Maherali *et al.*, 2006). P_{50} values typically range from -0.2 MPa to -14.0 MPa in trees, with more negative values corresponding to greater drought tolerance (Maherali*et al.*, 2004). However, network characteristics effecting this range of drought tolerance remain unknown. Consequently, scientists are unable to derive xylem network properties from the shape of PLC curves and transversely are unable to predict the drought tolerance of plants based on xylem network characteristics (Venturas *et al.,* 2017).

In this study, we investigated xylem network characteristics that influence hydraulic efficiency and embolism resistance of the xylem networks using laser ablation tomography (LATscan), a method that produces high-resolution two-dimensional images that can be reconstructed to three-dimensional networks. The goal was to explore the anatomical network characteristics of three ring-porous (*Quercus montana*, *Fraxinus pennsylvanica*, *Carya ovata*) and three diffuse-porous tree species (*Populus x canadensis*, *Fagus sylvatica*, *Liriodendron tulipifera*). Diffuse-porous tree

species typically exhibit a tight vessel size distribution across that annual growth rings, while ring-porous tree species exhibit a bimodal vessel distribution, with large vessels in the spring wood and small vessels in the latewood (Evert, 2006). Ring-porous tree species have a higher maximum hydraulic conductance than diffuse-porous tree species due to the larger vessels in the early growth periods of the season in comparison to diffuse-porous tree species (Carlquist, 1988; McCulloh et al., 2010). However, these large vessels are particularly vulnerable to air embolisms (Zimmermann, 1983; Wheeler *et al.*, 2005; Christman *et al*., 2012). We investigated the xylem vessel topology and intervessel connections of both wood types by tracing and reconstructing the xylem networks of all six species using methodologies that have been utilized previously to automatically segment brain vascular networks (Cruz Hernández *et al.*, 2019). We then simulated the robustness of the water flow in the network against blocked vessels and correlated these findings to P_{50} values. Comparing the different vessel arrangements of these two wood types with vulnerability curves will provide insight on how xylem networks are designed, e.g. vascular characteristics will provide a better understanding into the structure-function relationship of both ring- and diffuse-porous xylem networks in maintaining hydraulic conductance across water potential gradients.

5.2 Materials and Methods

Plant material

Two two-year-old branches of three individual trees of either ring-porous (*Quercus montana, Fraxinus excelsior, Carya ovata)* or diffuse-porous (*Fagus sylvatica,*

Populus x canadensis, Liriodendron tulipifera) tree species were harvested for each measurement between April 2016 and June 2017. Selected tree species were grown on Cornell University campus, and tree replicates were chosen based on their proximity to each other (Ithaca, NY; lat. 42.44° N, long. 76.44° W). Ithaca has a moderate continental climate with an average annual temperature of 8.5 °C and an average annual rainfall of 982 mm (Northeast Regional Climate Center 2019). Branches were harvested from the lower canopy (~3 m above ground) with a pole pruner. For anatomical measurements and laser ablation tomography, branches (10 – 20 cm long) were harvested during the day, while for hydraulic conductance measurement branches (60 – 100 cm long) were collected around midnight to prevent artificial embolism occurrence in the xylem conduits (Wheeler *et al.*, 2013). After harvesting, branches were brought to the lab. For anatomical measurements and hydraulic conductance measurements, samples were processed on either the same or the next day (please see respective section). Samples for laser ablation tomography were placed in a sealed plastic bag and shipped to L4iS (State College, PA), where samples were refrigerated until processing.

Anatomical measurements:

Sample length determination for xylem segmentation

Sample length for xylem segmentation was determined from the vessel length distribution, which was calculated for each species based on the silicon injection technique (Sperry *et al.*, 2005; Wheeler *et al.*, 2005). The cutting distance for the branches of each species was set to the 75^{th} percentile of the vessel class length for

diffuse-porous tree species and to the 50th percentile for ring-porous tree species (Table 5.1). These percentile thresholds were set differently for wood types because the number of images involved in sampling the long branch length of ring-porous tree species would have jeopardized the lifetime of the Canon camera used in this study.

For the vessel injection technique, six branches (each ~60 cm in length) per species were cut, brought into the lab, and flushed for 1 hour at 70 kPa with a 20 mM KCL solution to remove native embolisms (Sperry *et al.*, 1988). Then, basal ends of the branches were connected via silicon tubing to a nitrogen gas tank and injected with a 10:1 two-component silicone elastomer (RTV141 A&B, distributed by Hisco, Somerset, NJ, USA) at 70 kPa overnight. Prior to injection, the silicon mixture was degassed under vacuum and infused with a UV stain that was dissolved in chloroform (Ciba Uvitex OB, Ciba Specialty Chemicals, Tarrytown, NY) in order to separate silicone injected xylem vessels from empty vessels for imaging analysis. After the silicon cured (~2 days), branches were sectioned at six cutting distances from the injection site with a sliding microtome (American Optical, 680 sliding microtome, Spencer Lens Co., Buffalo, NY). The respective cutting distances (L_i) were determined with the following equation

$$L_i = L_{min}\left(\frac{L_{max}}{L_{min}}\right)^{\left[\frac{i-1}{N-1}\right]} \quad \text{(Eq. 5.1)}$$

with L_{min} equal to 0.5 cm beyond the injection point, and L_{max} the distance at which 2% of the vessels were detected under the fluorescence microscope, and N the total number of cuts. Then, cross-sections were mounted in glycerol and magnified with a 20x objective and imaged with a camera (Retiga Exi CCD camera, QImaging,

Burnaby, BC, Canada attached to a fluorescence microscope (Olympus BX50, Olympus Scientific Solutions, Waltham, MA, US). Fluorescent silicon injected vessels from the most recent formed year ring were counted and averaged over species. Last, the vessel length distribution and the average vessel length was calculated for each species on the basis of equations reported in previous studies (Christmann *et al.*, 2007; Christman *et al.*, 2009) with the objective to fit the silicon-injected vessel counts with a Weibull function and to use the best fit to calculate the second derivate, from which the vessel length distribution was calculated (vessel length distribution, Appendix 5).

Table 5.3: Sampling thresholds for laser ablation tomography and segmentation analysis.

Wood type	Tree species	Cutting distance between images (µm)	Total sample length (mm)	Intervessel threshold (µm)
Diffuse-porous	*F. sylvatica*	40	70.0	2
	L. tulipifera	50	62.9	3
	P. x canadensis	35	46.0	3
Ring-porous	*C. ovata*	50	98.0	4
	F. pennsylvanica	50	271.4	5
	Q. montana	50	167.0	5

Determining intervessel wall thickness

Scanning electron microscopy (SEM, Zeiss 1550, Oberkochen, Germany) was used to measure intervessel wall thickness as the distance between two adjacent vessels to determine the minimum distance at which two vessels were connected and to be used as the vessel connectivity criteria (Fig. 5.1a). Three branches per individual tree (nine

branches per tree species) were harvested and cut into 5 mm samples with a sliding microtome (American Optical, 680 sliding microtome, Spencer Lens Co, Buffalo, NY). Then, samples were dehydrated in a series of 25%, 50%, 70%, 95%, and 100% ethanol, and then dried down at room temperature. Samples were coated with gold-palladium for 20 seconds at a current of 20 mA and imaged at a voltage of 3.0 kV and a current of 0.21 nA. The intervessel wall thickness was measured in ImageJ (Rueden *et al.*, 2017) based on a minimum of 60 adjacent vessels. The 95th percentile of each data set was calculated and set as the criterion for intervessel connectivity. Intervessel distances equal to or smaller than the 95th percentile were counted as connected (Table 5.1).

a. b.

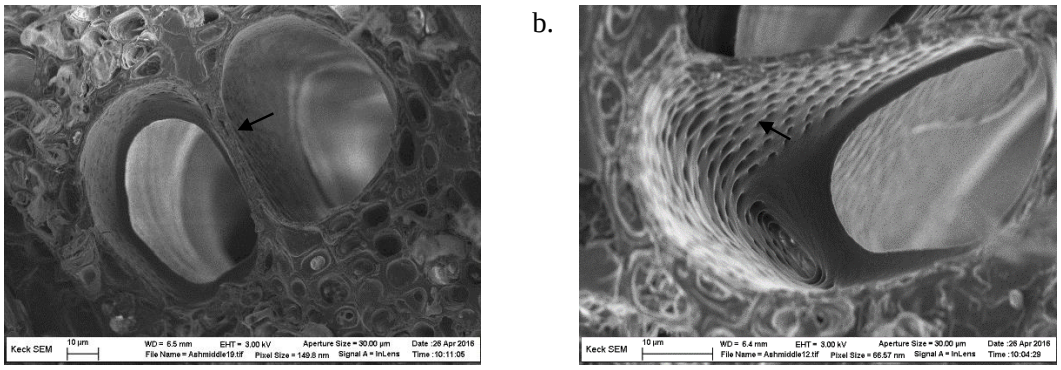

Figure 5.1: Scanning electron microscopy (SEM) images of two types of xylem vessel connections of *Fraxinus pennsylvanica*. Two vessels can be connected through intervessel pit connections (arrows) that are formed on adjacent vessel walls (a), or one vessel can bifurcate and turn into two separate xylem vessels (b).

Xylem segmentation: Image processing pipeline ranging from raw images to xylem network analysis

Many steps had to be accomplished in order to study the three-dimensional structure of xylem networks and to understand the fluid dynamics through these networks (Fig.

5.2). The individual task that led to the final analysis is laid out in the following paragraphs.

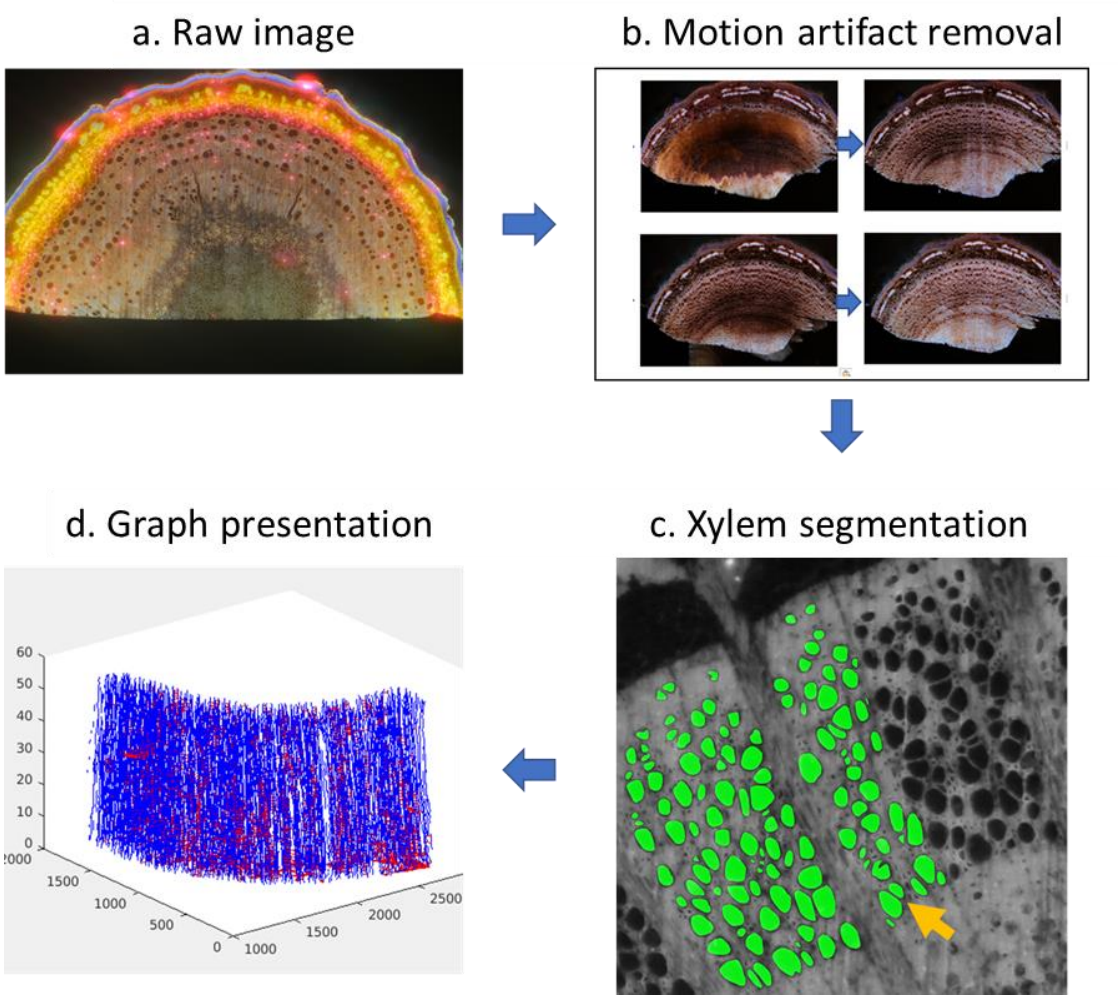

Figure 5.2: Complete image processing pipeline. Raw images (a) preprocessed for intensity normalization and motion artifact removal (b). The preprocessed images were segmented, and vessels segments and intervessel connections (yellow arrow) were detected (c). The segmentation and detection results are represented in the graph representation (d). The graph representation of 60 slices of images are illustrated (x-axis and y-axis represent pixels) (d). The xylem segments are shown in blue, and the intervessel pit connections are shown in red.

A) Image acquisition

Laser ablation tomography (LAT) was used to cut tree branches and acquire digital cross-sectional images (Fig. 5.2a). The laser source was a Coherent Avia 355-7000 Q-switched ultraviolet laser (Coherent, 5100 Patrick Henry Drive, Santa Clara, CA 95054 USA) with a pulse repetition rate of 25 kHz and wavelength of 355 nm. The pulse duration of the laser was less than 30 ns and supplied pulse energy of approximately 200 mJ. The galvanometer used to scan the laser beam to make the ablation plane was a Scanlab HurryScan 10 (Scanlab, Siemensstr 2a, 82178 Puchheim, Germany). Samples were fixed to a cantilever and connected to the mechanical stage along its travel axis, then fed into the ablation plane using an Aerotech linear drive stage (Aerotech, Inc., 101 Zeta Dr, Pittsburgh, PA 15238, USA), with the cutting distance ranging from 35 µm to 50 µm. Images were captured via a Canon 70D camera equipped with a Canon Macro Photo Lens MP-E 65 mm 1:2.8 1-5X. The images captures were 5472 x 3648 pixels at a resolution of 1 micron per pixel.

Setting cutting distance between images

To determine the maximum distance between cuttings that would allow for tracing and connecting vessels through consecutive images, a preliminary experiment was performed in which 31 slices of a branch sample of all six tree species were ablated with a cutting distance of 5 µm (total length of 150 µm). Then, a minimum of 100 xylem vessels per sample was selected and manually traced in all 31 slices using ImageJ (Rueden *et al.*, 2017) following manual segmentation protocol developed by Haft-Javaherian et al. (Haft-Javaherian *et al.*, 2019). The tracing similarity between

the first slice and the following slices were measured in Matlab based on the ratio of the intersection area of two consecutive vessel cross-sections and the first slice vessel cross-section area averaged over all detected vessels to determine the maximum distance between two images such that at least 50% averaged cross-sectional area overlaps were observed with an upper limit of 50 μm. From this analysis, the maximum cutting distances for LAT scans were determined (Table 5.1). Lastly, the manually traced xylem vessels were annotated as ground truth and later used for training the computer to develop tree species-specific xylem segmentation models (see below).

B) Motion artifact compensation

Laser ablation tomography is prone to motion artifacts that is one of the main challenges for image processing of 3D networks. Apparent motion can be caused by any combination of gradual shift due to sample curvatures, sudden shift, or rotation due to sample realignment, poor focus, and burned cross-section (Fig. 5.2b). In order to compensate for these different motion artifact cases, two different methods were utilized. For each method, the hyperparameters were optimized based on the raw images and type of motion artifacts detected in the analysis. Furthermore, the computational complexity and scalability also had to be considered in the motion artifact compensation, given that the 3D images could contain up to 5000 slices along their third dimension. Since there were no local artifacts due to distortion and motion in the images, a rigid registration (i.e., translation and rotation) was sufficient. A registration method consists of a similarity metric as an input to the cost function and

an optimizer to optimize the cost function finding the optimal registration parameters. Mean square error (*MSE*) was applied to correct motion artifacts (Eq. 5.2), where N and M are numbers of rows and columns in the image and I and I' are the intensity of a particular pixel in two images, as the similarity metric and the regular step gradient descent optimization, which follows the gradient of the cost function toward the direction of extrema with reducing the step function when the gradient changes direction.

$$MSE = \frac{1}{N \times M} \sum_{i=1}^{N} \sum_{j=1}^{M} \left(I_{i,j} - I'_{i,j}\right)^2 \qquad \text{(Eq. 5.2)}$$

A random grid search used to find the optimal hyperparameters for the optimizer detected two optimal sets of hyperparameters. The ensemble of two optimizers based on the optimal sets of hyperparameters was able to handle most of the cases and was successful when applied to the test cases with small sample sizes. The failure modes included uneven illumination, laser-burned cross-sections, color-distorted images, and sudden dramatic changes. However, even after multi-thread parallelization, this method had a long run time and required manual treatments for the remaining failure cases.

We devised the second method from the work of Evangelidis and Psarakis (Evangelidis and Psarakis, 2008) to overcome the drawbacks of the first method and to handle samples with large sample sizes. We adopted the enhanced correlation coefficient (Psarakis and Evangelidis, 2005) as the similarity measure. This measure is preferable due to its invariant to contrast and brightness differences (i.e., photometric distortions) as well as its corresponding linear approximation expression with a

closed-form solution to facilitate the optimization of the original non-linear measure. Additionally, Evangelidis and Psarakis proposed an iterative gradient-based on a searching function (e.g., forward additive refinement algorithm) to optimize the original non-linear measure using a linear approximation (Evangelidis and Psarakis, 2008). In order to tackle multi-scale motion artifacts, the transformation parameters were estimated in a pyramid fashion using 10x scaled-down version of the two images and then fine-tuned using the original parameter resolutions. Since the images did not suffer from local motion artifacts, only the estimation of the global transformation parameters within two consecutive images was required.

In order to parallelize the process, images were divided into groups of 10 consecutive images and registered independently based on the first image in the group. Then, starting from the second image group, the first image of each image group was aligned to the last image of the preceding image group and the rest of the images within the group were warped using the same transformation. Finally, a failure detector was implemented by using the mean structural similarity index (Wang *et al.*, 2004) between two consecutive images. Within every 11 consecutive pairs of images, the middle pair was considered a failure case if its similarity index was at least 5% lower than the median of the 11 similarity indexes. The failure cases were registered again using the same algorithm (or in rare cases manually if the algorithm failed repeatedly) followed by warping all the following images using the same transformation parameters. This process was repeated until no failure cases were detected.

C) Xylem vessel segmentation

After correcting for motion artifacts, the computer algorithm was trained using the manually segmented xylem vessels (ground truth). Due to the significant anatomical differences between vessel morphologies across tree species, it was not possible to develop a universal tracing model. Therefore, the computer algorithm developed individual segmentation models for each species (Fig. 5.2c). To implement the training program, the architecture and training scheme of a convolutional neural network (CNN) model with an optimal architecture for the 3D vasculature segmentation task and a customized cost function, DeepVess was adopted (Haft-Javaherian *et al.*, 2019). This architecture model was trained on each species using the ground truth data set corresponding to that species with intervessel xylem distances determined by previous measurements using scanning electron microscopy images (below). Since each sample data set contained between 1000 and 5000 images, each 500-image stack was stored in a separate HDF5 binary data format to be segmented using the CNN model. After this segmentation task, the binarized segmentation results were concatenated to form the complete segmentation data set for each sample. In order to remove minor segmentation artifacts, we applied a dilation morphological image filter with a disk kernel of radius 1 to remove the boundary of vessels followed by a 3D median filter with a 3-voxel box kernel to smooth the vessel boundary and fill the gaps (non-segmented areas) within the vessels.

D) Xylem network representation

Defining vessel connections and xylem segments

We implemented two different analyses to represent the xylem networks within this data set. (Fig. 5.2d and 5.3a,b, and d). The xylem segmentation results were utilized to generate the graph representation of xylem networks for both network analysis and fluid mechanic characterization. Since 3D xylem vessels traversed through the branch, they appeared in a 2D cross-section in each image slice. Xylem vessels were connected by two types of connections. Xylem vessels merged and bifurcated as they traversed the length of the branch. Bifurcation occurred when more than one xylem vessel merged into one xylem vessel, or one xylem vessel divided into two or more xylem vessels. The bifurcation was apparent in images when a cross-section from an image slice overlapped with more than one cross-section in the preceding or proceeding adjacent image slice. Therefore, depending on the cross-sectional overlaps in the segmented images, the 3D xylem segments and their junctions were identifiable. Due to the number of bifurcations detected in the segmentation analysis, xylem segments were defined as a xylem vessel that started and ended with a junction. Two cross-sections located within two adjacent slices belonged to the same 3D xylem segment if they overlapped. Xylem vessels were also connected through intervessel pit connections. Because intervessel pit connections were not directly visible in the images, they were identified based on the thickness of the wall between two xylem vessels. Intervessel connections were determined from the cryo-image anatomical analysis and were determined to occur in places where the distance between the boundaries of two separate cross-sections within an image slice was less than the pre-determined set-point that varied across species (Table 5.1). In this way, intervessel connections were only scored as present if the boundary thickness between two

adjoining vessels was less than the pre-determined intervessel boundary threshold (Table 5.1 and Fig. 5.1a).

Xylem-based, junction-based, and streamline network presentations were utilized to represent xylem traits such as xylem segments, intervessel connections, and bifurcation junctions. The xylem-based network (Fig. 5.3b) represents the 3D xylem segments as graph vertices, while the junction-based network (Fig. 5.3c) represents the bifurcation junctions as the graph vertices. Consequently, the xylem-based network represents the bifurcation junctions and intervessel connections using the graph edges, while the junction-based network represents 3D xylem segments and intervessel connections using the graph edges. Alternatively, the streamlined network (Fig. 5.3d) traces all the possible distinct water streamlines between two ends of the sample based on the bifurcations. Therefore, the streamline network represents the streamlines as the graph vertices and the intervessel connections between streamlines as the graph edges.

In order to characterize these networks using geometrical measures, each cross-section was fit to a centroid, and the shortest distance to the boundary was defined as the diameter. The diameter of each xylem vessel was defined as the median of the measured cross-sections. Correspondingly, the xylem segment length, number of intervessel connections, and total length of intervessel connections were measured for each xylem segment. Geometrical measures were calculated and represented for the xylem based and streamline networks. Junction-based networks; the inverse of the xylem based network was used to simulate fluid dynamics in xylem networks in response to embolism events (see “fluid dynamics in xylem networks” section).

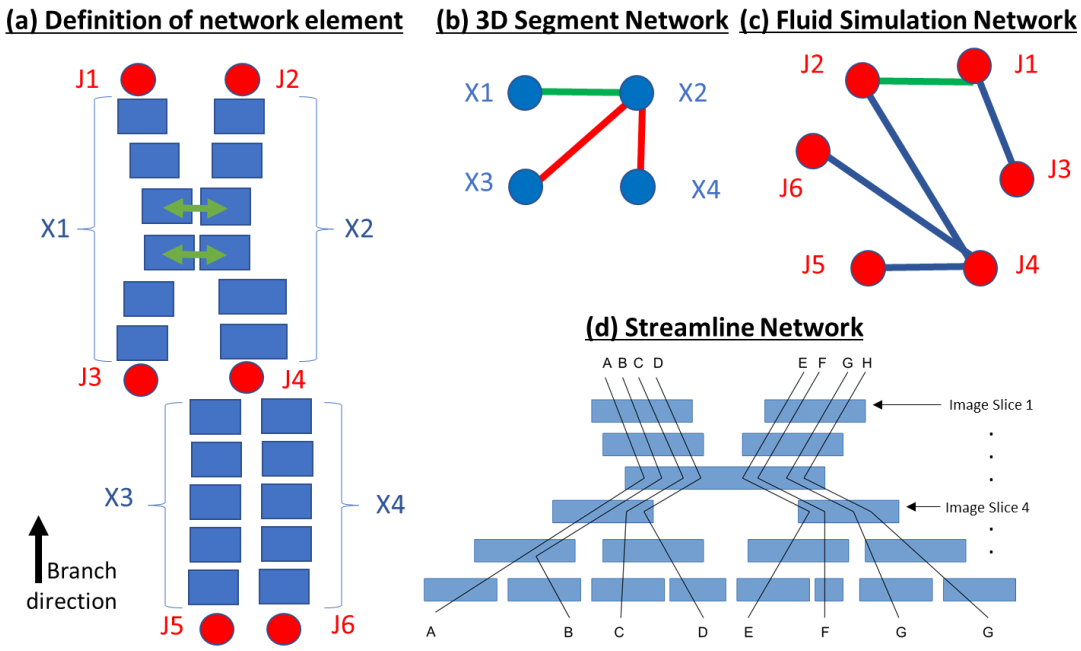

Figure 5.3: Three schematic representations of xylem networks. Blue boxes represent a segmented xylem cross-section, and each row of the blue boxes represents an image slice (a). 3D xylem segments (X1-X4) begin and end at junctions (J1-J6). Some xylem vessels were connected by intervessel connections (green arrows and graph edges) are identified based on threshold distances between xylem. The xylem-based (b) and junction-based graph representations (c) assign xylems and junctions to the vertices, respectively. In the streamline network representation (d), streamlines were defined as all possible paths for water to traverse the sample using junctions.

Network circle presentation

Network circles were also used to visually represent differences between xylem networks (Fig. 5.4). To generate these visualizations, the vessels in the first image of the image stack were numbered sequentially according to their nearest neighbor (e.g. starting at any vessel numbered 1, all nearest neighboring vessels were numbered 2 – n, then starting at vessel 2 all nearest neighboring vessels were numbered n+1 – m, etc.). Through the depth of the image stack, newly appearing vessels were assigned the next available number. After numbering all vessels and assigning them individual

identification numbers (ID numbers) in consecutive order in the network, the xylem-vessel segments or streamlines were aligned sequentially on the outside of a circle (segment ID numbers are not shown in representation). Then, intervessel pit connections and merged streamlines were made visible by connecting the xylem segments and streamlines on the outside of the circle via lines. The thickness of each line in the diagram corresponded to the number of connections between the two xylem-segments (e.g. the thinnest lines corresponded to a single connection). The length of the merged streamlines is not represented in the network circle because the complexity of the data would have made the circle presentation unreadable.

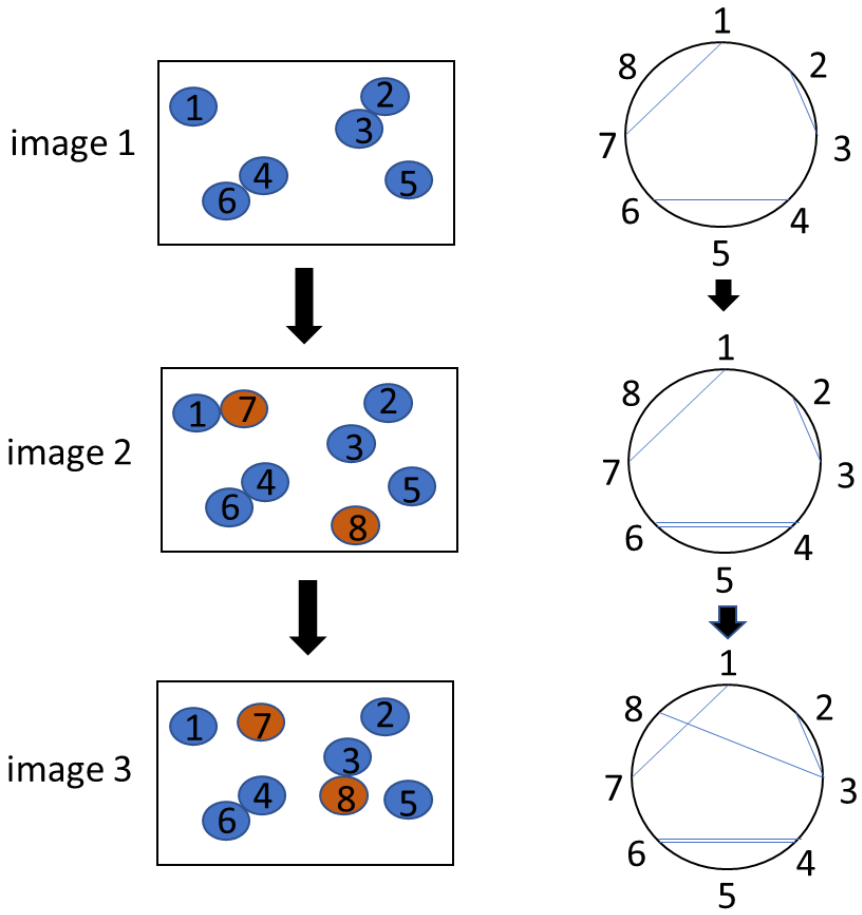

Figure 5.4: Schematic of circle network presentation based on 3D segment analysis. Images 1-3 are consecutive, with image 1 being the first image of the stack. In the first image, xylem vessels (blue circles) are consecutively numbered with xylem identification numbers (1-6); these numbers are assigned to vessels from left to the right and from top to bottom on the image. In subsequent images, new emerging xylem vessels (red circles) are assigned the next available identification number. This information is mapped onto the circle presentation (circles on the right hand side) with xylem ID numbers radially spaced around the circumference of the map. Then, for each image in the stack, adjacent xylem vessels in the network are connected with a line between their respective IDs on the circle presentation. As a result of this procedure, the number of lines between any two IDs represent the total number of images in which these corresponding xylem vessels were connected to one another. Xylem ID numbers are not shown in the presented figures in this study.

Fluid dynamics in xylem networks

Two different analyses were performed to examine fluid dynamics in xylem networks

under increasing stress conditions.

1) Experimental measurements of percent loss of hydraulic conductivity

Vulnerability curves were performed using the bench-top dry-down method (Tyree and Dixon, 1986). Around 60 cm long branches were cut around midnight, immediately double bagged, brought to the lab, and the cut end was put into water. The following morning, branches were spread out on the bench-top, single leaves were bagged to equilibrate the leaf with the branch water potential (Ψ_{branch}) and dried down for varying amounts of time to archive a range of different (Ψ_{branch}). During this timeframe, Ψ_{branch} was taken on the bagged leaves with a water status console (Soilmoisture Equipment Corp., Goleta, CA). After reaching the desired Ψ_{branch}, branches were double bagged, equilibrated for 12 hours, and remeasured. Then, branches were cut underwater to 10 cm long segments and inserted into a custom-built low-pressure flow meter (Melcher *et al.*, 2012) by attaching one end of the branch segment to a reservoir that was filled with a (0.1 µm) filtered 20 mM KCl perfusion solution, and the other end of the branch segment to an analytical balance (HR-200, A&D, Elk Grove, Il). The initial flow rate (Q) was measured when the flow rate (F, kg s^{-1}) was constant The hydraulic pressure difference between sample and solution reservoir was kept stable between 1.5 kPa and 3.0 kPa during the measurements depending on the tree species. Afterward, branch segments were flushed for 1 hour at 100 kPa with the perfusion solution, and the max flow rate was measured by reinserting the stem segments into the low-pressure flow meter. The unit-length hydraulic conductivity (K) was determined

by

$$\mathrm{K} = \mathrm{Q}\,\frac{L}{\Delta \mathrm{P}} \qquad (\mathrm{Eq.}\,5.3)$$

where, L is the length of the sample, and ΔP is the hydraulic pressure gradient. After the measurements, the xylem cross-sectional area was determined with a caliper and the specific hydraulic conductivity determined by dividing K by the cross-sectional area. The percent of hydraulic loss of conductivity (PLC) was calculated by

$$\mathrm{PLC} = \frac{100}{1 - \frac{K_{max}}{K_{in}}} \qquad (\mathrm{Eq.}\,5.4)$$

where, K_{max} is the maximum specific conductivity after flushing, and K_{in} is the initial specific hydraulic conductivity. The PLC data were fitted with an exponential sigmoidal equation of

$$\mathrm{PLC} = \frac{100}{1 + exp\big(a + (\Psi - \mathrm{b})\big)} \qquad (\mathrm{Eq.}\,5.5)$$

where, a and b are fitting parameters, whereby a describes the slope of the curve and b represents the position of the curve on the x-axis at 50% PLC (Pammenter and Van der Willigen, 1998). The significance levels of the parameters were calculated based on this fit.

2) Embolism simulation

The pressure drops within a 3D xylem segment were modeled based on the Hagen–Poiseuille law of a circular cross-sectional pipe with laminar flow. Correlating the fluid flow within the pipe (Q) with the pressure drop (ΔP) was formulated as in Eq.

5.6. Hence, the segment resistance is defined as Eq. 5.7, where, μ is the dynamic viscosity of water at 25°C, D is the xylem segment diameter, and L is the xylem segment length (Loepfe*et al.*, 2007).

$$Q = \frac{\pi D^4 \Delta P}{128 \mu L} \quad \text{(Eq. 5.6)}$$

$$R_x = \frac{\Delta P}{Q} = \frac{128 \mu L}{\pi D^4} \quad \text{(Eq. 5.7)}$$

Sperry and Hacke (Sperry and Hacke, 2004) modeled the resistance of the intervessel connections (R_i) as infinitely thin plates with perfectly circular pores with resistance as a function of the equivalent pore size (D_e) and the number of pores in the intervessel connection (n_p) defined in Eq. 5.8. We modeled the intervessel connection resistance (R_i) as a function of L_i, which is a proxy for the n_p based on the assumption that n_p is proportional to the intervessel connection length (L_i in Eq. 5.9), which were measured based on 3D images of samples (Eq. 5.9).

$$R_i = \frac{24 \mu}{D_e^3 n_p} \quad \text{(Eq. 5.8)}$$

$$D_e^3 n_p = \alpha L_i \quad \text{(Eq. 5.9)}$$

$$R_i = \frac{24 \mu}{\alpha L_i} \quad \text{(Eq. 5.10)}$$

The hydraulic network based on the xylem segments and intervessel connections was modeled using Eq. 5.7 and Eq. 5.10. The system was then represented in a linear system of equations, and the solution was acquired using one of the sparse systems of linear equation solver methods (e.g., Cholesky solver) depending on the characteristics of the linear systems. A unit pressure difference was applied between the two ends of the longest connected segment within each tree sample, and the flow within the

sample was measured to calculate the sample conductance (Q/ΔP). Thirty simulations were conducted for each dropout percentile ranging from 0% to 100% in order to simulate different embolism events. The relative conductance, which is the ratio of conductance to the baseline conductance at 0% dropout was reported for each sample. Embolism simulation was calculated based on xylem segmentation results. However, due to image qualities, fluid simulations could not be performed in all samples on the entire length of the segmented image stack (Table 5.2).

Table 5.2: Image stack length used for embolism simulation model for each species and replicate.

Tree species	**replicate**	**Analyzed sample length (mm)**	**Total sample length (mm)**
F. sylvatica	1	70.0	70.0
	2	70.0	70.0
	3	70.0	70.0
L. tulipifera	1	27.8	62.9
	2	62.9	62.9
	3	62.9	62.9
P. x canadensis	1	46.0	46.0
	2	46.0	46.0
	3	46.0	46.0
C. ovata	1	97.8	98.0
	2	97.8	98.0
	3	97.8	98.0
F. pennsylvanica	1	17.8	271.1
	2	70.9	271.1
	3	77.5	271.1
Q. montana	1	160.3	167.0
	2	153.7	167.0
	3	158.7	167.0

Statistics

Statistical analysis was performed in JMP Pro 14.0.0 (SAS Institute Inc., Cary, NC.) or Matlab. All tests were performed with a probability level $P < 0.05$. Differences between tree species were calculated using ANOVA, and multi-comparison corrections were done using the Tukey-Kramer method. For calculating differences in intervessel wall thickness among tree types, the dependent variable was log transformed to fulfill model assumptions.

5.3 Results

Xylem network representations

3D xylem segment-based and streamline-based network representations were utilized to perform geometrical comparisons between xylem networks. The comparisons of the average vessel segment, which is defined as a xylem vessel that starts and ends with a bifurcation, and average streamline diameter, which represents water pathways, revealed that ring-porous tree species have in both representations a significantly larger average xylem or streamline diameter than diffuse-porous tree species (Fig.5.5a and 5.6a, Table 5.3 and 5.4). Additionally, the comparisons showed that *C. ovata* has the smallest average xylem segment or streamline diameter within the ring-porous trees.

There were no significant differences for wood type effect for the remaining three geometrical comparisons (Fig. 5.5b-d and 5.6b-d, Table 5.3 and 5.4). However, multiple comparisons of xylem segment length and average intervessel pit connections per xylem segment indicated that *F. pennsylvanica* had a larger average xylem

segment length than the remaining tree species (ANOVA, $P < 0.05$, Table 5.3) but also fewer intervessel pit connections per xylem segment (ANOVA $P < 0.05$; Fig. 5.5b,c, Table 5.3). However, despite the low number of intervessel pit connections, the total length of intervessel connections of *F. pennsylvanica* is significantly longer than the pit connection length of the five remaining tree species (ANOVA, $P < 0.05$; Fig. 5.5d, Table 5.3). Conversely, the xylem network of diffuse-porous consists of short vessel segments with many pit connections that are generally very short (Fig. 5.5b-d, Table 5.3).

Comparisons of geometrical characteristics of streamlines did not concur with xylem-segment based comparisons. Streamline comparisons revealed that streamline length and total connection length did not differ significantly among tree species (Fig. 5.6b,d, Table 5.4). Additionally, the significant differences between streamline connections did not reveal any pattern between wood types or tree species (ANOVA, $P < 0.05$; Fig. 5.6c, Table 5.4).

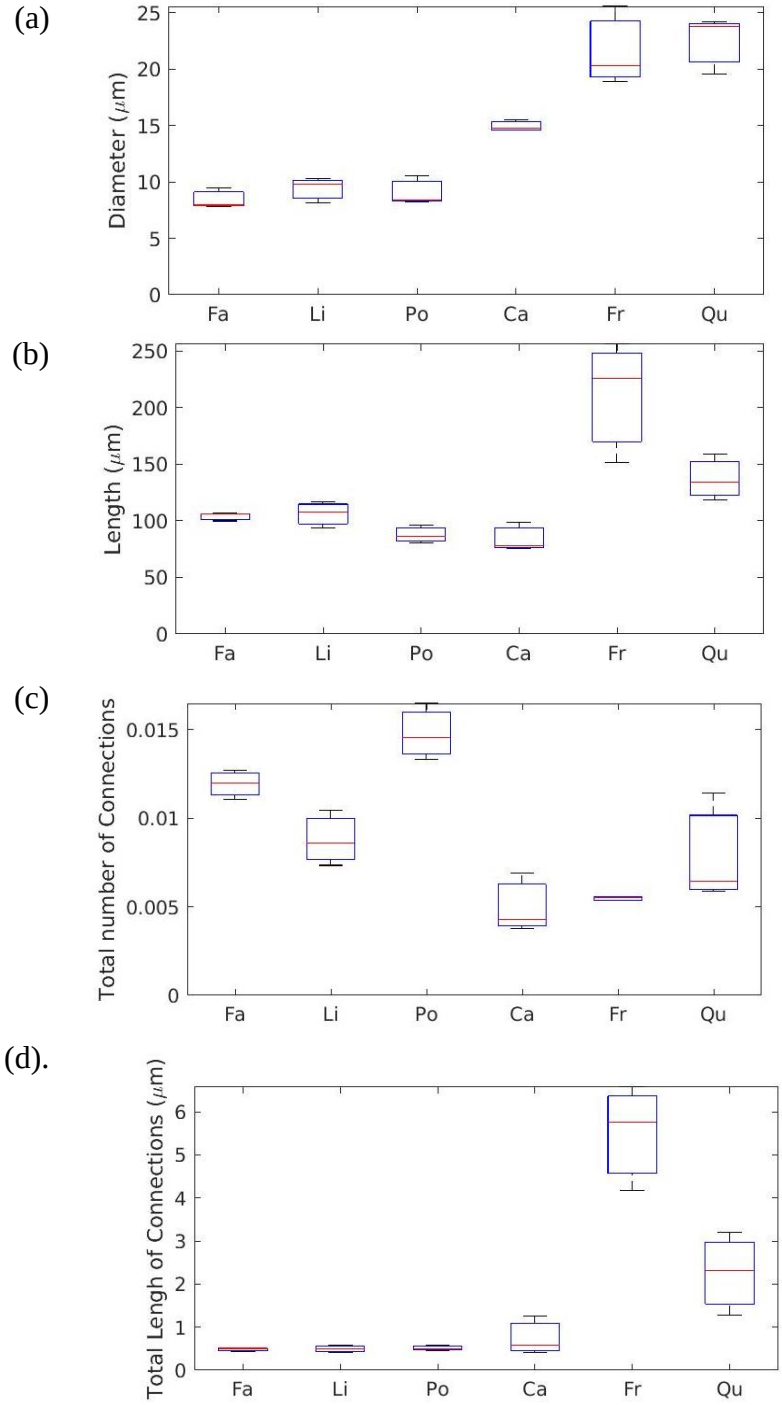

Figure 5.5: Comparisons of the vessel segment diameters (a), vessel segment lengths (b), amount of pit connections per vessel segment (c), and lengths of intervessel pit connections averaged over vessel segments (d) between three diffuse- (*F. sylvatica* (Fa), *L. tulipifera* (Li), *P. x canadensis* (Po)) and three ring-porous tree species (*C. ovata* (Ca), *F. pennsylvanica* (Fr), *Q. montana* (Qu)). Results were calculated based on the 3D xylem segment analysis. Statistical differences are given in Table 5.3.

Table 5.3: Comparisons between means of vessel segment diameter, vessel segment length, pit connection frequency and intervessel pit connections averaged over vessel segments length of three diffuse-porous (*F. sylvatica*, *P. x canadensis*, *L. tulipifera*) and three ring-porous tree species (*C. ovata*, *Q. montana*, *F. pennsylvanica*) based on the 3D segment analysis (ANOVA and Tukey-Kramer multi-comparison correction).

3D Segment Networks		Diameter (µm)		Length (µm)		Connection Frequency		Pit connection Length (µm)	
Species 1	**Species 2**	**Δµ**	**P**	**Δµ**	**P**	**Δµ**	**P**	**Δµ**	**P**
F. sylvatica	*L. tulipifera*	-0.99	0.987	-2.13	1.000	3.14E-3	0.292	-0.01	1.000
F. sylvatica	*P. x canadensis*	-0.65	0.998	16.64	0.958	-2.85E-3	0.385	-0.03	1.000
F. sylvatica	*C. ovata*	-6.54	0.014 *	20.08	0.912	6.94E-3	0.004 **	-0.26	0.996
F. sylvatica	*F. pennsylvanica*	-13.17	<.001 ***	-106.97	0.002 **	6.47E-3	0.006 **	-5.02	<.001 ***
F. sylvatica	*Q. montana*	-14.07	<.001 ***	-32.97	0.597	4.04E-3	0.112	-1.78	0.056
L. tulipifera	*P. x canadensis*	0.34	1.000	18.77	0.932	-5.99E-3	0.011 *	-0.02	1.000
L. tulipifera	*C. ovata*	-5.56	0.039 *	22.20	0.874	3.80E-3	0.147	-0.25	0.997
L. tulipifera	*F. pennsylvanica*	-12.19	<.001 ***	-104.84	0.002 **	3.32E-3	0.244	-5.01	<.001 ***
L. tulipifera	*Q. montana*	-13.09	<.001 ***	-30.84	0.658	8.99E-4	0.986	-1.76	0.058
P. x canadensis	*C. ovata*	-5.89	0.028 *	3.43	1.000	9.79E-3	<.001 ***	-0.23	0.997
P. x canadensis	*F. pennsylvanica*	-12.53	<.001 ***	-123.61	<.001 ***	9.32E-3	<.001 ***	-4.99	<.001 ***
P. x canadensis	*Q. montana*	-13.43	<.001 ***	-49.61	0.214	6.89E-3	0.004 **	-1.75	0.061
C. ovata	*F. pennsylvanica*	-6.63	0.013 *	-127.04	<.001 ***	-4.75E-4	0.999	-4.75	<.001 ***
C. ovata	*Q. montana*	-7.53	0.005 **	-53.05	0.166	-2.90E-3	0.368	-1.51	0.123
F. pennsylvanica	*Q. montana*	-0.90	0.991	73.99	0.030 *	-2.42E-3	0.545	3.24	<.001 ***

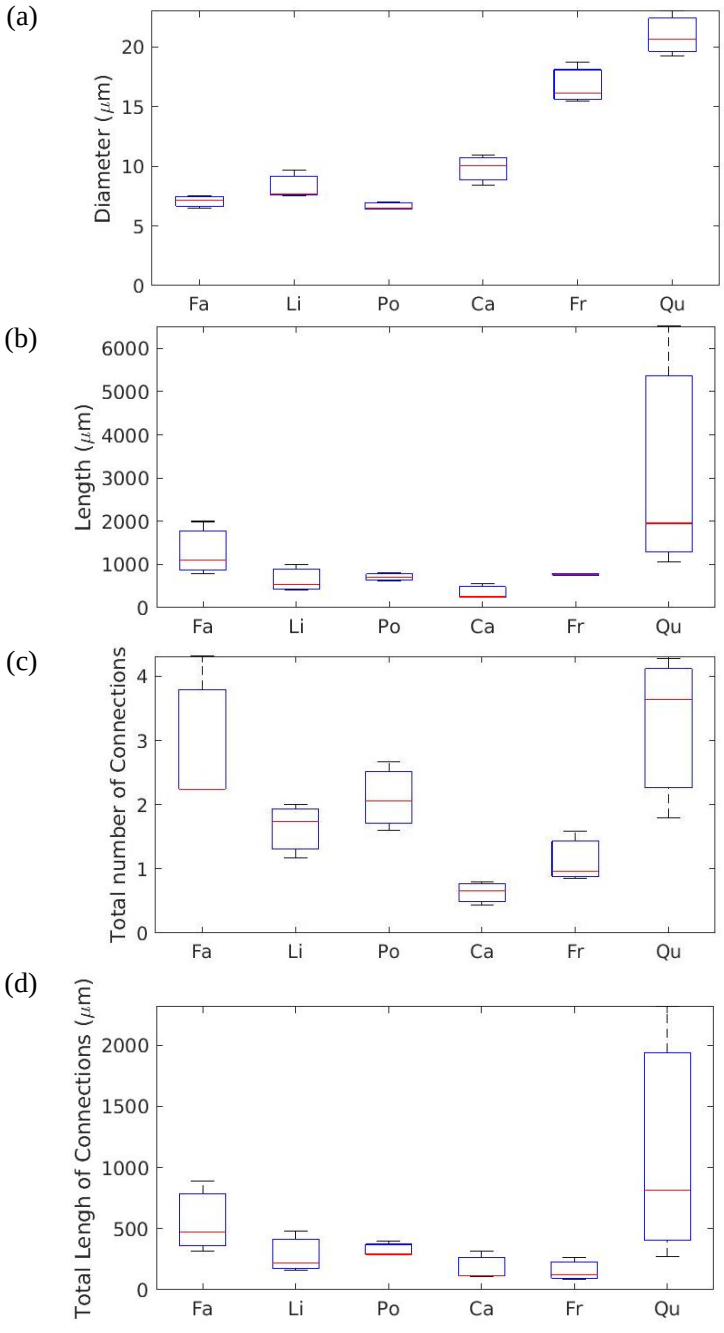

Figure 5.6: Comparisons of the streamline diameters (a), streamline lengths (b), amount of pit connections connecting streamlines (c), and lengths of pit connections averaged over streamlines (d) between three diffuse- (*F. sylvatica* (Fa), *L. tulipifera* (Li), *P. x canadensis* (Po)) and three ring-porous tree species (*C. ovata* (Ca), *F. pennsylvanica* (Fr), *Q. montana* (Qu)). Results were calculated based on the streamline analysis. Statistical differences are given in Table 5.4.

Table 5.4: Comparisons between means of streamline diameter, streamline length, number of pit connections between streamlines, and pit connection length averaged over streamlines of three diffuse- (*F. sylvatica*, *P. x canadensis*, *L. tulipifera)* and three ring-porous tree species (*C. ovata*, *Q. montana*, *F. pennsylvanica*) based on the streamline analysis (ANOVA and Tukey-Kramer multi-comparison correction).

Streamline Networks		Diameter (µm)		Length (µm)		Connection Frequency		Connection Length (µm)	
Species 1	**Species 2**	**Δµ**	**P**	**Δµ**	**P**	**Δµ**	**P**	**Δµ**	**P**
F. sylvatica	*L. tulipifera*	-1.25	0.833	642.79	0.985	1.30E+0	0.391	275.25	0.973
F. sylvatica	*P. x canadensis*	0.42	0.998	586.31	0.990	8.26E-1	0.789	235.66	0.986
F. sylvatica	*C. ovata*	-2.74	0.169	941.26	0.929	2.30E+0	0.035 *	379.40	0.905
F. sylvatica	*F. pennsylvanica*	-9.73	<.001 ***	526.58	0.994	1.80E+0	0.127	402.89	0.882
F. sylvatica	*Q. montana*	-13.93	<.001 ***	-1885.4	0.458	-3.06E-1	0.996	-571.80	0.655
L. tulipifera	*P. x canadensis*	1.67	0.618	-56.48	1.000	-4.69E-1	0.974	-39.59	1.000
L. tulipifera	*C. ovata*	-1.49	0.717	298.47	1.000	1.01E+0	0.634	104.15	1.000
L. tulipifera	*F. pennsylvanica*	-8.48	<.001 ***	-116.2	1.000	5.01E-1	0.966	127.64	0.999
L. tulipifera	*Q. montana*	-12.68	<.001 ***	-2528.2	0.193	-1.60E+0	0.203	-847.05	0.280
P. x canadensis	*C. ovata*	-3.16	0.089	354.95	0.999	1.48E+0	0.268	143.74	0.999
P. x canadensis	*F. pennsylvanica*	-10.15	<.001 ***	-59.73	1.000	9.70E-1	0.667	167.23	0.997
P. x canadensis	*Q. montana*	-14.35	<.001 ***	-2471.7	0.210	-1.13E+0	0.523	-807.46	0.323
C. ovata	*F. pennsylvanica*	-6.99	<.001 ***	-414.68	0.998	-5.07E-1	0.965	23.49	1.000
C. ovata	*Q. montana*	-11.19	<.001 ***	-2826.6	0.122	-2.61E+0	0.016 *	-951.19	0.187
F. pennsylvanica	*Q. montana*	-4.20	0.017 *	-2411.9	0.229	-2.10E+0	0.059	-974.69	0.170

Network circle analysis showed that xylem segments of diffuse-porous tree species were connected to xylem vessel segments with more distant ID numbers (identification numbers that were assigned to xylem-segments in consecutive order; Fig. 5.4), while ring-porous tree species connect rather with xylem vessel segments with consecutive ID numbers. However, these latter mentioned connections are longer than the more distant connections in diffuse-porous tree species (Fig. 5.7).

Contrary, the streamline circle analysis revealed that streamlines, especially in the diffuse-porous tree species, are connected to streamlines with ID numbers that are further apart than the xylem-segment analysis suggested (Fig. 5.8). The high connectivity of streamlines across the diagonal of the circle depicts a highly connected

streamline network for *F. sylvatica* and *P. x canadensis* (Fig. 5.8a,c). The streamline network of *L. tulipifera* also shows the connectivity between more distant ID streamlines, however these connections are not as distant as for the other two diffuse-porous tree species (Fig. 5.8b). The streamline network of *L. tulipifera* is comparable to the streamline networks of the two ring-porous tree species *C. ovata* and *Q. montana*, despite their differences in xylem segment connectivity (Fig. 5.8d,f). The streamline circle presentation for *F. pennsylvanica* primarily shows solitary, independent streamlines. A few streamline connections between neighboring ID or consecutive ID streamlines are visible, indicating that most of the water flows through the xylem vessels directly and not through pit connections.

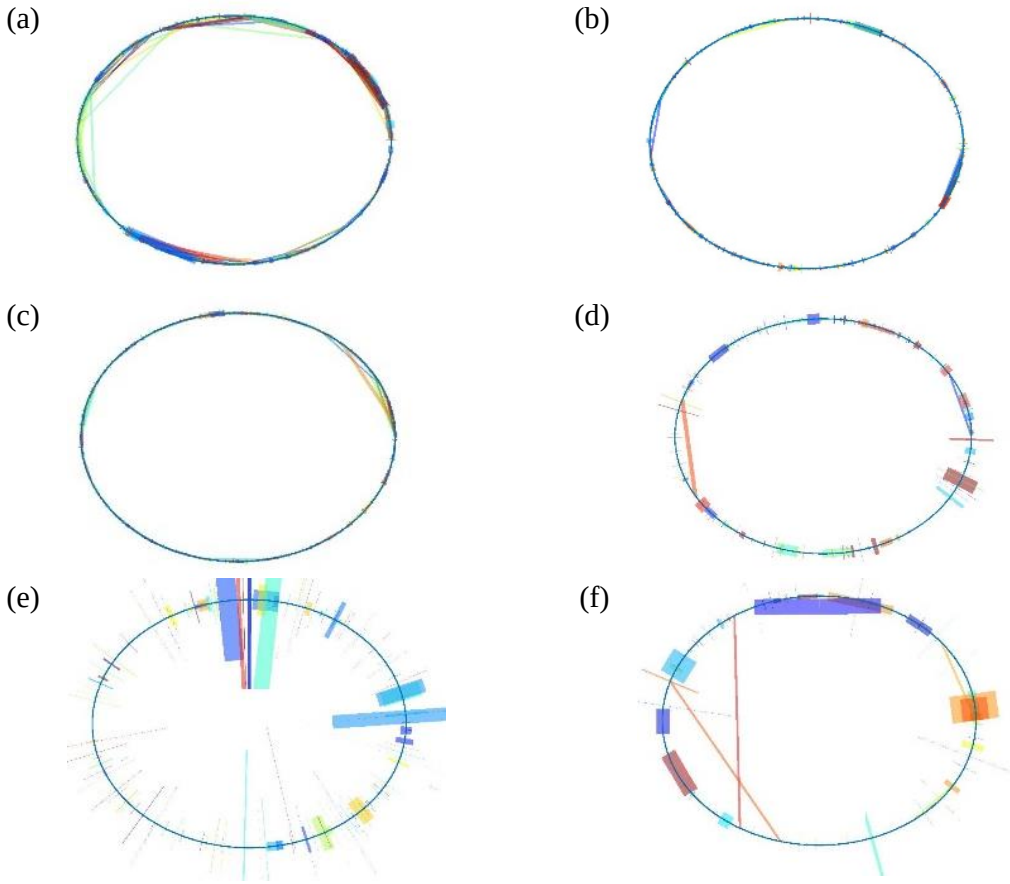

Figure 5.7: Network circle presentations of three diffuse- (*F. sylvatica* (a), *L. tulipifera* (b), *P. x canadensis* (c)) and three ring-porous tree species (*C. ovata* (d), *F. pennsylvanica* (e), *Q. montana (f))* based on 3D xylem segment analysis. One circle network per species is shown representative for three replicates per species. All vertices (xylem segments) are aligned along the circle perimeter and edges (connections) are drawn between vertices. The edge thickness perpendicular and parallel to the circle perimeter is proportional to the total length of the connection between two connected vertices.

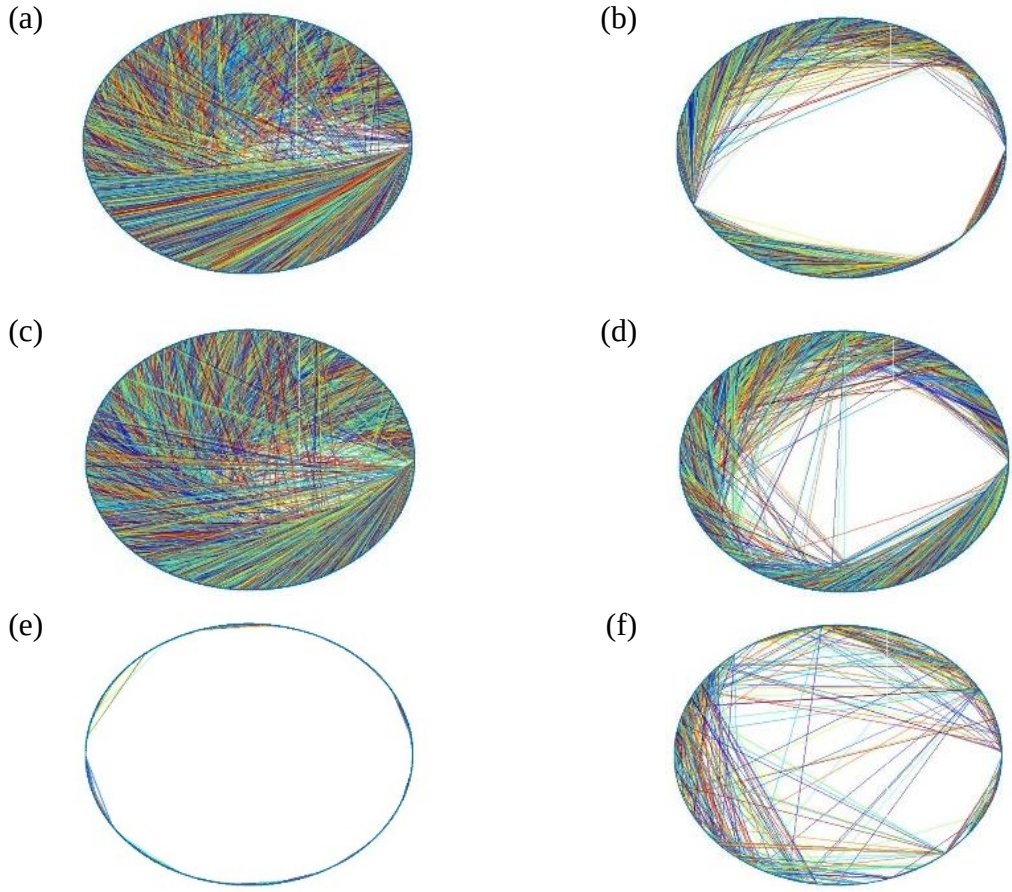

Figure 5.8: Network circle presentations of three diffuse- (*F. sylvatica* (a), *L. tulipifera* (b), *P. x canadensis* (c)) and three ring-porous tree species (*C. ovata* (d), *F. pennsylvanica* (e), *Q. montana (f))* based on the streamline analysis. One network per species is shown representative for three replicates per species.). All vertices (xylem segments) are aligned along the circle perimeter and edges (connections) are drawn between vertices.

Fluid simulations and P_{50} value comparisons

As a measure of robustness, we simulated the flow of water through a segment at constant pressure and characterized the change in flow due to the elimination of increasing fractions of randomly selected xylem vessels. Relative conductance decreased in all networks with an increasing vessel dropout probability (Fig. 5.9). The

ring-porous tree species *C. ovata* and *Q. montana* showed the highest decreasing rate in relative conductance, with a 100% conductance loss at a vessel dropout rate of 2% (Fig. 5.9d and f). In contrast, the dropout probability that causes a 100% conductance loss in *F. pennsylvanica* varies between 1-90% due to the high variability within the species (Fig. 5.9e). In the diffuse-porous tree species, *F. sylvatica* and *P. x canadensis* show a total conductance loss at 10% vessel dropout (Fig. 5.9a,c), while the 100% conductance loss of *L. tulipifera* varies between 10% and 38% due to the variability within the samples (Fig. 5.9b).

Based on the simulated decrease in relative conductance with increasing vessel dropout, simulated P_{10} and P_{50} values are calculated. Comparison of these values among species revealed that both the simulated P_{10} and P_{50} are not significantly different between the species (Fig. 5.10a,b). Simulated mean P_{10} values are reached between 0.002% and 0.005% vessel dropout (Fig. 5.10b), while simulated P_{50} values are reached between 0.01% and 0.04% vessel dropout probability (Fig. 5.10a). The simulated dropout rate does not differ either between tree species (Fig. 5.10c).

Experimentally determined, P_{50} values range from – 0.02 MPa for *F. pennsylvanica* to -2.07 MPa for *F. sylvatica* (Fig. 5.11a-f). Ring-porous tree species have higher P_{50} values than diffuse-porous tree species, with the exception of *C. ovata* and *P. canadensis*. *C. ovata's* P_{50} value of -0.9 MPa suggested a greater drought resistance compared to *P. canadensis* P_{50} value (-0.69 MPa). Fitting parameter a and b were all highly significant, except fitting parameter b for *F. pennsylvanica*, indicating that a more simplistic model fit would have been sufficient for this species (Table 5.5).

Comparisons between simulated P_{50} values and experimental P_{50} values did not

show any significant differences or patterns between tree species, all tree species were equally vulnerable to xylem vessel loss (Fig. 5.12). However, our data did not reveal at what pressure xylem segments dropped out. In our fluid simulation, we modeled water transport as a function of the pressure gradient across the network and did not include equations that connect the local pressure in the xylem to the xylem drop out procedure in the analysis. As a result, we are unable to fully connect the physics of cavitation to the fluid dynamic network properties.

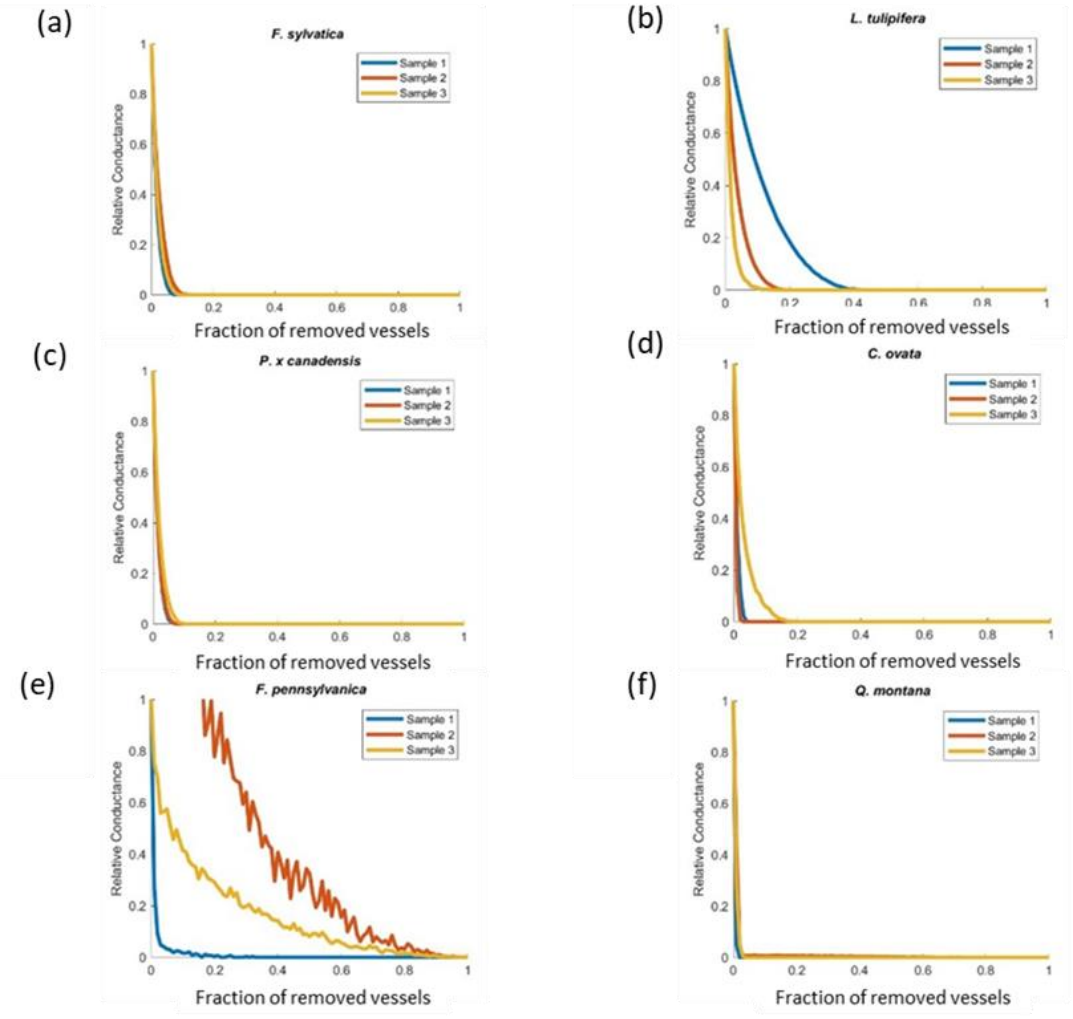

Figure 5.9: Simulated relative hydraulic conductance as a function of fraction of removed vessel (embolized vessels) of three diffuse- (*F. sylvatica* (a), *L. tulipifera* (b), *P. x canadensis* (c)) and three ring-porous tree species (*C. ovata* (d), *F. pennsylvanica* (e), *Q. montana (f))*. Represented are three replicates per species.

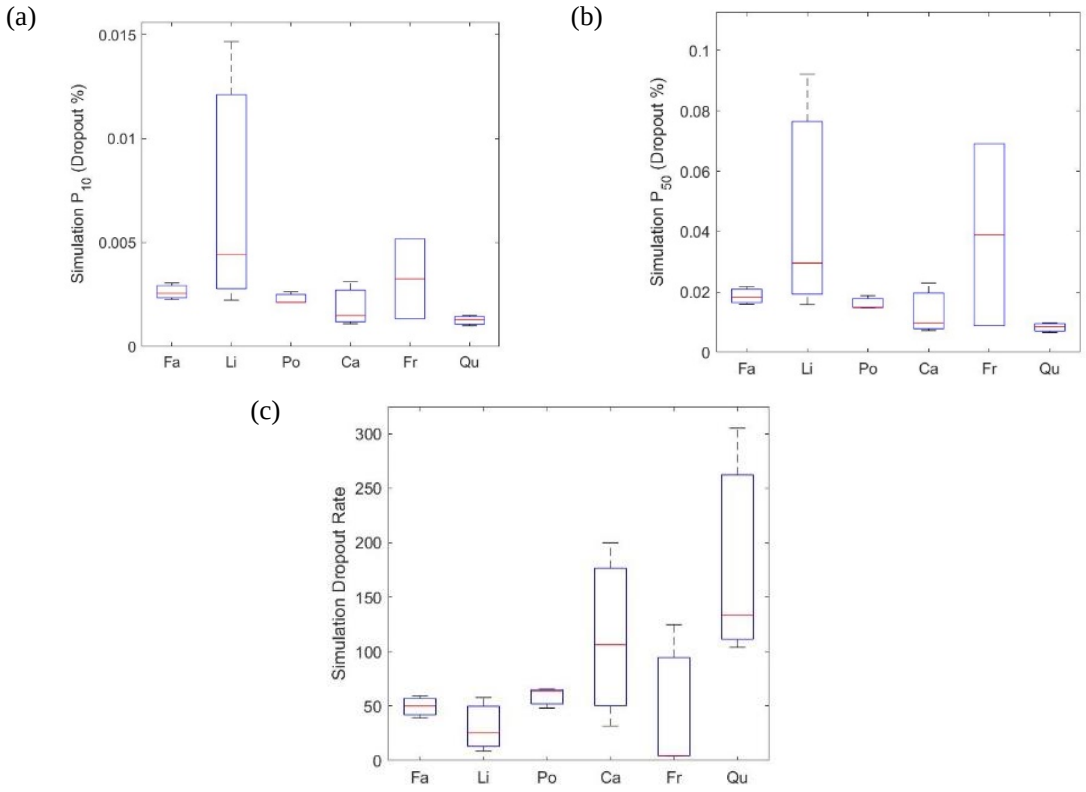

Figure 5.10: Comparison of simulated P_{10} values (a), simulated P_{50} values (b), and simulation dropout rate (c) based on embolism simulation analysis between three diffuse- (*F. sylvatica* (Fa), *L. tulipifera* (Li), *P. x canadensis* (Po)) and three ring-porous tree species (*C. ovata* (Ca), *F. pennsylvanica* (Fr), *Q. montana* (Qu)).

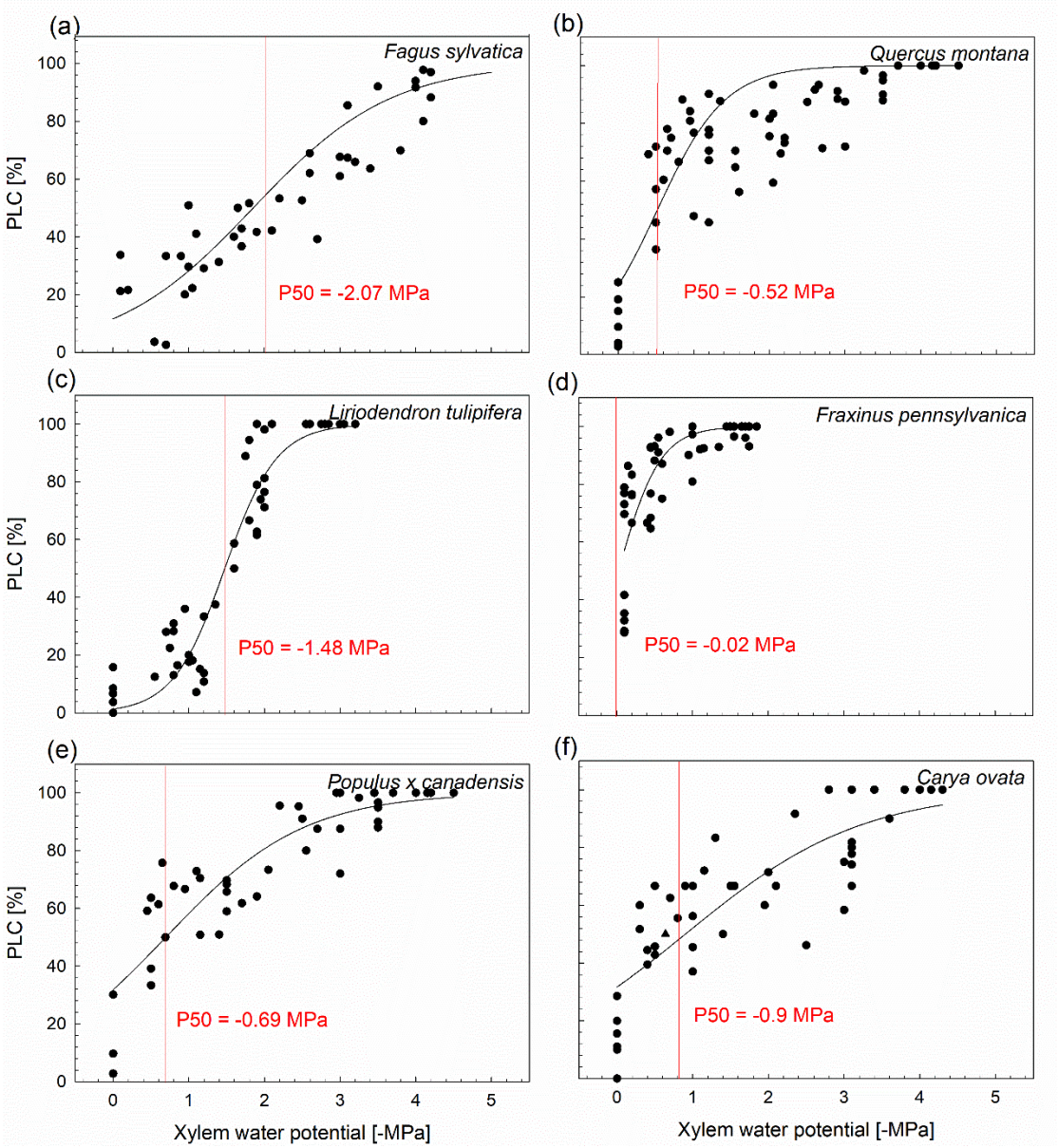

Figure 5.11: Percent loss of hydraulic conductivity curves (PLC curves) of three diffuse- (*F. sylvatica* (a), *Q. montana* (b), *L. tulipifera* (c)) and three ring-porous tree species (*F. pennsylvanica* (d), *P. x canadensis* (e), *C. ovata* (f)). Fitted lines were obtained by fitting the exponential sigmoidal equation PLC = 100/ (1 + exp{a[Ψ_x -b]}), to the data, where a describes the slope of the curve and b is the water potential (Ψ_x) at which PLC is reduced 50% (P_{50}, red line) (Pammenter and Vander Willigen, 1998). Values for a, b, are given in Table 5.5.

Table 5.5: Values of coefficients a and b from Eq. 5.10, where a describes the slope of vulnerability curves presented in Figure 5.11 and b is the predicted water potential at which 50% loss in hydraulic conductance occur. Significant parameters are marked by asterisks (**** = $P < 0.0001$; * = $P < 0.05$).

Tree species	a	b
F. sylvatica	0.84***	-2.07****
L. tulipifera	2.92***	-1.47****
P. canadensis	1.07***	0.69****
Q. montana	1.13***	-0.51****
F. pennsylvanica	3.64***	-0.02*
C. ovata	0.85***	-0.90***)

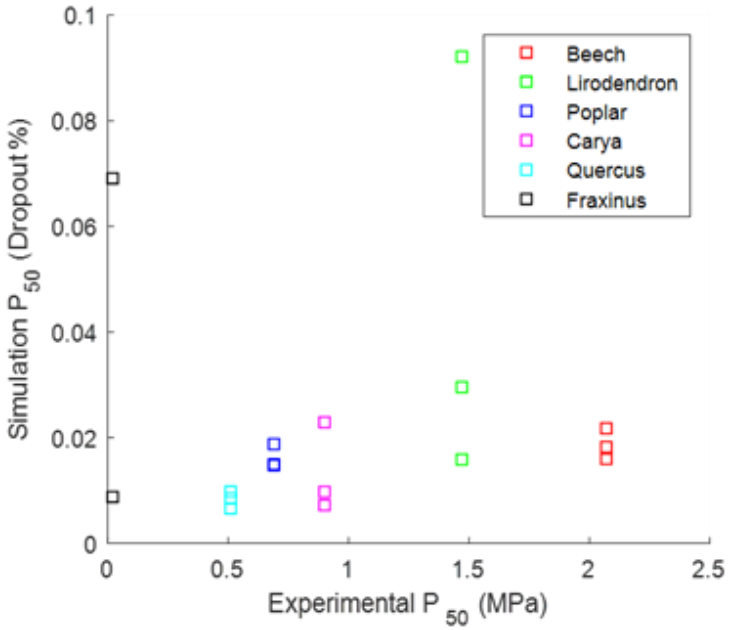

Figure 5.12: Comparisons between simulated P_{50} values from fluid simulation models and experimental determined P_{50} values from hydraulic conductivity measurements for three diffuse- (*F. sylvatica* (beech), *L. tulipifera* (liriodendron), *P. x canadensis* (poplar)) and three ring-porous tree species (*C. ovata* (Carya), *Q. montana* (Quercus), *F. pennsylvanica* (Fraxinus)).

5.4 Discussion

Network segmentation:

We present for the first time an analysis of xylem vascular networks that characterize the topology and connections of xylem vessels over several centimeter-long branches. The analysis was performed using a 3D-xylem segment model and a streamlined model that provided two different geometrical analyses to characterize the importance that certain anatomical/morphological features have on influencing xylem network function (Fig. 5.5a-d and 5.6a-d). While the 3D xylem segment analysis considered anatomical characteristics of xylem vessels, the streamline analysis examined water pathways (streamlines) through the xylem network. The combination of both analysis types aided our understanding of xylem network structures in more depth. For example, the xylem segment analysis revealed that the xylem networks of *F. pennsylvanica* consist of large volume xylem vessel segments that are poorly connected, while diffuse-porous trees have smaller volume vessels that are more connected (Fig. 5.5a-d). Contrary, the streamline analysis revealed, that the streamline lengths were comparable in all examined xylem networks (Fig. 5.5c). These results indicate that tree species have developed different strategies to efficiently move water through their network. These network patterns were also visually represented in the circle presentations (Fig 5.7a-f and 5.8a-f). Furthermore, circle presentations provided insight into how the structure of xylem networks vary across species (Fig. 5.7 and 5.8). While the circle presentation of xylem segment analysis showed that xylem segments of ring-porous tree species rarely have pit connections with xylem segments that are more distant, the streamline analysis revealed that water flow still is highly

connected, indicating that xylem networks have a plethora of redundant water passages that allow for water redistribution. However, caution is needed when interpreting the results of circle representations because the ascending vessel/ streamline (vertices) identification numbers (ID numbers), that were assigned in a consecutive order to vessels/ streamlines and are aligned at the outside of the circles do not truly represent the physical proximity of the vertices in the xylem network. It is assumed that ascending ID numbers correspond to neighboring vertices in the xylem network. However, while this assumption is generally true, there were instances when consecutive ID numbers were given to xylem vessels that were physically far apart. Additionally, it is important to stress that the selected and segmented area in our images were rectangular (Fig. 5.2c) to half-circular (Fig. 5.2a), meaning that the circle presentation does not represent the actual image geometry. In order to improve the quality of circle presentations, new methods should be explored that consider the real physical location of vertices in the networks such as bringing vertices in one plane, with newly emerging vertices placed radially inwards from the vertices that were present from the top of the image stack to illustrate not only their planar location but also their depth location within the xylem network.

In our analysis, we characterized xylem segments, xylem vessel sections between two junctions, instead of xylem vessels. The rationale for this is that the computer algorithm found a large number of xylem vessel bifurcations during the segmentation process (Fig. 5.1b). Xylem vessels can connect to each other in a longitudinal way via bifurcations, compared to intervessel pit connections that connected vessels laterally. Because of the plethora of detected bifurcations, it was difficult to determine the

beginning and the end of each xylem vessel. Therefore, xylem segments were defined as water-conducting conduits between two bifurcations. The exact number of bifurcations per network was not analyzed but given that the average xylem segment length in diffuse-porous trees is 100 µm over an average 5.9 cm long branch it appears that many bifurcations exist. To the best of our knowledge, bifurcations have not been described in xylem networks and therefore have not been considered in previous studies investigating xylem network structure (Loepfe *et al.*, 2007; Mrad *et al.*, 2018). Therefore, it is important to visually verify these connections to ensure that the algorithm is not falsely detecting imaging artifacts as bifurcations.

Fluid dynamics through xylem networks:

Computational fluid dynamic methods combined with stochastic dropout simulations allowed us to study the interaction of xylem segments and intervessel connections during water transport and their resistance to different degrees of embolism incidents. All species showed an extremely rapid decline in their relative conductance with increasing vessel dropout. Because vessel dropout occurred randomly in the simulation, these results correspond to randomly occurring cavitation events within the pore network. However, the model does not include the effects of air embolisms propagating from air seeding, and therefore, currently, we are unable to conclude if higher connectivity leads to more embolism resistant networks or more vulnerable networks. In order to simulate air-seeding in xylem networks, a follow-up simulation must be performed in which randomly dropped vessels will also trigger the removal of all connected vessels. The results of this study will answer the question if the rate

hydraulic conductivity loss is a function of vessel connectivity or not.

The simulated conductance loss of 50% occurred between 0.01-0.04% dropout probability for all species (Fig. 5.9a-f). The lack of significant differences in the simulated P_{50} value as well as the decreasing rate of relative conductance might be due to the variability between samples (Fig. 5.10a,c). Nevertheless, the low dropout rate that resulted in the observed extreme declines in conductance loss is much more sensitive to dropout compared to other vascular networks systems in other organisms, such as in the mouse and human cortical capillary networks. In these animal network systems, a 50% reduction in blood flow occurred when 20% of the capillaries were stalled with blood flow (Cruz Hernández *et al.*, 2019), which is several orders of magnitude higher than the plant vascular systems modeled in this study. However, comparing these two different networks might not be valid because of the differences in positive pressure-driven fluid flow velocities through the animal networks compared to the slower negative pressure fluid flow velocities in plant systems. While fluid transport in both networks is essential to life, the fluid flow in capillary brain systems must also flow permanently to provide the brain with sufficient nutrients and oxygen and to remove wastes and CO_2. Thus, a slowdown in fluid transportation would result in life-threatening conditions. Contrary, even though the xylem vascular network also supplies and distributes nutrients from the soil throughout the body of the plant, the velocity of the transpiration stream in trees can vary greatly, and can even slow down or stop under conditions that close stomates (at night in C3 plants or during the day in CAM plants, or during periods of drought stress etc.), but variation in transpiration rates does not result in short-term life-threatening conditions.

Furthermore, capillary networks in animal systems have sphincter-muscular system that can alter flow paths and change flow rates as well as blood volume through the network rapidly in response to changes in chemical signals, whereas these rapid changes do not occur in plant systems since they lack muscle tissue and capillary sphincters. However, vascular compression has been observed to occur in distal tissues in response to decreasing leaf water potentials which can alter hydraulic resistance when water potentials are low (Cochard *et al.*, 2004; Brodribb and Holbrook, 2005; Zhang *et al.*, 2016) altering fluid distributions. This vascular compression was not accounted for in this study. Therefore, even though both networks provide fluid transport and nutrient distribution, the needs of the tissues in the different systems are so vastly different that the function might be different and comparisons between them invalid.

In this study, we included on average 134,000 xylem vessels in our analysis for the ring-porous species. A 0.01% dropout represents the loss of 14 xylem vessels within a branch of 17.9 cm in length (the average analyzed sample length). To conclude that a loss of such a low number of xylem vessels causes the hydraulic conductance to decline by 50% seems questionable, even though large xylem vessels of ring-porous tree species have been described to be highly prone to cavitation events (Christman *et al.*, 2012). Our data and model suggest that the larger vessels may be playing a larger role than anticipated. Scaling these results to a 20-m tall tree would mean that 15,964 vessels would be blocked in to reduce hydraulic conductance by 50%. If a high percentage of these blocked xylem vessels are large-volume vessels, then it is reasonable that the conductance loss is affected, given that flow through vessels is

proportional to the vessel diameter to the fourth power (Eq. 5.6). However, because 15,964 vessels only constitute 0.01% of all vessels in a 20-m tall tree, the question remains: what is the function of the remaining 99.99% of vessels. Xylem networks have been described as being constructed of redundant xylem vessels that can take over water-conducting tasks if one vessel is blocked (Zimmermann, 1983; Ewers *et al.*, 2007). Nevertheless, it is important to stress, that we do not know which vessel diameter size class is being impacted in the 0.01% dropout rate by the resultant change in water potential. In a recent study, Huber et al. (unpublished data), showed that tree stems are very embolism resistant, even under severe drought stress conditions, meaning that it might be that the 0.01% dropout rate only occurs in trees under severe drought stress conditions. More research is needed to better understand the connection between the vulnerability of networks and the effects that low dropout rates have on the function of the vascular networks in plants.

Laser ablation tomography (LAT) was used as a sampling method to cut tree branches and acquire digital cross-sectional images of tree wood and used to reconstruct xylem networks, compare them to each other, and run three fluid simulations models. These models were tested to hydraulic PLC curves. The results demonstrate the high potential of this kind of analysis to understand vascular networks in plants. Because the collection of geometrical characteristics and fluid simulations revealed the complexity of this data set, we were unable to answer the original research objective: if xylem connectivity leads to more resistant or more vulnerable xylem networks. Likewise, we did not find a parameter that is dictating the robustness of xylem networks to fluid flow. To identify network metrics that are specific to ring-

and diffuse-porous xylem networks, we need more specific analyses, such as the suggested air seeding dropout simulation and validation of the fluid drop-out analysis. Additionally, the presented analysis needs further consideration in terms of the biological validity of the results, such as if the low simulated P_{10} and P_{50} values are biological valid, or if the methodology used in the analysis needs fine-tuning.

5.5 References

Aerts H, Fias W, Caeyenberghs K, Marinazzo D. 2016. Brain networks under attack: robustness properties and the impact of lesions. Brain: A Journal of Neurology **139**, 3063–3083.

Alder NN. 1997. Use of centrifugal force in the study of xylem cavitation. Journal of Experimental Botany **48**, 665–674.

Brodribb TJ, Holbrook NM. 2005. Water stress deforms tracheids peripheral to the leaf vein of a tropical conifer. Plant Physiology **137**, 1139–1146.

Carlquist S. 1988. *Comparative wood anatomy: systematic, ecological, and evolutionary aspects of dicotyledon wood*. Berlin, Heidelberg: Springer-Verlag.

Choat B, Lahr EC, Melcher PJ, Zwieniecki MA, Michele N. 2005. The spatial pattern of air seeding thresholds in mature sugar maple trees. Plant, Cell and Environment **28**, 1082–1089.

Choat B, Cobb AR, Jansen S. 2008. Structure and function of bordered pits: new discoveries and impacts on whole-plant hydraulic function. The New phytologist **177**, 608–25.

Christman MA, Sperry JS, Adler FR. 2009. Testing the 'rare pit' hypothesis for xylem cavitation resistance in three species of Acer. New Phytologist **182**, 664–674.

Christman MA, Sperry JS, Smith DD. 2012. Rare pits, large vessels and extreme vulnerability to cavitation in a ring-porous tree species. New Phytologist **193**, 713–720.

Christmann A, Weiler EW, Steudle E, Grill E. 2007. A hydraulic signal in root-to-shoot signalling of water shortage. The Plant Journal **52**, 167–174.

Cochard H, Badel E, Herbette S, Delzon S, Choat B, Jansen S. 2013. Methods for measuring plant vulnerability to cavitation: a critical review. Journal of Experimental Botany **64**, 4779–4791.

Cochard H, Froux F, Mayr S, Coutand C. 2004. Xylem wall collapse in water-stressed pine needles. Plant Physiology **134**, 401–408.

Cruz Hernández JC, Bracko O, Kersbergen CJ, *et al.* 2019. Neutrophil adhesion in brain capillaries reduces cortical blood flow and impairs memory function in Alzheimer's disease mouse models. Nature Neuroscience **22**, 413–420.

Evangelidis G, Psarakis E. 2008. Parametric image alignment using enhanced correlation coefficient maximization. IEEE Transactions on Pattern Analysis and Machine Intelligence **30**, 1858–1865.

Evert RF. 2006. *Esau's Plant Anatomy: Meristems, Cells, and Tissues of the Plant Body: their Structure, Function, and Development*. Hoboken, New Jersey: John Wiley & Sons, Inc.

Ewers FW, Ewers JM, Jacobsen AL, López-Portillo J. 2007. Vessel redundancy:

modelling safety in numbers. IAWA Journal **28**, 373–388.

Giordano R, Salleo A, Salleo S, Wanderlingh F. 1977. Flow in xylem vessels and Poiseuille's law. Canadian Journal of Botany **56**, 333–338.

Haft-Javaherian M, Fang L, Muse V, Schaffer CB, Nishimura N, Sabuncu MR. 2019. Deep convolutional neural networks for segmenting 3D in vivo multiphoton images of vasculature in Alzheimer disease mouse models. PloS one **14**, e0213539.

Hales S. 1727. *Vegetable staticks: or, an account of fome statical experiments on the sap in vegetables: being an essay towards a natural hiftory of vegetation. Alfo, a specimen of an attempt to analyse the air, by a great variety of chymio-statical experiments*. London: W. and J. Innys and T. Woodward.

Jacobsen AL, Ewers FW, Pratt RB, Paddock III WA, Davis SD. 2005. Do xylem fibers affect vessel cavitation resistance ? Plant Physiology **139**, 546–556.

Jansen S, Choat B, Pletsers A. 2009. Morphological variation of intervessel pit membranes and implications to xylem function in angiosperms. American Journal of Botany **96**, 409–419.

Lens F, Sperry JS, Christman M a, Choat B, Rabaey D, Jansen S. 2011. Testing hypotheses that link wood anatomy to cavitation resistance and hydraulic conductivity in the genus Acer. New Phytologist **190**, 709–723.

Loepfe L, Martinez-Vilalta J, Piñol J, Mencuccini M. 2007. The relevance of xylem network structure for plant hydraulic efficiency and safety. Journal of Theoretical Biology **247**, 788–803.

Maherali H, Moura CF, Caldeira MC, Willson CJ, Jackson RB. 2006. Functional

coordination between leaf gas exchange and vulnerability to xylem cavitation in temperate forest trees. Plant, Cell and Environment **29**, 571–583.

Maherali H, Pockman W, Jackson RB. 2004. Adaptive variation in the vulnerability of woody plants to xylem cavitation. Ecology **85**, 2184–2199.

Melcher PJ, Michele Holbrook N, Burns MJ, Zwieniecki MA, Cobb AR, Brodribb TJ, Choat B, Sack L. 2012. Measurements of stem xylem hydraulic conductivity in the laboratory and field. Methods in Ecology and Evolution **3**, 685–694.

Melcher PJ, Zwieniecki MA, Holbrook NM. 2003. Vulnerability of xylem vessels to cavitation in sugar maple. Scaling from individual vessels to whole branches. Plant Physiology **131**, 1775–1780.

Mrad A, Domec JC, Huang CW, Lens F, Katul G. 2018. A network model links wood anatomy to xylem tissue hydraulic behaviour and vulnerability to cavitation. Plant, Cell and Environment **41**, 2718–2730.

Northeast Regional Climate Center. 2019. NRCC The Ithaca Climate Page.

Pammenter NW, Van der Willigen C. 1998. A mathematical and statistical analysis of the curves illustrating vulnerability of xylem to cavitation. Tree Physiology **18**, 589–593.

Psarakis E, Evangelidis G. 2005. An enhanced correlation-based method for stereo correspondence with sub-pixel accuracy. Computer Vision, 2005. ICCV 2005. Tenth IEEE International Conference on. Beijing, China: IEEE, 907–912.

Rueden CT, Schindelin J, Hiner MC, DeZonia BE, Walter AE, Arena ET, Eliceiri KW. 2017. ImageJ2: ImageJ for the next generation of scientific

image data. BMC Bioinformatics **18**, 1–26.

Sperry JS, Donnelly JR, Tyree MT. 1988. Seasonal occurrence of xylem embolism in sugar maple (*Acer saccharum*). American Journal of Botany **75**, 1212–1218.

Sperry JS, Hacke UG. 2004. Analysis of circular bordered pit function I. Angiosperm vessels with homogenous pit membranes. American Journal of Botany **91**, 369–385.

Sperry JS, Hacke UG, Wheeler JK. 2005. Comparative analysis of end wall resistivity in xylem conduits. Plant, Cell and Environment **28**, 456–465.

Sperry JS, Sullivan JE. 1992. Xylem embolism in response to freeze-thaw cycles and water stress in ring-porous, diffuse-porous, and conifer species. Plant Physiology **100**, 605–13.

Tyree MT, Dixon MA. 1986. Water stress induced cavitation and embolism in some woody plants. Physiologia Plantarum **66**, 397–405.

Venturas MD, Sperry JS, Hacke UG. 2017. Plant xylem hydraulics: what we understand, current research, and future challenges. Journal of Integrative Plant Biology **59**, 356–389.

Wang Z, Bovik AC, Sheikh HR, Simoncelli EP. 2004. Image quality assessment: from error visibility to structural similarity. IEEE Transactions on Image Processing **13**, 600–612.

Wheeler JK, Huggett BA, Tofte AN, Rockwell FE, Holbrook NM. 2013. Cutting xylem under tension or supersaturated with gas can generate PLC and the appearance of rapid recovery from embolism. Plant, Cell and Environment **36**, 1938–1949.

Wheeler JK, Sperry JS, Hacke UG, Hoang N. 2005. Inter-vessel pitting and cavitation in woody Rosaceae and other vesselled plants: a basis for a safety versus efficiency trade-off in xylem transport. Plant, Cell and Environment **28**, 800–812.

Woodcock DW. 1989. Distribution of vessel diameter in ring-porous trees. Aliso: A Journal of Systematic and Evolutionary Botany **12**, 287–293.

Zanne AE, Sweeney K, Sharma M, Orians CM. 2006. Patterns and consequences of differential vascular sectoriality in 18 temperate tree and shrub species. Functional Ecology **20**, 200–206.

Zhang Y-J, Rockwell FE, Graham AC, Alexander T, Holbrook NM. 2016. Reversible leaf xylem collapse: a potential "circuit breaker" against cavitation. Plant Physiology **172**, 2261–2274.

Zimmermann MH. 1983. *Xylem structure and the ascent of sap*. New York: Springer Verlag.

CHAPTER 6

SUMMARY OF RESULTS

The impact of plant hydraulics on stomatal conductance in controlling the stomatal aperture at the beginning of drought stress periods is shown by the simultaneous recording of hydraulic, chemical, and electrical signals in *Helianthus annuus* during two different drought stress intensities, slow and fast dry-down treatments (Chapter 3). I found that the acoustic emission events (AE events) and changes in leaf-level turgor pressure were the only two signal types that preceded stomatal closure. Electrical and hormonal signals were observed to take place only during or after stomatal closure occurred, therefore these signal types were excluded as a mechanism used by plants to close stomata. The measured increase in AE events were found to be associated with increased tissue shrinkage and leaf level turgor changes. Since the AE events occurred first, it is proposed that they serve as a possible early hydraulic signaling mechanism because it started at the onset of both dry-down treatments. Thus, it may serve as a possible candidate for initiating stomatal closure. Additionally, the decrease of leaf turgor pressure is another possible signal candidate, as it was recorded shortly after AE events started in both the natural dry-down treatments and shortly after the addition of a -3.0 MPa polyethylene glycol solution in the fast dry-down treatment. Since, changes in leaf turgor pressure occurred concurrently with stomatal responses, AE events and leaf turgor changes were the two parameters most tightly linked to the measured onset of stomatal closure. The experimental results also showed that stomatal closure was initiated at similar leaf water potentials (Ψ_{leaf}) across all

treatments, which emphasizes the importance of the leaf water status in governing stomatal control at the beginning of drought stress periods. However, not all hydraulic signals played an important role in the initiation of stomatal closure, as the turgor loss point and cavitation events were observed after stomatal closure occurred.

During and after drought stress periods, the hydraulic status of plant organs (root, stem, leaf) were intensively studied in *Helianthus annuus* and *Populus x canadensis* and supported by the examination of four additional woody tree species (*Acer saccharum*, *Acer saccharinum*, *Picea glauca*, and *Tsuga canadensis*) (Chapter 4). The simultaneous measurements of organ water potential (Ψ), organ relative water content, and xylem vessel embolism thresholds (determined by using cryo-microscopy and a single vessel injection technique) enabled us to correlate hydraulic integrity of plant organs with stomatal closure. Data revealed that xylem vessels of petioles were most susceptible to embolism formation, while root and stem xylem vessels were highly drought resistant. Yet, stomatal closure was not correlated to xylem cavitation events in any organ, since cavitation only occurred during higher drought stress intensities. Air seeding threshold data revealed that root and petiole xylem vessels of *P. x canadensis* and *H. annuus* were equally more vulnerable to drought stress than stem xylem vessels. However, drawing conclusions based on Ψ alone is misleading, because Ψ measurements revealed a persistent water potential gradient between plant organs, with leaves experiencing more negative water potentials than the roots, even after stomatal closure occurred. This disequilibrium causes petioles of both species to reach the air seeding pressure threshold at lower drought stress intensities than roots and consequently, petioles were the organ suffering the most embolism events, while

stem and root exhibited little to no embolism. Thus, these findings suggest that overall Ψ_{plant} cannot be determined by covered Ψ_{leaf} measurements alone in *P. x canadensis* and *H. annuus*. Furthermore, comparison of the plant water status during the dry-down experiments and P_{50} values (predicted by plant hydraulic vulnerability curves) revealed that only two of the six examined species experienced water potentials lower than P_{50}, bringing into question the usefulness P_{50} values have on predicting drought stress resistance of plants during drought stress periods.

After drought stress recovery, the root was the only organ that recovered its water status to pre-drought stress conditions across plant species, highlighting the importance of root water uptake for plants' recreation after drought stress periods (Chapter 4). *H. annuus* showed embolism events in stem xylem vessels during the dry-down period that did not recover after rewatering. Contrary, while embolisms were not observed in stems of *P. x canadensis* and *A. saccharum* during the drought stress period, both species showed increased embolism events after two days of drought stress recovery. This observation was unexpected and speculated to be caused by the mechanical expansion of xylem conduits. Recovery of the hydraulic status of petioles occurred in all plant species, with the exception of *P. x canadensis*, which shed its leaves. However, despite the recovery of physiological and anatomical functions of leaves, stomatal conductance remained inhibited or low in plant species that did not show recovery of embolism events of stem xylem vessels to pre-drought stress conditions, suggesting that the stem plays an important role in recovering processes after drought stress.

To understand and predict embolism occurrence in the wood of tree species

remains challenging. To answer the question if xylem connectivity leads to more resistant or more vulnerable xylem networks, we acquired digital cross-sectional images of two-year-old tree branches of three ring- (*Quercus montana*, *Fraxinus pennsylvanica*, *Carya ovata*) and three diffuse-porous tree species (*Fagus sylvatica*, *Liriodendron tulipifera*, *P. x canadensis*) using laser ablation tomography. Then, we reconstructed xylem networks to understand the topology of vascular networks and compared them with each other. Additionally, we and ran fluid simulation models of each network to predict the resistance of hydraulic conductivity as a function of vessel dropout within the network (Chapter 5). The results of this analysis revealed not only the potential but also the complexity of this type of analysis. For example, we showed that the understanding of two different network analyses is essential to fully understand xylem networks: while the xylem segment analysis revealed that tree the xylem segment length differed across tree species, the streamline (water path) analysis showed that the streamline length did not differ across tree species, indicating that plants developed different pathway architectures to efficiently move water through their xylem network. Furthermore, fluid simulations showed that vessel removal between 0.01-0.04% of the original vessel population resulted in a 50% loss of hydraulic conductance across all tree species. In the current model, this dropout procedure was performed randomly and was not coupled to any information regarding the local water potential; therefore, we are unable to predict at which water potentials the xylem vessel will start to drop out (embolize). Based on these results we were not able to connect xylem vessel topology with embolism resistance, nor identify a parameter that indicates the robustness of xylem networks to fluid flow. Therefore,

further analysis will focus on the fine tuning of the methodology used in the analysis and the consideration of the biological validity of the results, such as if the low simulated P_{50} values (as measured by dropout percentage) are biologically relevant. The outcome of these studies will help connect PLC curves with the xylem topology of ring- and diffuse-porous tree species.

The results of the presented studies stress the importance of plant hydraulics in the drought response of plants at the beginning, during, and after drought stress periods. Foreseeing the impact of drought stress in plants becomes particularly crucial in times of climate change. The data gathered in these studies contribute to this endeavor and point towards changes in turgor pressure and Ψ_{leaf} as useful indicators to estimate stomatal closure at the onset of drought stress in plants and therefore could be used as a leading indicator for adjusting watering protocols in agricultural or viticulture settings. Contrary, P_{50} values, the recording of acoustic emission events, and the observation of cavitation events are not supportive parameters in predicting the drought stress resistance of plants; multiple sources of AE events confound the interpretation of their presence and organ xylem vessels can endure severe drought stress without cavitating. Additionally, results show that estimating the stem and the root water status of plants during drought stress periods based on covered leaf water potential measurements might be misleading because of water potential gradient we observed in our studies causing higher Ψ_{root} than Ψ_{leaf}. Therefore, more research is needed to understand the role of cavitation events and water potential gradients in plants, especially with regard to drought stress resistance in plants.

APPENDICES

Appendix 1

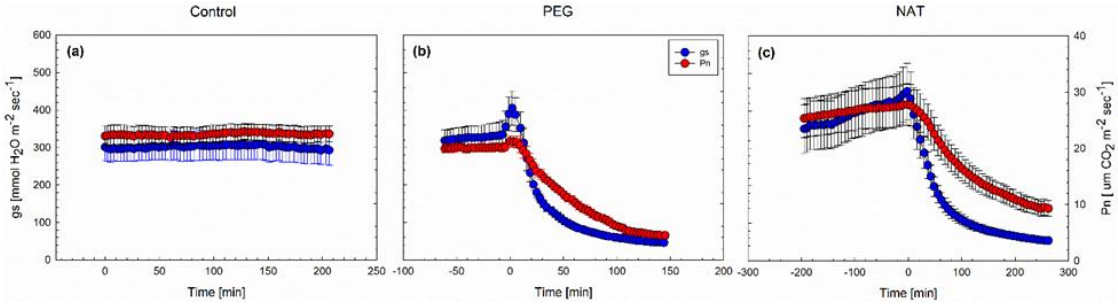

Figure A1: Mean and SE of stomatal conductance (gs; blue circles) and photosynthesis (Pn; red circles) of sunflower (*Helianthus annuus*) plants throughout the time course of the experiment. Sunflowers were either kept hydrated (control, n = 5 (a)), or exposed to either an induced (PEG, n = 8 (b)), or a natural dry-down treatment (NAT, n = 8 (c)). Time point 0 min. represents the beginning of the control experiment or the peak of gs in the dry-down treatments.

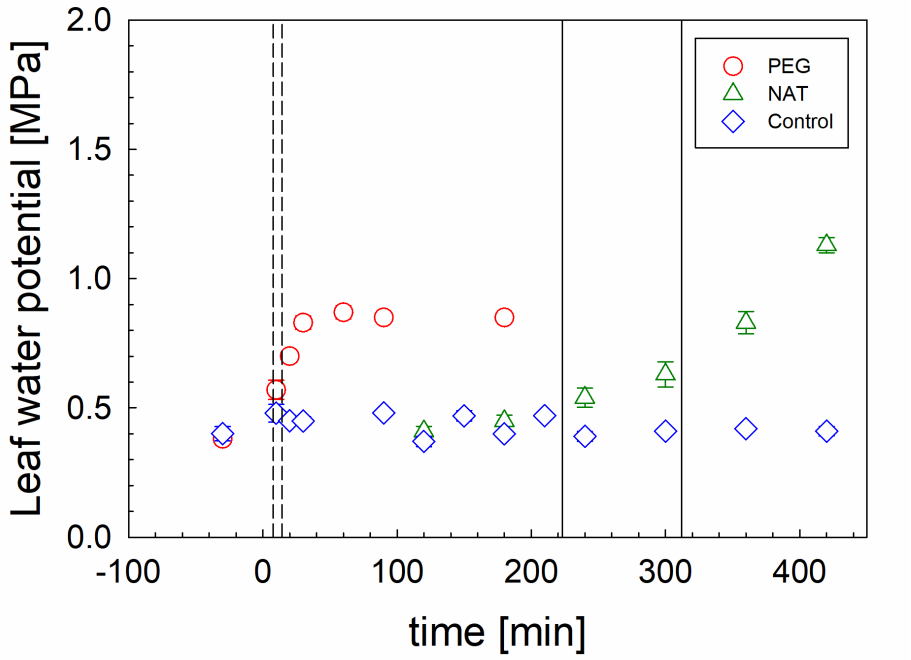

Figure A2: Covered leaf water potential of sunflower plants (*Helianthus annuus*) throughout the duration of the experiment. Sunflowers were either kept hydrated (control, blue diamond), or exposed to either an induced (PEG, red circle) or a natural dry-down treatment (NAT, green triangle) (n =5; respectively). The confidence interval of the max. stomatal conductance during the onset of stomatal closure is presented for the PEG (dashed lines) as well as the NAT dry-down treatment (solid line). Time point 0 min refers to the induction of the PEG 8000 solution in the PEG treatment or the beginning of the NAT dry-down treatment.

Appendix 3

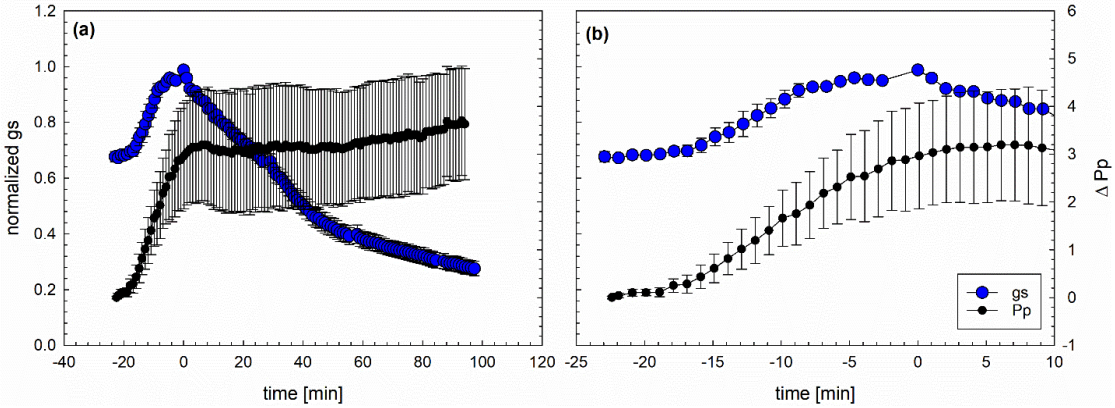

Figure A3: Stomatal conductance (gs, blue circles) and relative changes in the patch pressure of Yara ZIM probes (ΔPp) (ZIM Plant Technology GmbH, Henningsdorf Germany) of sunflower (*Helianthus annuus*) leaves throughout the entire PEG treatment (a) or zoomed into the period when stomatal were responding (n =5, mean ± SE). Pp is inversely correlated to changes in bulk leaf turgor (Zimmermann *et al.*, 2008).

Appendix 4

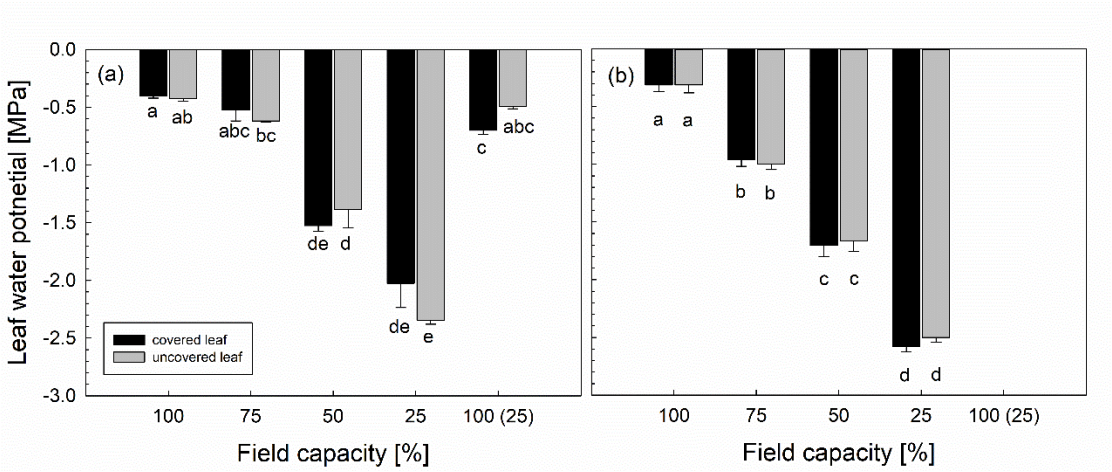

Figure A4: Comparison between mean (+/- SE) covered and uncovered leaf water potential of *H. annuus* (a) and *P. x canadensis* (b) (n = 4, respectively) measured at different field capacities (FC) that ranged from saturated (100% FC) to extreme drought (25% FC) followed by rewatering to saturation (100 (25)% FC). Data could not be collected for *P. x canadensis* leaves at 100 (25)% FC, because *P. x canadensis* shed its leaves after the 25% FC treatment. Columns with different letters are significantly different ($P < 0.05$).

Appendix 5

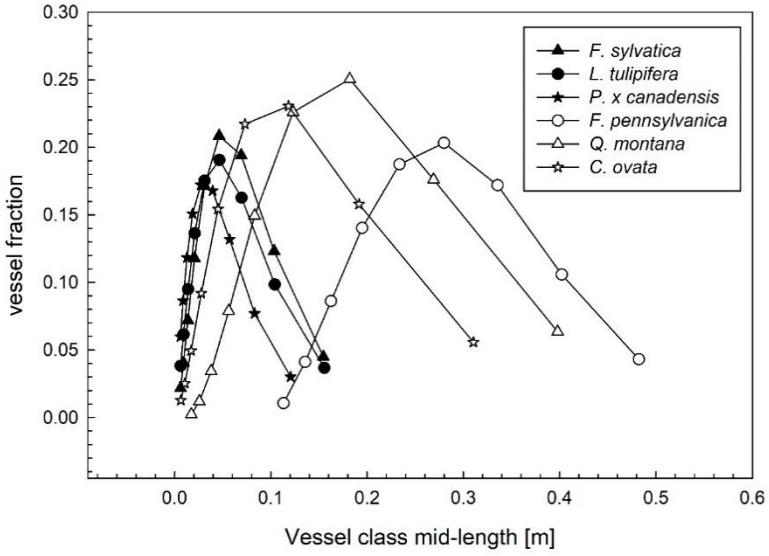

Figure A5: Vessel length distribution of three diffuse-porous (filled symbols) and three ring-porous (unfilled symbols) tree species. Six branches per species were sampled and compiled before fitting vessel distribution according to Christmann *et al.*, 2009.